DYNAMICS OF MYELINATION IN THE MAMMALIAN NERVOUS SYSTEM

BY MALTE SEBASTIAN KALLER

OF PEMBROKE COLLEGE



A THESIS SUBMITTED TO THE UNIVERSITY OF OXFORD

FOR THE DEGREE OF DOCTOR OF PHILOSOPHY

STUDENT ID: 683287

TRINITY 2019

ABSTRACT

Myelination was first understood to enable faster impulse propagation in axons more than 60 years ago, yet it took a long time to recognise the mechanistic complexity of this cellular process and the diverse roles that myelinating glia play in the formation and functioning of the vertebrate nervous system. Once considered a static insulator, myelinating glia are now increasingly recognised as dynamic and adaptive cell populations. The effective bidirectional signalling between axons and glia and dynamic changes in the Schwann cell population play a fundamental role in the injury response of the PNS. Furthermore, converging evidence now suggests that myelin in the CNS can be dynamically regulated by neuronal activity and continues to participate in nervous system plasticity beyond development, yet the functional role of such adaptive myelination remains unclear. While the dynamic natures and diverse functions of myelinating glia have now gained increased recognition, fundamental mechanisms and principles underlying these processes remain poorly understood. The aim of this thesis was to advance our understanding of myelin dynamics and the axon-glia communication regulating them. The first part of this thesis describes the development of myelinating co-cultures using human induced pluripotent stem cell-derived sensory neurons. Our work outlines how such a novel PNS co-cultures system can be used to provide insights into the cellular and molecular specialization of axoglial signalling, how pharmacological agents may promote or impede such signalling and the pathogenic effects of ganglioside antibodies. The second part of the thesis describes work aimed to investigate the role of neuregulin 1 (*Nrg1*) signalling in myelination in the PNS and CNS. While *Nrg1* plays an essential role in the myelination of Schwann cells, as demonstrated in this thesis, its role in CNS myelination remains elusive. The work presented indicated that conditional global deletion of *Nrg1* in mice leads to a behaviour deficit in a motor task. However, we found no conclusive evidence for a role of *Nrg1* in adaptive myelination and myelinating glia dynamics in the CNS. The third part of this thesis focuses on the functional role of dynamic and

adaptive myelination in the CNS, concentrating on the question if and how *de novo* myelination during adulthood facilitates and shapes motor behaviour and learning. The work presented replicates and extends previous findings indicating a causal relationship between adaptive myelination and behaviour change. However, not all aspects of evidence were faithfully replicated, and we conclude that further investigation is required to unravel the link between adaptive myelination and motor learning. Furthermore, our preliminary analysis of cellular and microstructural changes in CNS, acquired by combining histology and magnetic resonance imaging, remains partly inconclusive regarding the exact role that *de novo* myelination might play in skill acquisition. Overall, the major contributions of this thesis are the development of a novel and useful co-culture system using iPSC derived human cells and the thorough replication, critical evaluation and extension of important findings that indicated a causal link between myelin plasticity and behaviour change.

DECLARATION

This dissertation is the result of the author's own work. Exception to this are the few cases where explicit reference is made to the work and contributions of others and the sections of the work where credit and contributions of collaborators have been clear acknowledged in the 'Preface' section of this document. The work presented in this thesis has also not been submitted for another qualification to this or any other university. This dissertation does not exceed the page or word limit.

MALTE SEBASTIAN KALLER

ACKNOWLEDGMENTS

First, I would like to thank my supervisors, Heidi Johansen-Berg, David Bennett and Cassandra Sampaio Baptista. They are brilliant scientist who do outstanding work. They have always been extremely supportive, and they provided helpful and constructive feedback when it was needed. They did not give up on me, even in the most difficult times, for which I am deeply grateful. Heidi and Dave do such an excellent job of managing their research group, always being kind, constructive and respectful while supporting and encouraging people to give their best. They are a true inspiration and role models for what academic scientists in leadership positions should be. It has been a real privilege to work with them.

I would like to thank the members of the research groups of Heidi Johansen-Berg and David Bennett that I have worked with over the years and that have always provided a joyful and constructive work environment. In particular, I would like to thank Alex Clark for all that he has taught me and all his advice and support. I would also like to thank Ilaria Cervellini and Jorge Galino for their encouragement and constructive advice over the years as their adopted son. Furthermore, I would also like to thank David Bannerman, an invaluable source of support and constructive feedback for anything related to the *in vivo* experiments, as well as a great conversation partner for the latest in the word of football. I would also like to thank all the departmental staff in the Nuffield Department of Clinical Neuroscience and the animal facility of the Medical Science Division.

I am also grateful to all members of Pembroke College, Oxford. The staff members at Pembroke have provided a supportive and enjoyable environment for students. In my years as captain of the MCR football team, Bar manager for the MCR Bar, Welfare Rep and College Peer supporter I had the chance to really participate in college life. I have met countless amazing and inspiring people at countless college dinners and events and formed some true friendships over the years. Being part of this college has been a true privilege that I will never forget.

Last but not least, I would like to thank my friends and family that make my life worth living. You know who you are, but if you insist, I may spell your names out for the final version of this document. You have kept me sane over the years and I could not have done this without your love and support. Thank you.

PREFACE AND ACKNOWLEDGEMENTS OF COLLABORATORS

Part of the scientific work presented in this thesis has been conducted in collaboration with other researchers. To acknowledge their invaluable help and contributions, I have outlined the general contribution of collaborators below, followed by a detailed breakdown of the scientific contributions of others. Some further acknowledgments, such as for the gifting of anti-bodies and reprogramming of iPSC, are included in the relevant section of the Chapters.

GENERAL ACKNOWLEDGMENT FOR SCIENTIFIC COLLABORATORS

Part of this thesis has been published as a paper with shared first authorship:

> ***Clark AJ, Kaller MS****, Galino J, Willison HJ, Rinaldi S, Bennett DLH: Co-cultures with stem cell-derived human sensory neurons reveal regulators of peripheral myelination. Brain 2017, 140:898–913.*

All work presented in Chapter 2 of the thesis is derived from the paper mentioned above, as well as the results presented in Chapter 3 - 3.3.1 and Chapter 3 - 3.3.2. As a shared first author of this paper, I have played a major role in writing the document. I also shared the responsibility of planning and conducting the experiments, as well as collecting, analyzing and interpreting the data. Hence, I share the majority of the credit for this work with the other first author Alex J Clark, who has been an invaluable collaborator, laboratory partner and mentor.

The exception to this is the work involving the use of Anti-disialosyl antibodies, which is presented in Chapter 2, section 2.3.4 and 2.3.5. While I was involved in the data collection and analysis of the work presented in these sections, the planning and interpretation of these experiments were conducted by Alex J Clark and Simon Rinaldi, two brilliant scientists who deserve the credit for this work. However, I have included the results of these experiments in this thesis, as they demonstrate the

possibilities of the novel co-culture system that I helped to establishing and characterising, and as I have at least partly been involved in conducting the experiments.

Furthermore, I would like to acknowledge the work of Jorge Galino, who played a major part in collecting the Western Blot and electron microscopy data, together with Errin Johnson (EM facility, University of Oxford, UK), as well as designed the viral construct used in this study. I would also like to thank Florence Heath, who has helped with some of the perfusion.

Another part of this thesis has been previous published as a sole first authorship paper by the author of this thesis:

> Kaller, M.S., Lazari, A., Blanco-Duque, C., Sampaio-Baptista, C., Johansen-Berg, H., 2017. Myelin plasticity and behaviour—connecting the dots. Current Opinion in Neurobiology, Glial Biology 47, 86–92.

Sections 1.6 and Figure 1.4 and 1.5 of this thesis are derived from this review mentioned above. These sections have been predominantly written, and the figures have been designed by the author of this thesis. However, I would like to acknowledge the invaluable discussions, suggestions and corrections by the other 4 authors of this paper that formed an essential basis for this work.

Finally, I would like to acknowledge the contributions of the staff at the animal facility of the Medical Science Divison, Oxford, who have helped to manage the animal colonies, ensured the welfare of the animals and conducted all the tamoxifen administration via gavage.

DETAILED BREAKDOWN OF THE SCIENTIFIC CONTRIBUTIONS OF OTHERS

Alex J Clark, University of Oxford

- All experiments conducted with the iPSC-derived co-cultures have been conducted in collaboration with Alex Clark (Chapter 1 and 2) and he had a major contribution in designing and optimising the experimental protocol for establishing the co-cultures.
- Alex Clark conducted the majority of neuronal differentiation from iPSC that were used for the iPSC-derived co-cultures (Chapter 1 and 2).
- Alex Clark conducted a large proportion of the isolation of primary Schwann cells (Chapter 2-2.2.4).
- Alex Clark conducted or helped with the establishment and maintenance of the co-cultures, as well as the immunohistochemistry and confocal microscopy for the images and/or data presented in the following Figures: Figure 2.2A&I. Figure 2.3A,B&C. Figure 2.5, Figure 2.6, Figure 2.7, Figure 2.8.

Simon Rinaldi, University of Oxford

- Simon Rinaldi conducted or helped with the establishment and maintenance of the co-cultures, as well as the immunohistochemistry and confocal microscopy for the images and/or data presented in the following Figures: Figure 2.6, Figure 2.7, Figure 2.8.
- Simon Rinaldi planned and conducted the experiments involving the Anti-disialosyl antibodies, together with Alex Clark. The author of this thesis contributed to the maintenance of co-cultures and conducted the data analysis for this work.

Errin Johnson, EM facility, University of Oxford

- The fixation, section and part of the imaging of the co-cultures with electron microscopy was conducted by Errin Johnson at the Electron Microscopy Facility at the School of Pathology,

University of Oxford. Concerning the work presented in Figure 2.3D, we simply provided Errin Johnson with living co-cultures.

Ilaria Cervellini, University of Oxford

- Ilaria helped with the isolation of the primary rodent Schwann cells.
- Ilaria helped with the maintenance of the co-cultures with rodent Schwann cells.

Jorge Galino, University of Oxford

- Jorge helped with the imaging of the electron microscopy sections (Figure 2.3D)
- Jorge help us with the acquisition of the data using Western Blotting, doing most of the work in the process that resulted in the data presented in Figure 3.2G and Figure 3.3H.
- Jorge also designed the viral construct used for the work presented in Figure 3.2.

Laurence Brown, University of Oxford

- Laurence provided the hardware and software for conducting the activity monitoring of mice using passive infrared sensors and helped with the data analysis for the data presented in Figure 4.9, Figure 4.10 and Figure 4.11.

Florence Heath, University of Oxford

- Florence conducted a subset of perfusions of animals (n=20) for the ex vivo MRi imaging data set (described in Chapter 5.2.3).

Takahiro Shimizu, University College London

- Takahiro helped conducted the genotyping (n=40) for a subset of Myrf-cKO animals used in this thesis.

Staff at the animal facility, Department of Biomedical Services, University of Oxford

- The staff at the animal facility conducted the breeding, weaning and identification of all the mice used for the experiments presented in this thesis.
- The staff at the animal facility conducted all the tamoxifen administration via gavage described in this thesis.

Annette van der Toorn, Center for Image Sciences, UMCU, Netherlands.

- Annette conducted all the *ex vivo* MR imaging at the facility in Uetrecht, Netherlands, according to our instructions.

TABLE OF CONTENTS

CHAPTER 1 | .....GENERAL INTRODUCTION 1

1.1. STUDYING THE ROLE OF GLIAL CELLS IN THE NERVOUS SYSTEM 1
1.2. MYELIN AND MYELINATING GLIA OF THE MAMMALIAN NERVOUS SYSTEM 2
1.2.1 Myelinating glia 3
1.3. THE FUNCTIONAL ROLE OF MYELINATING GLIA IN THE NERVOUS(WOLPERT, DIEDRICHSEN AND FLANAGAN 2011; MAKINO *ET AL.* 2016) SYSTEM 6
1.3.1 Increase Speed of action potential propagation 6
1.3.2 Support of axonal integrity and metabolism.....7
1.4. THE DEVELOPMENT AND DYNAMICS OF MYELINATING GLIA 9
1.4.1 Development and dynamics of PNS myelination: Schwann cells.....9
1.4.2 Development and dynamics of CNS Myelination: Oligodendroglia.....11
1.5. AXON-GLIA SIGNALLING SHAPING THE MYELIN LANDSCAPE 14
1.6. MYELIN DYNAMICS IN THE CNS AND BEHAVIOUR 17
1.6.1 Association between behaviour and WM during development and ageing 17
1.6.2 Myelin plasticity may clarify the link between myelin and behaviour 19
1.6.3 Driver of behavioural change: myelin remodelling and conduction speed 22
1.6.4 Understanding the mechanisms underlying myelin plasticity will be essential to understanding its relevance for behaviour.....23
1.7. SCOPE OF THIS THESIS 25
1.7.1 Theme 1: Establish iPSC- derived myelinating co-cultures to model the axoglial relationship in vitro 26
1.7.2 Theme 2: Investigate the role of Nrg1-ErbB signalling in myelination 27
1.7.3 Theme 3: Replicating and extending evidence for role of de novo CNS myelination in motor learning 28

CHAPTER 2 | .....ESTABLISHING MYELINATION CO-CULTURES WITH IPSC-DERIVED SENSORY NEURONS TO STUDY PERIPHERAL MYELINATION..... 29

2.1. INTRODUCTION 29
2.1.1 Aim of the Chapter 31
2.2. MATERIALS AND METHODS 31
2.2.1 Ethics statement.....31
2.2.2 Induced pluripotent stem cell generation.....31
2.2.3 Induced pluripotent stem cell maintenance and differentiation 33
2.2.3.1 Neuronal differentiation..... 33
2.2.4 Schwann cell harvesting and culture.....34
2.2.5 Establishing the myelinating co-cultures.....35
2.2.6 Immunocytochemistry and confocal imaging 36
2.2.6.1 Quantification of myelination..... 36
2.2.7 Transmission electron microscopy.....38
2.2.8 Western blot.....39
2.2.9 Anti-disialosyl antibody treatment.....40
2.2.10 Statistics.....41

2.3. RESULTS 41
2.3.1 Alignment and myelination of human induced pluripotent stem cell-derived sensory neurons by rat Schwann cells 41
2.3.2 Node of Ranvier formation and maturation of the myelin sheath 44
2.3.3 Myelination increases over time 45
2.3.4 Anti-disialosyl antibodies impair myelination 45
2.3.5 A human anti-disialosyl IgM antibody induces demyelination 51
2.4. DISCUSSION 51

CHAPTER 3 | ..... THE ROLE OF NRG-ERBB SIGNALLING IN MYELINATION AND GLIA DYNAMICS 57

3.1. INTRODUCTION 57
3.1.1 Aim of this Chapter 59
3.2. MATERIALS AND METHODS 59
3.2.1 Establishing myelinating co-cultures 59
3.2.2 AAV transduction 60
3.2.3 Immunocytochemistry and confocal imaging of co-cultures 61
3.2.4 Pharmacological blockade of Nrg1- ErbB signalling 62
3.2.5 Animals 62
3.2.6 Tamoxifen treatment by oral gavage 63
3.2.7 Behaviour testing 63
3.2.7.1 Complex Running Wheel 63
3.2.7.2 Criteria for excluding animals from complex wheel data analysis 65
3.2.8 EdU supplementation in drinking water 65
3.2.9 Histological analysis of brain tissue 65
3.2.9.1 Perfusion of animals and tissue processing 65
3.2.9.2 Immunohistochemistry of free-floating brain sections 66
3.2.10 Statistics 67
3.3. RESULTS 67
3.3.1 Overexpression of Nrg1 type III influences levels of myelination 67
3.3.2 Pharmacological blockade of Nrg1-ErbB signalling leads to impaired myelination 69
3.3.3 Establishing co-cultures with rat OPC and human iPSC-derived sensory neurons – Pilot study 70
3.3.3.1 Oligodendrocytes did not remain stable over time in established co-culture conditions 73
3.3.3.2 Manipulating Nrg1-ErbB signalling in co-cultures with rat Oligodendroglia 73
3.3.4 Conditional knock out of Nrg1 affects performance on complex wheel running task. 78
3.3.5 The effect of wheel running and Nrg1 cKO on oligodendroglia dynamics 79
3.4. DISCUSSION 82

CHAPTER 4 | ..... REPLICATING AND EXTENDING BEHAVIOUR PHENOTYPE OF THE *MYRF*-CKO MODEL 89

4.1. INTRODUCTION 89
4.1.1 Aim of this Chapter 92
4.2. MATERIALS AND METHODS 93
4.2.1 Animals 93
4.2.1.1 Mouse breeding and Genetic background 93
4.2.1.2 Mouse Genotyping 94
4.2.1.3 Tamoxifen administration 94
4.2.2 Histological analysis of brain tissue 94
4.2.2.1 Perfusion of animals and tissue processing 94
4.2.2.2 Immunohistochemistry of free-floating brain sections 95

4.2.3 Behaviour Testing of mice 95
4.2.3.1 Complex Running Wheel 96
4.2.3.2 Passive infrared (PIR) activity monitoring 96
4.2.3.3 Accelerating Rotarod 97
4.2.3.4 Balance Beam 97
4.2.3.5 Criteria for excluding animals from complex wheel data analysis 98
4.2.4 Statistics 98
4.3. RESULTS 100
4.3.1 Preventing adult myelination by conditional deletion of myelin regulatory factor (Myrf) 100
4.3.2 Testing effects of conditional Myrf deletion on complex wheel running. 100
4.3.2.1 Testing for the effect of covariates on complex wheel running 102
4.3.2.2 Conditional knock-out (KO) of Myrf leads to reduced performance on complex wheel 104
4.3.2.3 Exploring variability in performance across animals 107
4.3.2.4 Quantifying running speed with finer time bins 109
4.3.2.5 Conditional KO of Myrf does not lead to a performance deficit on the Normal Running wheel 110
4.3.2.6 Performance of P-Myrf$^{(-/-)}$ animals on the CW was impaired within the first hours 110
4.3.2.7 P-Myrf$^{(-/-)}$ animals spent less time running the complex running wheel than P-Myrf$^{(-/+)}$ controls. 112
4.3.3 Investigating spontaneous locomotor activity of P-Myrf animals in the home cage using passive infrared (PIR) sensors 115
4.3.3.1 Assessing differences in spontaneous activity following CW running 115
4.3.3.2 Assessing differences in spontaneous activity prior to CW running 117
4.3.3.3 Potential confounds 119
4.3.4 No evidence for a general impairment in locomotor skills or coordination in P-Myrf$^{(-/-)}$ animals. 119
4.3.4.1 Accelerating rotarod assay revealed no differences between genotypes 121
4.3.4.2 Balance beam walking assay revealed no differences between genotypes 123
4.4. DISCUSSION 123

CHAPTER 5 | INVESTIGATING UNDERLYING BIOLOGICAL CHANGES IN WHITE MATTER OF *MYRF*-CKO MODEL 132

5.1. INTRODUCTION 132
5.1.1 Aim of this Chapter 135
5.2. MATERIALS AND METHODS 136
5.2.1 Animals and Behaviour testing 136
5.2.2 EdU treatment in separate cohort of animals 137
5.2.3 Perfusion and tissue preparation 137
5.2.4 Immunohistochemistry 137
5.2.5 MRI acquisition 138
5.2.6 MR processing and statistical analysis 138
5.3. RESULTS 141
5.3.1 Behavioural phenotype on the complex wheel of the sub-sample used for behavioural analysis 141
5.3.2 The effect of running and Myrf deletion on oligodendroglia dynamics in the anterior corpus callosum 143
5.3.2.1 Density of newly-differentiated OLs not affected by wheel running 143
5.3.2.2 OPC density and proliferation not affected by deletion of Myrf 145
5.3.3 Analysis of white matter integrity in Myrf-cKO model using MRI (Preliminary data) 146
5.3.3.1 Region of interest analysis in whole WM skeleton: Mean FA and MTR of the whole WM did not reveal an effect of wheel running or genotype 147
5.3.3.2 Voxel-wise analysis of fractional anisotropy (FA) and magnetic transfer ratio (MTR) in the white matter skeleton 147

5.3.3.3 Region of interest analysis in anterior corpus callosum: Mean FA and MTR in the anterior corpus callosum did not significantly correlate with histological measures..... 150
5.4. DISCUSSION.....152

CHAPTER 6 |GENERAL DISCUSSION.....160

6.1. SUMMARY OF THE KEY RESULTS 160
6.2. DISCUSSION AND FUTURE DIRECTIONS 162
6.2.1 Theme 1: Establish iPSC- derived myelinating co-cultures to model the axoglial relationship in vitro 162
6.2.2 Theme 2: Investigate the role of Nrg1-ErbB signalling in myelination 164
6.2.3 Theme 3: Replicating and extending evidence for role of de novo myelination in motor learning 166

BIBLIOGRAPHY.....169

SUPPLEMENTARY FIGURES.....189

TABLE OF FIGURES 195

MAIN FIGURES:.....195
SUPPLEMENTARY FIGURES:.....198
TABLES 198

LIST OF COMMON ABBREVIATIONS

Abbreviation	Explanation
APC	Adenomatous polyposis coli protein
CC1	Anti- Adenomatous polyposis coli protein (APC) Antibody, clone CC-1
CNS	Central Nervous system
DAPI	4′,6-diamidino-2-phenylindole
DTI	Diffusion Tensor Imaging
DWI	Diffusion Weighted Imaging
EdU	5-ethynyl-2'-deoxyuridine
EM	Electron Microscopy
ErbB	A family of proteins structurally related to the epidermal growth factor receptor.
MBP	Myelin Basic Protein
MRI	Magnetic Resonance Imaging
MTR	Magnetic Transfer Ratio
MYRF	Myelin regulatory Factor
NF200	Neurofilament Protein 200
NRG1	Neuregulin 1
OL	Oligodendrocyte
OPC	Oligodendrocyte Precursor Cell
PCR	Polymerase chain reaction
PDGF	Platelet-derived Growth Factor
PNS	Peripheral Nervous System
SC	Schwann cell

CHAPTER 1 | GENERAL INTRODUCTION

The acquisition of myelinating glia was a critical evolutionary advancement that enabled the development of increasingly complex nervous systems. Myelination was first understood to enable faster impulse propagation in axons more than 60 years ago (Huxley and Stampfli, 1949; Tasaki, 1939), yet it took a long time to recognise the mechanistic complexity of this cellular process and the diverse roles that myelination plays in the formation and functioning of the vertebrate nervous system (Nave and Werner, 2014).

1.1. STUDYING THE ROLE OF GLIAL CELLS IN THE NERVOUS SYSTEM

The nervous system conveys information using electrical impulses and neurons are highly specialized cells for rapid electrical transmission of signals. Research focusing on understanding the intricate functioning of the nervous system has long been focused on neuron-to-neuron communication. However, neurons in the nervous system are outnumbered (Verkhratsky and Butt, 2018) by a large and diverse group of highly specialized non-neuronal cells called glia, which for a long time have received relatively little attention. This was both a cause and a consequence of the poor understanding of what glial cells actually do.

Glial cells were first observed in close proximity with neurons by leading neuroscientists of the 19th century, including Rudolf Virchow, Santiago Ramón y Cajal and Pío del Río-Hortega (Chvátal and Verkhratsky, 2018). Lacking the methodological and theoretical means to investigate their role in the nervous system, glial cells were assumed to primarily function as “Nervenkitt”, the German word for nerve glue. These initial speculations eventually lead to their collective name “glia”, the ancient Greek word for glue.

While the name remains, our understanding of the functional role of glia has vastly expanded and continues to evolve. Indeed, glial cells seem to play a vital role in almost all aspects of nervous system function, ranging from development, maintenance, plasticity, recovery after injury and a range of pathological conditions. Over recent decades a renewed interest in glial cells, together with rapid technological advances, continues to provide unexpected insights into the roles of glial cells. Not merely supporting cells, glia are now thought to actively shape and influence information processing, participate in complex cognitive processes such a learning and memory, and may play central roles in common nervous system pathologies. Hence it has become ever more apparent that any advanced understanding of the nervous system, of its development, functioning and health, needs to consider and include the diverse contributions of glia.

1.2. MYELIN AND MYELINATING GLIA OF THE MAMMALIAN NERVOUS SYSTEM

A unique specialization of glia in vertebrates is the deposition of a subcellular structure called myelin. Myelin is the spiral extension of the glial plasma membrane arranged as multi-layered sheaths wrapping around an axon (Fig. 1.1). Each myelin sheath consists of multiple layers of membrane, numbering up to >150 in one sheath, which are eventually compacted to tightly wrapped spiral rings by a range of myelin specific proteins, such as myelin basic protein (MBP). These wraps of specialized cell membrane are contained in long segments of glial cytoplasm called internodes that surround axons (Figure 1.1). At the lateral ends of these myelin internodes, glia form a complex seal with the axon, which aid the formation of Nodes of Ranvier, gaps of unmyelinated ion-channel rich axonal membrane that are located between two internodes. Myelin internodes retain uncompacted cytosolic compartments, such as the innermost (adaxonal) and outermost (abaxonal) layers, which are radially connected to further cytosolic compartments that are predominately active during myelin sheath formation but remain open in mature internodes (Nave and Werner, 2014).

The evolution of vertebrate myelination first emerged in Paleozoic vertebrate fish around 500 million years ago (Zalc et al., 2008) and represented a fundamental evolutionary step for the development for the nervous system. Indeed, myelin and myelin-like structures are thought to have arisen independently at least three times in evolutionary history and can also be found in some families of invertebrate, where it is partly of axonal origin (Knowles, 2017).

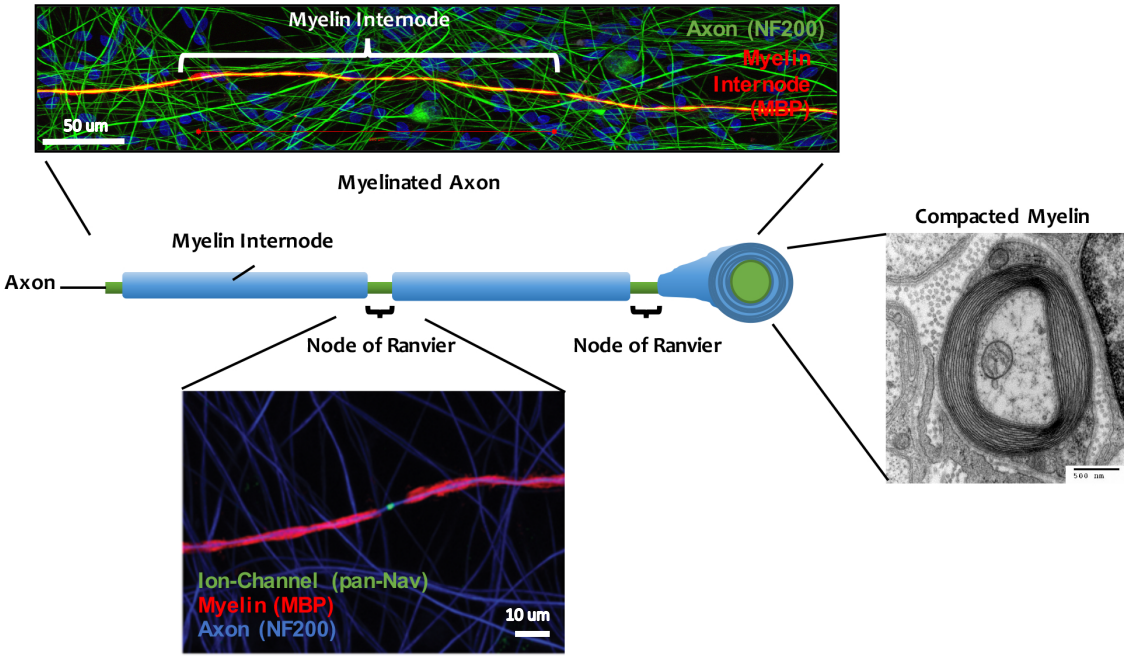


*Figure 1.1. **Myelin and the node of Ranvier**.*

Myelinating glia wrap long segments of axons with multi-layered sheaths of specialized membrane, which is compacted to form the complex intracellular structure we call myelin. Nodes of Ranvier, specialized axon-glia structures which contain a high density of axonal ion-channels necessary for the propagation of an action potential, form on the unmyelinated spaces between two myelin internodes. Myelin Internodes and Nodes of Ranvier increase the speed of delivery of impulses from one neuron to another, and changes in size or function can alter the timing at which information arrives at its destination.

1.2.1 MYELINATING GLIA

In mammals and most other vertebrates myelin is formed by two distinct types of myelinating glia. Schwann cells (SC) myelinate a subset of axons in the peripheral nervous system (PNS) and originate from neural crest cells (Monk et al., 2015) (Figure 1.2). Oligodendrocytes (OL) are the myelinating glia in the central nervous system (CNS) and derived from oligodendrocyte precursor cells (OPC)

that originate from neuroepithelial precursors (Bergles and Richardson, 2016) (Figure 1.3). Despite their different cellular origins, these two types of myelinating glia have several features in common, notably the morphology of the myelin internodes they form in the CNS and PNS. However, the molecular composition of myelin and the gene expression programme regulating myelination differ between the two cell types, although they share some similarities. The most striking difference between the two cell types is the overall morphology of their cell body, as SC interact and myelinate only with a single axon, while oligodendrocytes can form multiple myelin internodes on multiple axons. The similar-appearing structure and function of peripheral and central myelin are, thus, striking examples of convergent cellular evolution (Nave and Werner, 2014).

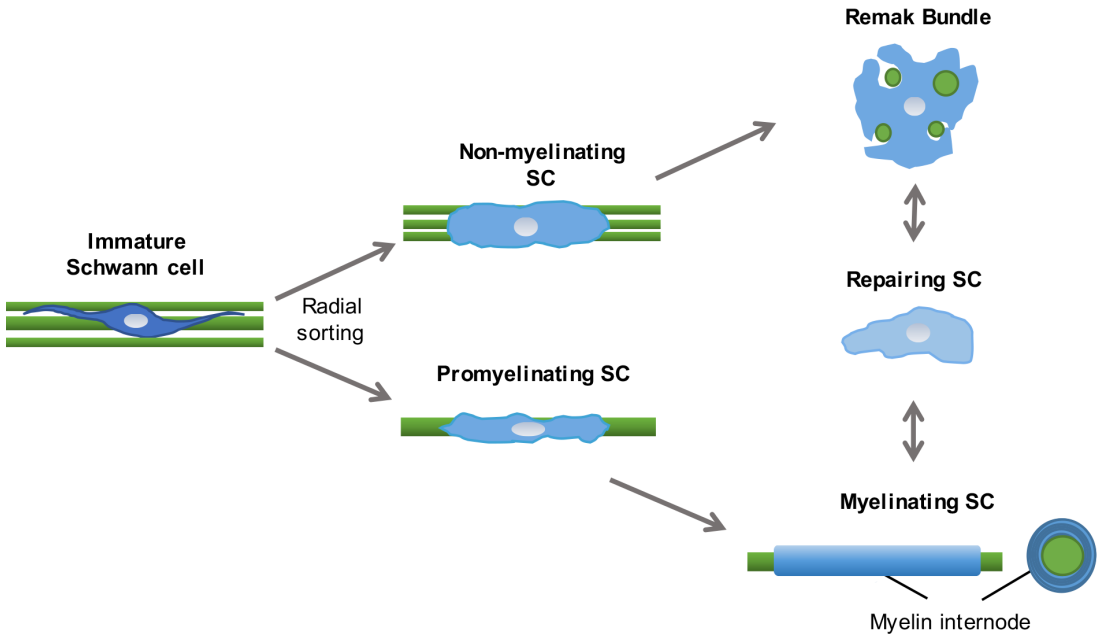


Figure 1.2. ***Development of Myelinating and Non-myelinating Schwann Cells in the PNS.***

Schematic illustration of Schwann cell (SC) (blue) in its developmental stages. Immature SCs are migrating along developing axons (green). Immature SCs can either stay associated with multiple axons, or associate exclusively with a single axon in a process called radial sorting. SCs associated with a single axon proceed into a promyelinating stage, activating the required transcriptional networks to eventually form a single mature myelin internode by wrapping and compacting a specialised glia membrane to a complex intracellular structure (show longitudinally and cross-sectionally). SCs associated with multiple axons eventually ensheath and bundle several axons in a structure called a Remak Bundle (depicted cross-sectionally). In pathological conditions such as nerve injury, SC of both phenotypes can change their differentiation state into a repairing SC. In this unique state, SC actively contribute to nerve repair and PNS regeneration by proliferating and forming long columns called band of Büngner to guide and support axonal growth. Repairing SC subsequentially re-differentiate into myelinating and non-myelinating SCs .

Immature Schwann cells migrate along axons in the PNS. Myelination of Schwann cells starts with a process of “radial sorting”, which describes a process in which immature Schwann cell’s cytoplastic processes extends into an axon bundle to “select” a single axon segment (Figure 1.2). Pro-myelinating Schwann cells that have radially sorted and wrapped around a single axon will activate a complex transcriptional programme. This transcriptional regulation is driven by factors including Sox10 and Oct6 and will eventually lead to expression of Krox20, the transcriptional master regulator essential for the expression of myelin genes (Herbert and Monk, 2017).

Myelinating oligodendrocytes are the most numerous glia cell in the adult CNS and differentiate from oligodendrocyte precursor cells (OPC), a proliferative and migratory cell population in the CNS (Figure 1.3). OPCs extend and retract numerous cytoplasmic processes, surveying their environment. OPCs establish initial contact with axons and can, providing the right intrinsic and/or external factors are given, start differentiating into a pre-myelinating oligodendrocyte. In this transitional cellular stage cytoplasmic processes make contact with several axons that can either

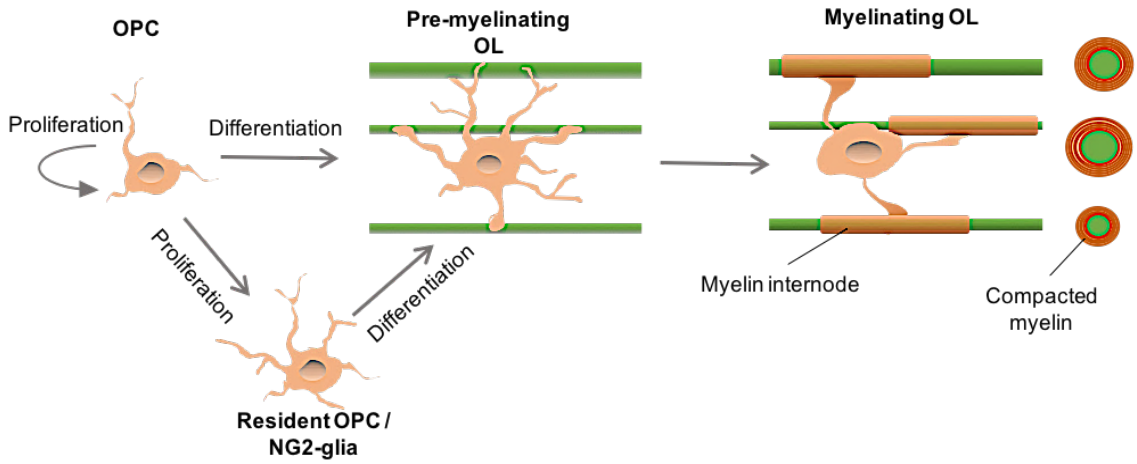


Figure 1.3. ***Development of Oligodendroglia in the CNS.***

Oligodendrocyte progenitor cells (OPCs), which form the majority of mitotic cells in the adult brain, can proliferate multiple times before differentiating into premyelinating oligodendrocytes, which eventually mature into myelinating oligodendrocytes. Mature oligodendrocytes can form myelin segments on multiple axons simultaneously. If and how each initial axon-glia contact matures to into myelin internodes can depend on a combination of a wide range of factors, including intrinsic and extracellular signalling, cellular identity and neural activity.

retract or develop into a myelin sheath. Some aspects of the transcriptional regulation of oligodendrogenesis are shared with Schwann cell development, such as Sox10 and Yy1, while others, such as Olig1 and Olig2 are specific to oligodendrocyte myelination (Sock and Wegner, 2019). The transcription factor Myelin Regulatory Factor (*Myrf*) is a key factor for the initiation of myelination, analogous to the role that Krox20 plays in Schwann cells (Herbert and Monk, 2017; Simons and Nave, 2016).

1.3. THE FUNCTIONAL ROLE OF MYELINATING GLIA IN THE NERVOUS SYSTEM

1.3.1 INCREASE SPEED OF ACTION POTENTIAL PROPAGATION

The key function of myelination is the ability to increase conduction velocity along axons. Myelin does that by insulating the axonal membrane, reducing the ability of current to leak out of an axon and thus increasing the distance a local electrical current can flow passively. In myelinated axons the active and time-consuming part of action potential generation, orchestrated by voltage-gated ion channels regulating the current flow across the membrane, is limited to the Nodes of Ranvier. The resulting action potential propagation has been termed “saltatory”, as electrical current passively “jumps” from one Node to the next (Huxley and Stampfli, 1949; Ranvier and Weber, 1878; Seidl, 2014; Tasaki, 1952, 1939). This remarkably sophisticated axon-glia interaction can accelerate nerve conduction 20-100-fold, compared to non-myelinated axons of the same diameter and temperature.

The conduction speed of a myelinated axon is determined by several aspects of the axon-glia geometry. The most important factors are the diameter of the axons and the thickness of their associated myelin sheets; a relationship usually quantified as the g-ratio, which is estimated by calculating the fraction of the inner diameter over the outer diameter of the myelin sheath (Rushton, 1951; Waxman, 1975). The optimal g-ratio for a maximum improvement in conduction velocity is around 0.6 (Chomiak and Hu, 2009). The length of the internode, or the space between two nodes of Ranvier is another factor influencing conduction velocity with mature myelin

internodes reaching a length of up to 1.5mm (Friede, 2017; Friede et al., 1981). It is of note that the passive current in a myelinated axon is usually sufficient to skip a node, which is likely to provide a safety mechanism ensuring consistent nerve conduction. Another important factor is the morphology of the nodes of Ranvier, which can vary considerably in the CNS (Arancibia-Cárcamo et al., 2017).

Increasing the speed at which information can flow through an organism became an evolutionary advantage with the emergence of complex multicellular organisms. Once nervous systems had evolved, two main strategies for increasing conduction velocity developed: (i) enlargement of axon calibres, with the giant squid axon as a prominent example and (ii) myelination (Castelfranco and Hartline, 2016; Xu and Terakawa, 2013). A key advantage of myelination is that it leads to increased impulse propagation without the need for exponential axonal enlargement, providing improved yet spatially efficient nerve conduction. For comparison, an unmyelinated squid axon requires a diameter of about 500 µm to conduct at a speed of 25 m/sec, whereas a mammalian myelinated axon with a diameter of a only a few µm can conduct with a similar velocity while requiring 5000 times less energy (Murdoch 1982; Snaidero and Simons 2014). Hence, myelination was an essential evolutionary step for the development of fast operating, complex, yet spatially compact nervous systems, including the ones that are now pondering their own remarkable complexity.

1.3.2 SUPPORT OF AXONAL INTEGRITY AND METABOLISM

The role of myelinating glia in the nervous system is more diverse than just the regulation of conduction speed. Indeed, Schwann cells and oligodendroglia play an important role in maintaining neuronal health and fuelling axonal energy demand (Nave, 2010a; Simons and Nave, 2016). Glial cells that engulf axons without myelinating them are a feature of almost all nervous systems and even unmyelinated axons in the PNS are still contained in Remake bundles (Figure 1.2). While physical separation of electrically active axons may limit cross talk, perturbation of Remak bundles in mice causes progressive degeneration of the associated axons (Chen et al., 2003; Haney et al.,

1999), indicated a role of ensheathing glia cells in axonal health. Indeed, cells of the myelinating cell lineage release a range factors promoting axonal survival and integrity (Keswani et al., 2004; Simon et al., 2010), cellular signalling that seems especially important during development in which loss of Schwann cells leads to secondary loss of motor neurons and most dorsal-root ganglia neurons, resulting in perinatal death in mice (Riethmacher et al., 1997). Genetic and acquired conditions that affect myelinating glia often lead to secondary axonal damage during adolescence and adulthood, further indicating the dependence of neurons on glia support (Fehmi et al., 2018; Nave, 2010b; Stassart et al., 2018).

The reasons for such a cellular dependence become apparent when considering the enormous dimensions of long-range projecting neurons in the PNS and CNS. The axon of a cortical neuron with a dimeter of ~1 µm can project ~100 cm into the corticospinal tract. Klaus Nave compares these dimensions as analogous to a 4 m wide subway tunnel with a length of 4000 km (Nave, 2010a). This enormous size provides large logistical and metabolic challenges for the cellular machinery to maintain the essential and demanding cellular functions that ensure precise action potential generation. While myelin provides no significant overall net benefit in terms of energy consumption for the organism after considering the cost of developing and maintaining myelination (Harris and Attwell, 2012), it significantly reduces the metabolic cost of neuronal activity. However, myelin also provides a significant barrier for the diffusion of essential metabolites. Solving a problem they partially create, recent studies have highlighted that oligodendrocytes provide active metabolic support in the form of lactate and pyruvate, transported in open cytosolic channels of the myelin sheath, a process that may partly be linked to neuronal activity (Saab and Nave, 2017). Growing evidence also suggests that Schwann cells may play a critical role in peripheral nerve metabolism (Jha and Morrison, 2018). Myelinating glia also contribute to the ion and water homeostasis of nerves and the brain, as emphasised by congenital disorders affecting such relevant cellular functions (Min and Knaap, 2018).

1.4. THE DEVELOPMENT AND DYNAMICS OF MYELINATING GLIA

Discovering glia's wider roles in maintaining neuronal integrity and homeostasis emphasises the importance of the intimate axon-glia relationship for a functional nervous system. Historically, myelinating glia were believed to be ensheathing insulators that remained static and quiescent after nervous system development. Yet their functional importance goes beyond providing static support, as myelinating glial cell populations are and remain surprisingly dynamic and plastic even in the adult nervous system. These glia dynamics differ significantly between the PNS and CNS and the function of dynamic changes in the oligodendroglia population are just beginning to be revealed.

1.4.1 DEVELOPMENT AND DYNAMICS OF PNS MYELINATION: SCHWANN CELLS

During early embryonic development, nerves in the PNS are a dynamic structure consisting of tightly packed axons and flatted Schwann cell precursor processes without a basal lamina, extracellular matrix or extracellular space. Schwann cell precursor cells are a pluripotent cell population that can differentiate into a variety of cell types, including melanocytes, fibroblasts and parasympathetic neurons. Yet, the phenotype of early nerves changes radically when this precursor population starts to differentiate into immature Schwann cells at around E14 in mice. A collagen rich extracellular space appears, blood vessels and fibroblasts are appearing, and Schwann cell start forming a basal lamina. At E16 in mice, separate axon Schwann cell bundles have formed which are embedded in collagen rich extracellular matrix containing blood vessels. Additionally, an early perineurium, a sheath of connective tissue surrounding a bundle of nerve fibres, has been formed at this stage. There is little evidence for the existence of a resident Schwann cell precursor population beyond this developmental time point. Shortly after this development radial sorting is initiated. Proliferation and apoptosis within the Schwann cell population control glia numbers to acquire the right numbers needed by the axons present. Myelination in the PNS is initiated around birth and continues rapidly during early post-natal development (Jessen et al., 2015; Jessen and Mirsky, 2019; Salzer and Zalc, 2016).

Once developed and matured, the peripheral nervous system forms a remarkably stable structure. Highly-specialized fibroblast-like cells tightly associate to form protective cellular barriers around nerve fascicles that contain axons and Schwann cells tightly embedded in vascularized extra cellular matrix. Myelinating glia are the most abundant cell type within peripheral nerve trunks, followed by non-myelinating Schwann cells in a 2:1 ratio. Schwann cells in the developed PNS are remarkably quiescent and myelinating Schwann cells, once matured, seem to remain for a lifetime. Labelling the cell population for their proliferative potential has only revealed very occasional replacement of Schwann cells (Stierli et al., 2018). The stability of PNS, consisting of motor, sensory and autonomic nerves, may be due to their main function; building a reliable and stable connection between the tissues and organs and the CNS.

However, Schwann cells retain an immense capacity for dynamic and adaptive changes in case of nerve insult and injury. Indeed, the dynamic response within the Schwann cell population is considered one of the main reasons why peripheral nerves are able to efficiently regenerate after injury, in contrast to the CNS (Jessen and Mirsky, 2016). Remarkably, mature, established and quiescent Schwann cells can “reprogram” and “de-differentiate” into a progenitor-like state within days of the injury (Stierli et al., 2018). In this progenitor-like state so-called “repairing” or “Bunge” Schwann cells proliferate *en masse* and orchestrate the response to nerve injury (Figure 1.2). This successful injury response is not even hindered by the genetic ablation of over 70% of the Schwann cells at this stage, emphasising their remarkable adaptive capacity (Gerber et al., 2019). The function of repairing Schwann cells is diverse, and includes the coordination of other cells by secretion of a range of different factors, the clearing of debris and the formation of a bridge between the two nerve ends to aid axonal regrowth (Jessen and Mirsky, 2016). Once axons have regenerated, reciprocal interaction with axons leads to the re-differentiation of Schwann cells, which adopt either the myelinated or non-myelinated phenotype. While regenerated nerves contain overall higher cell populations, increased axonal sprouting and denser extracellular matrix, proportions of cellular

population and cellular dynamics return to the homeostatic state acquired before injury (Stierli et al., 2019).

1.4.2 Development and dynamics of CNS Myelination: Oligodendroglia

The emergence of oligodendroglia starts with the birthing of oligodendrocyte precursor cells (OPCs) during embryonic development, occurring in three distinct waves in time and space (Michalski and Kothary, 2015). Starting at around embryonic day 12, migrating OPCs originate from the ventral ventricular zone, followed by a second smaller wave originating from the dorsal ventricular zone about two days later. A third wave of OPC differentiation occurs postnatally (Michalski and Kothary, 2015; Richardson et al., 2006; Sevc et al., 2014). Interestingly, cells from these three temporal migrations compete with each other for space and display compensatory redundancy, meaning that ablation of a single wave is compensated for by the others without interfering with CNS development (Kessaris et al., 2006). Myelination starts shortly before birth and advances rapidly in early postnatal development. The large part of myelination in CNS happens during early postnatal development, yet OPC differentiation and myelination continues way into adulthood, though seems to slow down with age (Barkovich et al., 1988; Bartzokis et al., 2010; Deoni et al., 2011; Hill et al., 2018; Young et al., 2013). The spatiotemporal sequence of myelination in the CNS is complex and seems to follow a stereotypical order, extending roughly from deep to superficial brain regions in a posterior to anterior pattern in the human brain (Barkovich et al., 1988; Kinney et al., 1988; Paus et al., 2001).

In contrast to the PNS, the myelinating glia population in the CNS never seems to enter a quiescent phase, but continues to be plastic and dynamic throughout life, although these dynamics seem to change gradually over time (Hill et al., 2018; Young et al., 2013). In contrast to Schwann cell precursor cells that seem to fade in early PNS development, OPCs remain resident in the CNS and form the largest progenitor population in the developed brain (Figure 1.3). Interestingly, OPCs enter a controlled state of equilibrium in the grey and white matter of the adult CNS, each occupying its

unique pocket of space established through mutually repulsive cues and maintained by proliferation, migration and controlled cell death (Hughes et al., 2013). This resident population of OPCs represents about 5-10% of the total cell population in the developing and adult CNS and remains the major source for the generation and maintenance of myelinating oligodendrocytes under physiological and pathological conditions (Dawson et al., 2003; Dimou and Gallo, 2015). The population of resident OPCs is often referred to as NG2 glia and beginning to be considered as a unique class of glia cells to emphasise their potential function beyond being a progenitor cell for oligodendrocytes. Indeed, the abundance of resident OPCs, their expression of voltage-gate sodium channels and glutamate receptors, as well as the discovery of synapse formation between NG2-glia and neurons lead to increased interested into their functional role in the nervous system (Chorghay et al., 2018; de Faria et al., 2018). Finally, converging evidence suggests that oligodendroglia in the CNS are more heterogeneous than previously thought (Bechler et al., 2015; Marques et al., 2016; Tomassy et al., 2014; Zonouzi et al., 2019), with potential variations of their intrinsic myelination capacity, morphological phenotype, their intrinsic proliferation and differentiation potential and their expression of ion-channels and cell surface receptors (Dimou and Simons, 2017; Spitzer et al., 2019). The functional importance of this heterogeneity and cellular features like spatiotemporal variation in ion-channel expression remain relatively unclear but imply a complexity in their functional roles not previously appreciated.

OPCs continue to proliferate and differentiate into myelinating oligodendrocytes throughout adulthood (Hill et al., 2018; Young et al., 2013). Compared to the PNS, the CNS is much less capable of efficient regeneration after injury despite the abundance of such a resident progenitor population of myelinating glia, suggesting that nerve repair and injury response may not be their primary purpose. Understanding the glia dynamics and their functional role in the CNS has been challenging and limited by the lack of methods to study myelination over time in sufficient resolution. However, recent evidence using longitudinal *in vivo* two photon imaging in mice has provided remarkable

insides into life-long OPC proliferation and differentiation in the sensory cortex of mice (Hill et al., 2018; Hughes et al., 2018). In mice, about half of the myelinating oligodendrocytes were formed after 4 months, which is considered the time taken for a mouse to reach adulthood. While OPC proliferation and myelination were slowly changing the myelin landscape, the observed OPC differentiation into myelinating glia was surprisingly inefficient, with over half of differentiating cells dying before maturation. Yet, once developed, newly formed myelinating oligodendrocytes were remarkably stable over time (Tripathi et al., 2017). Additionally, such studies revealed that the dynamics of myelinating glia can be influenced by changes in the sensory experience of mice, with an increase in myelinating glia integrating into the neural circuit due to increased sensory stimulation.

Ground-breaking studies like these are part of a refreshed interest in myelin and myelination as a potential mechanism of lifelong brain plasticity. Indeed, over recent years converging evidence has indicated that myelin in the CNS can be dynamically regulated by neuronal activity and experience (Chang et al., 2016; Fields, 2015; Purger et al., 2016; Sampaio-Baptista and Johansen-Berg, 2017). Although this phenomenon has been recognised in cell culture studies for some time (Demerens et al., 1996; Stevens et al., 1998), its demonstration *in vivo*, and its potential contribution to behaviour change and learning, has been suggested only recently (McKenzie *et al.* 2014; Xiao *et al.* 2016). Indeed, converging evidence from a number of different experimental approaches, including neuroimaging studies in humans (Scholz *et al.* 2009; Caeyenberghs *et al.* 2016; Lakhani *et al.* 2016) and rodents (Sampaio-Baptista *et al.* 2013), genetically modified mice (McKenzie *et al.* 2014) as well as manipulation of neural activity in both rodents and zebrafish (Gibson *et al.* 2014; Hines *et al.* 2015; Mensch *et al.* 2015; Mitew *et al.* 2018), indicate that myelin dynamics and plasticity may be an additional route by which experience can shape brain structure and function.

1.5. AXON-GLIA SIGNALLING SHAPING THE MYELIN LANDSCAPE

Myelination in the nervous system requires close and dynamic interactions between myelinated axons and their associated myelinating cells. A good example is the formation of the complex nodal structure, which is an intricate process that depends on a range of reciprocal axon-glia communication (Fehmi *et al.* 2018). Investigating the complex cellular interactions regulating the formation and maintenance of the myelinated axon structure is critical for understanding the many pathological conditions that can affect myelin in the PNS and CNS. Interestingly, the intra- and extra-cellular signalling pathways regulating myelination can differ significantly between the PNS and CNS, which may partially explain why congenital or acquired myelin pathologies almost exclusively effect either CNS myelin or the PNS myelin, but not both (Nave and Werner 2014).

Substantial progress has been made in understanding the factors regulating PNS myelination. The best understood and most important extrinsic signals are either axonal derived, such as neuregulin 1 Type III (TIIINRG1), or part of the extracellular matrix, such as laminin and collages and their respective receptors (Salzer 2015). Another important factor required for PNS myelination is the G-protein coupled receptor Gpr126, essential for the regulation of intracellular cAMP levels in Schwann cells. The tight axo-glia signalling leads to a stereotypical formation of PNS myelination, so that axons with a diameter of 1 μm or above are fully myelinated along their length whereas smaller axons do not receive any myelination. Furthermore, there is a tight correlation between axon dimeter and myelin sheath thickness in order to optimise conduction velocity in these larger calibre axons (Salzer 2015). Nrg1-erbB signalling has been identified as the key regulator driving this stereotypical PNS myelination profile (Mei and Nave 2014).

While the factors driving PNS myelination have been identified, we are only beginning to comprehend the complex factors driving myelination in the CNS. In contrast to the PNS, myelination of oligodendrocytes does not seem to follow a relatively simple guidance like myelinating axons of a certain size and does not seem to be an “all-or-nothing” phenomenon either. While axonal

morphology can still influence myelin sheath thickness, CNS axons with a diameter as small as 0.2 µm can be myelinated and there is a large overlap in axon calibre between myelinated and unmyelinated axons (Hildebrand *et al.* 1993). Furthermore, axons in the CNS exhibit a wide variation the length and thickness of myelin sheaths and distribution pattern of the myelin sheaths along their length (Williamson and Lyons 2018). Additionally, the density of myelination differs between different regions and its influence by axonal and oligodendroglia identity, with different oligodendroglia preferring different cellular targets and different sub-classes of neurons presenting different profiles of myelination (Tomassy *et al.* 2014; Bechler *et al.,* 2015; Zonouzi *et al.* 2019). How such a complex landscape of myelination develops is relatively unclear, and the signals that regulate it are just beginning to be identified.

Other glia cells in the CNS, such as astrocyte and microglia, can affect myelination by influencing oligodendroglia dynamics during development and after injury (Kıray *et al.* 2016; Dutta *et al.* 2018; Fields and Dutta 2019). Indeed, the fact that several congenital leukodystrophies affect astrocyte and microglia associated genes hints at a complex cellular interdependence ensuring the appropriate development, maintenance and dynamics of myelination (Nave and Werner 2014). Additionally, a range of repulsive and inhibitory signals, such as Eph-ephrin molecules, are also likely to play an important role in CNS myelination, as cellular structures such as dendrites are not myelinated (Almeida 2018).

Interestingly, electrical activity of axons has emerged as a key regulator of myelination, influencing oligodendroglia dynamics in developing zebrafish as well as in developing and adult mice (Czopka 2016; de Faria *et al.* 2018; Mitew *et al.* 2018; Korrell *et al.* 2019). Blocking synaptic transmission can impair myelination and remyelination *in vivo* (Wake *et al.,* 2011; Hines *et al.* 2015; Mensch *et al.* 2015; Korrell *et al.* 2019). However, myelination can also occur in the absence of neuronal activity and vesicular release of glutamate (Bechler, Byrne and ffrench-Constant 2015; Etxeberria *et al.* 2016). Furthermore, oligodendrocytes can myelinate axon like structures in the absence of any

neuron derived signals (Bechler *et al*., 2015), while being clearly sensitive to axonal derived signals in different experimental paradigms (Gibson *et al.* 2014; de Faria *et al.* 2018; Mitew *et al.* 2018), which suggest that no extrinsic signals are essential for CNS myelination.

An emerging explanation for such contradicting results is the existence of two distinct modes of myelination: an intrinsic mode requiring only an axon-shaped substrate, and an adaptive mode of myelination in which oligodendroglia become sensitive to external signals that can subsequently modulate the process (Bechler *et al.,* 2018). According to this theory the two modes act as a sequential mechanism regulating myelination during CNS development. While myelination is initially driven by the intrinsic mode by default, oligodendroglia can be switched into an adaptive and faster mode of myelination to become sensitive to neuronal activity. The apparent co-existence of these different modes of myelination has been demonstrated in the developing nervous system of zebrafish (Koudelka *et al.* 2016). Evidence for a switch between the two modes has been provided by *in vitro* studies, indicating that growth factors such as brain derived neurotrophic factor (BDNF) or neuregulin 1 (NGR1) can regulate glutamate receptor expression in OPCs and their subsequent sensitivity to neuronal activity (Lundgaard *et al.* 2013). That means that axonal derived signals, for example activity-dependent vesicular release of growth factors, could modulate the sensitivity of oligodendroglia to glutamate, while the response of oligodendroglia could depend on age and phenotype specific expression of relevant receptors (Bechler *et al.*, 2018; de Faria *et al.* 2019; Spitzer *et al.* 2019).

Such intricate control of myelination would be similar to the development of many neuronal circuits in CNS, which start with dynamic scaffold that is optimised by neuronal activity (Dan and Poo 2006; Turrigiano 2011). However, it is becoming increasingly obvious that the mechanisms regulating the development and dynamics of myelination are complex and still poorly understood and it is unclear how and why they eventually lead to the complex and adaptable myelin landscape found in the CNS.

1.6. MYELIN DYNAMICS IN THE CNS AND BEHAVIOUR

The emerging complexity of oligodendroglia dynamics and myelin plasticity in the CNS naturally leads to the question of their functional role in the CNS and if and how they contribute to complex behaviour like learning. Our current understanding of brain plasticity is mainly centred around the concept of synaptic plasticity, which is supported by widely acknowledged theoretical frameworks, decades of experimental work and neural modelling (Kreutz and Sala 2012). In contrast, evidence for the plasticity of myelin has only started to converge in recent years and consequently its functional significance and underlying mechanisms remain poorly defined. Hence, it is still not clear if and how experience leads to dynamic and specific changes in myelination that may drive behavioural change (Figure 1.4).

1.6.1 ASSOCIATION BETWEEN BEHAVIOUR AND WM DURING DEVELOPMENT AND AGEING

White matter (WM) gets its colour from the abundance of myelinated axons in the connective tracts of the CNS, which make up about half of the brain volume in an adult human. Correlated changes in WM and cognitive functions over the human lifespan offer a link between myelin and cognitive and sensorimotor development. For instance, maturation of sensorimotor or language-related tracts are associated with the development of these basic skills in childhood (Nagy *et al.* 2004; Fields 2008; Simmonds *et al.* 2014), whereas maturation of fronto-parietal (Nagy *et al.* 2004; Mabbott *et al.* 2006; Peters *et al.* 2014; Bells *et al.* 2019) and fronto-striatal (Liston *et al.* 2011; Bos *et al.* 2015; Darki and Klingberg 2015) WM pathways correlates with protracted development of executive functions and behavioural control during adolescence and early adulthood. At the other end of the lifespan, ageing is accompanied by axon and myelin deformation and degeneration even in the absence of specific pathological conditions, as indicated by post-mortem histological studies (Peters 2002; Marner *et al.* 2003). Mirroring the observed loss of myelinated fibres, changes in WM diffusion metrics are reliably associated with ageing (Cox *et al.* 2016). Interestingly, ageing seems to predominantly affect a network of higher-

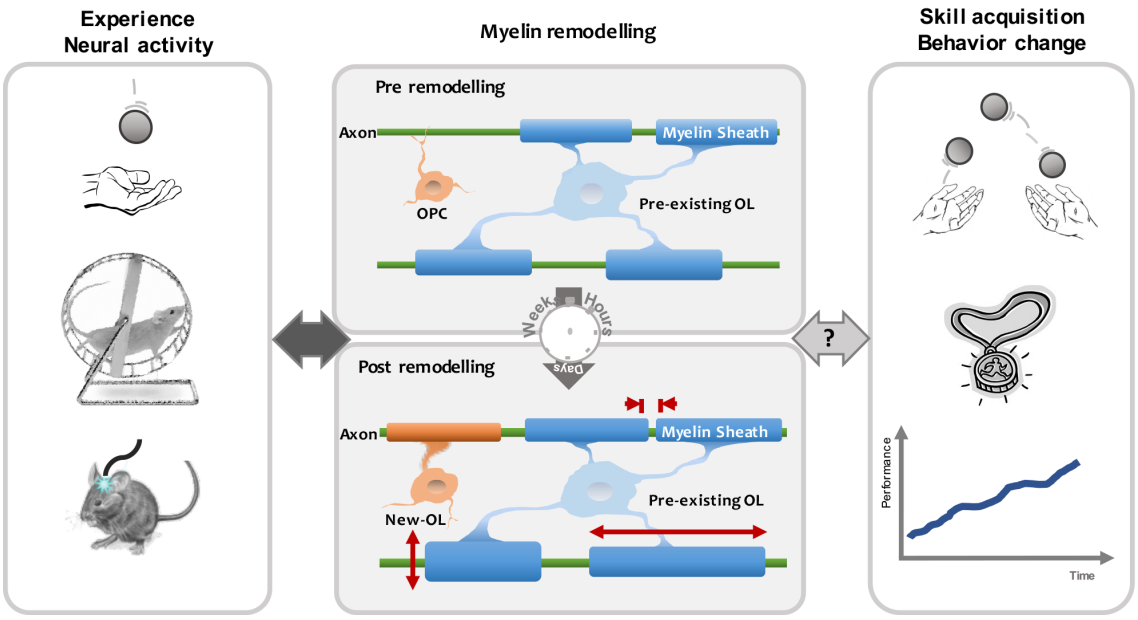


*Figure 1.4. **Myelination can be dynamically remodelled by neural activity and experience even during adulthood, yet its role in learning remains elusive.***

Experiences such as learning to juggle (Scholz et al. 2009) or playing a computer game (Hofstetter et al. 2013) are associated with structural changes in white matter pathways in humans, while learning a motor skill can lead to changes in myelination in rodents (Sampaio-Baptista et al. 2013). Indeed, neural activity can regulate changes in myelin- forming cells within an active circuit, as demonstrated by in vivo optogenetic techniques in awake, behaving mice (Gibson et al. 2014). Such myelin plasticity may occur through many different routes (see Figure 1.5). While changes in myelination have mainly been investigated after days or weeks, recent evidence suggests an active requirement of New-OL within the first hours of skill acquisition (Xiao et al. 2016). However, if and to what extent adaptive changes in myelination can facilitate behavioural change and skill acquisition remains poorly understood. Learning more about the underlying biological mechanism, such as the speed at which experience can be translated into adaptive changes in myelination, will be critical to understand the role that myelin plasticity plays in the nervous system.

order brain regions that myelinate relatively late during adolescence and seem especially vulnerable to disorders during early and late development (Douaud *et al.* 2014). Accumulating evidence indicates that such age-related decline in cerebral WM integrity may contribute to cognitive deficits associated with ageing (Bennett and Madden 2014), although this relationship remains a subject of debate. However, while developmental and age-related WM changes indicate an important association between myelin and healthy brain function, such associations are hindered by a wide range of concomitant lifespan-related biological changes and can provide little mechanistic insight into whether or how myelin can shape behaviour.

1.6.2 MYELIN PLASTICITY MAY CLARIFY THE LINK BETWEEN MYELIN AND BEHAVIOUR

While brain plasticity has mainly been studied in the context of activity-dependent changes at the synapse, converging evidence from animal and human studies now indicates that similar mechanisms can also regulate myelination. This previously overlooked phenomenon, termed myelin plasticity, may provide a complementary route through which experience shapes the brain (Fields 2015). Indeed, in healthy adults, evidence for a link between changes in WM structure and skill learning in humans is accumulating (Scholz *et al.* 2009; Taubert *et al.* 2010; Hofstetter *et al.* 2013). Using myelin-sensitive imaging methods (Alonso-Ortiz *et al.* 2015; Groeschel *et al.* 2016; Heath *et al.* 2018), a recent study found experience-dependent changes in myelin that were associated with changes in skilled movements in healthy young adults (Lakhani *et al.* 2016). However, in most studies, concurrent changes in other WM cells as well as in grey matter make it challenging to infer the functional relevance of myelin plasticity for any associated behavioural change. Allowing the possibility for more direct experimental interventions, rodent studies can provide important insights into the link between changes in myelin and behaviour (Blumenfeld-Katzir *et al.* 2011; Sampaio-Baptista *et al.* 2013; Gibson *et al.* 2014; McKenzie *et al.* 2014), although potential differences in oligodendroglia dynamics between humans and other animals have to be considered (Young *et al.* 2013; Yeung *et al.* 2014). Conditional knock-out of the gene encoding the transcription factor *Myrf* (Myelin Regulatory Factor) in adult mice has provided the only evidence for a direct causal link between experience-dependent myelin plasticity and skill acquisition (McKenzie *et al.* 2014; Xiao *et al.* 2016). By preventing the maturation of newly generated OLs in adult mice (Figure 1.5A&B), this knock-out seems to interfere with the mice's ability to master running on a complex wheel with irregularly spaced rungs (McKenzie *et al.* 2014; Xiao *et al.* 2016). If the mice had been exposed to the complex wheels prior to the genetic manipulation, their performance was unimpaired, suggesting that newly forming OLs play a specific role in acquisition of a novel skill. However, it remains to be determined whether these findings translate to other forms of learning and precisely which aspects of the behaviour are impaired. Using a

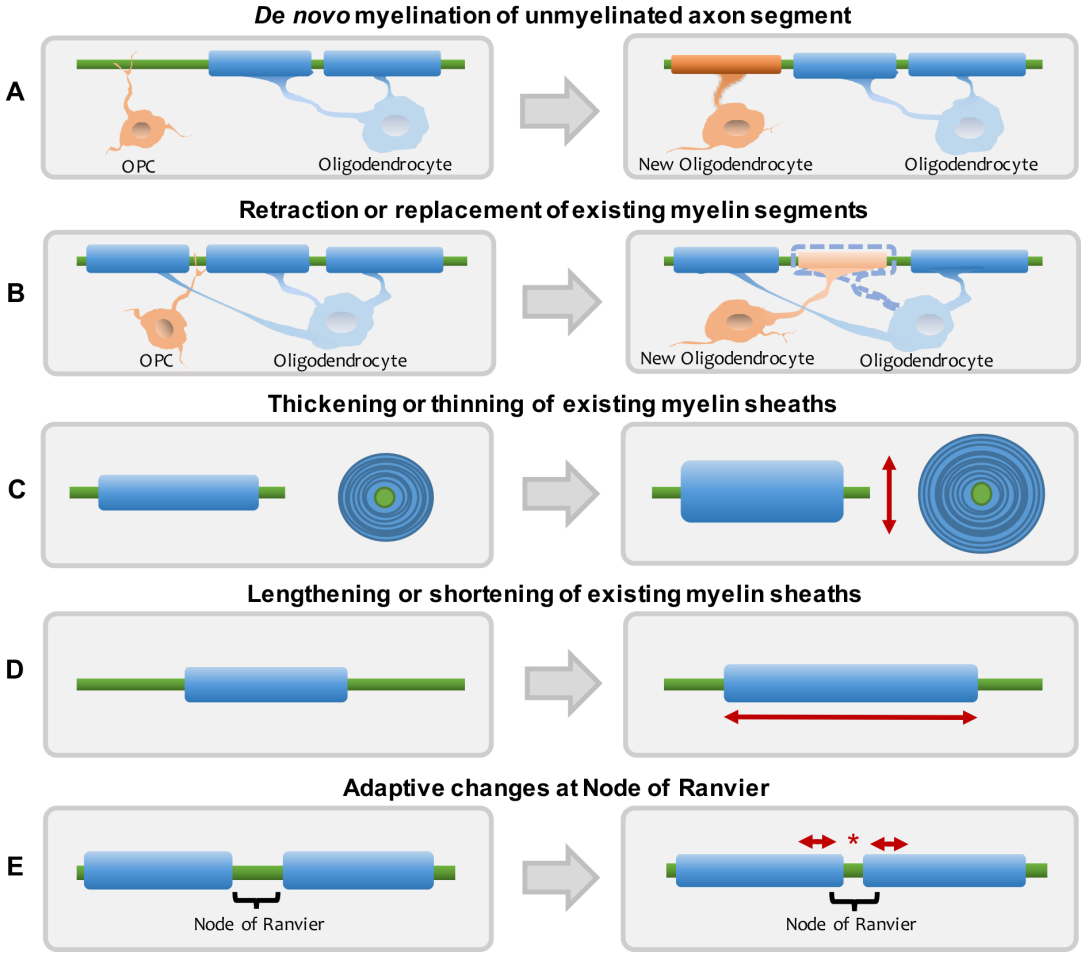


Figure 1.5. ***Different cellular processes may lead to dynamic changes in myelination during adulthood.*** *Axons (green) in the CNS can be wrapped by myelin segments (blue), which are formed by oligodendrocytes (OLs) during development. Converging evidence indicates that myelination can be dynamically remodelled by activity-dependent and experience-dependent mechanism, even during adulthood.* ***(A)*** *Oligodendrocyte precursor cells (OPCs, orange) are an abundant proliferating cell population in the adult CNS and have the potential to differentiate into new myelinating oligodendrocytes (Hill et al. 2018) . Such de novo myelination (orange segment) can occur at previously unmyelinated segments, or* ***(B)*** *can replace retracting or damaged myelin segments of pre-existing OLs.* ***(C,D)*** *Additionally, pre-existing oligodendrocytes may also adjust structural parameters of their myelin sheath to modify nerve conduction velocity. Such myelin remodelling can be achieved by (C) altering the thickness of myelin segments though the addition or removal of membrane layers (Jeffries et al. 2016), or* ***(D)*** *varying the length of myelin segments (Etxeberria et al. 2016). Yet, it remains unclear if and to what extent myelin remodelling in the adult CNS can be mediated by pre-existing OLs.* ***(E)*** *Additionally, adjustment of Node of Ranvier length has been suggested as another potential mechanism for tuning the arrival time of information in the CNS (Arancibia-Cárcamo et al. 2017). While all of these mechanisms have the potential to change the information flow within neural networks, their relative contribution to adaptive myelin plasticity, as well as their mechanistic complexity, remain poorly understood.*

different transgenic approach, another group indicated that the continuous generation of new OLs in the adult brain of mice may play a role in the maintenance of nodal integrity, and consequently, in the maintenance of motor functions, yet the study did not investigate motor learning (Schneider *et al.* 2016).

Alongside myelin formed by newly differentiating OLs, remodelling of the existing myelin sheath represents another putative mechanism by which experience can shape brain structure (Figure 1.5C,D). Yet it remains unclear if and to what extent myelin remodelling in the adult CNS can be mediated by pre-existing OLs. To address this, a recent study demonstrated that conditional upregulation of cellular signalling pathways in pre-existing OLs of adult mice was sufficient to induce a subtle increase in myelination in the CNS that was mainly driven by the addition of new myelin to existing sheaths, rather than *de novo* myelination of naked axons (Jeffries *et al.* 2016). Additionally, a concurrent increase in nerve conduction velocity indicated that the observed myelin remodelling resulted in functional changes. To probe whether such upregulation of myelin gives incremental benefits or rather disturbs homeostatic fine-tuning, the authors assessed a variety of behaviours and only found evidence for slightly enhanced hippocampal-dependent emotional learning; motor learning and object recognition remained unaffected. While this study supports the notion that myelin remodelling in pre-existing myelin sheaths is a probable mechanism for myelin plasticity (Goebbels *et al.* 2010; Snaidero *et al.* 2014), these findings also suggest that subtle and globally induced hypermyelination during adulthood does not lead to general cognitive or motor behavioural change. This could mean that behavioural performances is not consistently sensitive to subtle changes in myelination during adulthood. However, it is also possible that the CNS can compensate for such artificially induced hypermyelination, mechanisms of adaptive myelination related to learning remain largely unaffected by the genetic manipulation, and/or the influence of myelin remodelling on behaviour depends on the specific demands of the behaviour in question.

Overall, these considerations are an important reminder that the link between myelin remodelling and behavioural adaptation remains poorly understood (Figure 1.4).

1.6.3 DRIVER OF BEHAVIOURAL CHANGE: MYELIN REMODELLING AND CONDUCTION SPEED

Considering myelin's traditional function in modulating nerve conduction velocity, myelin plasticity may play a vital role in facilitating the flow and integration of information (de Hoz and Simons 2015). Additionally, precise timing of nerve impulses is essential for certain forms of synaptic plasticity (Dan and Poo 2006; Chang *et al.* 2016) and regulation of oscillatory neuronal activity in large and complex neural networks (Pajevic *et al.* 2014). However, it has been methodologically and experimentally challenging to study how experience can influence nerve conduction velocity. Etxeberria and colleagues demonstrated that visual deprivation via monocular eyelid suture can lead to shortening of myelin sheath length in the respective optic nerve, which in turn reduced nerve conduction velocity (Etxeberria *et al.* 2016). Additionally, genetically induced increases in CNS myelin sheath thickness have been linked to changes in nerve conduction speed and subtle behavioural effects (Jeffries *et al.* 2016). Recently, changes in the nodes of Ranvier have been considered as another mechanism by which experience can modulate nerve conduction speed (Ford *et al.* 2015; Arancibia-Cárcamo *et al.* 2017), as altering the length of a node can change the node capacitance and the axial resistance for current flow into the internode (Figure 1.5E). Modelling of conduction speed based on nodal lengths imaged in the mouse CNS has shown that variations in the length of nodes can change the conduction velocity by about 20%, which is comparable to the changes produced by alterations in myelin sheath thickness or length (Arancibia-Cárcamo *et al.* 2017). Interestingly, the change in membrane area needed to achieve a given change of conduction speed was estimated to be >270-fold smaller for a change in nodal length than for an alteration of the myelin sheath thickness or length, making it a potentially faster and more energy efficient mechanism.

Furthermore, it is noticeable that structural parameters of myelinated axons can deviate significantly from the canonically assumed relationship between axon dimeter and myelin thickness

(Chomiak and Hu 2009). While investigating parts of the auditory system responsible for sound localisation, Ford and colleagues observed that structural parameters of myelin sheaths and nodes can differ significantly between different axons that compute different sound frequencies, and can even vary along a single axon (Ford *et al.* 2015). Importantly, the authors claim, backed by simulations and *in vivo* and *in vitro* recordings, that such structural arrangements of myelination can play a significant role in information processing in the investigated network. While these observations describe myelination established during development, such findings are a reminder that the relationship between the myelin sheath and conduction velocity is complex, a fact that will need to be considered when investigating functionally significant myelin remodelling.

1.6.4 UNDERSTANDING THE MECHANISMS UNDERLYING MYELIN PLASTICITY WILL BE ESSENTIAL TO UNDERSTANDING ITS RELEVANCE FOR BEHAVIOUR

Understanding the biological mechanisms underlying adaptive myelination is a key issue surrounding myelin plasticity, and one that will likely require intense translational efforts across disciplines, from molecular biology to neuroimaging (Walhovd *et al.* 2014). A good example of this is the question of how fast myelin can be dynamically modulated by experience, which in turn has vast implications for its potential role in behavioural adaptation. Changes in WM microstructure, as assessed by MRI, have been detected after just 2 hours of playing a video game (Hofstetter *et al.* 2013). However, MRI metrics do not provide a direct measure of myelin. Hence, it is unclear if and to what extent myelin remodelling could contribute to such a rapid signal change, as most animal studies have investigated experience-dependent or activity-dependent changes in myelination in the timeframe of days or weeks (McKenzie *et al.* 2014; Etxeberria *et al.* 2016). A recent experiment, however, indicated a causal link between behaviour changes and OL dynamics within a few hours. By identifying a novel marker of early OL differentiation (Enpp6), Xiao and colleagues were able to track OL differentiation in adult mice to show that maturation of newly forming OLs was increased within the first 2.5 hours of exposure to a complex running wheel (Xiao *et al.* 2016). Interestingly,

preventing the differentiation of new OLs caused a deficit in running performance in the same 2–3 hours time window, suggesting a very early and active requirement for newly differentiating OLs in learning.

Understanding the speed at which myelin can be remodelled may be important for unravelling its function in the nervous system. Myelin remodelling could be understood as a slower, secondary process that reacts to changes in the dynamics of neural networks. The purpose of such secondary plasticity could be the consolidation of learning by means of adjusting myelination patterns to the new needs of the neural network, as well as providing important homeostatic control. The evidence presented by Xiao and colleagues suggests that myelin plasticity can act in a similar temporal window as fast, primary plastic changes provided by synaptic plasticity. This suggests that these two mechanisms may interact more synergistically than previously thought. However, it remains unclear how such rapid changes in conduction velocity can be achieved. A subpopulation of oligodendrocyte precursor cells (OPCs) may be primed to rapidly respond to novel experience by differentiating into myelinating OLs (Xiao *et al.* 2016). Such new OLs could establish the location of their new myelin segments within a few hours, as indicated by *in vitro* and *in vivo* zebrafish models (Watkins *et al.* 2008; Czopka, ffrench-Constant and Lyons 2013). Nevertheless, it is unclear how such early processes can lead to significant alteration in conduction velocity. While it is possible that just one or a few wraps of new myelin might have beneficial effects, newly forming pre-myelinating OLs may also influence neural activity independent of *de novo* myelination — for example, through clustering of nodal components at 'pre-nodes', which can be induced by OL-secreted factors (Freeman *et al.* 2015), or early metabolic coupling between newly differentiating OLs and axons (Fünfschilling *et al.* 2012). Additionally, remodelling of existing myelin sheaths (Jeffries *et al.* 2016), as well as adjustment of nodes of Ranvier length (Ford *et al.* 2015; Arancibia-Cárcamo *et al.* 2017) provide alternative and fast routes by which myelin could adapt to neuronal activity changes. However,

neither the relative contribution, nor the temporal dimensions of these mechanisms have been investigated.

Furthermore, it is still unclear if myelin plasticity is bi-directional. The vast majority of work in this area has investigated whether increasing activity results in increased number, length or thickness of myelin internodes. However, given the requirements for homeostasis in any biological system, it is plausible that a reciprocal phenomenon occurs, whereby certain types of activity could result in downregulation of myelin, analogous to long-term depression at the synapse. Indeed, social (Liu *et al.* 2012a; Makinodan *et al.* 2012) or sensory deprivation (Etxeberria *et al.* 2016; Sinclair *et al.* 2017) have been associated with a reduction of internodes or the number of myelin wraps that form during development. Auditory deprivation in adult mice can lead to a decrease in myelination on functionally associated large calibre axons (Sinclair *et al.* 2017), suggesting an activity-dependent mechanism that leads to a decrease in pre-existing myelination.

The emerging complexity of myelination in the CNS complicates the task of unravelling the functional role of myelin plasticity, yet it may simultaneously be an indicator of its significance. However, the role of adaptive myelination in facilitating and shaping behavioural change remains elusive and fundamental mechanisms underlying myelin remodelling are still poorly understood. In order to unravel the mystery of its function, it is important to detect functionally relevant changes in myelination and to establish a conclusive link between adaptive myelin and behavioural change.

1.7. SCOPE OF THIS THESIS

This thesis aimed to contribute to our understanding of myelin dynamics and the axon-glia communication regulating them. For this purpose, this thesis aimed to develop novel *in vitro* models to study myelination and to approach novel scientifically relevant questions in order to provide a valuable contribution to the field. Additionally, this thesis aims to replicate and critically investigate

previous scientific findings that had a large impact on the field of study, as such practise is an essential cornerstone of scientific progress.

Understanding the intricacies and functional significance of dynamic myelination requires the employment of a range of scientific approaches and methods, some of which have been used in this thesis. Co-cultures between neurons and myelinated glia can provide useful *in vitro* models to study and manipulate specific aspects of cellular interaction, such a Nrg1-ErbB signalling, in an isolated and controlled environment. How such cellular interactions can potentially influence experience-dependent processes, however, requires complementing *in vivo* studies using model organisms like rodents. *In vivo* studies also allow the investigation of the functional role of adaptive myelination, by genetically ablating myelinating glia dynamics *in vivo* and testing its effect on complex aspects of behaviour such as motor skills and learning. Combining histological analysis of cellular processes with magnetic resonance imaging of tissue microstructure in such *in vivo* models can provide further complementing insights into the extent and relevance of adaptive and dynamic cellular changes associated with observed behaviour.

Overall the research presented in this thesis focuses broadly on three different scientific themes and sets of questions, which have been outlined below.

1.7.1 Theme 1: Establish iPSC- derived myelinating co-cultures to model the axoglial relationship in vitro

Myelinating co-culture systems from rodent cells have significantly contributed to our understanding of the complex mechanisms involved in myelination, both in the PNS and CNS. These studies most frequently use primary dorsal root ganglion cells in combination with myelinating glia, either SC or OL. However, the rapidly advancing field of induced pluripotent stem cell (iPSC) technology offers the promising opportunity to develop novel *in vitro* cell culture systems, which allows the investigation of signalling pathways, characterisation of disease pathogenesis and the screening of new drugs using human cells (Yu *et al.* 2013).

In an attempt to develop a novel method to study myelination, our aim was to establish myelinating co-culture systems using human iPSC-derived neurons which can be efficiently differentiated and remain stable for a long period of time (Chambers *et al.* 2012). In an initial step, we tested if rodent derived myelinating glia, Schwann cells and oligodendroglia, can be used to create myelinating co-cultures with human neurons. We aimed to investigate if such mix-species co-cultures can recreate the canonical features of myelinated axons, such as the formation of internodes, nodal structures and important signalling pathways. Furthermore, we aimed to take advantage of the presence of human antigens in the co-cultures system by testing the effect of anti-bodies associated with auto-immune neuropathies on the formation and maintenance of myelinating co-culture.

1.7.2 THEME 2: INVESTIGATE THE ROLE OF NRG1-ERBB SIGNALLING IN MYELINATION

Whether or not an axon in the PNS will be myelinated by a Schwann cell is largely regulated by the Nrg1-ErbB signalling pathway. In contrast, experimental perturbations of Nrg1 signalling in vivo revealed only minor differences in developmental myelination of the CNS (Taveggia *et al.* 2005; Roy *et al.* 2007; Brinkmann *et al.* 2008) and OL have the surprising capacity to indiscriminately myelinate in the absence of any instructive cue in vitro (Lee *et al.* 2012). While these studies revealed a striking difference between the mechanism regulating myelination in the PNS and CNS, a recent study by Lundgaard and colleagues (2013) indicated that *Nrg1* might play an important, although quite different, role in CNS myelination (Lundgaard *et al.* 2013). Using a co-culture system in which rat dorsal root ganglion (DRG) neurons are myelinated by forebrain OL, their results raise the interesting possibility that the extent of activity-dependent changes in myelination maybe dynamically regulated by specific signalling pathways, such as Nrg1-ErbB, allowing the CNS to control when and where activity may lead to adaptive changes in nervous system function.

Our aim is to investigate this hypothesis by a combination of *in vitro* and *in vivo* studies. We aim to use the co-culture system developed in Theme 1 for our *in vitro* investigation. Our aim was to manipulate *Nrg1* expression via viral transduction of a subset of neurons. While a soluble isoform

of Nrg1 Type I was used in previous studies, it is unclear if Nrg1 Type III expressed at the axonal surface could have a similar effect on OL myelination, as suggested by a social isolation study in mice (Makinodan *et al.* 2012).

For our in vivo experiment we aimed to test if experimental perturbations of Nrg1-ErbB signalling disrupt motor skill learning and/or corresponding adaptive changes in oligodendroglia dynamics, using a behaviour task that has previously been shown to induce experience dependent changes. For this experiment we used a conditional knock-out model previously characterized in David Bennett's lab, which allows the conditional knock-out of all *Nrg1* isoforms (CAG-Cre-ERTM; $Nrg1^{(fl/fl)}$).

1.7.3 Theme 3: Replicating and extending evidence for role of de novo CNS myelination in motor learning

Myelination can be dynamically remodelled by neural activity and experience even during adulthood, yet the function of this adaptive process remains poorly understood. One source of myelin plasticity is the continuous creation of new myelin-forming oligodendrocytes (OLs) in the healthy adult brain. Previous work by McKenzie *et al.* (2014) and Xiao *et al.* (2016) demonstrated that conditionally ablation of *de novo* myelination impaired the mice's ability run on a complex running wheel with irregular rung spacing, indicating an active role of myelin plasticity in motor skill acquisition.

Given the importance and impact of this finding, we aimed first to replicate and extend the behaviour phenotype of this transgenic model. Furthermore, we aimed to investigate the association between skill acquisition, oligodendroglia dynamics and brain wide changes in metrics of tissue microstructure acquired by *ex vivo* magnetic resonance imaging. For this purpose, we established a colony of the same transgenic mice used by Mckenzie *et al.* (2014) in our laboratory and acquired a set-up of the complex wheel behaviour test.

Chapter 2 | ESTABLISHING MYELINATION CO-CULTURES WITH IPSC-DERIVED SENSORY NEURONS TO STUDY PERIPHERAL MYELINATION

2.1. INTRODUCTION

There is a close anatomical and metabolic relationship between axons and Schwann cells such that the health of each cell type is intimately dependent on the other. Axoglial signalling is critical for myelination and can be disturbed in pathological states (Taveggia *et al.* 2010). Co-cultures recapitulate many of the sequential features of myelination observed *in vivo*, including Schwann cell alignment to axons, ensheathment of the axon by the Schwann cell process and finally membrane wrapping and compaction. The intercellular interactions between axons and Schwann cells during myelination result in the formation of axonal domains with specialised molecular constituents (Rasband and Peles 2016). For instance, voltage gated sodium channels (VGSCs) are clustered at the node of Ranvier, flanked by the paranodes where tight adherence of the Schwann cell paranodal loops to the axon act as a diffusion barrier, separating VGSCs from potassium channels in the juxtaparanode.

Human induced pluripotent stem cells (iPSCs) are increasingly used in model systems of neurological disorders (Wu Yi-Ying *et al.*; Sandoe and Eggan 2013; Corti *et al.* 2015). They facilitate the study of human proteins in their normal cellular context, and, through the reprogramming of patient-derived samples, allow the impact of mutations to be investigated within a relevant polygenetic background.

They can be used for pharmacological studies, toxicity screening, to investigate immunopathological mechanisms, and to assess the reactivity of cells/antisera towards human antigens. Culture protocols have advanced such that instead of focussing on single cell types it is possible to investigate intercellular interactions and more complex tissues. This approach has been used to investigate central myelin (Czepiel *et al.* 2015) but has not previously been used to study axoglial signalling and myelination in the peripheral nervous system. We report here that sensory neurons differentiated from human iPSCs can be effectively and reliably myelinated by rat Schwann cells. These myelinating co-cultures display the expected features of axonal and Schwann cell specialization.

In inflammatory neuropathies such as Guillain Barré syndrome (GBS) and chronic inflammatory demyelinating polyneuropathy (CIDP), axoglial proteins and glycolipids are important targets for the underlying autoimmune process (Willison and Yuki 2002; Devaux *et al.* 2012; Kamil *et al.* 2019). In a subset of patients, neuropathy-associated antibodies specifically target neo-epitopes formed by cis and trans interactions between different axonal and glial molecules (Querol *et al.* 2013; Rinaldi *et al.* 2013). Recreating these interactions in solid phase systems has proved difficult. Problems with existing assays are further evidenced by the inconsistent relationship between antibody binding *in vitro* and pathogenic effects *in vivo* (Greenshields *et al.* 2009). Anti-disialosyl ganglioside antibodies, which bind to alpha2-8 linked disialic acid residues (as found in GD3, GD1b, GT1b and GQ1b), are associated with predominantly sensory and/or ataxic neuropathies. Disialosyl antibodies of the IgM class are a defining feature of CANOMAD (chronic ataxic neuropathy with ophthalmoplegia M-protein, cold agglutinins and anti-disialosyl anti- bodies). This neuropathy shows both axonal and demyelinating features on electrophysiology (Willison *et al.* 2001). Disialosyl antibodies of the IgG class have been found in acute sensory neuropathies, some with unequivocal electrophysiological evidence of demyelination in the form of temporal dispersion (Wicklein *et al.* 1997; Miyazaki *et al.* 2001). However, immunization of rabbits with GD1b that raised IgM and IgG antibodies induced a sensory neuropathy characterized pathologically by down-regulation of the neurotrophin-3 receptor,

trkC, and by the degeneration of sensory axons and DRG neurons (Kusunoki *et al.* 1996; Hitoshi *et al.* 1999). In this report, we exploit the myelinating co-cultures to show that both mouse IgG and human, neuropathy-associated IgM type anti-disialosyl antibodies bind to human iPSC- derived sensory axons at the nodal axolemma and, in addition to inducing acute complement mediated axonal degeneration, have deleterious, complement-independent effects on myelination.

2.1.1 Aim of the Chapter

The aim of this chapter was to establish myelinating co-culture systems using human iPSC-derived neurons. Furthermore, we aimed to take advantage of the presence of human antigens in such a co-cultures system by testing the effect of anti-bodies associated with auto-immune neuropathies on the formation and maintenance of myelination in the co-culture system.

2.2. Materials and methods

2.2.1 Ethics statement

Human iPSC lines used in this study were derived from human skin biopsy fibroblasts, following signed informed consent. Three control cells lines were used in this study – AD2-1 (iPSC line 1), AH017-7 (iPSC line 2) and NHDF1 (iPSC line 3). AH017-7 and NHDF1 were reprogrammed with approval from research ethics committee: National Health Service, Health Research Authority, NRES Committee South Central, Berkshire, UK (REC 10/H0505/71).

2.2.2 Induced pluripotent stem cell generation

NHDF1 (from 44-year-old female) was reprogrammed with Yamanaka retroviruses SOX2, KLF4, OCT3/4, c-MYC and NANOG (Takahashi and Yamanaka 2006), and has previously been described (Hartfield *et al.* 2014). AH017-7 (from 67-year- old female) has also previously been described (Handel *et al.* 2016) and was reprogrammed using the SeVdp(KOSM)302L Sendai virus system, containing genes for KLF4, OCT3/4, SOX2 and c-MYC, expressed from a single transcript and packaged into a single Sendai virus to ensure consistency of gene dosage ratio (Nishimura *et al.* 2011, 2013).

AD2-1 (from 51-year-old male) was reprogrammed using the CytoTuneTM- iPS Reprogramming Kit (ThermoFisher). The fibroblasts to generate AD2-1 were obtained from a commercial source (Lonza, CC-2511). Reprogramming was performed as directed by the manufacturer's instructions. The CytoTune reprogramming kit contains four Sendai virus-based reprogramming vectors each capable of expressing one of the four Yamanaka factors (*KLF4*, *OCT3/4*, *SOX2* and *c-MYC*). Briefly, after fibroblast transduction with the four Sendai virus-based reprogramming vectors, cells are cultured for 5-6 days, with medium changes every other day (DMEM, high glucose (Sigma), 10% FBS (ThermoFisher), 1% Pen/Strep (100x, ThermoFisher), 200mM L- glutamine (Sigma), 1% non-essential amino acids (ThermoFisher)). The transduced fibroblasts are then passaged using 0.05% Trpsin-EDTA onto pre-prepared feeder layer plates containing mitotically inactivated mouse embryonic fibroblasts (MEF). 3-4 weeks after transduction, colonies should have grown to an appropriate size to allow for manual picking. Using an inverted microscope, a single colony displaying iPSC morphology is cut into 5-6 pieces using a 25 gauge needle, transferred into iPS media (KO-DMEM (ThermoFisher), 25% Knock Serum Replacement (ThermoFisher), 1% nonessential amino acids (100x, ThermoFisher), 200mM L-glutamine (Sigma), 1% Pen/Strep (100x, ThermoFisher), 8 ng/ml human FGF2 (Miltenyi Biotec)) and plated onto pre-prepared MEF plates. Colonies are allowed to attach for 48 hours, and thereafter medium changes are performed daily. iPSCs were adapted to feeder-free conditions onto Matrigel (Scientific Laboratory Supplies)-coated plates in mTeSR1 medium (ScienCell). Bulk passaging was by 0.5 mM ethylenediaminetetraacetic acid (EDTA) to make large-scale, quality-controlled stocks that were cryopreserved in liquid nitrogen. The number of feeder-free passages was kept to a minimum. When selecting iPSCs from frozen stocks for differentiation, vials with the same passage number were selected for each cell line throughout all experiments performed in this study. The iPSC line AD2-1 were reprogrammed by and obtained through the IMI/EU sponsored StemBANCC consortium via the Human Biomaterials Resource Centre, University of Birmingham, UK (http://www.birmingham.ac.uk/facilities/hbrc). iPSC lines were also subject to strict quality control checks before the initiation of differentiation. Quality control for AD2-1 included tests for Sendai virus

clearance, FACS for pluripotency markers, genomic integrity checks and embryoid body tri-lineage differentiation experiments. Cells are also confirmed as negative for Mycoplasma before cryopreservation.

2.2.3 INDUCED PLURIPOTENT STEM CELL MAINTENANCE AND DIFFERENTIATION

iPSCs were defrosted, plated onto Matrigel coated plastic and maintained in mTeSR1 medium, which was exchanged daily. iPSCs were passaged when 90% confluent onto Matrigel coated plasticware using TrypLE express (ThermoFisher). Rho-associated, coiled-coil containing protein kinase (ROCK) inhibitor (ScienCell) (10 mM) was included in the medium for 24h after each passage. Prior to the start of differentiation, iPSCs were plated onto Matrigel coated 6-well plates. Twenty-four hours later, the medium was exchanged from mTeSR1 to mouse embryonic fibroblast conditioned medium (ScienCell) supplemented with 10ng/ml human recombinant FGF2. Cells were allowed to expand in MEF-conditioned medium until about 50% confluent, at which time differentiation was started according to Chambers *et al*. (2012).

2.2.3.1 Neuronal differentiation

The medium was exchanged to knockout serum replacement (KSR) medium (Knockout-DMEM (ThermoFisher), 15% knockout-serum replacement (ThermoFisher), 1% Glutamax (100x, ThermoFisher), 1% nonessential amino acids (100x, ThermoFisher), 100 µM β-mercaptoethanol (ThermoFisher), 1% antibiotic/antimycotic (100x, ThermoFisher)) containing the SMAD inhibitors – SB431542 (Sigma, 10 µM) and LDN-193189 (Stratech, 100 nM). The medium was gradually transitioned from KSR medium to N2 medium (Neurobasal medium (ThermoFisher), 2% B27 supplement (ThermoFisher), 1% N2 supplement (ThermoFisher), 1% Glutamax (ThermoFisher), 1% antibiotic/antimycotic (ThermoFisher)) over an 11 day period. On day 2, the small molecules - CHIR99021 (Apollo Scientific, 3 µM), SU5402 (R&D Systems, 10 µM) and DAPT (Sigma, 10 µM), were included together with the dual SMAD inhibitors in the medium. Whilst not in the original description by Chambers *et al*. (2012), we found it optimal to passage the cells on day 2 or 3 of the differentiation,

which allowed more growing area for the neurons to develop into. On day 6, the SMAD inhibitors were removed, leaving only the 3 small inhibitors in the medium. On day 11, the now immature neurons were replated using TrypLE (Gibco) onto Matrigel coated coverslips (25,000 per 13 mm coverslip) in 100% N2 medium containing human recombinant NGF, GDNF, BDNF and NT3 (all at 25 ng/ml, Peprotech). CHIR99021 (3 µM) was included in the medium until day 14, and laminin (1 µg/ml, ThermoFisher) was supplemented into the medium from day 20 onwards. Medium changes were performed twice weekly after replating onto coverslips. If required, Cytosine β-D-arabinofuranoside (araC, 2 µM, Sigma) was included in the medium soon after replating to kill the few non-neuronal dividing cells remaining in the culture. AraC was withdrawn from the medium once a pure neuronal culture was obtained, as judged by the absence of morphologically non-neuronal cells on phase-contrast light microscopy. This state was typically achieved 2-3 weeks after replating.

2.2.4 SCHWANN CELL HARVESTING AND CULTURE

All work using animals conformed to UK Home Office legislation (Scientific Procedures Act 1986). Schwann cells were harvested from the sciatic nerve and brachial plexus of postnatal Day 3 or 4 rats. Rat Schwann cells are used, as well-established culture protocols exist and they can be successfully expanded several times *in vitro* in order to create cryopreserved stocks. Nerves were enzymatically digested with a collagenase (Sigma, 3mg/ml) and dispase II protease (Sigma, 2.5mg/ml) incubation for 1h at 37°C. Nerves were gently triturated using a P1000 pipette tip and plated onto PDL/laminin coated plastic in Schwann cell expansion medium [DMEM/F12 (ThermoFisher), 10% foetal bovine serum (ThermoFisher), 200ng/ml NRG1-b1 EGF domain (R&D Systems), 10 ng/ml NGF (recombinant-murine, Peprotech), 4mg/ml forskolin (Sigma)]. Cells were serially treated with 5–10mM araC to eliminate fibroblasts. After approximately four passages, each time doubling the growing area, cells were frozen in a Mr Frosty freezing container (ThermoFisher) and stored in liquid nitrogen.

2.2.5 ESTABLISHING THE MYELINATING CO-CULTURES

To establish the co-cultures, a frozen vial of Schwann cells was thawed in warm water, centrifuged in phosphate-buffered saline (PBS) and resuspended in Schwann cell basal medium [DMEM/ F12 (ThermoFisher), 5 mg/ml insulin (Sigma), 100 mg/ml transferrin (Millipore), 25 ng/ml NGF (recombinant-human, Peprotech), 25 ng/ml Selenium (Sigma), 25 ng/ml thyroxine (Sigma), 30 ng/ml progesterone (Sigma), 25 ng/ml triiodothyronine (Sigma), 8 mg/ml putrescine (Sigma)]. The medium on the neuronal cultures was changed from N2 to Schwann cell basal medium. Schwann cells (25 000) in a 25 ml droplet were slowly pipetted onto a single coverslip containing the iPSC-derived neurons, with care taken not to touch the coverslip with the pipette tip. The Schwann cell droplet was evenly distributed over the coverslip. Cultures were carefully put back into the incubator to allow Schwann cell adherence. The culture medium was changed 2 days later. At this stage abundant Schwann cells can be observed adhered to the coverslip. An additional Schwann cell basal medium change was performed 4 days after adding the Schwann cells. During the 1-week period when the human iPSC-derived neurons are cultured in Schwann cell basal medium we observe no detrimental effects to the neurons, such as neurite blebbing. Myelination was induced 1 week after Schwann cell addition, by exposing the cells to myelination medium [N2 medium, 1:300 phenol-free Matrigel (Scientific Laboratory Supplies), 5% charcoal-stripped FBS (ThermoFisher), 25ng/ml NGF (recombinant-human, Peprotech), 50mg/ml ascorbic acid (Sigma)]. Medium changes were performed twice weekly from then on.

When optimizing the culture conditions required to establish myelinating co-cultures, we observed that the Schwann cells proliferate and align to the human axons during the week after seeding them onto the neurons; this is aided by keeping the co-cultures in Schwann cell basal medium. However, we noticed that simply supplementing the Schwann cell basal medium with ascorbic acid (as usually performed when culturing primary DRG neurons and Schwann cells together) resulted in only the occasional formation of myelin internodes. Furthermore, after 3–4 weeks these cultures gradually

began to show signs of a decline in neuronal health, such as neurite blebbing. We therefore adapted commonly used protocols when generating myelinating co-cultures using primary rodent cells, by using myelination medium that is largely formulated to encourage the growth and wellbeing of the neurons. We found that using the neuronal medium, with the addition of Matrigel and ascorbic acid greatly improved both neuronal health, alignment by Schwann cells and the levels of myelination. This adaptation in medium allowed us to establish healthy and stable myelinating co-cultures between rat Schwann cells and human iPSC-derived neurons that could be kept for many months without signs of a gradual decline in cellular health.

2.2.6 IMMUNOCYTOCHEMISTRY AND CONFOCAL IMAGING

For immunocytochemistry, coverslips were transferred to PBS, and fixed in 1% paraformaldehyde for 20min. Cells were washed three times in PBS and then permeabilized in ice cold methanol for 20min. Following three PBS washes, cells were blocked [5% donkey serum, 0.3% milk powder, 1% bovine serum albumin (BSA), 0.1% sodium azide, 1% dimethyl sulphoxide (DMSO)], washed in PBS, and incubated with the primary antibody overnight at 4°C. Cells were then washed with PBS, and incubated with the secondary antibody for 2h at room temperature. The secondary antibody was washed off with PBS, and the coverslips were mounted onto Superfrost Plus microscope slides (Thermo Scientific) in Vectashield mounting medium (Vector Laboratories). Primary antibodies used and their dilations are outlined in Table 1. Secondary antibodies used were Alexa Fluor 568, 546, 488, 405 or Pacific Blue.

2.2.6.1 Quantification of myelination

Myelination was quantified via confocal microscopy using systematic random sampling to ensure objective sampling across the coverslip. Zen Black Software (Zeiss, Germany) was used to create a digital diamond shape of 13 points (2 mm horizontal/vertical distance between each point) that was centred on each coverslip. A tile scan (each 1792 µm x 1792 µm in size, using either a 10x or 20x objective) was taken at each point, resulting in 13 non-overlapping images that equally sampled all

quadrants of the coverslip (31.4% of the total area). Images were processed and analysed using ImageJ software (Version 1.48J). A condition-blinded investigator then created binary images for each channel (MBP (Myelin Basic Protein), NF200 (Neurofilament Heavy Chain) & DAPI) by adjusting the threshold to acquire the maximum signal-to-noise ratio, and area measurements for each channel were recorded. The proportion of axonal area covered by myelin was then calculated.

Table 1. ***Primary Antibodies used for immunohistochemistry and their dilutions.***

Antigen	Company	Dilution
MBP	Abcam	1:400
NF200	Sigma, Abcam	1:400 1:10,000
S100	Dako	1:400
BRN3A	Millipore	1:500
Collagen type-V	Millipore	1:500
N-Cadherin	BD Biosciences	1:400
c-JUN	Cell signalling	1:400
SOX10	Santa Cruz	1:500
Krox20	Covance	1:500
Caspr	Gift from Prof. Baht	1:400
Pan-Nav	Sigma	1:400
Kv1.2	Neuromab	1:200
APC(CC1)	Calbiochem	1:200
GFP(YFP)	Avas	1:500
PDGF-Rα	New England Biolabs	1:400

Since measuring MBP area was a novel approach to quantify myelination, we cross-validated our results by comparing them to the most commonly used method (myelin internode count). We counted the number of internodes and quantified the myelin area in 18 separate myelinated co-culture coverslips within a single neuronal differentiation and found both set of results were highly correlated (Pearson's R; r = 0.962, n = 18, P<0.001; Figure 2.1). Hence, measurement of MBP surface area was used to quantify myelination, as it provided the more time efficient method. When comparing between conditions, the proportion of the total axonal area covered by myelin (MBP area/NF200 area) was calculated, and expressed as a fold change from control. To acquire cell numbers, DAPI positive nuclei were quantified using 'Particle Analyser' provided by ImageJ software.

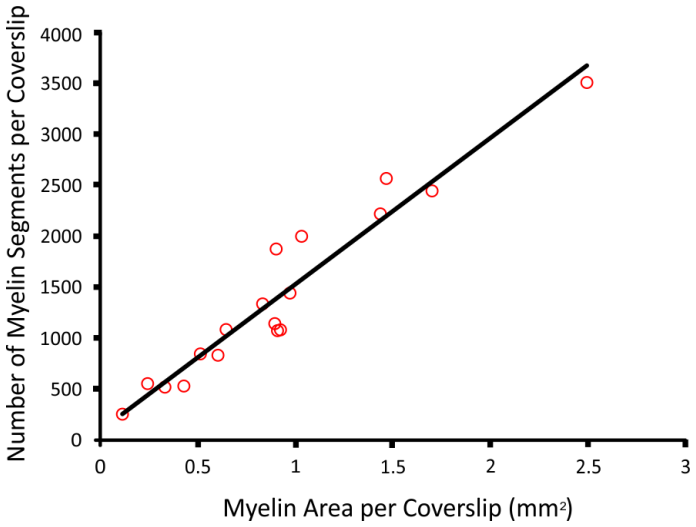


Figure 2.1. ***The number of MBP positive internodes and MBP area (as a proportion of NF200 immunoreactive axons) is highly correlated (Pearson's R; r = 0.962, n =18, P <0.001).***

2.2.7 TRANSMISSION ELECTRON MICROSCOPY

Cells adhered to coverslips were fixed in pre-warmed fixative (2.5% glutaraldehyde + 4% PFA (Agar Scientific) in 0.1 M PIPES (Sigma) buffer at pH 7.2) for 1 hour at room temperature, then incubated at 4 °C overnight. Cells were thoroughly washed in 0.1 M PIPES buffer 5 times for 15 minutes each. The fourth wash included 50 mM glycine in 0.1 M PIPES to quench free aldehydes. Cells then underwent a secondary fixation in 1% osmium tetroxide (TAAB Laboratories) in 0.1 M PIPES at 4 °C for 1 hour, after which they were washed in milliQ water 5 times for 10 minutes each. Cells then

underwent a tertiary fixation in 0.5% uranyl acetate (Agar Scientific) overnight at 4 °C in the dark, then rinsed with milliQ water for 5-10 minutes. Cells were then dehydrated in 30%, 50%, 70%, 80%, 90% and 95% ethanol (Sigma), each for 10 minutes, then incubated in 100% ethanol for 90 minutes with 3 solution changes during this time. To infiltrate with epoxy resin, cells were incubated with 3:1 100% dry ethanol:Agar100 resin(Agar Scientific) for 1 hour, then 1:1 100% dry ethanol:Agar100 resin for 2 hours, and 1:3 100% dry ethanol:Agar100 resin for 1 hour in a fume hood. Cells were then incubated in 100% Agar100 overnight at room temperature, and the resin changed twice the next day. The cells were embedded by inverting the coverslip onto Beem capsules filled with fresh 100% Agar100 resin. Blocks were polymerised for 24 hours at 60°C, then submerged in liquid nitrogen and the coverslip snapped off, leaving cells embedded as a monolayer on the surface of the block. Ultrathin sections (90 nm) were taken using a Diatome diamond knife on the Leica UC7 ultramicrotome and mounted onto 200 mesh Cu grids. Sections were post-stained with Reynold's lead citrate (Reynolds, 1963) for 5 minutes, washed with degassed water and dried. Samples were transferred to a FEI Tecnai 12 transmission electron microscope and imaged at 120kV. Images were acquired using a Gatan OneView CMOS camera with Digital Micrograph 3.0 software.

2.2.8 WESTERN BLOT

Cells were washed with PBS, and then lysed in NP40 buffer. Mechanical dissociation through a 25 gauge needle was used to facilitate breakdown of the cellular material. The lysates were spun at 13,000 rpm for 15 min and the protein concentration of the supernatant was determined using a BCA Protein Assay kit (ThermoFisher). Protein homogenate (30 µg) was loaded on precast 10-14% SDS-polyacrylamide gels (Biorad), and transferred to PVDF membranes (ThermoFisher), blocked in 3% BSA for 1 hour and immunoblotted with antibodies against *Nrg1* (Neuregulin-1α/β1/2 (C-20) SantaCruz SC-348; 1:500) and Calnexin (Endo Life ADI-SPA-860; 1:10,00). Secondary antibodies were anti-rabbit IgG horseradish peroxidase linked (GE Healthcare NA9340V; 1: 10,000). ECL prime western blotting detection system (GE Healthcare) was used to develop the film (GE Healthcare).

2.2.9 ANTI-DISIALOSYL ANTIBODY TREATMENT

The mouse monoclonal IgG antibodies MOG12 and EG4 were produced and purified from hybridomas cloned by limiting dilution after GT1b or GQ1b ganglioside immunization (respectively) of GD3-synthase deficient mice, as previously described (Boffey *et al.* 2005). The human monoclonal IgM antibody HA1 was cloned after EBV transformation of peripheral blood mononuclear cells taken from a patient with CANOMAD, as previously described (Willison *et al.* 1996). All of these anti-ganglioside antibodies cross-react with structurally similar gangliosides containing disialosyl groups, including GD1b, GD3, GT1a, GT1b and GQ1b. Herein, they are referred to as 'anti-disialosyl' antibodies to reflect this reactivity. Normal mouse IgG was obtained from Abcam. To identify topographical binding patterns, the culture media of mature co-cultures were supplemented with anti-disialosyl antibodies at 100mg/ml and incubated at 37°C for 16h. To assess the effects of complement, culture media were subsequently supplemented with 20% normal human serum and re-incubated at 37°C for 2h. Immunocytochemistry and confocal imaging were then performed, as described above. To assess their effects on myelination, anti-disialosyl antibodies were added to every change of medium for the first 4 weeks after myelination was induced, at both low (10mg/ml) and high (EG4 40mg/ml, MOG12 and HA1 50mg/ml) concentrations, without the addition of normal human serum. Experiments were repeated with three different iPSC differentiations. Controls were treated with myelination medium only, or with identical concentrations of normal mouse IgG. After 4 weeks, cells were fixed, the entire axonal field was imaged, and the proportion of the NF200 positive axonal area covered by MBP positive myelin was calculated as before.

To assess effects on established myelin, co-cultures aged 9 to 12 months from three different iPSC lines were used. At baseline, myelination medium was supplemented with fluoromyelin red (Fisher Scientific) at a 1:300 dilution, and incubated at 37° C for 16 h. The extent of baseline myelination was recorded by imaging live cells over a 2688 mm x 2688 mm centred grid at 10 x objective magnification. Images took less than 3 min to acquire per coverslip. Automated stage movement with

defined coordinates were used to allow serial imaging of the same areas. After baseline imaging, myelination medium was replaced. From this point on, the human IgM HA1 was added to each change of medium for the next 4 weeks. Control coverslips were treated with standard myelination medium only. After 4 weeks, cultures were fixed and axon and myelin coverage was assessed by immunofluorescence with NF200 and MBP primary antibodies, as before. To identify areas of demyelination, the fluoromyelin image from baseline was overlain with the MBP channel image at 4 weeks, in which the background had been made transparent. The area of fluoromyelin signal (at baseline) without a corresponding MBP signal (after 4 weeks) was calculated using ImageJ, and expressed as a proportion of the total fluoromyelin area at baseline. Areas of ongoing demyelination, identified by 'fragmented' MBP staining replacing linear fluoromyelin staining, were also imaged at higher power (63x objective) to assess the integrity of demyelinated axons.

2.2.10 STATISTICS

Statistical analysis was performed using IBM SPSS Statistics for Mac (Version 25). Student's t-test was used for comparison of two groups, one-way ANOVA using Tukeys or Dunnet's *post hoc* correction was used for more than two groups. The experimental units (means n) of analysis for the presented *in vitro* experiments represent separate individual coverslips from the same neural differentiation, unless otherwise indicated. Correlation was analysed using Pearson's R. Results are reported as mean±SEM. Asterisks indicate the level of significance (***P<0.001, **P<0.01, *P<0.05).

2.3. RESULTS

2.3.1 ALIGNMENT AND MYELINATION OF HUMAN INDUCED PLURIPOTENT STEM CELL-DERIVED SENSORY NEURONS BY RAT SCHWANN CELLS

We found that the key step in promoting myelination in co- cultures of human iPSC-derived sensory neurons and rat Schwann cells was to use a neuronal base medium with Matrigel in the myelinating medium stage rather than a Schwann cell basal medium. This gave rise to long-lasting stable co-cultures in which neuronal health was maintained and a much greater efficiency of myelination. To

investigate how human iPSC-derived sensory neurons interacted with primary rat Schwann cells, co-cultures were investigated for canonical markers of the Schwann cell-axon relationship. Initially, sensory neurons were first differentiated using the previously published protocol (Chambers *et al.* 2012). These neurons grew extensive arborized neurites, and >90% of cells were positive for the sensory neuron transcription factor BRN3A (Figure 2.2A). After allowing the neurons to mature and

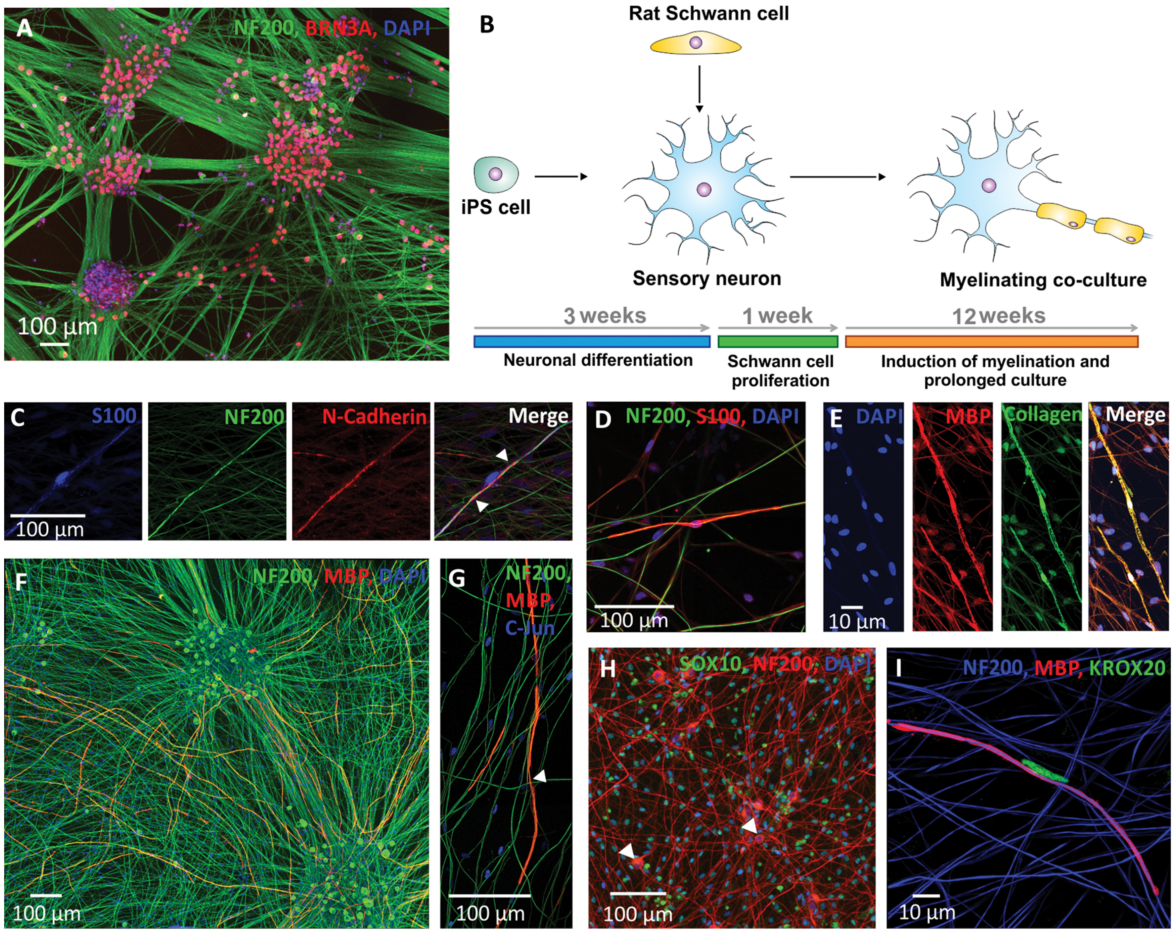


Figure 2.2. ***Rat Schwann cells align and myelinate human iPSC-derived sensory neurons.***

(A) Sensory neurons can be differentiated from iPSCs, identified through BRN3A positive nuclei, and these grow extensive NF200 immunoreactive neurite processes. (B) Schematic showing the establishment of the myelinating co-cultures. (C) As rat Schwann cells migrate and come into contact with human axons, N-cadherin expression is upregulated at the interface between the axon and Schwann cell (arrowheads). (D) The S100 immunoreactive Schwann cell tightly aligns to the human axon. (E) Collagen expression is upregulated as the basal lamina forms around the Schwann cell/axon complex. (F) MBP positive internodes are abundant throughout the co-cultures after 6 weeks of myelination. (G) Myelinating Schwann cells do not express c-Jun (arrowhead highlights a c-Jun negative nucleus) in contrast to non-myelinating Schwann cells. (H) Rat Schwann cells are SOX10 positive, whereas the neurons (NF200 positive, arrowheads) do not express SOX10. (I) Myelinating Schwann cells express KROX20.

grow widespread neurite processes for 2 weeks, rat Schwann cells were added in suspension, these adhered to the coverslip and were allowed to migrate and come in contact with axons for 1 week before myelination was induced (schematic and timeline of co-culture shown in Figure 2.2B). In that time, alignment and Schwann cell-axon interaction was observed by the expression of N-cadherin at the cell-to-cell interface (Figure 2.2C, arrowheads), as has been described in primary co-cultures of DRGs and Schwann cells (Wanner and Wood, 2002). Staining the Schwann cell cytoplasm with an antibody directed against S100 revealed the typical bipolar Schwann cell morphology that was closely aligned to the NF200 positive axon of the sensory neuron (Figure 2.2D). As the tightly associated rat Schwann cell begins to form the axon/Schwann cell complex before the onset of myelination, increased levels of extracellular matrix are observed (collagen IV), indicating the beginning of basal lamina formation (Figure 2.2E). The first MBP positive internodes were observed after ~2 weeks of ascorbic acid supplementation, and gradually increased over time in culture (Figure 2.4). After 6 weeks of myelination, abundant MBP positive internodes are detected throughout the culture (Figure 2.2F). On a transcriptional level, Schwann cells followed a typical transition into a mature myelinating state; basal expression of the transcription factor SOX10 was present in all Schwann cells, but not in neuronal nuclei (arrowheads, Figure 2.2H). Upon induction of myelination, rat Schwann cells associated with MBP positive internodes showed strong upregulation of KROX20 (Figure 2.2I), while the expression of c-JUN was not detected in these cells (Figure 2.2G, arrowhead depicts a Schwann cell nucleus associated with an MBP positive internode that is negative for c-JUN), consistent with the cross antagonistic relationship between these transcription factors (Parkinson *et al.* 2008). Taken together, these myelinating co-cultures of rat Schwann cell and human iPSC-derived sensory neurons express the canonical markers of an axoglial relationship, and we demonstrate for the first time that there is successful cross-species signalling in order to initiate alignment, basal lamina formation and myelination.

2.3.2 NODE OF RANVIER FORMATION AND MATURATION OF THE MYELIN SHEATH

We detected characteristic nodal structures in our 6-week myelinated co-cultures using antibodies directed against proteins localized to the specialized axonal domains that form at the node of Ranvier, the paranode and the juxta-paranode. Caspr (contactin-associated protein)-positive paranodes encompassed dense clusters of voltage gated sodium channels at the nodes (using an antibody that recognizes a sequence from the intracellular III-IV loop present in all vertebrate Na_v channels) (Figure 2.3A and B). The shaker type voltage gated potassium channel ($K_v1.2$) was localized in adjacent juxtaparanodes (Figure 2.3A). Nodes of Ranvier were abundantly detected throughout the culture at this time point, with the occasional heminode also present (Figure 2.3C).

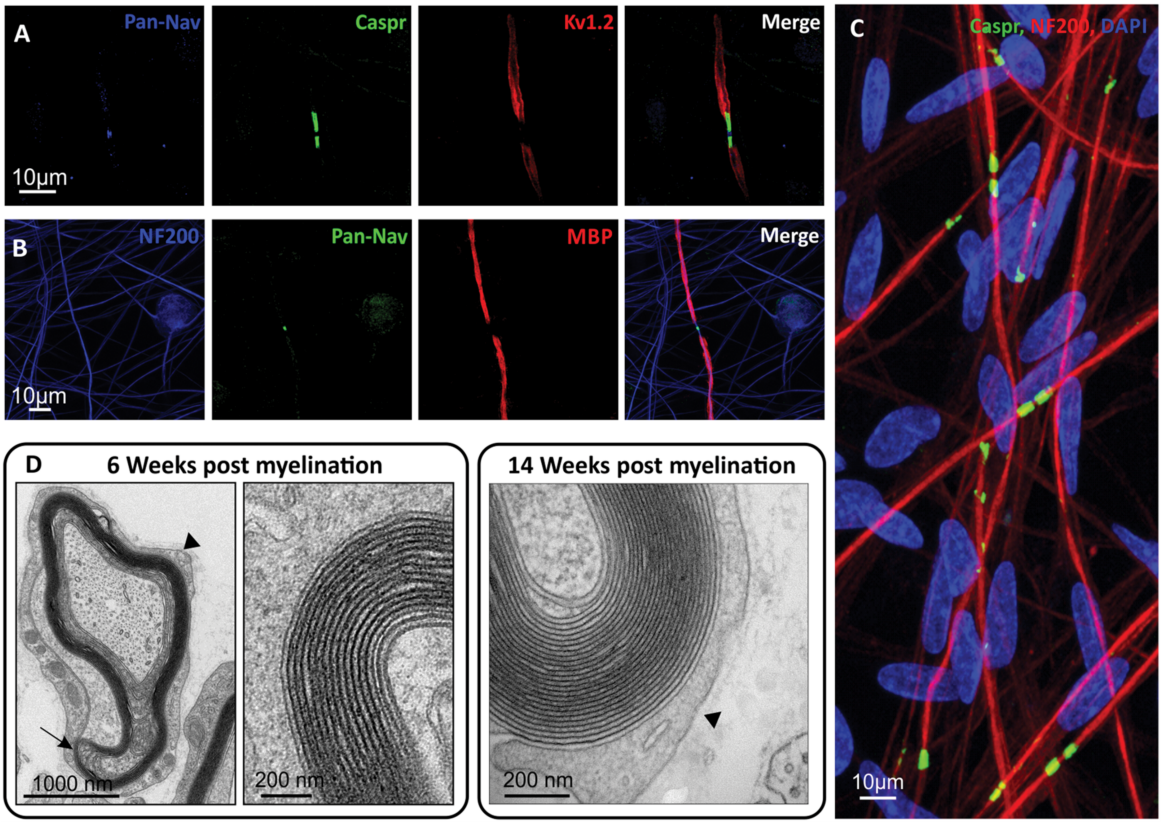


Figure 2.3. ***Nodes of Ranvier and the basal lamina successfully form in co-cultures.***

(A) Clustering of voltage gated sodium channels at the node, Caspr at the paranode and Kv1.2 at the juxtaparanode is detected after 4 weeks of myelination. (B) Sodium channels cluster between the MBP positive internodes. (C) Abundant Caspr positive paranodes are detected after 6 weeks of myelination. (D) At the electron microscopy level, the basal lamina can be observed (arrowheads) as well as individual myelin wraps. Not all the myelin wraps are tightly compacted at 6 weeks (arrow), whereas after 14 weeks of myelination, the number of wraps has increased and are tightly compacted. Compacted myelin was abundant in all co-culturs analysied via electron microscopy (n=6), but was not quatified.

Myelin sheath ultrastructure was viewed with electron microscopy at 6 and 14 weeks post-myelination (n=6 coverslips per timepoint). At this resolution individual myelin wraps and the basal lamina around the Schwann cell/axon complex could be observed (arrowheads, Figure 2.3D). At the earlier time point, several axons were observed where the myelin wraps were not compacted (arrow Figure 2.3D). Increasing numbers of myelin wraps and a more compacted myelin structure were observed at the later time point indicating the typical maturation of the myelin sheath (Figure 2.3D).

2.3.3 MYELINATION INCREASES OVER TIME

To investigate the time course of myelination in the co-cultures, myelin coverage was quantified at 2, 3, 4, 6 and 14 weeks post-induction. Representative images used for the quantification are illustrated in Figure 2.4(A–E). As expected, an overall significant increase in the quantity of myelin was observed over time [Figure 2.4G, one-way ANOVA, $F(4,17) = 9.616$, $p<0.001$], however the axonal coverage did not significantly change over time [Figure 2.4F, one-way ANOVA, $F(4,17) = 2.735$, $p>0.05$], indicating that the increase in myelin is not simply due to greater axonal outgrowth. Furthermore, these cultures are extremely stable, and have been maintained for over 9 months with no loss of myelin or neuron integrity (Figure 2.5).

To assess the levels of myelination across different iPSC lines, we differentiated three separate control lines to sensory neurons and co-cultured them with rat Schwann cells as described in the methods. All three iPSC-derived neuronal cultures were successfully myelinated and the levels of myelination were very similar between cell lines (Figure 2.6) demonstrating the reproducibility of this co-culture system.

2.3.4 ANTI-DISIALOSYL ANTIBODIES IMPAIR MYELINATION

Gangliosides containing disialosyl moieties are known to be expressed by sensory neurons (Svennerholm et al., 1994). Auto-antibodies directed against these gangliosides are associated with acute (IgG) and chronic sensory/ataxic neuropathies (IgM) with electrophysiological evidence of both axonal degeneration and demyelination (Wicklein et al., 1997; Miyazaki et al., 2001; Willison et al.,

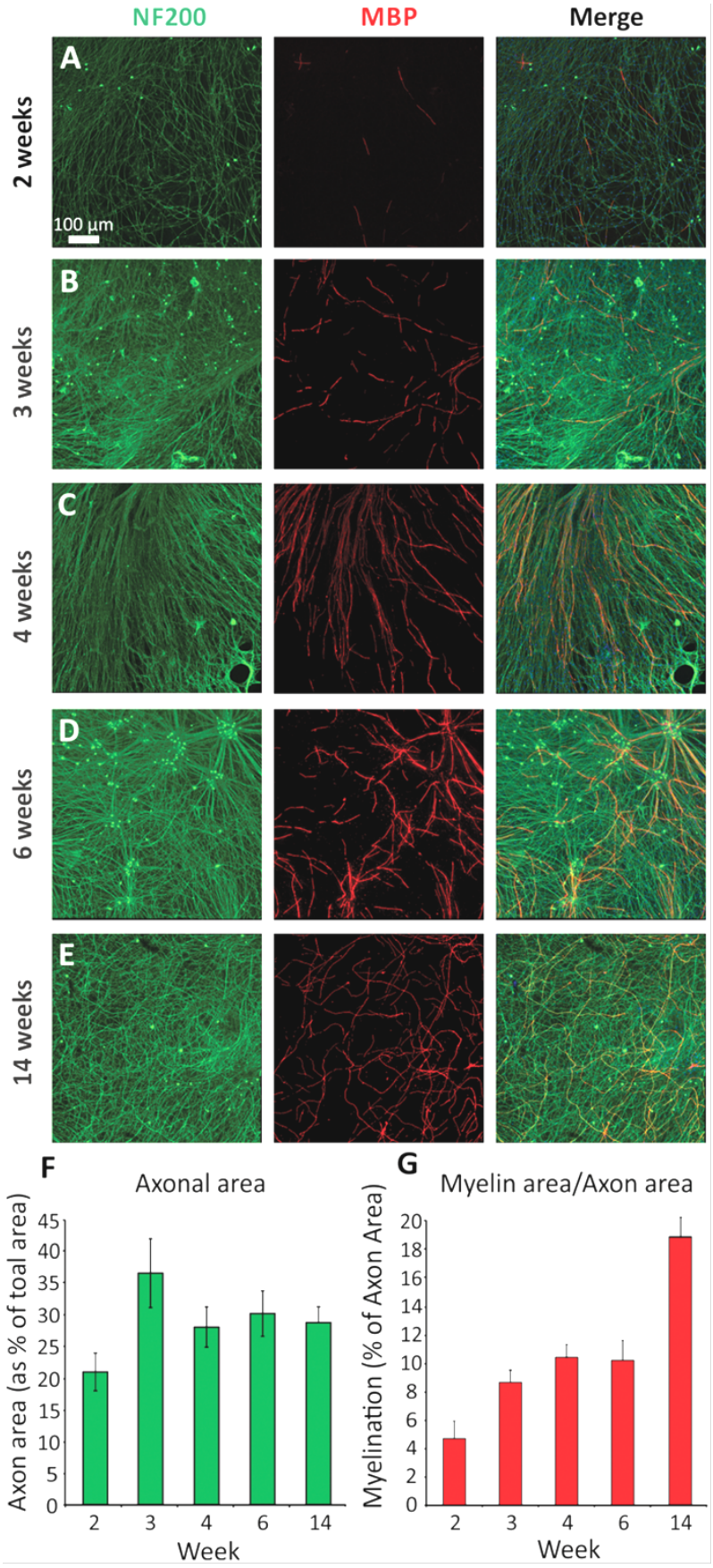


Figure 2.4. ***Myelination increases over time in culture.***

*Cultures were fixed and immuno-cytochemistry performed at (**A**) 2, (**B**) 3, (**C**) 4, (**D**) 6 and (**E**) 14 weeks post-induction of myelination. (**A**) The first MBP-positive internodes can be detected at ~2 weeks. Myelination was quantified (**G**) as a proportion of NF200-positive staining (**F**). Levels of myelination steadily increase over time, whereas axonal area remains unchanged from 4 weeks (n=3-4 per group). Results are reported as mean±SEM*

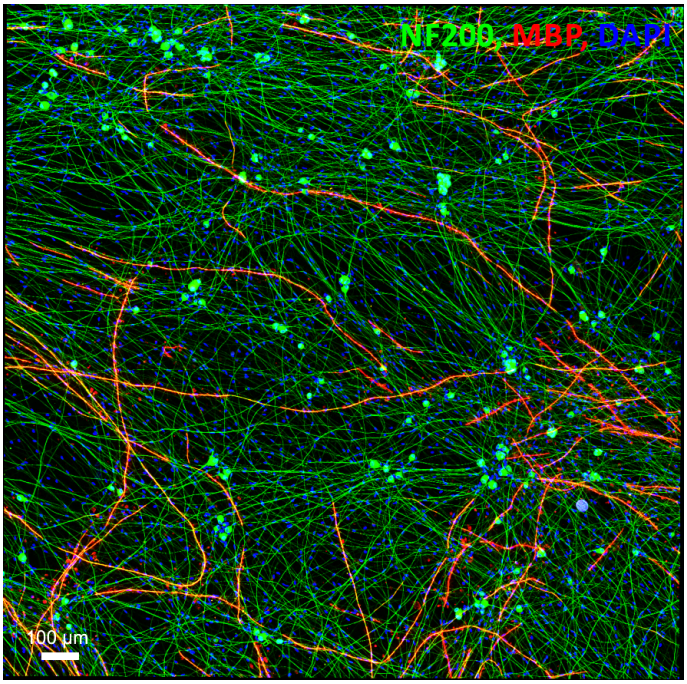


Figure 2.5. ***Myelinating co-cultures can be maintained in culture for many months.***
This image illustrates a 9 month old myelinating coculture. The neurons show no signs of cellular stress such as neurite blebbing and there are abundant MBP positive internodes throughout the culture.

2001). We therefore investigated the topographical targets and pathological effects of anti-disialosyl antibodies using two mouse IgG3 monoclonal antibodies (MOG12 and EG4) and the human IgM monoclonal, HA1. After overnight incubation, all antibodies had bound to exposed axolemma (at both the nodes of Ranvier) (Figure 2.7A and Figure 2.8A) and unmyelinated axons (Figure 2.7A and Figure 2.8B) within the mature co-cultures Nodal reactivity was sharply delimited by the paranodal junction protein Caspr indicating that tight junctions at the paranode are likely excluding access of these antibodies to the internodal regions (Figure 2.7A and Figure 2.8A). We did not observe binding to Schwann cells. After overnight incubation with either mouse or human ADAs at 10 or 100 mg/ml, the addition of normal human serum as a source of complement produced axonal deterioration and myelin blebbing within 2 h (Figure 2.7B and Figure 2.8E). These changes were not seen with antibody or normal human serum alone (Figure 2.7B, and Figure 2.8C and D). The prolonged addition of the low concentrations of mouse IgG anti-disialosyl antibodies (10mg/ ml), without normal human

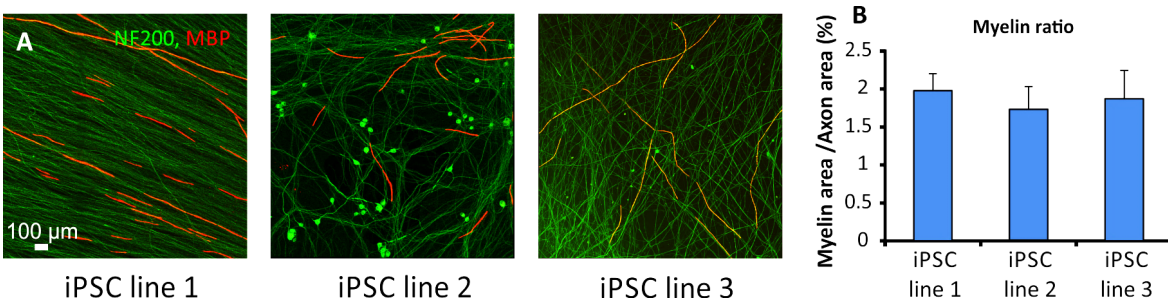


Figure 2.6. ***The levels of myelination are similar across three different iPSC lines.***

*When three different iPSC lines were separately differentiated to neurons (**A**) and myelinated with rat Schwann cells, the levels of myelination were very similar when quantified at 4 weeks (n=4 per group) (**B**). Results are reported as mean±SEM*

serum, started at the onset of myelination, significantly reduced the proportion of myelination at 4 weeks (Figure 2.7D and G) [n=3, mean (95% confidence interval, CI) reduction versus control = 66% (35% to 96%), p<0.01, one-way ANOVA with Tukey correction], without reducing the total axonal area itself (Figure 2.7D and F). Unlike the changes observed following the addition of normal human serum, this condition did not result in axonal degeneration. Likewise, there were no morphological changes in the axons after 4 weeks, when compared to control conditions without antibody (Figure 2.7H and I). Prolonged incubation with higher concentrations of mouse IgG ADAs (50 mg/ml) almost entirely prevented myelination [Figure 2.7E and G, n = 3, mean (95% CI) reduction versus control = 96% (64% to 127%), p<0.001, one-way ANOVA with Tukey correction], but also produced wide-spread irregularities in the axonal neurofilament-heavy staining (Figure 2.7E and J). There was no significant difference between the two different mouse IgG anti-disialosyl antibodies in terms of their observed effects on myelination at either the high or low concentration (both P>0.05, unpaired t-test), and these results were pooled for the final analysis. No significant effect on myelination was seen with control antibodies (normal mouse IgG, Abcam) at either high (50 mg/ml) or low (10 mg/ml) concentration (P>0.05, one-way ANOVA with Dunnett correction) (Figure 2.9).

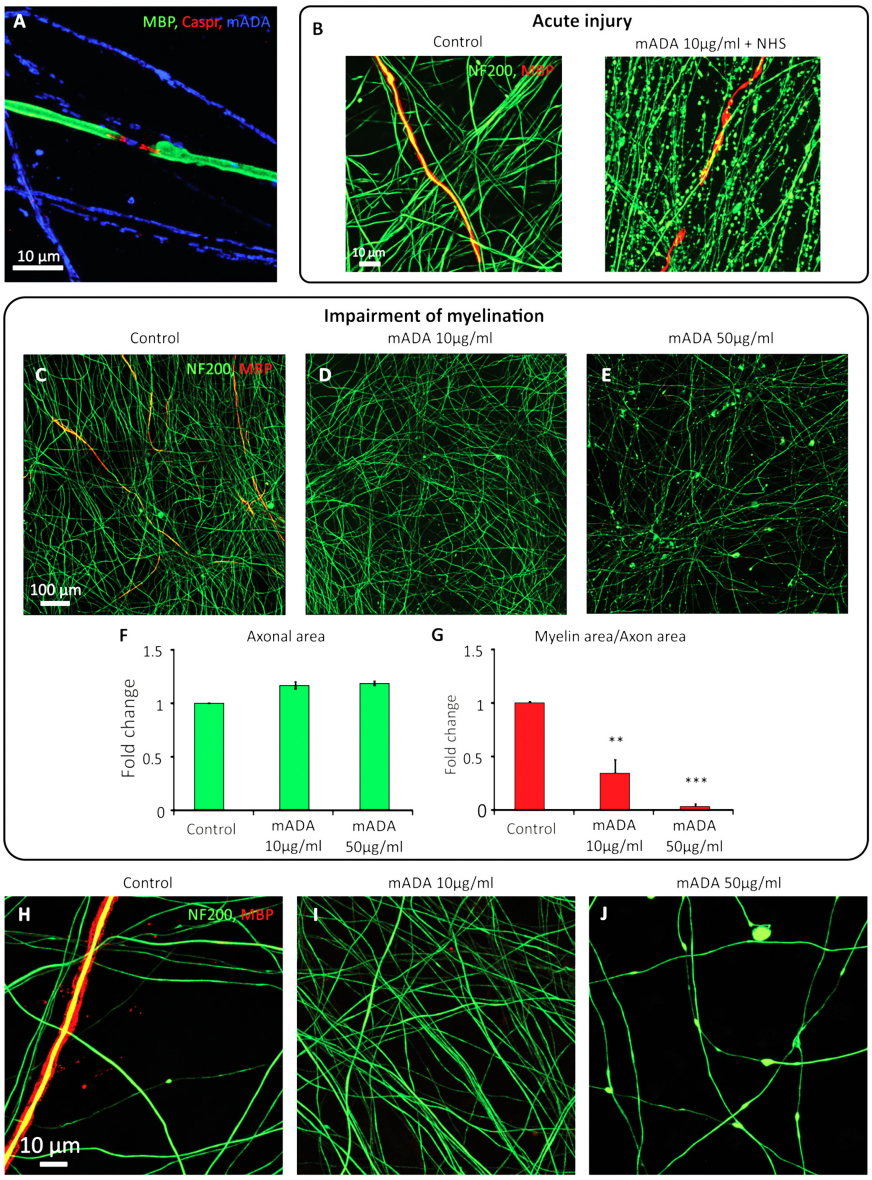


Figure 2.7. ***Mouse IgG anti-disialosyl antibodies cause acute, complement dependent axonal degeneration while prolonged application without a source of complement impairs myelination.***

*Both mouse IgG3 antibodies (mADAs, example shown is EG4, blue) bind to unmyelinated axons and the nodal axolemma, but do not cross the paranodal junction (marked by Caspr, red). (**B**) With the additional provision of normal human serum (NHS) as a source of complement, axonal degeneration can be observed after 2 h. (**C–E** and **G**) Prolonged culture with mouse anti-disialosyl antibodies without a source of complement significantly reduces the extent of myelination at 4 weeks at both low (10 µg/ml, $^{**}P<0.01$) and high (40 µg/ml EG4, 50 µg/ml MOG12, $^{***}P< 0.001$) antibody concentrations. (**F**) Axonal area in antibody-treated cultures is not reduced over this time period. Graphs show pooled data from three separate experiments using both anti-disialosyl antibodies (EG4 and MOG12). Example images were treated with MOG12 ('mADA') or myelination medium only ('Control'). (**H–I**) Axonal morphology is no different from controls after 4 weeks of continuous incubation with low dose (10 µg/ml) mouse anti-disialosyl antibodies without NHS, but (J) irregular axonal staining and blebbing is seen at 50 µg/ml.*

The prolonged addition of the human IgM monoclonal, HA1, started at the onset of myelination, likewise resulted in a dose-dependent reduction in axonal coverage by myelin at 4 weeks [n=3, (95% CI) reduction at 10 mg/ml versus control = 56% (35% to 77%), p<0.001, mean (95% CI) reduction at 50 mg/ml versus control = 75% (54% to 96%), P<0.0001, one-way ANOVA with Tukey correction]

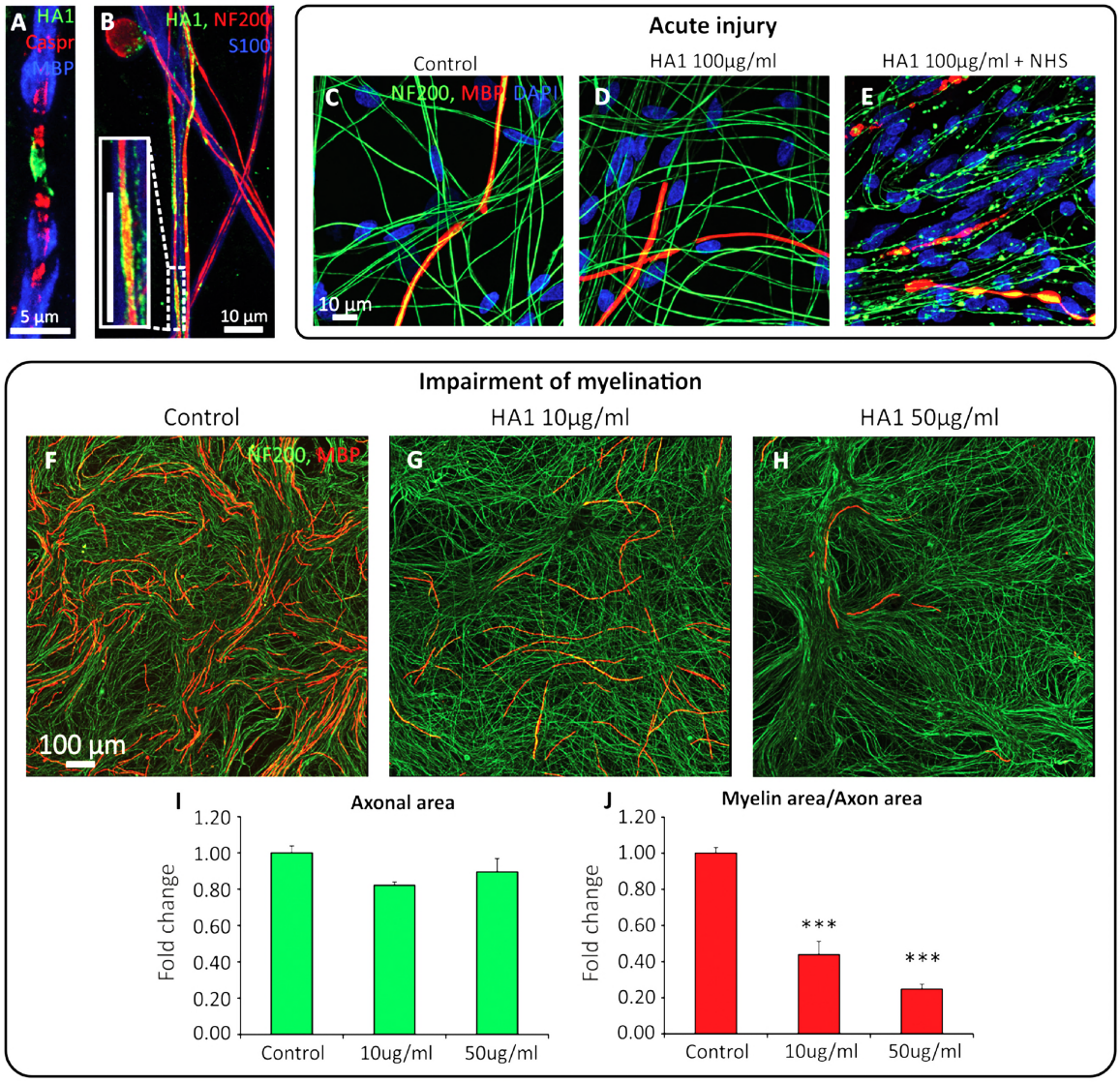


Figure 2.8. ***A CANOMAD associated human IgM anti-disialosyl antibody (HA1) also causes acute, complement dependent axonal degeneration while prolonged application without a source of complement impairs myelination.***

*(**A**) HA1 (green) binds to nodal axolemma (flanked by Caspr, red) and to (**B**) unmyelinated axons (NF200, red), without any reactivity to Schwann cells (S100, blue, n=3). (**C–E**) Short-term incubation with HA1 followed by normal human serum as a source of complement leads to (**E**) acute axonal degeneration (n=3). (**F–H**) Prolonged incubation with HA1, without provision of complement, leads to a dose-dependent reduction in myelination over 4 weeks (n= 3 coverslips per group), quantified in (**J**). No significant alteration to (**F–H**) axonal morphology or (**I**) axonal coverage was observed (*** $p < 0.001$ versus control).*

(Figure 2.8F–J). Neither antibody concentration caused visible changes to axonal morphology (Figure 2.8F–H) or a significant change in axonal area [one-way ANOVA with Tukey correction, $F(2,6) = 0.9833$, $p>0.05$] (Figure 2.8I).

2.3.5 A HUMAN ANTI-DISIALOSYL IGM ANTIBODY INDUCES DEMYELINATION

To establish whether ADAs could induce demyelination, in addition to preventing myelination, established co-cultures aged 9–12 months were used. With prolonged exposure to HA1 at 50mg/ml, numerous myelin internodes present at baseline (revealed by live cell FluoroMyelinTM staining) were absent on repeat images taken after 4 weeks (Figure 2.10B). In comparison, under control conditions, the majority of internodes remained stable over the same time period (Figure 2.10A). Higher power images revealed no differences in axonal morphology between the groups (Figure 2.10C and D). Furthermore, in HA1 treated cultures, presumed ongoing demyelination could occasionally be observed, with clumps of disintegrating myelin surrounding intact axons (Figure 2.10D). When quantified at 4 weeks, there was no significant difference in axonal area between HA1 treated and control cultures [mean (95% CI) coverage difference for HA1 versus control = 0.05 (-1.24 to 1.13), $p = 0.9039$, unpaired t-test] (Figure 2.10E). However, the extent of myelin loss (demyelination) was significantly higher in the HA1 group [mean (95% CI) increased myelin loss with HA1 versus control = 10.54% (3.92 to 17.17), $p = 0.0115$, unpaired t-test] (Figure 2.10F).

2.4. DISCUSSION

Our aim was to establish myelinating co-cultures from iPSC-derived sensory neurons and use them to investigate the physiology and pathology of axoglial interactions within the peripheral nervous system. We found that, surprisingly given the species difference, human iPSC-derived sensory neurons can be reliably and efficiently myelinated by rat Schwann cells. These co-cultures feature the expected markers of a specialized axoglial relationship, including the widespread formation of nodes of Ranvier. The cultures are also extremely stable over time, which is a significant advantage

compared to primary myelinating co-cultures, and will enable axoglial physiology and disease pathogenesis to be investigated over long time periods.

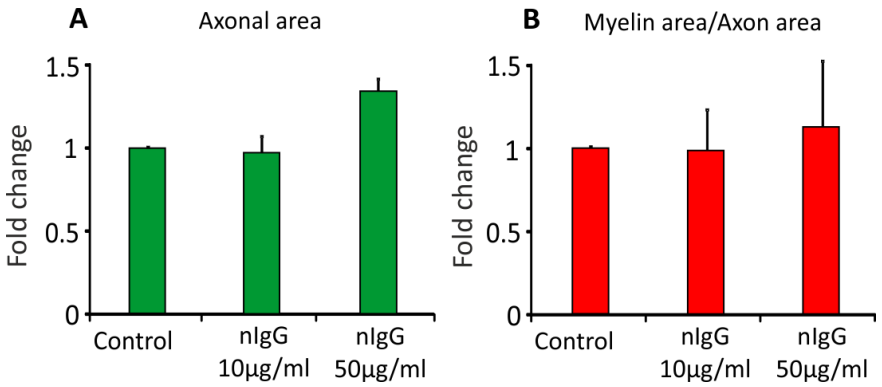


Figure 2.9. ***Prolonged (4 week) incubation with control antibodies (normal mouse IgG, nIgG) does not significantly alter either (A) axonal or (B) myelin coverage.***

iPSCs have become a fundamental tool for disease modelling, drug and toxicology screening and regenerative medicine. With the intrinsic capability of almost limitless self-renewal, the theoretical capacity to differentiate into essentially every cell type, and the potential to model a pathogenic genotype by reprogramming cells from an affected individual, iPSCs have attracted considerable attention (Soldner and Jaenisch 2012; Sterneckert *et al.* 2014; Hockemeyer and Jaenisch 2016). This led to rapid advances in the field, both in terms of reprogramming methods and in the development of novel and improved differentiation protocols for a large variety of cell types (Mertens *et al.* 2016). The differentiation protocol for sensory neurons used in the current study is exemplary (Chambers *et al*., 2012). Using a combination of five small molecular pathway inhibitors, this method produces a sensory neuronal population within 2 weeks at an efficiency of >90%. Further characterization defined these neurons as molecularly and functionally comparable to human sensory neurons derived from mature dorsal root ganglia. The protocol was originally developed with the aim of

generating nociceptors, most (but not all) of which have small diameter, unmyelinated axons. However, the neurons generated are heterogenous (Young *et al.* 2014).

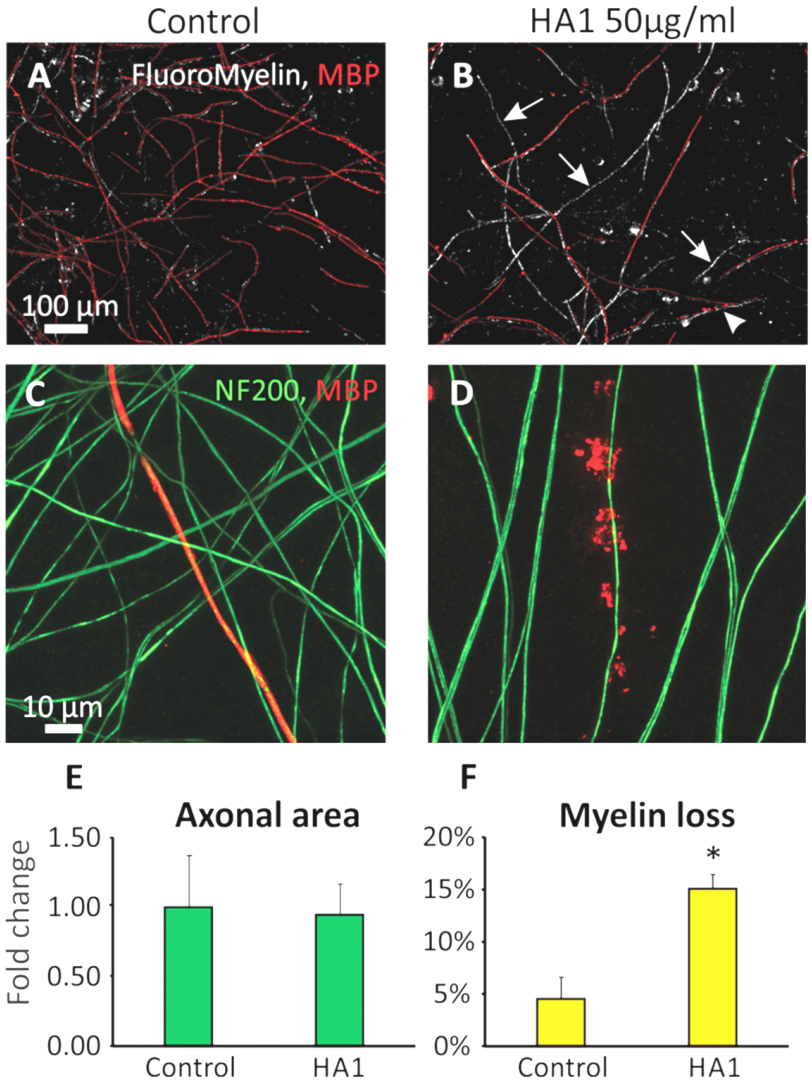


Figure 2.10. ***A CANOMAD associated human IgM anti-disialosyl antibody induces complement independent demyelination without evidence of axonal injury****.*

*(A and B) Superimposed images of the same field of view of an established myelinating co-culture 4 weeks apart. (A) Under control conditions the pattern and extent of myelination at baseline (assessed by FluoroMyelin™ staining, white) was largely maintained after 4 weeks further culture (assessed by MBP immunofluorescence, red). (C) Myelin and axons were morphologically normal in these aged co-cultures. (B) With prolonged exposure to HA1, numerous internodes present at baseline were no longer apparent after 4 weeks (arrows). In some areas (arrowhead) fragmentation of myelin could be seen. (D) At higher power in fixed tissue, myelin degeneration in such areas could be observed without loss of the underlying axon. (E) When quantified, there was no significant difference in axon area between HA1 treated and control cultures, but (F) the proportion of myelin loss was significantly greater with HA1 (*P < 0.05).*

We noted approximately a third of neurons generated using this protocol had action potential characteristics of non-nociceptive afferents (unpublished observation) and all axons were immunoreactive for neurofilament heavy chain, a characteristic of large diameter axons. We therefore investigated whether these sensory axons could be myelinated. We observed that iPSC-derived sensory neurons were indeed able to engage in the highly complex cell-to-cell interactions with Schwann cells, and successfully undergo myelination. Direct comparisons of myelination with primary co-cultures of rat DRG neurons with rat Schwann cells have not been conducted however, qualitatively the onset and nature of myelination is very similar. The longevity of our co-cultures is substantially greater than primary rat/rat co-cultures, so whilst similar levels of myelination may be initially observed after several weeks, we observe a progressive increase in myelination over time. Co-cultures could be maintained for >9 months without loss of myelin or axonal integrity (Figure 2.5), qualifying them for studies that require extremely long timeframes.

The activation of the myelination process (Figure 2.2) and the formation of nodal structures (Figure 2.3), require sequential and highly complex reciprocal cellular interaction (Salzer 2015). While many factors play a role in myelination, including cAMP, brain-derived neurotrophic factor (BDNF), Notch 1, cell-adhesion molecules, and G-protein-coupled receptors, Nrg1-ErbB signalling has been established as a key regulator of this process (Taveggia 2016), as demonstrated and further discussed in Chapter 3 of this thesis.

iPSC-based assays also offer advantages in the investigation of autoimmune diseases. Indeed, non-myelinating cultures of iPSC-derived motor neurons have recently been used to study the immunopathology of multifocal motor neuropathy associated anti-GM1 antibodies (Harschnitz et al., 2016). Dysimmune processes underlying other inflammatory neuropathies are known to target distinct topographical regions of the peripheral nerve, including the myelin sheath and specialized axonal domains formed at the node of Ranvier and flanking paranodal and juxta-paranodal domains (Devaux *et al.* 2012; Querol *et al.* 2013). These structures are not formed in pure neuronal cultures,

further highlighting the benefits of myelinating co-cultures. Currently, the specific antigen target in many inflammatory neuropathies is elusive and the exact nature of their pathology is uncertain. This is likely to be because solid phase serological assays fail to recapitulate the complex antigen environment created by cis-interactions within neural membranes, and the trans-interactions, which characterize axoglial connections and signalling. Such assays provide little to no insight into pathological mechanisms. The co-culture system thus has great promise for strengthening clinical-serological correlations, identifying new antigen targets, establishing pathological mechanisms, and testing therapeutic strategies. A further advantage of this culture system is its stability over time, facilitating the more realistic study of longer term pathological processes. Ganglioside antibodies have previously been shown to cause acute axonal deterioration in the presence of complement (O'Hanlon *et al.* 2001; McGonigal *et al.* 2010), which is again confirmed by this study. We have now shown that both mouse- and patient-derived anti-disialosyl ganglioside antibodies disrupt myelination independently of complement. The finding that these antibodies bind to the axolemma and not directly to Schwann cells emphasizes the importance of axon-derived signals in the formation and maintenance of healthy myelin. These observations correlate with the demyelinating electrophysiological pattern seen in some acute sensory neuropathies associated with anti- GD1b antibodies of the IgG class (Wicklein *et al.* 1997), and with CANOMAD (associated with IgM anti-disialosyl antibodies), which shows both axonal and demyelinating features (Willison *et al.* 2001). These antibodies not only induce demyelination, but also block *de novo* myelination in this experimental system. Anti-ganglioside antibodies have previously been shown to reduce axonal regeneration in culture (Rozés Salvador *et al.* 2016), and their persistence in patients with GBS is associated with delayed recovery (Bech *et al.* 1997). Our observations also suggest that they may impair repair associated remyelination, with potential implications for the optimal timing and duration of immunomodulatory therapy in patients. The anti-disialosyl antibodies in this study also react with GT1b, a known ganglioside ligand for myelin associated glycoprotein (MAG) providing one potential mechanism for altered axo-glial interactions (Yang *et al.* 1996). MAG is involved in the

maintenance of myelin, whereas evidence of its role in the initiation of peripheral nervous system myelination is conflicting (Owens *et al.* 1990; Owens and Bunge 1991; Montag *et al.* 1994). Mice with disrupted ganglioside synthesis do however display increased axonal degeneration and demyelination within their peripheral nerves, possibly because the ganglioside-MAG interaction is absent (Sheikh *et al.* 1999). Whether anti-disialosyl antibodies bound to axonal gangliosides block this specific signal, affect another unidentified pathway, or simply act as a non-specific physical barrier to axoglial interaction, remains to be determined.

In summary, we have developed a myelinating co-culture system using human iPSC-derived sensory neurons and rodent Schwann cells, which faithfully recapitulates the canonical markers of axoglial relationship. Additionally, this co-culture system can be used as a model system to investigate the immunopathology of the inflammatory neuropathies.

Chapter 3 | THE ROLE OF NRG-ERBB SIGNALLING IN MYELINATION AND GLIA DYNAMICS

3.1. INTRODUCTION

Myelination in the nervous system requires close and dynamic interactions between myelinated axons and their associated myelinating cells. The use of primary rodent cells (dorsal root ganglion neurons and Schwann cells) in the generation of myelinating co-cultures led to great progress in understanding the interactions between these two cell types, showing for instance that the axolemma contains a signal that could promote Schwann cell proliferation (Wood and Bunge 1975; Salzer *et al.* 1980). This was subsequently identified as neuregulin-1 (Morrissey *et al.* 1995). The type III neuregulin-1 isoform (TIIINRG1) is expressed on the axolemma of large diameter axons and signals in a juxtacrine manner (via erbB 2 and erbB 3 heterodimers expressed by Schwann cells) to promote axon ensheathment and myelination in the PNS (Garratt *et al.* 2000; Michailov *et al.* 2004; Taveggia *et al.* 2005). The expression profile of TIIINRG1 on a PNS axon determines not only whether or not an axon is myelinated, but also regulates the thickness of the myelin sheath formed by a Schwann cell, making it a key regulator of PNS myelination during development.

An investigation of Nrg1-erbB signalling in CNS myelination, however, revealed that it serves distinct functions in myelination of the PNS and CNS. Oligodendrocytes express a subset of erbB receptors (predominatly ErbB3 and ErbB4) and respond to overexpression or supplementation of *Nrg1* by increased differentiation, survival and myelination *in vitro* (Canoll *et al.* 1996, 1999; Vartanian *et al.* 1997; Flores *et al.* 2000; Lundgaard *et al.* 2013). However, extensive investigation of transgenic mouse lines with a lack or impairment of Nrg1-erbB signalling indicated that neuregulin signalling was

not essential for developmental myelination in the CNS (Brinkmann *et al.* 2008). Neither neuronal deletion of *Nrg1* nor the deletion of oligodendrocyte-specific deletion of erbB3 and erbB4 had any qualifiable effect on myelination or glia morphology or branching within the first postnatal weeks of development. In contrast, other *in vivo* studies indicate the CNS myelination can be influenced by manipulation of Nrg1-erbB signalling. Mild hypomyelinations have been reported in transgenic mice with reduced expression of TIIINRG1 (Taveggia *et al.* 2008) and transgenic mice expressing a dominant negative erbB receptor in oligodendrocytes exhibit changes in oligodendrocyte morphology, number, and function (Roy *et al.* 2007). It still unclear why a reduction in Nrg1-erbB signalling can affect CNS myelination, while its deletion has little effect. Neuregulin appears to have a diverse set of functions in CNS, including the assembly of neural networks and synaptic function and plasticity (Mei and Nave 2014), yet its role in CNS myelination remains poorly understood.

One proposed hypothesis suggests that Nrg1-erbB plays a role in adaptive, but not developmental myelination by manipulating the glia's sensitivity to electrical activity. This idea is based on the observation that oligodendroglia become sensitive to the electrical activity of DRGs in myelinating co-cultures in the presence of Nrg1-erbB signalling (via addition of an extracellular domain of Nrg1 to culture medium) by increasing the current flowing through oligodendroglia's glutamate receptors (Lundgaard *et al.* 2013). Indeed, a link between Nrg1-erbB signalling and adaptive myelination has been suggested by Makinodan and colleagues (2012), who showed that social isolation of mice in early postnatal development leads to impaired myelination in the prefrontal cortex of mice along with a reduction in *Nrg1* expression. Interestingly, this specific hypomyelination, only observed in a "critical period" of development, was phenocopied by loss of oligodendrocyte ErbB3 receptors at a similar age (Makinodan *et al.* 2012). Yet, it remains unclear if Nrg1-erbB signalling can drive adaptive changes in oligodendroglia dynamics and myelination *in vivo* and if this effect can be observed in a context other than stress through social isolation in early life.

3.1.1 AIM OF THIS CHAPTER

The aim of this chapter was to study the effect of Nrg1-ErbB signalling manipulation on myelination in the PNS and CNS. To do that we first set out to investigate the effect of Nrg1-erbB signalling manipulation in our established PNS myelinating co-cultures with iPSC-derived sensory neurons. The aims were to demonstrate that Nrg1-erbB signalling plays a key role in the PNS myelination that we observe in our mixed species co-culture model established in Chapter 2. Secondly, we aimed to establish analogous myelinating co-cultures with myelinating glia from the CNS in order to study and contrast the role of Nrg1-erbB signalling on oligodendroglia dynamics *in vitro*. Finally, we employed a mouse model that allowed the conditional ablation of *Nrg1* during adulthood (cKO-*Nrg1*). Mice lacking both copies of *Nrg1* were tested on a motor task that has previously been shown to trigger dynamic changes in the oligodendroglia dynamics, the complex running wheel (McKenzie *et al.* 2014). The aim of this study was to investigate the potential role of Nrg1-erbB signalling on experience-dependent adaptive white matter changes *in vivo*.

3.2. MATERIALS AND METHODS

3.2.1 ESTABLISHING MYELINATING CO-CULTURES

For the generation, maintenance and differentiation of iPS cells, as well as the establishment and maintenance of myelinating co-cultures with rat Schwann cells, please refer to the Material and Methods section in Chapter 2. To establish the co-cultures with oligodendrocytes, rat oligodendrocyte precursor cells (also referred to as rat glia precursor [GPC]) cells were purchased from ThermoFisher (Cat-No:N7746100). Those rat OPCs were isolated from the cortices of newborn Sprague-Dawley rats at day 2 after birth (P2). The cells were isolated under sterile conditions using dissociation and magnetic bead separation, and expanded in complete StemPro® NSC SFM containing 10 ng/mL Platelet Derived Growth Factor AA Homodimer (PDGF-AA). The cells were cryopreserved at passage 2 in 90% complete StemPro® NSC SFM with 2 mM GlutaMAX^{TM}-I supplement and 10 ng/mL PDGF-AA, plus 10% DMSO. To establish co-cultures with iPSC-derived sensory neurons, a frozen vial

of rat OPCs was thawed in warm water, centrifuged in phosphate-buffered saline (PBS) and resuspended in OPC-P medium [DMEN/Neurobasal 50:50 (Gibco), B27 supplement, Sato Mix, N-acetyl cysteine (5 μg/ml), 10ng/ml D-biotin (Sigma), Anti/Anti (Gibco), GlutaMAX (Gibco), 1 ng/ml NT-3 (R&D), 10 ng/ml PDGF-AA (R&D)]. The medium on the neuronal cultures was changed from N2 to OPC-P. Glia precursor cells (25 000 per coverslip) in a 50 ml droplet were slowly pipetted onto a single coverslip containing the iPSC-derived neurons, with care taken not to touch the coverslip with the pipette tip. Droplets containing OPCs were evenly distributed over the coverslip. Cultures were carefully put back into the incubator. The culture medium was changed 2 days later. An OPC-P medium change was performed 4 days after adding the Glia precursors.

The OPC-P medium was optimised to promote glia health and proliferation by the addition of both PDGF-AA and NT-3 (Richardson *et al.* 1988; Sim *et al.* 2009). After one week in culture, the medium of the co-cultures was switched to OPC-D medium, which contains the same reagents as the OPC-P medium, with the exception of PDGF-AA. The withdrawal of PDGF-AA with continued NT-3 supplementation has been shown to promote Oligodendrocyte differentiation (Dugas and Emery 2013a, 2013b).

3.2.2 AAV TRANSDUCTION

For AAV8-Nrg1 type-III production, rat NRG1 type-III was subcloned into an AAV vector. Type-III-β1a constructs were a gift from Dr Douglas L. Falls (Emory University, Atlanta, USA) (Wang *et al.* 2001). A 2.3kb EcoNI/PsiI insert was cloned from the original PcDNA3.1 vector into the EcoR1 site of a pAAV-CAG vector. The AAV viral packaging, CsCl purification and viral genome titration were performed by Vector Biolabs. Neuronal cultures were transduced 3 weeks after plating neurons onto coverslips. After infection, neurons were left for 7 days before the addition of Schwann cells or OPCs. The stock virus was diluted in N2 medium to the correct multiplicity of infection (MOI) based on 25000 cells per coverslip. N2 medium containing the AAV was then transferred to the neuronal cultures, and left for 3 days. An N2 plus neurotrophins medium change was performed on Days 3 and 5 after infection,

and glia cells were added on Day 7. Co-cultures were then kept in Schwann cell basal medium or OPC-P medium for 7 days, before inducing myelination (as described in Chapter 2).

3.2.3 IMMUNOCYTOCHEMISTRY AND CONFOCAL IMAGING OF CO-CULTURES

For the methods used for myelinating co-cultures with rat Schwann cells, please refer to the methods described in Chapter 2. For immunocytochemistry of co-cultures with rat OPCs, coverslips were transferred to PBS, and fixed in 1% paraformaldehyde for 20min. Cells were washed three times in PBS. Following three PBS washes, cells were blocked [5% donkey serum, 0.3% milk powder, 1% bovine serum albumin (BSA), 0.1% sodium azide, 1% dimethyl sulphoxide (DMSO)], washed in PBS, and incubated with the primary antibody overnight at 4°C. Cells were then washed with PBS, and incubated with the secondary antibody for 2h at room temperature. The secondary antibody was washed off with PBS, and the coverslips were mounted onto Superfrost Plus microscope slides (Thermo Scientific) in Vectashield mounting medium (Vector Laboratories). Primary antibodies used and their dilations are indicated Table 1). Secondary antibodies used were Alexa Fluor 568, 546, 488, 405 or Pacific Blue.

Myelination was quantified via confocal microscopy using systematic random sampling to ensure objective sampling across the coverslip. Zen Black Software (Zeiss, Germany) was used to create a digital diamond shape of 13 points (2 mm horizontal/vertical distance between each point) that was centred on each coverslip. A tile scan (each 1792 µm x 1792 µm in size, using either a 10x or 20x objective) was taken at each point, resulting in 13 non-overlapping images that equally sampled all quadrants of the coverslip (31.4% of the total area). Image analysis was performed using Fuji/ImageJ (NIH). NF200-positive surface area was taken as a measurement of axon area. MBP positive cells were counted and classified in one of two categories, (1) Intact Oligodendrocyte (Figure 3.5A), if cell body was intact and partial overlap with surrounding axons could be observed, or (2) Fragmented Oligodendrocyte (Figure 3.5B), if MBP+ surface area was fragmented and dissociating.

3.2.4 PHARMACOLOGICAL BLOCKADE OF NRG1- ERBB SIGNALLING

Pharmacological inhibition of ErbB/Nrg1 signalling was performed using the selective and irreversible ErbB inhibitor, PD168393 (7 and 70nM, reconstituted in DMSO, Calbiochem), and the β-secretase inhibitor IV (50 and 500nM, reconstituted in DMSO, Calbiochem) that binds to BACE1 active site, blocking its proteolytic activity.

Compounds were included in the cell culture myelination medium at all medium changes, at the stated concentrations. Control conditions included the vehicle of the compound (DMSO) at the same concentration. Co-Cultures with Schwann cells were cultured for 4 weeks with twice weekly medium changes before fixation and image processing. Co-cultures with OPCs were cultured for 3 weeks with twice weekly medium changes before fixation and image processing.

3.2.5 ANIMALS

All animal work carried out conformed to UK Home Office legislation (Scientific Procedures Act 1986). CAG-Cre-ER^{TM}; Nrg1$^{fl/fl}$ mice and Nrg1$^{fl/fl}$ were bred by crossing Nrg1$^{fl/fl}$ mice with CAG-Cre-ER^{TM} mice [JAX(r) mice 004682], respectively; as described previously (Cheret *et al.* 2013; Fricker *et al.* 2013; Bartus *et al.* 2016). CAG-Cre-ER^{TM}; Nrg1$^{fl/fl}$ mice had a C57Bl6 background and both sexes were used for the experiment. The generation and genotyping of mutant mice with floxed alleles of *Nrg1* (Nrg1$^{fl/fl}$) mice has previously been described (Yang et al., 2001; Brinkmann et al., 2008; Fricker et al., 2013). These mice are null for α-isoforms of *Nrg1* in the absence of Cre recombination as they carry a premature stop codon in exon 7, which encodes the α-EGF domain (Li et al., 2002). The loxP sites flank exons 7–9, and exon 8 encodes the β-EGF domain. Cre recombination therefore results in ablation of all remaining β isoforms. To detect the CAG-Cre-ER^{TM} construct, PCR of genomic DNA was carried out (Primer details: Forward: 5'-CTCTAGAGCCTCTGCTAACC-3', Reverse: 5'-CCTGGCGATCCCTGAACATGTCC-3'). In CAG-Cre-ER^{TM} mice, a tamoxifen inducible form of Cre recombinase is expressed ubiquitously, driven by a chimeric promoter constructed from a cytomegalovirus intermediate-early enhancer and a chicken β-actin promoter/enhancer (Hayashi

and McMahon 2002). CAG-Cre- ER^{TM} expression and induction was previously evaluated in our laboratory group (Fricker *et al.* 2013) and other groups (Meyer and Birchmeier 1995). In short, tamoxifen administration leads to a ubiquitous deletion of *Nrg1* in almost all cell types, including cells of the PNS and CNS.

3.2.6 TAMOXIFEN TREATMENT BY ORAL GAVAGE

Tamoxifen (Sigma T5648) was dissolved at 40 mg/ml in corn oil on a shaker overnight at room temperature (RT) and by subsequent sonicating at 21°C for one hour. Nrg1$^{(-/-)}$ mice were generated by administering tamoxifen (0.25mg/g body weight in corn oil) by oral gavage for five consecutive days to CAG-Cre- ER^{TM}; Nrg1$^{fl/fl}$ mice, starting at P82-84. After this treatment, animals were left for at least 3 weeks before experimental procedures. Tamoxifen control animals from the same batch were used for comparison, which contained the floxed alleles of the *Nrg1* gene (Nrg1$^{fl/fl}$), but not the CAG-Cre-ER^{TM} regions. During, and for a week after tamoxifen treatment, nutritious jelly and mash were provided for all mice to prevent excessive weight loss due to adverse effects of the drug.

3.2.7 BEHAVIOUR TESTING

Experimenters were kept blinded to the genotype of the animals until all experimental procedures had been carried out. Wherever possible, we included equal numbers of animals of each gender in each experimental group. All mice were maintained on a 12-hour artificial light-dark cycle (9:00 – 21:00). Food and water was provided *ad lib.*

3.2.7.1 Complex Running Wheel

Cages with running wheels were purchased from Lafayette Neuroscience (SCURRY MOUSE MISSTEP WHEEL Model 80821S). This voluntary running wheel cage comes equipped with a wheel (circumference = 0.389 m) that allows individual rungs to be removed to create a complex wheel or rung configuration (Liebetanz *et al.* 2007; McKenzie *et al.* 2014). The mice were provided with a "complex wheel" (CW) with 16 out of 38 rungs removed to create a wheel with an irregular pattern of 22-rungs (Figure 3.1), a configuration that was adapted from (McKenzie *et al.* 2014). For behaviour

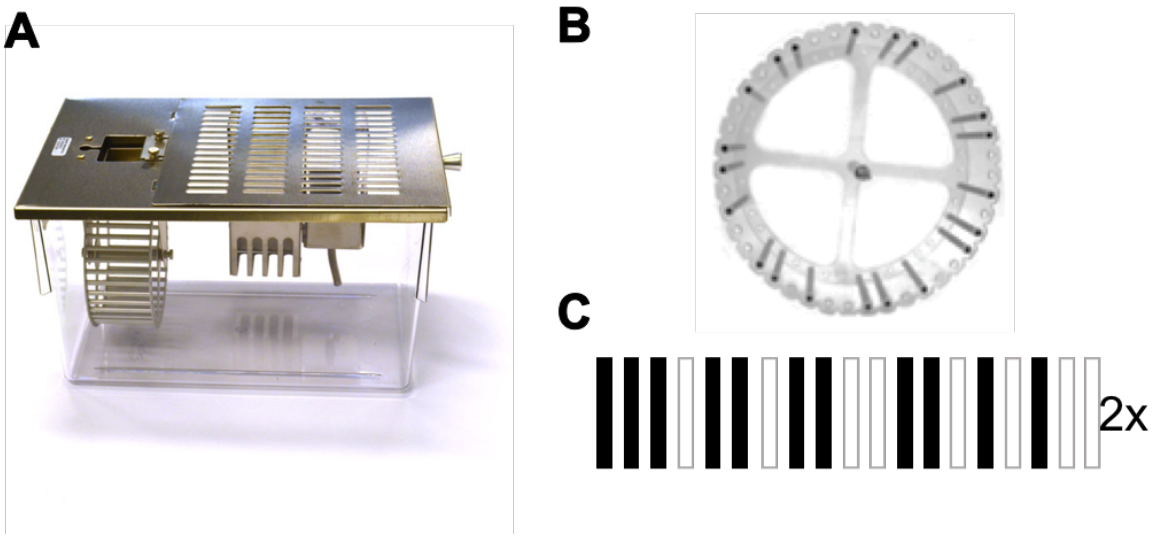


Figure 3.1. ***Equipment used for behavior testing with a complex wheel.***

(A*) Image of the cage in which mice were single house during the behavioral experiment.* ***(B)*** *A complex running wheel was created by removing 16 of the 38 potential rugs.* ***(C)*** *This created an irregular sequence of 11 rugs with varying gabs between them, which was repeated ones.*

testing, mice were single caged with the running wheel, a paper house filled with nesting material and wood chippings to cover the floor of the cage. Mice were accustomed to the cage for 30 mins before being provided access to the running wheel by removing a dividing wall to the compartment where the wheel was located. Mice were placed in the wheel cages up to 2 hours before the start of the dark period. Mice ran spontaneously, without artificial reward. Food and water were available *ad lib* within the specialised running wheel cages.

Infrared sensors recorded wheel rotation, which allowed computer-controlled recording of wheel rotation as a function of time for more than 20 cages simultaneously for 24h a day (The Scurry Activity Monitoring Software, Lafayette Neuroscience, Model 86165). For data analysis, counts of full wheel rotations were exported into a spreadsheet and divided into time bins of 10 seconds. The following running parameters were derived from the baseline activity data: 1) Distance travelled, which represents the total number of wheel rotations × wheel circumference. 2) Active Intervals, which represent the number of 10 second intervals in which at least one full wheel rotation was recorded.

3) Average speed, which represents the sum of the distance run divided by the number of active intervals, multiplied by 6 to measure m/min. 4) Maximum speed, which was calculated by determining the average speed in the 1% of fastest intervals run 5) Cruising speed, which was acquired by calculating the mode of the fastest 50% of intervals run by the animal. This metric was calculated to measure the most frequent speed at which an animal ran during their fastest running periods.

3.2.7.2 Criteria for excluding animals from complex wheel data analysis

Previous experiments reveal that a small subset of healthy untreated animals show unusually low engagement in voluntary wheel running. To prevent such outliners to skew overall group performance and increase the variability within the sample, we set the following pre-determined exclusion criteria for analysis of complex wheel behaviour performance: animals were excluded from the analysis if: 1) they ran less than 1km in 8 Days, or 2) ran less than 100 meters per day for at least half of the days recorded. One animal from each group met the predetermined exclusion criteria due to a consistent lack of running behavior. Running wheel data without sample exclusion is presented in Supplementary Figure 1.

3.2.8 EdU SUPPLEMENTATION IN DRINKING WATER

To investigate cellular proliferation *in vivo*, we administered 5-ethynyl-2'-deoxyuridine (EdU, Invitrogen) in the drinking water (0.2 mg/ml) for 12 days, starting 4 days before behaviour testing. Drinking water containing EdU was protected from light and replaced with a newly prepared solution every 4 days.

3.2.9 HISTOLOGICAL ANALYSIS OF BRAIN TISSUE

3.2.9.1 Perfusion of animals and tissue processing

Animals were deeply anaesthetized (Euthatal: 80mg/kg, i.p) with sodium pentobarbital and transcardially perfused with 10 ml PBS, followed by 30 ml paraformaldehyde (4% w/v in 0.1 M phosphate buffer) with the help of a perfusion pump (Flow rate: 4ml/min). The brain was dissected

out of the skull and was post-fixed in paraformaldehyde (4% w/v in 0.1M phosphate buffer) for 30 mins at room temperature, then overnight (~16 hours) at 4°C. Brain tissue was subsequently cryoprotected in 30% Sucrose PBS solution until tissue no longer floated in the solution. The tissue was then embedded in OCT and frozen on dry ice before being stored at -80°C until further processing.

3.2.9.2 Immunohistochemistry of free-floating brain sections

For Immunohistochemical analysis, coronal cryosections (30 μm) were cut (anterior to posterior) from the first section at which the anterior corpus callosum was visible and continuously connected from one hemisphere to the other. Brain sections were collected and washed in Tris-buffered Saline (TBS; Sigma) and processed as floating sections. All incubations and washes were performed on a shaker at 60 rpm. Sections were blocked in TBS containing 10% Normal Goat Serum (Sigma), 0.5% Triton-X (Sigma) and 1% BSA for 2 hours at room temperature. The primary antibody was directed against platelet-derived growth factor receptor alpha (anti-PDGF-Rα, rabbit, New England Biolabs, 1:400 dilution), which was diluted in TBS containing 10% of the blocking solution (see above) at 4°C. After washing steps, AlexaFluor-488 Click-iT detection kit (Invitrogen) was used for EdU labelling, following the manufacturer's instructions. Samples were then incubated with corresponding fluorophore conjugated secondary antibodies (1:500, Alexa FluorO-488 or 546, Thermo Fischer Scientific), diluted in blocking solution (1:10) for 2h at room temperature. Samples were mounted and dried for ~10 mins before being sealed under a glass cover with Vectorshield anti-fade mounting medium (Vectorshield laboratories) and viewed by a Zeiss L subse SM-700 confocal microscope and ZEN software. Cells were counted in low-magnification photo-micrographs (x20 objective) of non-overlapping fields of coronal sections (320μmx320μm each) of the corpus callosum, between the dorsolateral corners of the lateral ventricles (6 fields per section, three sections per animal), as illustrated in Figure 3.10A. The surface area of corpus callosum was calculated for each animal to determine cellular density. Image analysis was performed using Fuji/ImageJ (NIH).

3.2.10 STATISTICS

Statistical analysis was performed using IBM SPSS Statistics for Mac (Version 25). The experimental units (means n) of analysis for the presented *in vitro* experiments represent separate individual coverslips from the same neural differentiation, unless otherwise specified. Student's t-test was used for comparison of two groups, one-way ANOVA using Dunnet's t *post hoc* correction was used for more than two groups and for subsequent pair-wise comparisons against the control condition. A repeated mixed ANOVA was used to analyse behaviour performance on the complex wheel, including Sex and Age at Behaviour testing as categorical and continuous variables, respectively. Two-way ANOVAs were run to examine the effect of running (CW vs Home Cage) and genotype ($Nrg1^{(+/+)}$ vs $Nrg1^{(-/-)}$) on cell density.

3.3. RESULTS

3.3.1 OVEREXPRESSION OF NRG1 TYPE III INFLUENCES LEVELS OF MYELINATION

Neuregulin 1 Type 3 (TIIINRG1) expression at the axonal surface has been established as one of the key regulators of myelination. To investigate the role of TIIINRG1 in the present co-culture system, human iPSC-derived neurons were transduced with an AAV containing a TIIINRG1 construct at a range of MOIs ($1x10^4$ to $1x10^6$, Figure 3.2B–D). Viral transduction was well tolerated by iPSC-derived neurons, as no difference in axon area (Figure 3.2E; one way ANOVA, $F(3,17) = 1.103$, $p>0.05$) or visible signs of cellular stress were observed across different MOI conditions (Figure 3.2A–D). Neuronal overexpression of TIIINRG1 type caused a significant increase in the formation of myelin at 4 weeks (Figure 3.2F), when assessed for statistical significance using a one-way ANOVA $F(3,17) = 47.87$, $p<0.001$) with *post hoc* pairwise comparison using Dunnett's t correction. This represents a 4.8-fold and 13-fold increase in myelination relative to control with $1x10^5$ and $1x10^6$ MOI, respectively. Full-length (FL) and the cleaved-terminal fragment (CTF, formed following proteolytic processing) of TIIINRG1 protein expression was increased in the $1x10^5$ and $1x10^6$ MOI condition compared to untransduced basal expression (Figure 3.2G), which significantly increased the levels of

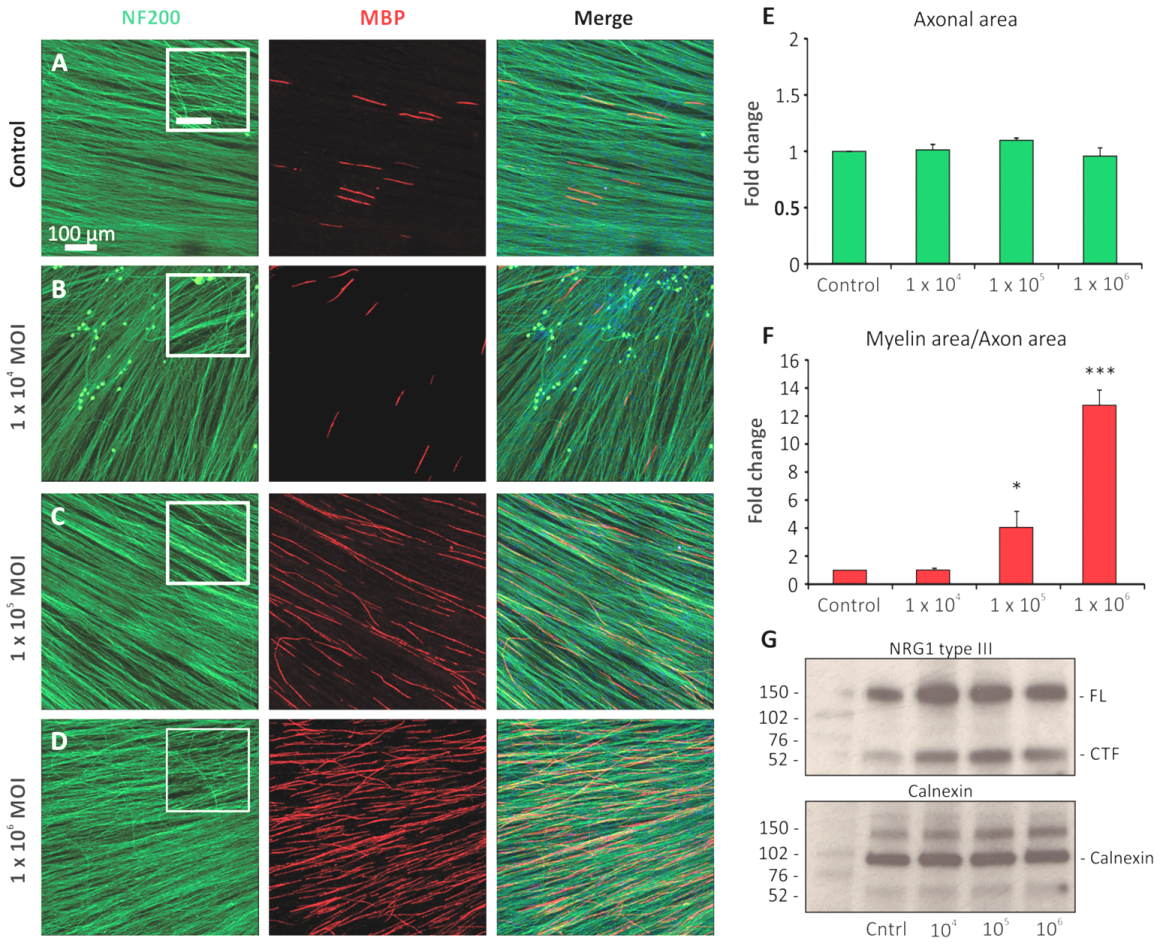


Figure 3.2. ***Overexpression of TIIINRG1 significantly increases myelination in the co-cultures.***

(A–D) *Human iPSC-derived neurons were transduced with an AAV containing a TIIINRG1 construct at a range of MOI's. Cultures were fixed for immunocytochemistry or lysed for protein extraction at 4 weeks post-induction of myelination.* ***(E)*** *Viral transduction had no effect on axonal outgrowth or morphology, with no visible signs of neurite blebbing (insets in* ***A–D****). Scale bar = 50 µm.* ***(F)*** *Myelination was similar in* ***(A)*** *untransduced and (B) 1 × 10^4 MOI conditions, whereas a significant and dose dependent increase in myelination was observed in* ***(C)*** *1 × 10^5 (*p < 0.05) and* ***(D)*** *1 × 10^6 (***p < 0.001) conditions, if compared to the control condition. Data presented as Mean ± SD* ***(G)*** *In the transduced neurons, western blot shows the increase in both the full-length (FL) (135 kDa) and cleaved-terminal fragment (CTF) (60 kDa) of TIIINRG1 compared to untransduced control. The calnexin control demonstrates an even protein loading across conditions. Statistical test used was a one-way ANOVA using Dunnett's post hoc correction.*

myelination in both conditions (Figure 3.2F). Interestingly, viral transduction with 1x10^4 MOI concentration led to some increase in the protein levels of both the full-length and cleaved-terminal fragment (Figure 3.2G), without significantly influencing the levels of myelination (Figure 3.2F) suggesting a possible threshold effect. Furthermore, assessing total *Nrg1* levels is only a partial reflection of TIIINRG1 protein at the axoglial interface.

3.3.2 PHARMACOLOGICAL BLOCKADE OF NRG1-ERBB SIGNALLING LEADS TO IMPAIRED MYELINATION

Neuregulins belong to the family of EGF domain-containing proteins and interact with and activate receptor tyrosine kinases of the ErbB family expressed by Schwann cells (ErbB2 and ErbB3). The selective and irreversible ErbB inhibitor PD168393 was used to block ErbB receptors and prevent TIIINRG1 signal transduction. As expected, a dose-dependent reduction in myelination was detected in the presence of PD168393 (Figure 3.3B, C & F) [one-way ANOVA, $F(2,14) = 14.87$, $p<0.001$, *post hoc* analysis (Dunnet's t)]. TIIINRG1 requires proteolytic cleavage by proteases to expose its active EGF-domain (Hu *et al.* 2006; Willem *et al.* 2006; Fleck *et al.* 2013). The cell-permeable isophthalamide that binds to BACE-1 active site was used to block its proteolytic activity (referred to as 'BACE-1'). The presence of the BACE1 inhibitor significantly reduced myelination when compared to the control conditions (Figure 3.3D–F) [ANOVA, $F(2,13) = 7.421$, $p<0.01$]. These results indicate that interference with Nrg1-ErbB signalling reduced myelination in our co-culture system. Neither the ErbB inhibitor (ANOVA, $F(2,14) = 2.311$, $p> 0.05$) nor the BACE1 inhibitor (ANOVA, $F(2,13) = 1.452$, $P>0.05$) had a measurable effect on axonal density (Figure 3.3B–E). To assess whether the pharmacological blockade of NRG/ErbB signalling led to a reduction in Schwann cell numbers, we quantified the number of DAPI positive cell nuclei in our cultures, of which only the Schwann cell ones should vary due to treatment. While PD treatment had an overall effect on the number of DAPI positive nuclei in the culture (One-way ANOVA; $F(2,13)=10.877$, $p=0.02$) *post hoc* analysis (Dunnet's t) indicated that only the highest concentration of PD168393 resulted in a reduction in overall cell numbers (Figure 3.3G). This is consistent with the fact that Nrg1 promotes Schwann cells proliferation via ErbB signalling. When we assessed the protein levels of the full-length and cleaved-terminal fragment of TIIINRG1 after neurons have been treated with the BACE1 inhibitor, we found indication that there was a reduction in the amount of cleaved-terminal fragment, and an increase in the full-length levels with both concentrations of BACE1 inhibitor. This corresponds to the inhibition of the proteolytic cleavage of full-length TIIINRG1, resulting in an accumulation of the full-length (FL) and a reduction

in the cleaved-terminal fragment (CTF). Similar results were observed when assessing full-length and cleaved fragment levels in the Bace1$^{-/-}$ mouse (Hu *et al.* 2006; Willem *et al.* 2006).

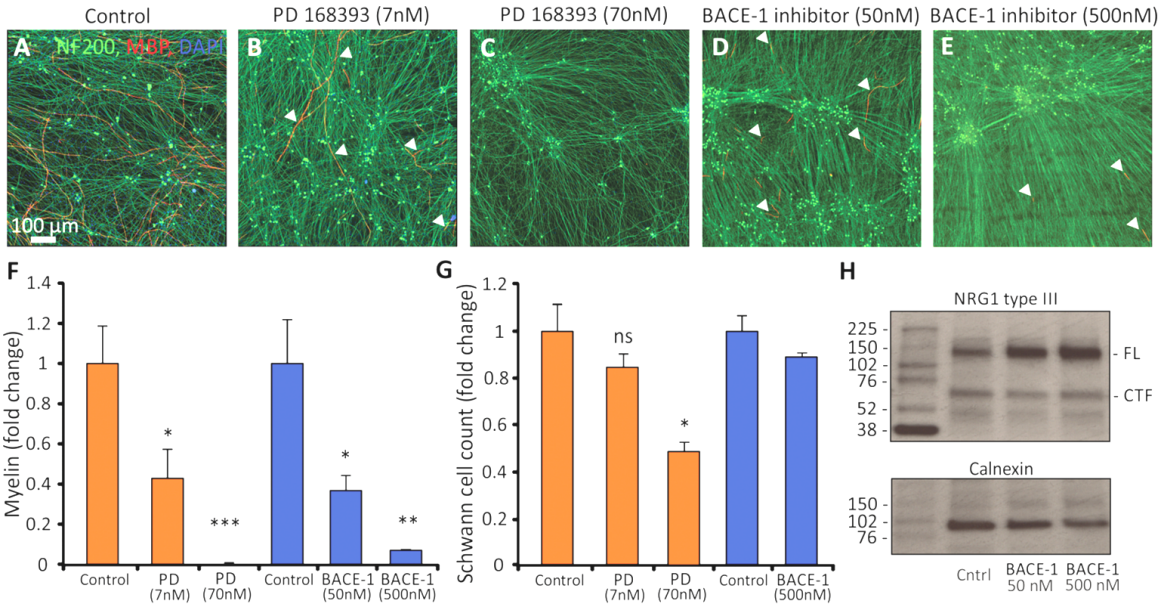


Figure 3.3. ***Pharmacological blockade of NRG1/ErbB signalling impairs myelination in the human/rat co-cultures.***

Irreversible blockade of ErbB receptors with PD168393 at (B) 7 nM and (C) 70 nM dose-dependently reduces the formation of MBP positive internodes compared to ***(A)*** *control cultures. Inhibition of the ß-secretase protease (BACE1) with* ***(D)*** *50 nM and* ***(E)*** *500 nM also results in a dose-dependent reduction in the formation of myelin. The few remaining myelin internodes are indicated in* ***B, D*** *and* ***E*** *with arrowheads.* ***(F)*** *Quantification of the myelin levels relative to an internal control (n=3-4).* ***(G)*** *Schwann cell numbers are reduced only with the highest concentration of PD168393 (n=3-4).* ***(H)*** *Treatment of iPSC-derived sensory neurons with BACE1 results in an accumulation in full-length (FL) TIIINRG1, and a reduction in the cleaved-terminal fragment (CTF). Data presented as Mean ± SD. Statistical test used was a one-way ANOVA using Dunnett's post hoc correction in pairwise comparison. Asterisks indicate statistical significance in post hoc analysis : ***p<0.001. **p<0.01, *p<0.05.*

3.3.3 Establishing co-cultures with rat OPC and human iPSC-derived sensory neurons – Pilot study

The basic concept of establishing co-cultures with iPSC-derived sensory neurons was adapted from the co-cultures with rat Schwann cells (see Chapter 2). A schematic illustration of the experimental sequence can be found in Figure 3.4A. The culture medium was adapted from work that had successfully established myelinating co-cultures between primary dorsal root ganglion cells and primary oligodendroglia cells (Wang *et al.* 2007; Pang *et al.* 2012; Lundgaard *et al.* 2013). Initially,

sensory neurons were first differentiated using the previously published protocol (Chambers *et al.* 2012), as described in Chapter 2 (Figure 2.2A). After allowing the neurons to mature and grow widespread neurite processes for 3 weeks, rat OPCs were added in suspension. For the first week in co-culture, the culture medium was supplemented with both PDGF-AA and NT-3 to encourage OPC proliferation. PDGF-AA was subsequently withdrawn from the medium to promote OPC differentiation (Dugas and Emery 2013a). Cells staining positive for the Oligodendrocyte marker MBP were widespread across the culture after 3 weeks (Figure 3.4B). The MBP-positive area was predominantly co-localized with NF200 positive axons, indicating close interaction between glia and axons (Figure 3.4C and D). Cells positive for the Astrocyte marker glia fibrillary acidic protein (GFAP) were also detected (Figure 3.4E), indicating that a subset of OPCs differentiated into Astrocytes. This kind of bi-polar differentiation potential of OPCs is well established (Dimou and Gallo 2015). Neuronal and axonal health did not seem to be adversely affected by the medium conditions or presence of glial cells, as no visible signs of cell death or neurite blebbing was observed (Figure 3.4B-E).

While we observed many MBP-positive Oligodendrocytes with intact cell morphology (Figure 3.4C,D; Figure 3.5A) that was comparable to images provided by other laboratories (e.g. Lundgaard et al., 2013), we also observed a large amount of MBP-positive cells with a seemingly fragmented cell morphology (Figure 3.5B). Altering the fixation protocol (e.g. percentage of PFA, time or temperature of fixation) did not alter the fact that those two distinct cell morphologies could be found in the same culture, making it unlikely to be result of a fixation artefact. To determine the fraction of “intact” to “fragmented” Oligodendrocytes, the cultures (n=3 with counts given as Mean±SD across cultures) were immunolabeled with antibodies against MBP (to identify differentiated oligodendrocytes) and NF200 (to identify the sensory neurons) after 3 weeks in culture (Figure 3.5). MBP-positive cells were classified as “fragmented” if MBP-positive surface area was present and localised in a specific area but was broken up in different fragments. Quantification revealed that the number of MBP-positive

cells with fragmented morphology (M=41±SD=3) was about equal to the number of intact and healthy looking MBP-positive oligodendrocytes (M=44±SD=9.54)(Figure 3.5D).

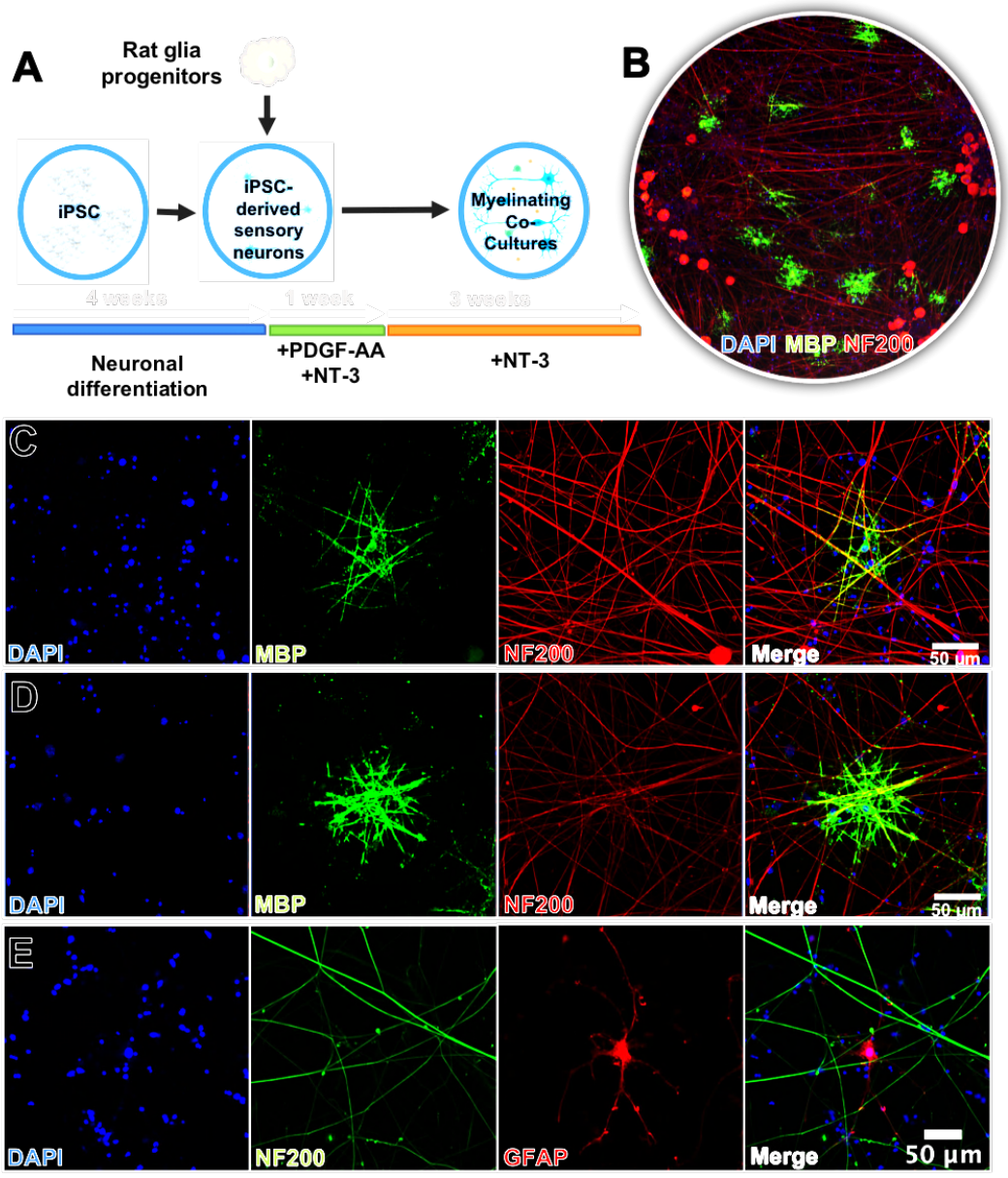


Figure 3.4. ***Co-cultures of rat OPCs and iPSC-derived sensory neurons.***

(A) *Schematic illustration showing the establishment of the myelinating co-cultures with rat OPCs.* ***(B)*** *MBP positive cells were abundant throughout the co-cultures after 2 weeks in culture.* ***(C, D)*** *Representative images of MBP positive oligodendrocytes found in the co-cultures. MBP positive stain colocalised with NF200 positive axons, indicated a close interaction between Oligodendrocytes and axons.* ***(E)*** *Example of a GFAP-positive astrocytes, which were also present in the culture at 2 weeks.*

3.3.3.1 Oligodendrocytes did not remain stable over time in established co-culture conditions

We set out to test the stability of the co-cultures and the reproducibility of the experimental paradigm by setting up another batch of co-cultures with rat OPCs. As with the PNS myelinating co-cultures, we tested how the co-cultures developed over time. MBP-positive cells were quantified (n=3 coverslips per condition, with cell counts reported as Mean±SD) at week 1, 2 and 3, and were classified as either "fragmented" or "intact". Representative images of co-cultures at week 2 and 3 are shown in Figure 3.6A and B, respectively. No MBP-positive cells were present in the co-cultures after one week in co-culture. After two weeks, the number of fragmented OLs per mm^2 (3.11±0.21) was larger than the number of intact OL (1.47±0.31). After 3 weeks, the number of fragmented OLs (1.95±0.27) was reduced when compared to week 2 and very few intact OLs were detected (0.58±0.16), yet some were still present (Figure 3.6C). Differences were tested statistically using a mixed model ANOVA, with the independent variables (IV) of Cell Morphology (two levels; Fragmented, Intact) and Week (two levels: Week 2, Week 3). There was a significant main effect of Week ($F(1, 4) = 484$, $p<0.001$), indicating that cell numbers were not stable, but that cells were lost over time. There was also a significant main effect of Cell Morphology ($F(1, 4) = 48.65$, $p<0.01$), with significantly more fragmented cells in the co-cultures than intact ones. Additionally, an independent t-test revealed a significant difference between the total number of MBP-positive cells per mm^2 at 3 weeks between first experiment (M=6.22, SD=.89, Figure 3.5) and second experiment (M=2.52, SD=.39, Figure 3.6) conducted ($t(4)=6.59$, $p<0.01$), indicating that the numbers of OPCs that differentiated into MBP-positive oligodendrocytes were not consistent between the experiments. Astrocytes were still present in the co-culture system (Figure 3.6E).

3.3.3.2 Manipulating Nrg1-ErbB signalling in co-cultures with rat Oligodendroglia

Neuregulins belong to the family of EGF domain-containing proteins and interact with and activate receptor tyrosine kinases of ErbB3 and ErbB4 expressed by Oligodendroglia cells. To test whether

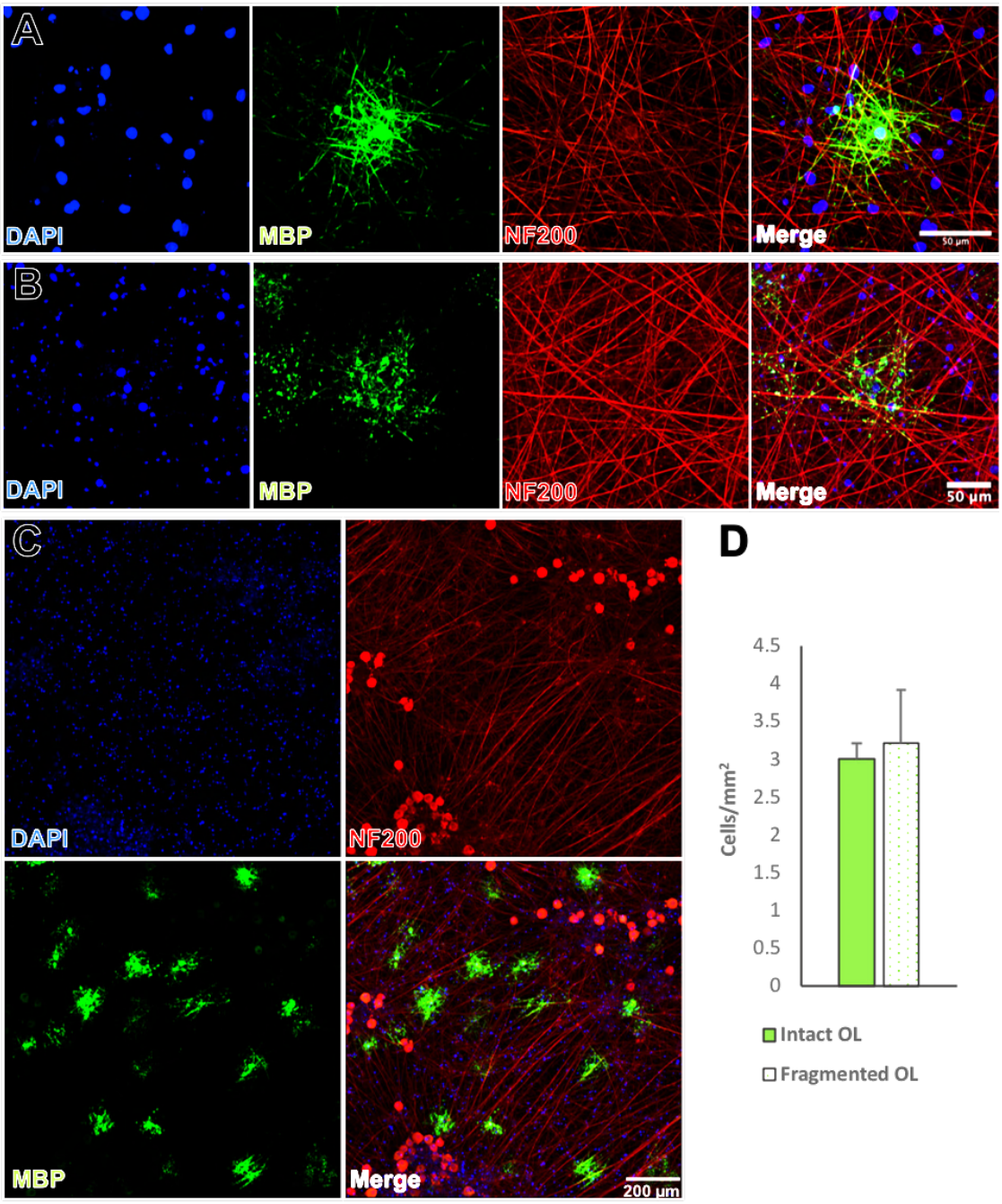


Figure 3.5. ***Co-cultures in the pilot experiment contained both intact and fragmented Oligodendrocytes.***

(A) *A representative image of an MBP-positive Oligodendrocyte cell with an non-fragmented intact cell morphology.* ***(B)*** *Representative image of an MBP-positive Oligodendrocyte with clear signs of a fragmented cell morphology.* ***(C)*** *Representative of image used for quantitative analysis of co-cultures after 3 weeks in culture.* ***(D)*** *Quantification of the density of "intact" and "fragmented" Oligodendrocytes (OL) after 3 weeks in co-culture. n=3 coverslips per group. Data presented as Mean±SD.*

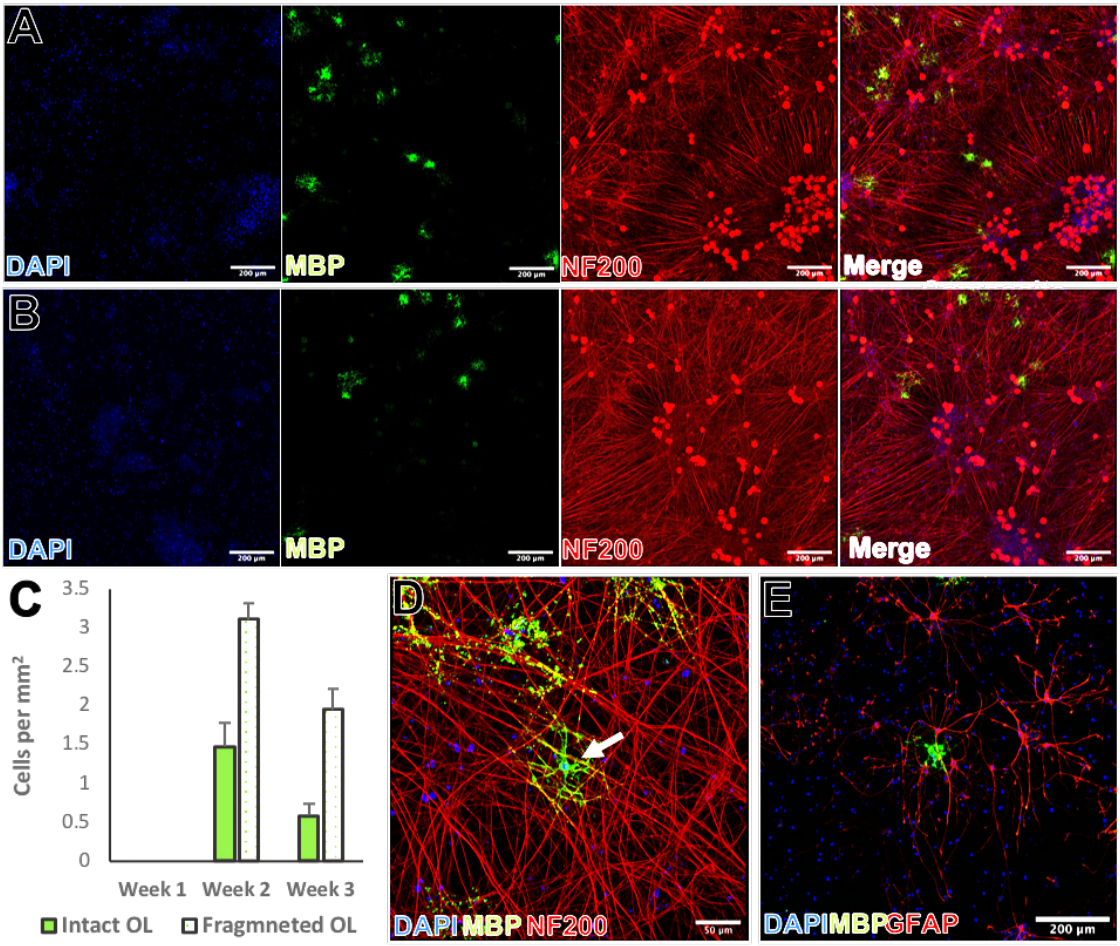


Figure 3.6. ***Oligodendrocyte do not remain stable across experiments.***

Representative images of the co-cultures after ***(A)*** *2 weeks and* ***(B)*** *3 weeks in co-culture (scale bar = 200 µm).* ***(C)*** *Quantification of the density of "intact" and "fragmented" Oligodendrocytes (OL) over the 3 weeks in co-culture. n=3 coverslips for Week 2. n=4 coverslips for Week 3. . Data presented as Mean±SD.* ***(D)*** *High magnification image of co-cultures, showing an "intact" oligodendrocyte at week 3 (white arrow), next to several other MBP-positive cells with fragmented cell morphology.* ***(E)*** *GFAP-positive Astrocytes were also observed in the co-cultures. The images represents an area with especially high astrocyte density*

manipulation of neuregulin 1 Type III-ErbB signalling influences oligodendroglia dynamics and integrity, we set up an experiment in parallel to the one described in the previous paragraph (Section 3.3.4). For a schematic experimental design please refer to Figure 3.7A. To investigate the role of TIIINRG1 in the present co-culture system, human iPSC-derived neurons were transduced with an AAV containing a TIIINRG1 construct at $5x10^5$ MOI one week before co-culturing (NRG1 condition). PD168393 (PD; 7ng/ml) was used to block ErbB receptors and prevent Nrg1 signal transduction from

the first day of co-culture. A control condition received normal culture medium. Cell proliferation was measured by 5-ethynyl-2'-deoxyuridine (EdU) supplementation (10 nM) to the culture medium (n=4 coverslips per condition) for the first week of co-culture. Co-cultures were then fixed and analysed with immunocytochemistry (Figure 3.7). The mean number of EdU+ cells (per mm^2) was lower in the control condition (M=35.22±SD=9.12) and PD condition (M=39.33±SD=14.29) when compared to the NRG1TIII condition (M=53.24±SD=12.47), as depicted in Figure 3.7C, yet statistical analysis (One-way ANOVA) found no significant difference between the three conditions ($F(2, 11) = 2.41$, $p=0.114$). The total number of DAPI positive cell nuclei per mm^2 was similar between the groups (Figure 3.7D). To analyse OPC differentiation, co-cultures were fixed and stained for MBP, NF200 and DAPI, as shown in Figure 3.6. Low numbers of "intact" OLs were detected in both conditions. A one-way ANOVA revealed no significant difference in the amount of intact OLs between conditions ($F(2, 8) = 0.731$, $p=0.520$), indicating that Nrg1-erbB signalling had no effect on oligodendrocyte survival or differentiation (Figure 3.7E). Viral transduction or PD supplementation had no effect on axonal area (Figure 3.7F).

In summary, established co-cultures of rat Oligodendrocyte precursor cells and human iPSC-derived sensory neurons did show the presence of MBP-positive oligodendrocytes aligning with axons. However, an equal or larger number of MBP-positive cells were visibly fragmented, and the overall numbers of MBP-positive cells was not consistent between experiments or timepoints. This observed variability together with the low number of viable Oligodendrocytes detected in different experimental conditions made it clear that the established co-cultures system, at its current stage of method development, was not a suitable and viable *in vitro* model to study the potential effect of the Nrg1-ErbB signalling manipulation on oligodendroglia dynamics.

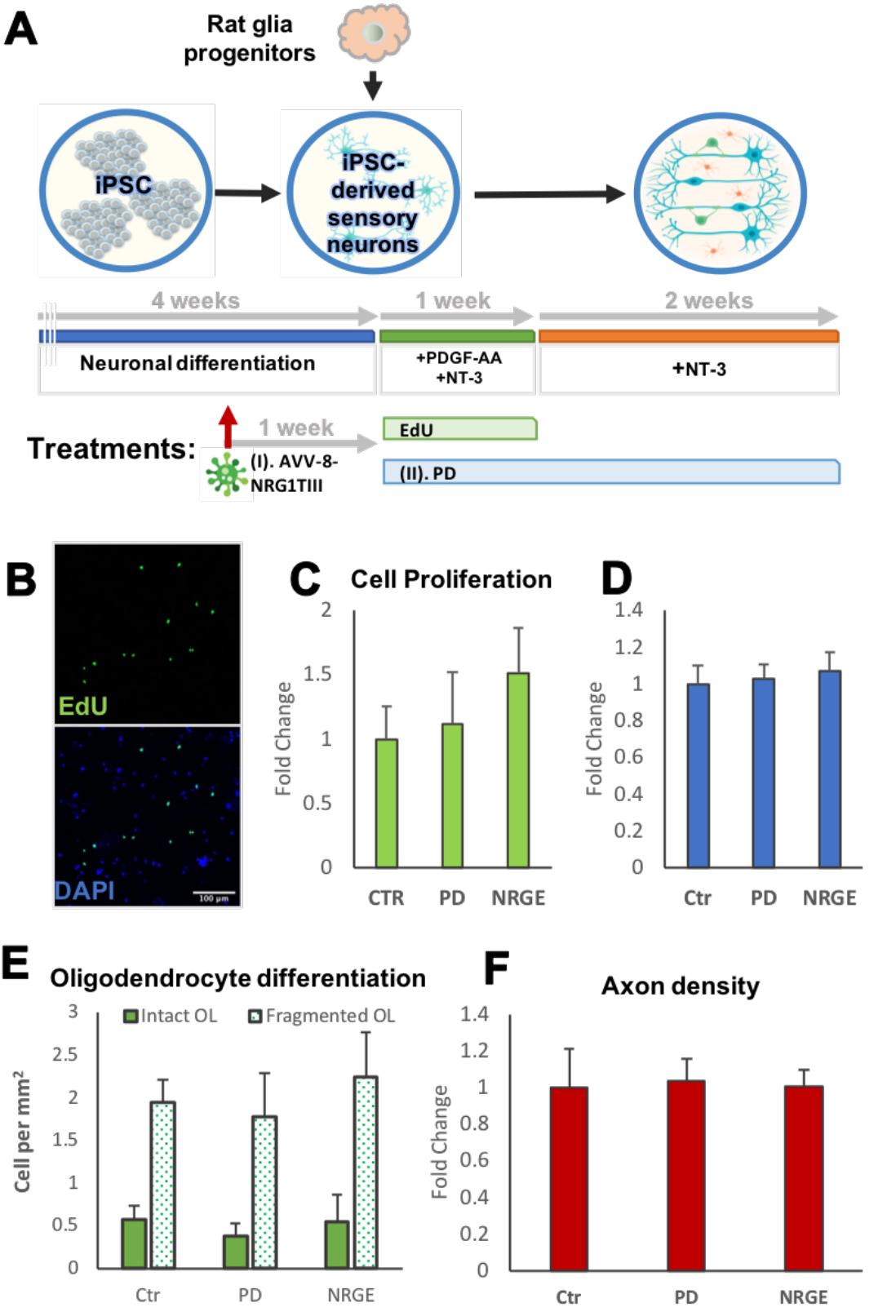


Figure 3.7. . ***Experiment to investigate Nrg1-ErbB signaling in co-culture system with Oligodendrocytes.***

Schematic showing the establishment and maintenance of the myelinating co-cultures with OPCs. Cultures were setup in 3 conditions: I. A condition in which neurons were infected with the… (continue on next page)

(Figure 3.7. continuation from previous page) …AAV8-Nrg1-type-III viral construct one week before co-culturing. II. A condition in which co-culture medium was supplemented with PD(7 nM), and III. a control condition. A subset of cultures in each condition was supplemented with EdU for 1 week to investigate cell proliferation. ***(B)*** *Representative image of a stain for EdU used for quantitative analysis of cell proliferation.* ***(C)*** *EdU positive cells per condition as fold changed to control condition.* ***(D)*** *DAPI positive cells did not significantly differ between the conditions.* ***(E)*** *Quantification of the density of "intact" and "fragmented" Oligodendrocytes (OL) per condition after 3 weeks in co-culture.* ***(F)*** *The different conditions had no effect on axonal outgrowth or morphology, with no visible signs of neurite blebbing. Data presented as Mean±SD.*

3.3.4 CONDITIONAL KNOCK OUT OF *NRG1* AFFECTS PERFORMANCE ON COMPLEX WHEEL RUNNING TASK.

Voluntary wheel running is a common behaviour paradigm to assess physical performance and endurance in mice and can be used as an intervention to provide valuable insight into the adaptation of numerous physiological outcomes. There is growing evidence that such behavioural experiences including exercise and environmental enrichment induce significant changes in oligodendrocyte lineage cells (Tomlinson *et al.* 2016). Testing animals on a running wheel with irregularly spaced rungs ("complex wheel") is a variation of this paradigm that has been employed to assess latent motor deficits (Liebetanz *et al.* 2007) and/or motor learning in mice (McKenzie *et al.* 2014). It has also been shown to stimulate OPC proliferation and OL production (Xiao *et al.* 2016). Our aim was to test if Nrg1-erbB signalling influenced the effect of this behaviour paradigm on oligodendroglia dynamics.

To test the behavioural performance of mice on the complex wheel in the absence of neuregulin 1 signalling, a global deletion of both alleles of the *Nrg1* gene was induced. The resulting $Nrg1^{(-/-)}$ mice (n=7; 3 females) were compared to control littermates that lacked the tamoxifen inducible Cre-construct (CAG-Cre-ER^{TM}) necessary for the deletion (n=11; 5 females). Body weights (in g) before behaviour testing were not different between groups (males: $Nrg1^{(+/+)}$: M=22.45, SD=0.839; $Nrg1^{(-/-)}$:M=20.29, SD=0.819; t(8)=1.756, p=0.117; females: $Nrg1^{(+/+)}$: M=18.23, SD=0.274; $Nrg1^{(-/-)}$:M=16.48, SD=0.83; t(4)=0.849, p=0.637). A schematic illustration of the experimental design is displayed in Figure 3.8B. Animals were tested on the complex wheel 4-5 weeks after tamoxifen treatment at P82-84. Each animal was singly housed in a specialised cage (Figure 3.1A) with free access to a complex wheel for 8 consecutive days. Animals' behaviour performance was assessed by calculating their

average and maximum running speed (Figure 3.8C&D). Two male animals, one from each genotype group, met the predetermined criteria for exclusion from the behaviour analysis due to a consistent lack of running behaviour (run <1km in 8 days; Supplementary Figure 1). Running speed on the complex wheel was slightly lower for $Nrg1^{(-/-)}$ animals, especially on the last two days (Figure 3.8C&D). Statistical analysis of daily running speeds using a repeated mixed ANOVA (within factor: Days; fixed factors: Genotype, Sex, Age) revealed a significant Day*Genotype interaction for average daily speed ($F(7,49)=2.541$, $p=0.021$ – effect size $\eta_p^2 =0.188$, Observed Power=0.856) and maximum daily speed ($F(7,49)=2.796$, $p=0.016$ – effect size $\eta_p^2 =0.285$, Observed Power=0.874). A *post-hoc* simple effect analysis looking at the first and last day of running indicated that running parameters were significantly different between groups on the last day (Average Speed: $F(1,11)=13.012$, $p=0.004$; Maximum speed: $F(1,11)=10.276$, $p=0.008$), while differences on the first day were not significant between genotypes. Conditional KO of *Nrg1* had no significant effect on neither the total distance run by the animals, nor the total number of active intervals on the complex running wheel (Figure 3.9A and B). This was confirmed by statistical analysis of daily distance run and daily active intervals using a repeated mixed ANOVA (within factor: Days; fixed factors: Genotype, Sex, Age), which found no significant main effect of genotype for distance ($F(1,11)=0.17$, $p= 0.899$) or active intervals ($F(1,11)=1.632$, $p= 0.318$), nor a Day*Genotype interaction. Additionally, the hours of the day at which the mice were active did not differ between genotype groups. All in all, these results indicate that conditional KO of *Nrg1* affected the mice's ability to improve their running performance on the complex wheel over time, while having no effect on their overall activity level on the wheel.

3.3.5 The effect of wheel running and Nrg1 cKO on oligodendroglia dynamics

To assess how wheel running and conditional KO of *Nrg1* affect oligodendroglia dynamics, animals were culled after 8 days of behaviour testing and a randomly selected subset of their tissue (n=3 per group) was processed for immunohistochemistry. Additionally, these animals were compared to age

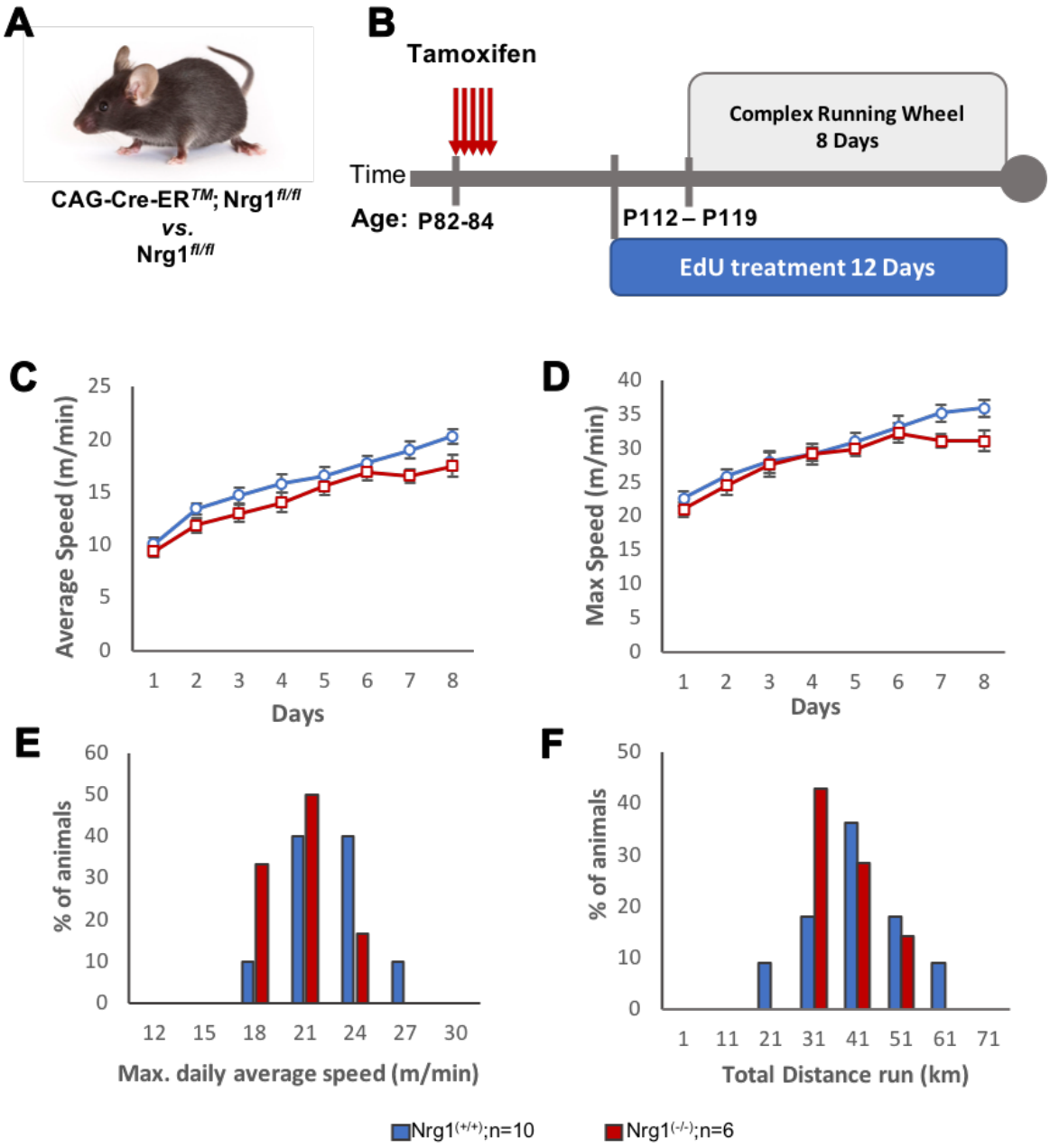


Figure 3.8. ***Conditional KO of Nrg1 caused a deficit in performance on complex wheel running.***

(A) *CAG-Cre-ER^{TM};Nrg1$^{fl/fl}$ animals were compared to tamoxifen control Nrg1$^{fl/fl}$ animals, which did not possess the CAG-Cre-ER^{TM} region.* ***(B)*** *Schematic illustration of the experimental design. Animals were treated with tamoxifen for 5 consecutive days at the age of P82-P84. Behavior testing was performed between 30 to 39 days later. EdU was administered in drinking water for 12 days, starting 4 days before behavior testing.* ***(C)*** *Average running speed and* ***(D)*** *maximum running speed for each respective genotype. A mixed model ANOVA found a significant interaction between "Day of Running" and "Genotype group" for both average running speed ($F(7,49)=2.541$, $p=0.021$) and maximum running speed ($F(7,49)=2.796$, $p=0.016$). Running Speed data presented as Mean±SEM. Frequency distribution of the* ***(E)*** *maximum daily average speed and* ***(F)*** *total distance run over the 8 days of testing indicated a slight shift towards lower values in the distribution for the Nrg1$^{(-/-)}$.*

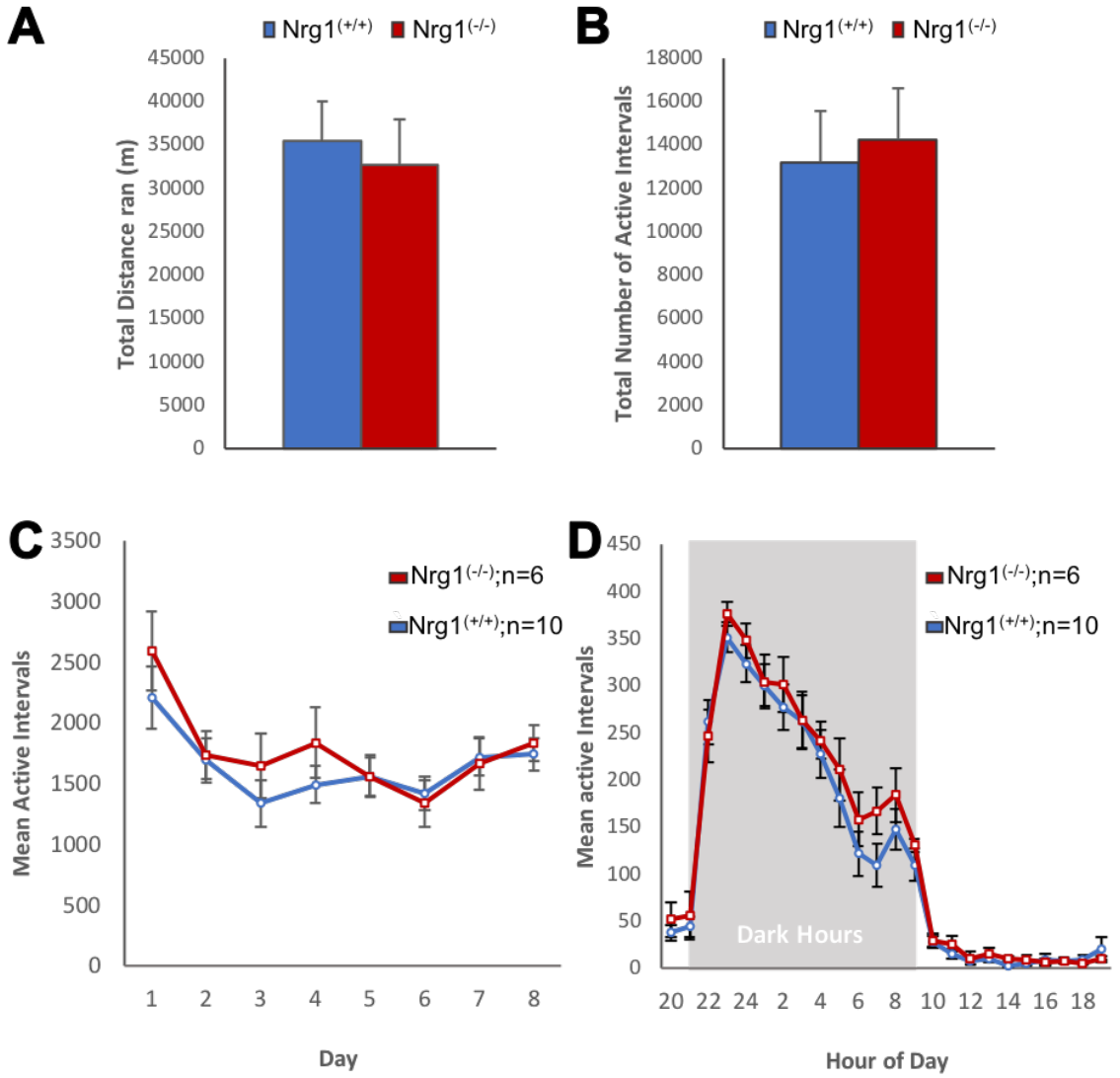


Figure 3.9. ***Conditional KO of Nrg1 did not effect total running distance or spontaneous activity patterns in mice.***

(A) *The mean accumulative distance run over the 8 days was not significantly different between the two genotype groups and* ***(B)*** *the total number of active intervals (10 second intervals in which >1 wheel rotation were recorded) was similar between the two genotypes.* ***(C)*** *The highest number of active intervals were recorded on the first day and was similar between Nrg1-cKO and controls.* ***(D)*** *Mice were most active during the first hours of the dark hours and showed almost no wheel running activity during the light hours, indicating a normal dark/light cycle activity pattern. Data presented as Mean±SEM.*

matched animals (n=3 per genotype group) that remained group housed in a regular home cage, instead of being transferred to a running wheel cage. These home cage control animals were offspring from the same breeding pairs, but not littermates with the animals that ran the wheel. EdU was administered via the drinking water for a total of 12 days, starting 4 days before behaviour testing (see Figure 3.8A). Density of cells was determined in the anterior corpus callosum, as illustrated in

Figure 3.10A-C. To assess overall cell proliferation, the numbers of EdU+ cells were quantified. The numbers of PDGF-Rα+ cells were counted to assess OPC cell density which allowed us to determine the density of proliferating OPCs (Edu+|PDGF-Rα+). As the vast majority of proliferating cells in the adult white matter are PDGF-Rα+ OPCs (>90%, McKenzie et al., 2014; Xiao et al., 2016), Edu+|PDGF-Rα- cells predominantly mark OPCs that have recently differentiated and can therefore be considered as an indicator for the quantity of OPC differentiation.

Two-way ANOVAs were run to examine the effect of running (CW vs Home Cage) and genotype ($Nrg1^{(+/+)}$ vs $Nrg1^{(-/-)}$) on cell density (n=3 per group). There were no significant differences in density of PDGF-Rα+ OPCs between groups (Figure 3.10D). Running had a statistically significant main effect for the number of proliferating EdU+ cells overall ($F(1,12)=9.528$, $p=0.020$ – effect size $\eta_p^2=0.544$, Observed Power=0.730), as well as the density of recently differentiated OPCs as quantified by Edu+|PDGF-Rα- cells ($F(1,12)=21.809$, $p=0.002$ – effect size $\eta_p^2=0.757$, Observed Power=0.978), with greater densities found in runners compared to home cage controls. No main effect of Running was found for proliferating Edu+|PDGF-Rα+ OPCs ($F_{(1,12)}=3.180$, $p=0.118$ – effect size $\eta_p^2=0.312$, Observed Power=0.338). There was no statistically significant main effect for Genotype, nor a Running*Genotype interaction for any of the assessed parameters.

Overall, the experiments indicate that animals exposed to a running wheel in a novel environment show an increase in cell dynamics in the corpus callosum. However, our statistical analysis does not support the hypothesis that oligodendroglia dynamics can be affected by ablation of Nrg1-ErbB signalling.

3.4. DISCUSSION

The aim of this chapter was to study the role of Nrg1-ErbB signalling manipulation in the PNS and CNS. We demonstrated that Nrg1-erbB signalling manipulation had a significant effect on myelination in the stable myelinating co-cultures between iPSC-derived sensory neurons and Schwann cells. We

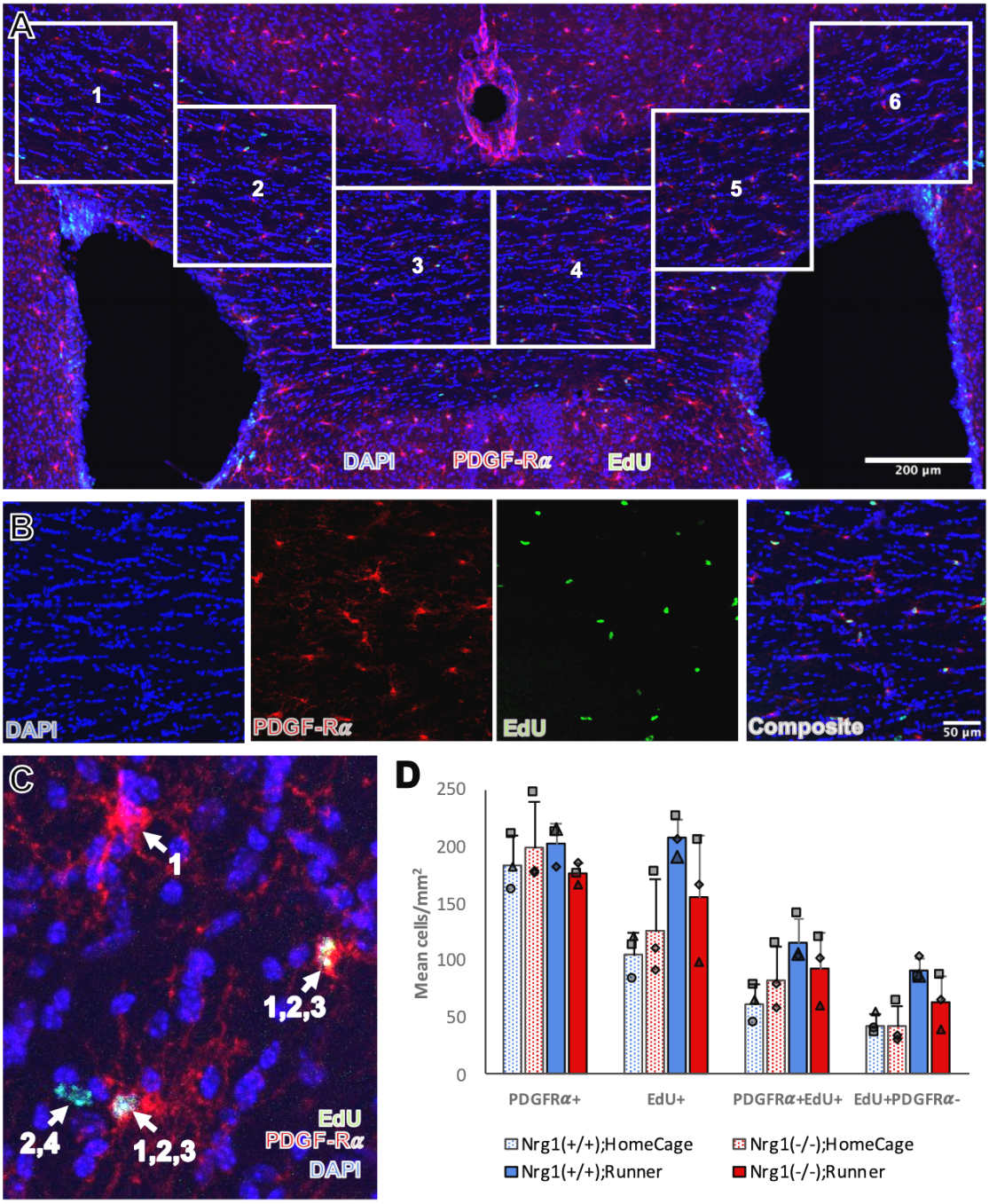


Figure 3.10. ***Effect of running and cKO of Nrg1 on oligodendroglia dynamics.***

Brain slices were stained for the OPC marker PDGF-Rα, proliferating cells marker EdU, and cell nuclei were visualized with DAPI. ***(A)*** *A representative image of the anterior corpus callosum used for the analysis. Six images (framed in white) were taken from each slice and 3 slices were analyzed per animal.* ***(B)*** *Representative individual image used for the analysis.* ***(C)*** *Cells were classified as (1)PDGF-Rα-positive (PDGF-Rα), (2) EdU-positive (EdU+), (3) PDGF-Rα-positive & EdU-positive(PDGF-Rα+EDU+), and/or (4) EdU-positive & PDGF-Rα-negative (EDU+PDGFRα-). Animals which were tested on the complex running wheel (Runners, n=3 per group) were compared to animals that were single house in a home cage (HomeCage) for the same time period while being treated with EdU.* ***(D)*** *Quantification of cell densities for the different groups indicated a statistically significant increase in EDU+PDGFRα- cells in Runners, compared to HomeCage controls, but no difference between genotype groups. Data presented as Mean±SD.*

also established an analogous co-cultures system between iPSC-derived sensory neurons and oligodendroglia cells, which produced MBP-positive myelinating oligodendrocytes. Yet, this model of CNS myelination lacked temporal stability and reproducibility between experiments, which prevented a conclusive investigation of the role of Nrg1-erbB signalling on myelinating glia of the CNS. Conditional ablation of *Nrg1* in young adult mice *in vivo* led to a behaviour deficit on the complex wheel. While finding evidence for an experience-dependent effect on oligodendroglia dynamics *in vivo*, our current data does not provide evidence for a role of Nrg1-erbB signalling on oligodendroglia dynamics.

All *Nrg1* isoforms contain an epidermal growth factor (EGF)-like signalling domain that can act on heterodimeric ErbB2-ErbB3 receptors expressed at the Schwann cell membrane; the membrane-bound type III isoform is thought to be the most important signalling molecule for the regulation of myelination in the PNS (Michailov *et al.* 2004; Taveggia *et al.* 2005; Birchmeier and Bennett 2016). Using an AAV-mediated overexpression system or pharmacological inhibition, we find that TIIINRG1 expressed on human axons could strongly promote myelination (Figure 3.2& Figure 3.3). Levels of *Nrg1* in the peripheral nervous system are regulated by proteolytic cleavage by a range of secretase enzymes, including BACE1 (Hu *et al.* 2006; Willem *et al.* 2006; Fleck *et al.* 2013). The role of Nrg1-ErbB signalling in myelination of the rodent peripheral nervous system is well established, and we have now shown that modulating TIIINRG1 expression on human sensory axons also has a key role in regulating myelination.

Co-cultures also have potential for drug and toxicology screening (Figure 3.3). In the last decade, BACE1 has emerged as an important target for experimental therapies in Alzheimer's disease. In addition to the proteolytic processing of Nrg1, BACE1 is one of the β-secretase enzymes required for the endoproteolysis of the amyloid precursor protein (APP), and hence the production of the 42-amino acid long b- amyloid peptide (amyloid-b42), widely considered to be neurotoxic and crucial during the early onset of Alzheimer's disease (Vassar 2004). As a result, BACE1 inhibitors are currently

in human clinical trials (Vassar *et al*, 2014). Given the profound effect on the myelination of human axons, the potential for BACE1 inhibition to produce deleterious effects on peripheral nerve function is highlighted by this study. This may be a particular problem for patients with pre-existing neuropathies (up to 8% of the elderly population) (Martyn and Hughes 1997), in which ongoing repair may be critically important. *Nrg1* is now also being considered as a target for clinical intervention. Human-based myelinating co-cultures should prove a useful tool for screening the effects of drugs targeting this signalling pathway.

While co-cultures between iPSC-derived sensory neurons and Schwann cells provided a stable and reproduceable model that allowed the investigation of neuron-glia signalling, the analogous model between iPSC-derived neurons and oligodendroglia lacked those crucial qualities. MBP-positive oligodendrocytes developed (Figure 3.4) with a cellular morphology comparable to the ones observed in *in vitro* cultures studies using dorsal-root ganglion cells (DRG) and oligodendroglia (Wang *et al.* 2007; Dugas and Emery 2013b; Lundgaard *et al.* 2013). This indicates that the established conditions in the current study were permissive to OL differentiation and axon-glia interaction. Yet, the high percentage of MBP-positive cells with fragmented morphology (Figure 3.5), which increased over time (Figure 3.6), were not reported in previous *in vitro* studies. Experimentally, it was not clear what caused this lack of oligodendrocyte survival and maintenance. Co-culture medium conditions may not have been fully optimised for co-cultures with iPSC-derived sensory neurons, despite being adapted from successful previous studies with DRGs (Lundgaard *et al.* 2013). While oligodendrocytes have an intrinsic tendency to wrap myelin around any permissive structure *in vitro* (Bechler *et al.* 2015) *,* a range of negative signals exist that inhibit myelination (Almeida 2018; Harboe *et al.* 2018). It is not clear if the expression profile of cell-surface molecules in human iPSC-derive sensory neurons is permissive for a prolonged axon-glia interaction, or what role the species differences could have played. Recent *in vivo* live imaging studies suggest that a large proportion of differentiation OLs in somatosensory cortex of adult mice indeed undergo programmed cell death after differentiation (Hill

et al. 2018), a process which seems to be partly modulated by experience-driven factors (Hughes *et al.* 2018). Yet, it is unlikely that the current study recreated the complex conditions found in the *in vivo* environment driving this poorly understood process. A limitation of our study was the use of commercially available OPCs, instead of harvesting them ourselves. This provided a lack of control over the quality of OPCs and introduced a potential risk factor for a lack of reproducibility between experiments.

Previous *in vitro* studies have demonstrated that *Nrg1* signalling affects oligodendrocyte differentiation, myelination, and survival (Canoll *et al.* 1996, 1999; Vartanian *et al.* 1997; Flores *et al.* 2000; Calaora *et al.* 2001). In the current study, manipulation of Nrg1-erbB signalling had no significant effect on the survival or differentiation of OLs (Figure 3.7), indicating that the high number of fragmented OLs and the low cellular density of MBP-positive cells in the established co-cultures were caused by factors independent of Nrg1-erbB signalling. Taken together, the established myelinating co-cultures between iPSC-derived sensory neurons and oligodendroglia did not provide a valid model for the study of Nrg1-erbB signalling on CNS myelination at the current stage of development.

The complex running wheel behaviour paradigm was initially developed to detect central motor deficits of coordinated motor skill performance (Schalomon and Wahlsten 2002; Liebetanz *et al.* 2007). In the current study we detected that mice with a conditional homozygous deletion of the *Nrg1* gene during early adulthood leads to a subtle reduction in running performance on the complex wheel over time compared to littermate controls (Figure 3.8). The homozygous deletion of neuregulin 1 was global in this mouse model, rather than localised to a region or cell type of interest. Hence, it is difficult to establish a causal link between the observed behaviour deficit and a specific biological process, as Nrg1-erbB signalling has a broad range of functions in the central nervous system, including neurotransmission and synaptic plasticity (Mei and Nave 2014). Deficits in motor coordination have previously been reported in mice that lack one copy of the *Nrg1* gene ($Nrg1^{+/-}$)

during development (Schneider *et al.* 2017), in which Nrg1-erbB signalling contributes to a wide range of processes including neuronal migration, axonal pathfinding and neuronal circuit assembly (Mei and Nave 2014). Interestingly, the total number of active intervals animals spent on the complex running wheel was not affected by conditional deletion of neuregulin 1 (Figure 3.9) in the current study. This indicates that a potential lack of motivation to run and/or reduced spontaneous locomotor activity, which was previously reported in animals with abnormal Nrg1-erbB signalling (Karl *et al.* 2007), did not contribute to the observed behaviour deficit on complex wheel running performance.

Running on a complex wheel has previously been shown to stimulate dynamic changes in oligodendroglia dynamics, triggering OPC proliferation and OLs production (McKenzie *et al.* 2014; Xiao *et al.* 2016). Our aim was to investigate if this experience-dependent change in oligodendroglia dynamics would be affected by impairing Nrg1-erbB signalling. In our experiment, we found that running significantly increased the number of Edu+|PDGF-Rα- cells (Figure 3.10D). As previous studies found that the vast majority (>90%) of EdU+ cells in the white matter of mice with comparable ages were also Sox10+ oligodendrocyte lineage cells (Xiao *et al.* 2016), those Edu+|PDGF-Rα- predominantly represent newly differentiated oligodendrocytes. Indeed, the increase in oligodendrocyte differentiation triggered by complex wheel running is similar to the one reported by McKenzie *et al.* (2014), who found a higher density of newly-differentiating oligodendrocytes after 11 days of running the complex wheel. Proliferation of OPC was not affected by wheel running at day 8 of the experiment in the current study. This is in line with previous studies, which found that CW running leads to a transient increase in OPCs proliferation that is only detectable around day 4 of running on the complex wheel (McKenzie *et al.* 2014), yet not at a later time point. However, the homozygous deletion of *Nrg1* did not significantly influence the observed oligodendroglia dynamics and hence our current data does not support the hypothesis that Nrg1-erbB signalling may affect the adaptive response to experience in the myelinating glia population.

Our *in vivo* experiment with cKO-Nrg1 model had several limitations. Firstly, we did not directly label cells for their mature Oligodendrocyte identity or myelination, limiting our ability to detect cell specific changes. Secondly, our current histological analysis does not include all collected tissue and is underpowered for the detection of a smaller effect size. In fact, we did not expect a large effect of *Nrg1* deletion on the oligodendroglia dynamics, as Nrg1-erbB signalling is one potential factor among many other factors that are likely to influence adaptive myelination in the CNS (Mount and Monje 2017; Bechler *et al.* 2018). Thirdly, we only investigated oligodendroglia dynamics in the anterior corpus callosum. However, it is possible that adaptive changes due to neuregulin signalling in oligodendroglia may be region-specific (Makinodan *et al.* 2012; Tomassy *et al.* 2016). Lastly, we did not control for the environmental factors that come with introducing animals to the complex wheel cages, as we compared runners to animals that remained in their home cage environment. Hence, the observed changes in oligodendroglia dynamics may be influenced by factors other than complex wheel running, such as novelty and/or environmental enrichment.

In summary, we could confirm the major role of Nrg1-ErbB signalling in PNS myelination in co-cultures between iPSC-derived sensory neurons and rat Schwann cells. Establishing an analogous co-culture system with rat oligodendroglia cells did not provide a model system suitable for the study of Nrg1-erbB signalling, as oligodendrocyte differentiation within the culture system was not stable and reliable enough. This emphasizes the importance of a stable model system to allow the study the effect of Nrg1-erbB signalling on oligodendroglia *in vitro*. Our *in vivo* experiment demonstrated that oligodendroglia dynamics can be dependent on experience, yet our study provides no conclusive evidence that Nrg1-erbB signalling influences experience-dependent changes in oligodendroglia dynamics triggered by running a complex wheel.

Chapter 4 | REPLICATING AND EXTENDING BEHAVIOUR PHENOTYPE OF THE *MYRF*-cKO MODEL

4.1. INTRODUCTION

Oligodendroglia dynamics can be influenced by experience even during adulthood, as we have demonstrated in Chapter 3. Yet, the role of such adaptive changes in learning and skill acquisition remains elusive. Converging evidence from many elegant studies indicates a link between changes in WM structure and skill learning (Scholz *et al.* 2009; Hofstetter *et al.* 2013; Lakhani *et al.* 2016). Experiences such as learning to juggle (Scholz *et al.* 2009) or playing a computer game (Hofstetter *et al.* 2013) are associated with structural changes in white matter pathways in humans. Rodent *in vivo* studies have demonstrated that experience can change the dynamics of oligodendroglia in the mature cortex (Hughes *et al.* 2018). However, concurrent changes in other WM cells as well as in grey matter make it challenging to infer the functional relevance of myelin plasticity for any associated behavioural change. Hence, it is not well understood if and to what extent these adaptive changes in brain structure facilitate behavioural change and skill acquisition.

A set of influential studies from the Richardson group (UCL), with transgenic mice have provided the only evidence for a direct causal link between experience-dependent myelin plasticity and skill acquisition (McKenzie *et al.* 2014; Xiao *et al.* 2016). Breeding together a set of mouse strains, the researchers created a transgenic rodent model that allowed the conditional knock-out of the gene encoding the transcription factor *Myrf* (Myelin Regulatory Factor), a factor critical for the initiation and maintenance of myelination by oligodendrocytes (Emery *et al.* 2009; Koenning *et al.* 2012).

Crucially, their model abolished *Myrf* expression only in PDGF-Rα-positive oligodendrocyte precursors (OPCs), not mature oligodendrocytes, which allowed them to experimentally abolish the differentiation of new myelinating oligodendrocytes at a developmental age of their choosing without affecting existing myelinating oligodendrocytes. Their data suggests that mice with homozygous deletion of *Myrf* in OPCs (P-Myrf$^{(-/-)}$) at postnatal day 60 showed no visible signs of myelin loss, nor behaviour deficits such as tremors or a reduced performance on the accelerating RotaRod, despite a ~90% reduction in the formation of new oligodendrocytes (McKenzie *et al.* 2014). Testing for a behaviour phenotype in these mice, McKenzie *et al.* (2014) employed the complex running wheel paradigm, which we also employed in Chapter 3 to test the behaviour of cKO-Nrg1 mice.

Voluntary wheel running on a normal running wheel is a frequently used as a behaviour paradigm to investigate locomotor activity and the effects of environmental enrichment and exercise in rodents (Manzanares *et al*. 2019). Wheel running are used by rodents even if no extrinsic reward is provided, surprisingly also by wild mice outside the lab environment (Meijer and Robbers 2014). Wheel running on a normal wheel is not considered as a motor learning task and is likely to be predominantly driven by circuits controlling locomotion. These circuits involve spinal central pattern generators that receive synaptic inputs from brain-stem reticulospinal neurons, which are themselves controlled by upstream locomotor centers such as the mesencephalic and the diencephalic locomotor regions (Grätsch *et al.* 2019).

The complex running wheel design, with several rungs removed in an irregular pattern (Figure 3.1), was designed to make wheel running more difficult in such a way that improved running abilities would require motor skill learned on a supraspinal (cortical) level and would thus depend on bihemispherical integration through the corpus callosum (Liebetanz and Merkler, 2006). Indeed, the difficulty of adapting the gait to be able to run on a surface with irregular gabs is likely to involve feedback-based reinforcement learning mechanisms that may engage circuits in sensorimotor areas

of the cortex, cerebellum and basal ganglia (Makino *et al.* 2016) to find a strategy for coping with the novel environment. Yet, learning to run the complex wheel is also likely to require the recalibration of a well-trained movement (locomotion) after the initial phase, which is a form of motor adaptation. Motor adaptation is usually distinguished from motor skill learning, as it is more dependent on sensory prediction error processing in the cerebellum (Diedrichsen and Kornysheva 2015, Wolpert 2011).

However, the complex wheel was initially employed not as a learning task, but to detect latent motor deficits in mice with a surgically transacted corpus callosum (Schalomon and Wahlsten, 2002). Testing mice with cuprizone-induced callosal demyelination (Liebetanz and Merkler, 2006), or with MPTP-induced nigrostriatal dopaminergic degeneration (Liebetanz et al., 2007), a separate research group found that the complex wheel design can detect latent motor behaviour deficits in mice that did not show corresponding deficits on more established tests for motor coordination (e.g., Balance Beam, RotaRod or normal running wheel).

McKenzie *et al* (2014) observed that mice with a conditional ablation of *Myrf* (P-Myrf$^{(-/-)}$) at P60 showed significantly lower running speeds on the complex wheel, when compared to their siblings that retained one functional copy of the gene (P-Myrf$^{(+/-)}$). At the same time, learning to run on the complex wheel was demonstrated to trigger changes in oligodendroglia dynamics, stimulating OPC proliferation and oligodendrocyte differentiation. If the mice had been exposed to the complex wheel prior to the genetic manipulation, their performance remained unimpaired, indicating that ablation of *Myrf*-expression in OPCs affects mice's ability to learn to run the complex wheel. Interestingly, this genotype difference in behaviour performance was already apparent after 2-3 hours of testing, and was accompanied by an early cellular and region-specific response within the oligodendroglia cell population (Xiao *et al.* 2016). Despite this genotype difference in running performance, McKenzie *et al.* (2014) found no difference in the time P-Myrf$^{(-/-)}$ mice actively engaged with the running wheel. Taken together, these results suggested that newly forming oligodendrocytes may play an active and

specific role in acquisition of a novel skill. Additionally, the authors suggested that the very early requirement for oligodendrocytes indicate a direct and active role of adaptive oligodendroglia dynamics in learning, on a time-scale usually only associated with synaptic plasticity.

However, it is not clear precisely which aspects of the behaviour were impaired by ablating the differentiation of new oligodendrocytes. Video recording of mice running suggested that mice adopt a general strategy to successfully run the complex wheel, changing their general gait rather than memorizing specific stepping patterns. This idea is supported by the finding that changing the pattern of rungs on the wheel does not impact running performance in experienced mice (McKenzie *et al.* 2014). Deficits in learning to run the complex wheel have previously been shown in mice with experimentally induced damage to white matter tracks or dopaminergic neurons (Liebetanz and Merkler 2006; Liebetanz *et al.* 2007) and it is not clear how these different experimental interventions can lead to a similar behavioural phenotype. Nonetheless, providing a causal link between a behaviour deficit and experimental manipulation of oligodendroglia dynamics, the *Myrf*-cKO mouse model provides an important tool to understand the link between behaviour change and adaptive changes in myelinating glia in the CNS.

4.1.1 Aim of this Chapter

Given the importance and implications of the described studies, our motivation for this third chapter was to replicate and extend the key behaviour phenotype of the *Myrf*-cKO model in a different experimental environment and research group. We were also aiming to further explore the behaviour phenotype of *Myrf*-cKO mice in terms of spontaneous locomotor activity and motor skills with a wider battery of relevant tests. Provided that we were able to detect a behavioural phenotype in *Myrf*-cKO mice on the complex wheel, we also then aimed to further explore the link between behaviour deficits and underlying biological changes in oligodendroglia dynamics and white matter integrity in Chapter 5.

4.2. MATERIALS AND METHODS

4.2.1 ANIMALS

All work carried out conformed to UK Home Office legislation (Scientific Procedures Act 1986).

4.2.1.1 Mouse breeding and Genetic background

Mice used in this study were originally created in the Richardson laboratory (McKenzie *et al.* 2014), UCL by crossing *Pdgfra-CreER^{T2}* transgenic mice (Rivers *et al.* 2008) with Cre-conditional reporter mice *Rosa26R-YFP* (*R26R-YFP*) (Srinivas *et al.* 2001) to generate double-homozygous offspring. *Cre* and *YFP* reporter lines in the Richardson Laboratory were maintained separately by crossing (more than 10 generations) with C57B6 females (Charles River; Margate, UK). These *Pdgfra-CreER^{T2} :Rosa26R-YFP* were crossed with *Myrf$^{(fl/fl)}$* mice (Emery *et al.* 2009) to obtain *Pdgfra-CreER^{T2}: R26R: Myrf$^{(+/fl)}$* offspring, which were sibling-mated to obtain *Myrf$^{(fl/fl)}$* and *Myrf$^{(+/fl)}$* littermates. These animals were finally crossed to generate cohorts of *Pdgfra-CreER^{T2}: R26R- YFP: Myrf $^{(fl/fl)}$* and *Myrf $^{(+/fl)}$* littermates for behavioural testing and further breeding. In the Richardson Laboratory, *Myrf$^{(fl/fl)}$* mice were obtained originally (in 2010) on a mixed 129/CBA/C57B6 background. After crossing into a double-homozygous *Pdgfra-CreER^{T2}*: *Rosa-YFP* background (predominantly C57B6; 3 generations) they were maintained in the Richardson Lab by sibling crosses for more than 6 generations and they generated exclusively agouti offspring in their original study (McKenzie *et al.* 2014). They were therefore mixed C57B6/CBA/129 with the major contribution being C57B6 (though agouti coat-colour is CBA-derived).

Five breeding pairs of *Pdgfra-CreER^{T2}: R26R- YFP: Myrf$^{(fl/fl)}$* and *Pdgfra-CreER^{T2}: R26R- YFP: Myrf* $^{(+/fl)}$ (referred to as P-Myrf$^{(fl/fl)}$and P-Myrf$^{(+/fl)}$) were sent to our laboratory from the Richardson Lab, UCL in 2016 and were used to breed animals for our study by crossing P-Myrf$^{(fl/fl)}$ with P-Myrf$^{(+/fl)}$ mates. Mice carried copies of *Pdgfra-CreER^{T2}* on both alleles and were either *R26R-YFP$^{(fl\|fl)}$*or *R26R-YFP$^{(+/fl)}$*. Two generations of animals were bred before behaviour testing started for the current studies and

animals from a total of 4 consecutive generations were used for behaviour testing. Hence, P-Myrf$^{(fl/fl)}$and P-Myrf$^{(+/fl)}$ were maintained by sibling crossing for 6 generations in our facilities. In our laboratory, we found a mix between black coat-colour (C57B6 derived) and agouti coat-colour (CBA-derived), suggesting a mixed and diverse background across the population.

4.2.1.2 Mouse Genotyping

Genotyping for Cre-ER^{T2} (Cre 5'-TCG ATG CAA CGA GTG ATG AG and Cre 3'-TTC GGC TAT ACG TAA CAG GG; Product Size 481bp) and R26R-YFP (R26WTF1-AAA GTC GCT CTG AGT TGT TAT, R26WTR1-GGA GCG GGA GAA ATG GAT ATG, R26KOF1-GCG AAG AGT TTG TCC TCA ACC) was by PCR amplification of genomic DNA. Myrf$^{(fl/fl)}$ mice were genotyped by PCR amplification of genomic DNA using primers within intron 7 flanking the first lox site (5'-AGGAGTGTTGTGGGAA-GTGG and 5'-CCCAGGCTGAAGATGGAATA), which gives a 281 bp product for the wild-type allele and a 489 bp product for the *loxP*-flanked allele (Emery *et al.* 2009).

4.2.1.3 Tamoxifen administration

Tamoxifen (Sigma T5648) was dissolved at 40 mg/ml in corn oil on a shaker overnight at RT and by subsequent sonicating at 21°C for one hour. P-Myrf$^{(+/-)}$ and P-Myrf$^{(-/-)}$ mice were generated by administering tamoxifen (0.3mg/g body weight in corn oil) by oral gavage for four consecutive days to *Pdgfra-CreER^{T2}:R26R- YFP:Myrf $^{(flox/flox)}$* and *Pdgfra-CreER^{T2}:R26R- YFP:Myrf $^{(+/flox)}$*. Animals were left for at least 2 weeks before experimental procedures. During, and for a week after tamoxifen treatment, nutritious jelly and mash were provided for all mice to prevent excessive weight loss due to the adverse effects of the drug.

4.2.2 HISTOLOGICAL ANALYSIS OF BRAIN TISSUE

4.2.2.1 Perfusion of animals and tissue processing

Animals were deeply anaesthetized (Euthatal: 80mg/kg, i.p) with sodium pentobarbital and transcardially perfused with 10 ml PBS, followed by 30 ml paraformaldehyde (4% w/v in 0.1 M phosphate buffer) with the help of a perfusion pump (Flow rate: 4ml/min). For the analysis of

oligodendrocyte differentiation using anti-APC(CC1) and anti-GFP/YFP antibodies (Table 1), brains were initially kept in the dissected skull and post-fixed in paraformaldehyde (4% w/v in 0.1M phosphate buffer) for 30 mins at room temperature, followed by another 24h post fixation at 4°C. This tissue was subsequently stored in PBS at 4°C and was used for MRI, before being dissected out of the skull, cryoprotected in 30% Sucrose PBS solution, embedded in OCT and frozen on dry ice before being stored at -80°C until further processing.

For the analysis using EdU and PDGF-Rα, brains were dissected out of the skull and post-fixed in paraformaldehyde (4% w/v in 0.1M phosphate buffer) for 30 mins at room temperature then overnight (~16 hours) at 4°C. Brain tissue was subsequently cryoprotected in 30% Sucrose PBS solution until tissue no longer floated in the solution. The tissue was then embedded in OCT and frozen on dry ice before being stored at -80°C until further processing.

4.2.2.2 Immunohistochemistry of free-floating brain sections

For Immunohistochemical analysis, coronal cryosections (30 µm) were cut (anterior to posterior) from the first section at which the anterior corpus callosum was visible and continuously connected from one hemisphere to the other. Processing of free-floating brain sections has been described in detail in Chapter 3. Primary antibodies used were anti-PDGF-Rα (rabbit, New England Biolabs, 1:400 dilution), anti-APC (clone CC1; mouse, Calbiochem, 1:200 dilution) and anti-GFP(YFP) (chicken, Avas, 1:500).

4.2.3 Behaviour Testing of mice

Assessment of behavioural phenotype was conducted by the same researcher. Wherever possible, equal numbers of animals and of each gender were included in each experimental group. For experiments for which data collection was not automated, researchers were blinded to the Genotype of the animals during data collection and analysis. All mice were maintained on a 12-hour artificial light-dark cycle (9:00-21:00). Food and water were provided *ad lib.*

4.2.3.1 Complex Running Wheel

The procedure and equipment for testing animals on the complex wheel have been described in Chapter 3 (Figure 3.1). Running speed of animals (Distance/Time) was conducted using timebins of 10 sec. McKenzie *et al.* (2014) calculated the average running speed by quantifying wheel spins during a 1 min timebin. Yet, in the current study between 35-40% of continuous running bouts were found to be shorter than 1 minute long (Supplementary Figure 2A&B). That meant that average running speed was often underestimated when using 1 min intervals to calculate speed. Hence, data were mainly processed in 10 sec bins, and only processed in 1 min bins if directly comparing data from our study to findings provided by previous research, as in Figure 4.3 and Figure 4.5.

4.2.3.2 Passive infrared (PIR) activity monitoring

The method and equipment for Passive infrared (PIR) activity monitoring was directly adapted from Brown *et al* (2017), who helped with the set-up and maintenance of the equipment. The cages used in the study were MB1 mouse cages (North Kent Plastic Cages, Overall size: 450 × 280 × 130mm), with wire tops. An accurate measurement of activity and rest relies on the infrared radiation from the mouse being able to reach the sensor at all times. For this reason, the small gaps under the food and water hoppers on the MB1 cages were blocked using Perspex blocks to prevent access by the animal and no environmental enrichment was used that could fully obscure the animal (e.g. Perspex tubes). The nesting materials used in the study were cotton fibre Nestlets (Datesand Group, Manchester, UK), with a minimum of 10g in each cage. Excessive nesting materials could potentially obscure the mouse from the sensor and nesting boxes will prevent the accurate assessment of activity. A polling time, means the frequency of individual data collection points, of 100msec was used by the sensors. With 10s bins this provides 100 separate 100msec measurements per time bin. A serial message containing all the activity data and a single measurement of environmental light from the LDR is then sent to the PC connected via USB, where it is stored alongside a timestamp. Data was exported in spreadsheets for further analysis.

4.2.3.3 Accelerating Rotarod

Mice were tested on a standard RotaRod apparatus (Ugo Basile, Italy). Mice were tested for their ability to stay on a rod 3 cm in dimeter (Figure 4.12A). The apparatus allowed simultaneous testing of up to 5 mice, yet a maximum of 3 mice were tested at the same time. Mice were habituated to the testing room for 30 mins before behaviour testing, by placing the their cages into the room. Mice were trained for three trials on the rotarod at a constant speed (4 rpm), 120 s each trial, 2 days before behaviour testing, at which speed all mice stayed on the rod for the duration of the trial.

On the day of testing, each mouse was held by the tail and allowed to grasp the rotating rod. If it was still in place after 10 s, then the rotation of the rod was accelerated by 20 rpm to a maximum speed of 40 rpm. The time at which each mouse fell off the rod was recorded, starting from the moment of acceleration. If a mouse managed to stay on the rod for longer than 150 s, the trail was stopped, and a time of 150 s was recorded. Each mouse was tested 3 times on the same day. Animals were allowed to rest for 10 minutes between trials.

4.2.3.4 Balance Beam

The beam apparatus consists of 1 meter round smooth wooden beams of 15 mm or 7.5 mm diameter positioned 50 cm above the table. A soft foam matt was placed beneath the beam to cushion any potential fall. The beam rested on the edge of a wooden box on one side, at which animals were placed for testing. On the other side, the beam rested on the edge of the animal's home cage (Figure 4.12C). The beam was slightly angled (~10 degrees) so that animals had to walk uphill to reach their home cage. A lamp (with a 60 watt light bulb) was used to shine light above the start point and serve as an aversive stimulus, and the light inside the room was slightly dimmed. Mice were habituated to the testing room for 1 hour before behaviour testing, by placing their cage inside the room. Three days before behaviour assessment on the Balance beam, mice were trained to cross the beam. Training was done by placing the mice on the beam (1.5 cm) opposite the home cage. During training mice were freely allowed to cross the beam and reach their home cage. This procedure was repeated

3 times with a 1-min rest time between attempts. Training was conducted as almost all mice freeze and/or stop on the beam, or try to turn around in the middle, during the first exposure to the apparatus. Only after learning the location of their home cage during training, mice reliably cross the beam without stopping and turning around, which allows reliable and comparable data collection. All mice successfully crossed the beams during training at least one time.

For testing, mice were placed on the beam and freely allowed to cross the beam. Mice were first tested on the wider beam (1.5 cm diameter). After a 5-min resting time in the home cage, the beam was exchanged for the narrow (0.75 cm) beam and the same animal was tested again. All animals successfully crossed the beams without falling. The apparatus was cleaned with ethanol (70%) before testing another animal.

Testing was recorded using an HD camera placed on the side of the beam opposite the home cage. Videos were analysed by a blinded experimenter. Foot slips (A slip is defined as the foot coming off the top of the beam) and the number of steps taken to cross the beam were quantified.

4.2.3.5 Criteria for excluding animals from complex wheel data analysis

Previous experiments reveal that a small subset of healthy untreated animals show unusually low engagement in voluntary wheel running. To prevent such outliners from skewing overall group performance, we set the following pre-determined exclusion criteria for analysis of complex wheel behaviour performance: animals were excluded from the analysis if: 1) they ran less than 1km in 8 Days (P-Myrf$^{(+/-)}$; n=4, females; P-Myrf$^{(-/-)}$; n=1), or 2) ran less than 100 meters per day for at least half of the days recorded (P-Myrf$^{(+/-)}$; n=2, females; P-Myrf$^{(-/-)}$; n=1). In total, eight P-Myrf animals were excluded based on these criteria (P-Myrf$^{(+/-)}$; n=6; P-Myrf$^{(-/-)}$; n=2).

4.2.4 STATISTICS

Statistical analysis was performed using IBM SPSS Statistics for Mac (Version 25). The statistical test used for a particular analysis are mentioned during the data presentation in the result sections. As in

previous chapters, normality of the data and assumptions of homogeneity of variance were tested (e.g. with Levene's Test) before using parametric statistical analysis. If these assumptions were not met, non-parametric alternative tests were used for statistical analysis, or the test parameters were adjusted to account for the lack of homogeneity of variances (e.g. using un-pooled variances and a correction to the degrees of freedom for unpaired t-test) whenever possible.

Performance on the complex wheel or the PIR activity monitoring cages were analysed using a mixed two-way ANOVA. However, sample data did not always meet the assumption of normality due to a tendency towards bimodal distribution in the sample population. After consultation with several behaviour scientist we, however, proceeded to apply this statistical analysis, as I) this statistical analysis shows a certain robustness to type 1 error due to moderate violation of assumptions of normality at the range of sample sizes used in this study (Arnau *et al.* 2013; Blanca *et al.* 2017, 2018), II) no ideal alternative non-parametric statistical analysis exist for a mixed model ANOVA, III) the same statistical analysis was used for the data set that we are attempting to replicate. If the assumption of sphericity (Mauchly's Test) was violated in the mixed two-way ANOVA, Greenhouse-Geisser or Huynh-Feldt procedures were used to estimate epsilon in order to correct the degrees of freedom of the F-distribution. In this case, adjusted degrees of freedom are presented.

The effect of potential covariates (Age at Testing, Age at Tamoxifen treatment, Sex, Generation, Experiment) was assessed by running mixed two-way ANOVA analysis with these factors as fixed factors or continuous covariates, without the between-subject factor of Genotype included. If a covariate had a statistically significant influence on the performance, it was included in the main statistical analysis to control for the induced variability. Significant interactions of Day*Genotype in the mixed two-way ANOVA were further analysed by a planned pairwise comparison of Genotype on the first and last day of running, using the Bonferroni adjustment for multiple comparisons, in order to test if the effect was present in the beginning and at the end of behaviour testing. Asterisks are used to indicate statistical significance when appropriate: *=$p<0.05$, **=$p<0.01$ ***=$p<0.001$.

4.3. RESULTS

4.3.1 PREVENTING ADULT MYELINATION BY CONDITIONAL DELETION OF MYELIN REGULATORY FACTOR (*MYRF*)

Myelin regulatory factor (*Myrf*) is a transcription factor required for oligodendrocytes to initiate myelination. *Myrf* is not expressed in OPCs, any other CNS cell, or any cell of the PNS. McKenzie and colleagues (2014) bred several mouse lines together to obtain Myrf$^{(fl/fl)}$ and Myrf$^{(+/fl)}$ on a PDGF-Rα-Cre-ER^{TM}:R26R-YFP background (referred to as P-Myrf). Administering tamoxifen induces Cre-mediated recombination, inactivating one or both alleles of *Myrf* in PDGF-Rα expressing OPCs while simultaneously labelling the OPCs with yellow fluorescent protein (YFP). Immunolabelling for YFP and the mature Oligodendrocyte marker APC(CC1) hence allows to identify the quantity of OPCs that have differentiated into mature oligodendrocytes (YFP+|CC1+) since the administration of tamoxifen (Figure 4.1). Using this method, we found a statistically significant reduction in the density of YFP+|CC1+ cells per mm^2 (Figure 4.1D&E) in the P-Myrf$^{(-/-)}$ animals (n=11; M=12.507, SD=4.610) compared to P-Myrf$^{(+/-)}$ animals (n=12, M=89.03, SD=41.60)(unpaired t-test, t(10.25)=6.068, p<0.001). This indicates a significant reduction in the amount of differentiating oligodendrocytes by ~86%. The quantity of YFP+|CC1- cells were also slightly lower in the P-Myrf$^{(-/-)}$ (M=88.11, SD=21.86) compared to the controls (M=105.86, SD=24.59), yet this difference did not reach statistical significance (unpaired t-test, t(21)= 1.832, p=.081). This confirms that the differentiation of new oligodendrocytes is significantly reduced in P-Myrf$^{(-/-)}$ animals in the current study, when compared to their P-Myrf$^{(+/-)}$ siblings that are used as an experimental control.

4.3.2 TESTING EFFECTS OF CONDITIONAL MYRF DELETION ON COMPLEX WHEEL RUNNING.

To analyse the behaviour performance of P-Myrf $^{(-/-)}$ and P-Myrf $^{(+/-)}$ littermates a total of 132 animals were tested on the CW (P-Myrf$^{(+/-)}$; n=65, 28 females; P-Myrf$^{(-/-)}$; n=67, 28 females) that were bred in

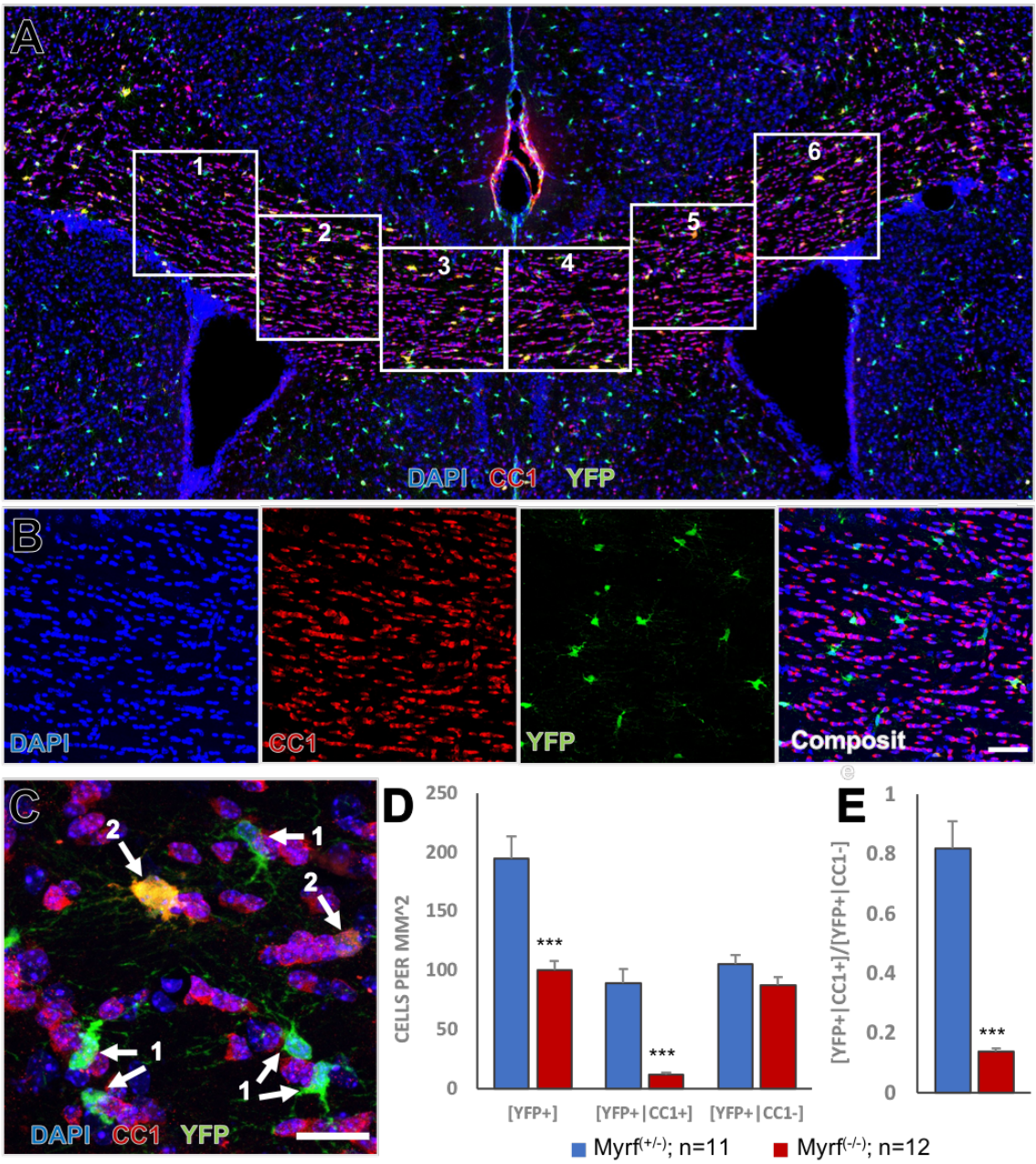


Figure 4.1. ***Deleting Myrf expression in OPCs significantly reduced the formation of new oligodendrocytes.***

*Representative image of a brain slices showing the anterior Corpus Callosum region used for quantification of YFP+ positive OPCs and CC1+ mature Oligodendrocytes. Six images were taken from each section (three sections per animal), as illustrated by the white frames in the image. (**B**) Representative individual images, split into its separate channels. DAPI was used to identify individual cell nuclei (Scale bar 50 um). **(C)** CC1+ and YFP+ cells were quantified and labelled as either (1) an OPC that is YFP+|CC1-, or (2) a recently matured Oligodendrocyte that was YFP+|CC1+. **(D)** Quantification confirmed a significant reduction of the density of YFP+|CC1+ recently matured oligodendrocytes in the P-Myrf$^{(-/-)}$ animals. **(E)** The ratio between recently matured Oligodendrocytes (YFP+|CC1+) and labelled OPCs (YFP+|CC1-) was significantly lower in the P-Myrf$^{(-/-)}$animals. Data presented as M±SEM, unpaired t-test used for statistical comparison. *** represents statistical significance of p<0.001.*

4 consecutive generations. Schematic illustrations of the experimental designs and sequences employed for each generation are displayed in Figure 4.2. Three different experimental designs were used to test the behavior phenotype of P-Myrf animals. Animals were semi-randomly assigned to either run a complex wheel with rungs removed or a normal running wheel. Two generations of animals were tested using this design (G1 and G2) (Figure 4.2A). Generation 3 (G3) of P-Myrfs was tested for their spontaneous locomotor activity (7 day home cage activity) and motor skills (Rota Rod & Balance Beam) after their completed testing on the complex wheel (Figure 4.2B). The spontaneous locomotor activity of P-Myrf animals from Generation 4 (G4) was assessed before allocating animals to a running wheel cage equipped with either a complex wheel (CW) or a fixed wheel (Complex wheel unable to rotate) (Figure 4.2C). A total of 8 animals (P-Myrf$^{(-/-)}$:n=2; P-Myrf$^{(+/-)}$:n=6) were excluded from the complex wheel running analysis due to them meeting predetermined criteria for exclusion (see methods for details and Supplementary Figure 3 for running wheel data without exclusions).

4.3.2.1 Testing for the effect of covariates on complex wheel running

Before testing for effects of genotype on behaviour, we assessed whether a number of different covariates might influence our findings, in order to determine which covariates to include in subsequent analyses. First, to test for a potential effect of the generations and sex on the performance on the CW, a mixed two-way ANOVA (Within subject factor: days (over 8 days of running); Between subject factors: Sex, Generation) was used to analyse daily running speed (average or maximum). This analysis revealed that Sex, but not Generation, had a significant effect on average (Sex: $F(1,117)=21.699$, $p<0.001$) and maximum (Sex: $F(1,117)=20.641$, $p<0.001$) running speeds on the complex wheel, with females consistently outperforming males (Supplementary Figure 4A&B). Apart from consistently running longer distances on the CW (Supplementary Figure 4D), females also spent more time on the CW than males over a period of 8 consecutive days (Supplementary Figure 4E&F). While there was an expected difference in body weight between sexes, there was no

difference in body weight between P-Myrf$^{(-/-)}$ and P-Myrf$^{(+/-)}$ animals for either sex (Supplementary Figure *4*C) at the start of behaviour testing.

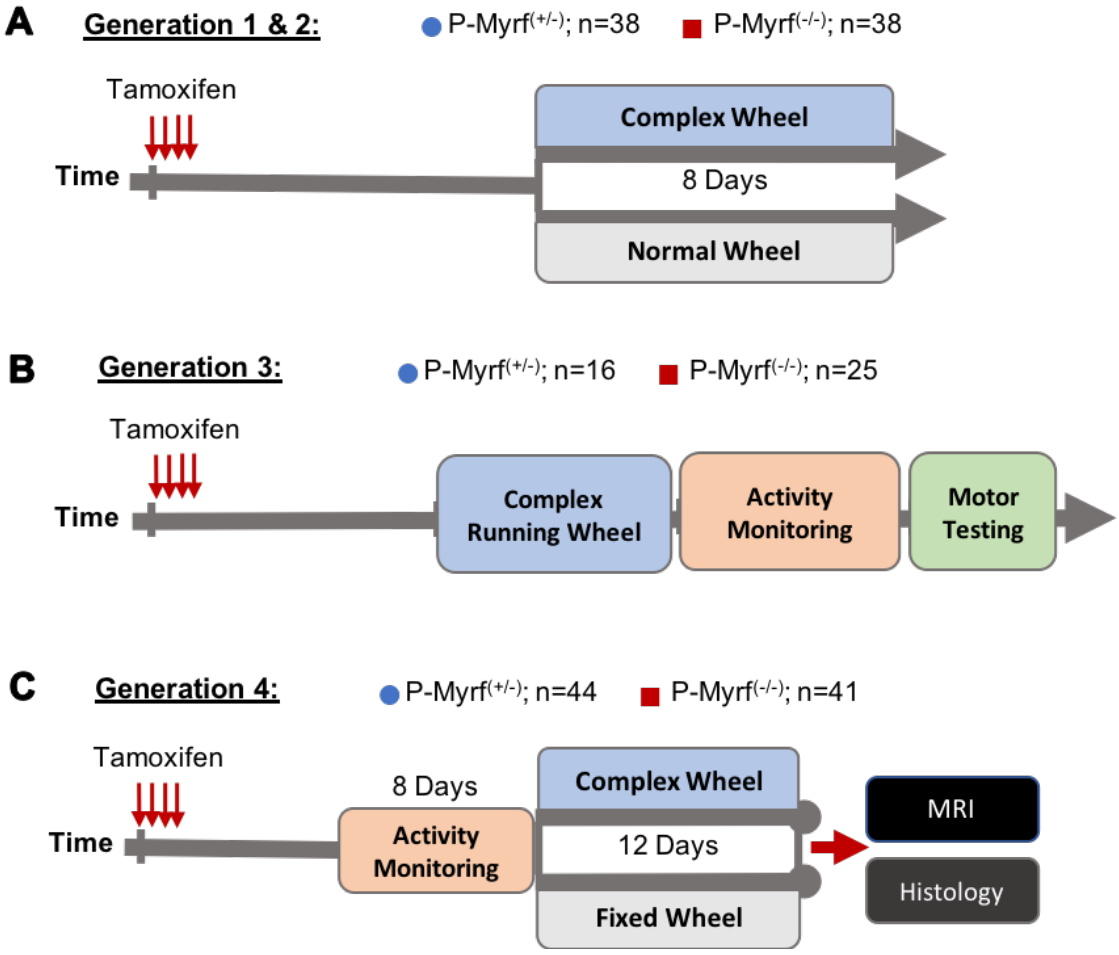


Figure 4.2. ***Schematic illutrations of experimental designs used to test the phenotype of P-Myrfs.***

(A) *Experimental design to test and compare the behaviour performance of mice on the complex and the normal running wheel* ***(B)*** *Experimental design to test performance of mice on the complex wheel, as well as the their wider behavioural phenotype regarding spotanous locomotor activity and motor skills.* ***(C)*** *Experimental design to test spontaneous locomotor activity in experimentally naiive animals, the effects of complex wheel running on cellular and microstrucual changes in the brain. The active control condition in this experimental design exposed mice to a complex wheel that was prevented from rotating (fixed wheel, FW) in the same environmental and cage (Figure 3.1) and set up. The biological phenotype of these animals was then assessed by ex vivo magnetic resonance imaging (MRI) and immunohistochemistry (Chapter 5).*

The age of tamoxifen treatment (Range: P58-93, M=77.11 SD=8.48), the age at behaviour testing (P92-135, M=109.92, SD=7.94) and the days between tamoxifen treatment and behaviour testing (P21-43, M=32.28, SD=7.52) varied between animals and generations (Table 2). As the formation of new Oligodendrocytes was prevented in an age range in which myelination is still ongoing (Young *et*

al. 2013; Hill *et al.* 2018), interfering with developmental myelination at different ages and for different lengths of time could lead to different behavioural phenotypes. However, we found no significant correlation between the performance of the P-Myrf$^{(-/-)}$ on the CW (average running speed) and any of the age parameters mentioned above in the compiled data set of all P-Myrf animals (Supplementary Figure 5). Yet, it is of note that our experiments were not specifically designed to compare the effect of these age parameters on running performance and age parameters varied between generations (Table 2).

In summary, of the potential covariates tested, only Sex was found to be significantly associated with running behaviour and so this factor was included as a fixed factor in all subsequent analyses of genotype differces to control for the induced variability.

4.3.2.2 Conditional knock-out (KO) of Myrf leads to reduced performance on complex wheel

Performance of P-Myrf$^{(-/-)}$ and P-Myrf$^{(+/-)}$ littermates on the complex running wheel was analysed using the combined data from all four separate generations of animals (P-Myrf$^{(+/-)}$; n=59, 28 females); P-Myrf$^{(-/-)}$; n=65, 28 females). A schematic illustration of experimental design can be seen in Figure 4.3B. Overall, the mean daily average and maximum speeds achieved by the P-Myrf$^{(-/-)}$ group were lower than their P-Myrf$^{(+/-)}$ siblings (Figure 4.3C&D). Statistical analysis using a mixed two-way ANOVA (within subject factor: Day, between subject factor: Genotype, Sex) revealed a significant Day*Genotype interaction for both average daily speed ($F(2.354,282.4)= 6.258$, $p=0.001$, effect size $\eta_p^2 =0.050$, Observed Power=0.935, Figure 4.3C) and maximum daily speed ($F(2.524,302.9)= 6.512$, $p=0.001$, effect size $\eta_p^2 =0.048$, Observed Power=0.940, Figure 4.3D).

Table 2. ***Variability of animal's age at important experimental timepoints within different generations of Myrf-cKO animals.***

Age is presented in days after birth (postnatal day).

Generation	n	Age at tamoxifen treatment	Age between tamoxifen treatment and CW	Age at beginning of CW testing
G1	17	Range=69-84 Mean=73.5 SD=3.9	Range=31-42 Mean=36.5 SD=5.5	Range=100-126 Mean=109.8 SD=6.5
G2	19	Range=58-93 Mean=74.6 SD=13.1	Range=34-42 Mean=38.1 SD=4.1	Range=92-135 Mean=112.4 SD=13.1
G3	39	Range=64-83 Mean=71.4 SD=5.9	Range=30-43 Mean=37.8 SD=5.9	Range=96-114 Mean=109.14 SD=4.04
G4	49	Range=79-88 Mean=83.7 SD=21-30	Range=21-30 Mean=25.4 SD=2.9	Range=102-116 Mean=109.1 SD=2.9

The significant interactions of Day*Genotype were further analysed by a planned pairwise comparison of Genotype on the first and last day of running, using the Bonferroni adjustment for multiple comparisons. On the first day, performance was lower in the P-Myrf$^{(-/-)}$ for both average and maximum speed, but not statistically significantly different between the two genotype groups. On the last day of running, P-Myrf$^{(-/-)}$ had a significantly lower running performance, for both average running speed ($F(1,106)=8.406$, $p=0.010$, $\eta_p^2=0.073$, Observed Power=0.819) and maximum running speed ($F(1,106)=13.265$, $p<0.001$, $\eta_p^2=0.111$, Observed Power=0.950). We also calculated the overall improvement in maximum running speed achieved per animal on the complex wheel (Overall maximum speed – maximum speed within the first hour of running on the wheel) which confirmed

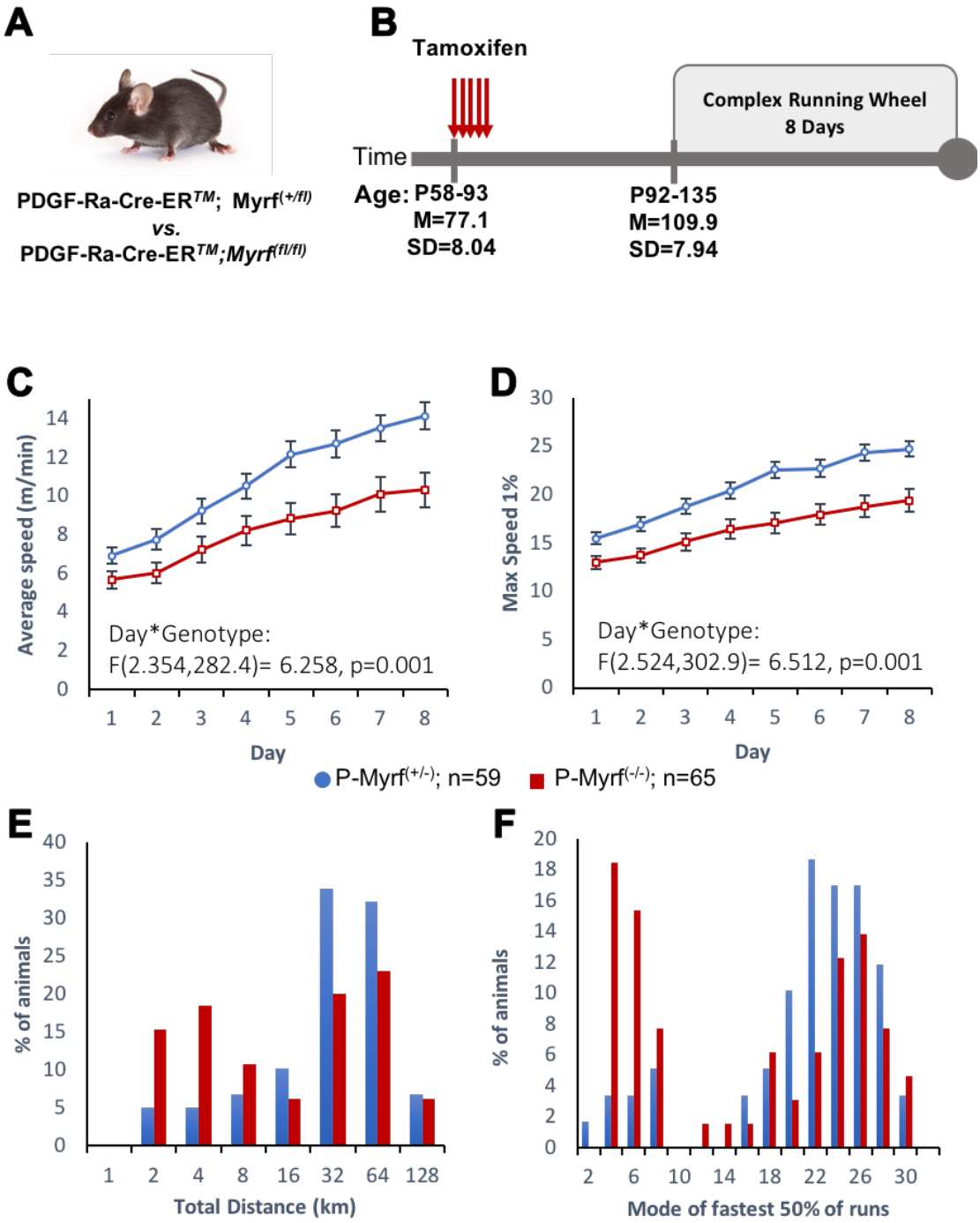


Figure 4.3. ***Preventing differentiation of new OL leads to impaired performance on the complex wheel.***

(A) *Animals, bred on a PDGF-Ra-Cre-ER^{TM}; with two floxed alleles of Myrf were compared to animals only have a single allele floxed.* ***(B)*** *Schematic illustration of experimental design. Data presented is merged from several experiments derived from 4 generations of animals. For both* ***(C)*** *Average and* ***(D)*** *Maximum speed a statistically significant effect for Genotype*Day was detected using a Mixed Two-way ANOVA.* ***(E)*** *The frequency distribution of Total running distance in 8 days reveals a large spread, ranging from around 64 km run in 8 days to around 2 km.* ***F.*** *Frequency distribution of the maximum daily cruising speed (defined as the Mode of the fastest 50% of active intervals) revealed a bimodal distribution in running performance that was especially prominent in the P-Myrf$^{(-/-)}$. Data presented as Mean ±SEM. Data processed in 1 minute long intervals for comparison with McKenzie et al. (2014).*

that P-Myrf$^{(-/-)}$ showed an overall significantly lower improvement in running performance (Kolgomorov-Smirnov non-parametric test, p<0.022, Figure 4.4A). Taken together, these results replicate the main behavioural results obtained by McKenzie *et al.* (2014) (Figure 4.5A&B).

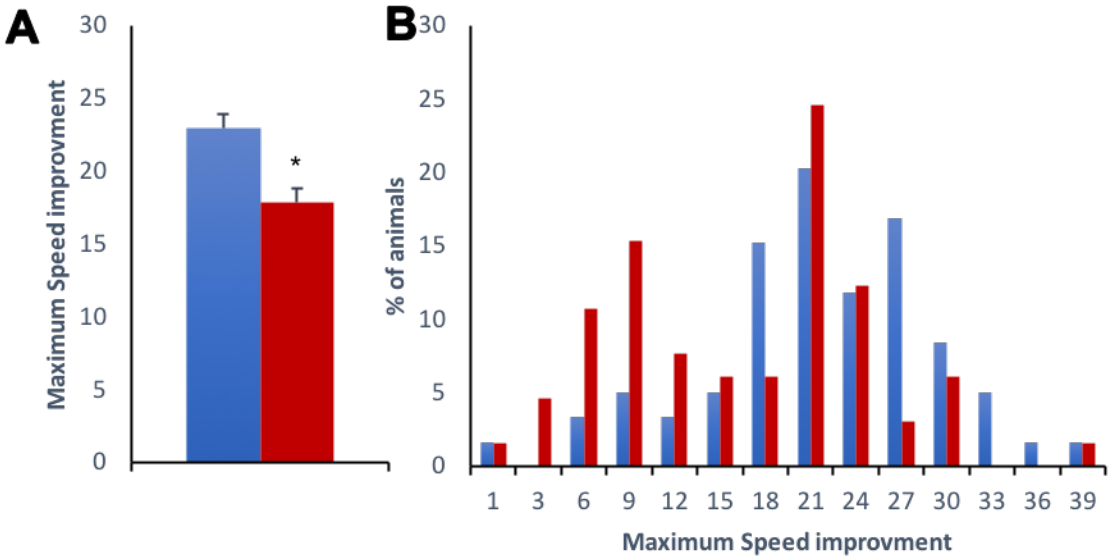


*Figure 4.4. **P-Myrf$^{(-/-)}$ animals had a significantly lower improvement of their overall running speed.** Improvement of maximum running speed was calculated by subtracting the maximum running speed achieved within the first hour of the first night from the overall maximum running speed achieved within 8 days. **(A)** The mean improvement in maximum running speed on the complex wheel was significantly lower for P-Myrf$^{(-/-)}$ animals, when compared to their P-Myrf$^{(-/-)}$ littermates (*p=0.022). Data presented as Mean ± SEM. Kolgomorov-Smirnov non-parametric test was used to test the difference statistically. **(B)** The frequency distribution of maximum speed improvements indicated bimodal distribution with in the P-Myrf$^{(-/-)}$ population.*

4.3.2.3 *Exploring variability in performance across animals*

The distance run by each animal varied greatly, ranging from <2 km to >73km (M=25.03, SD=20.69). The frequency distribution of the total distance run per animal over 8 days indicates a bimodal distribution within the P-Myrf$^{(-/-)}$ animals, which was much less prominent in the control group (Figure 4.3E, Independent sample Mann-Whitney U, p=0.013). The most frequent running speed (Mode) within the 50% fastest active intervals on an animal's fastest day (referred to as 'top cruising speed') is a parameter of running performance that most clearly visualises a bimodal distribution in running performance in the P-Myrf$^{(-/-)}$ animals (Figure 4.3F). A large proportion P-Myrf$^{(-/-)}$ animals

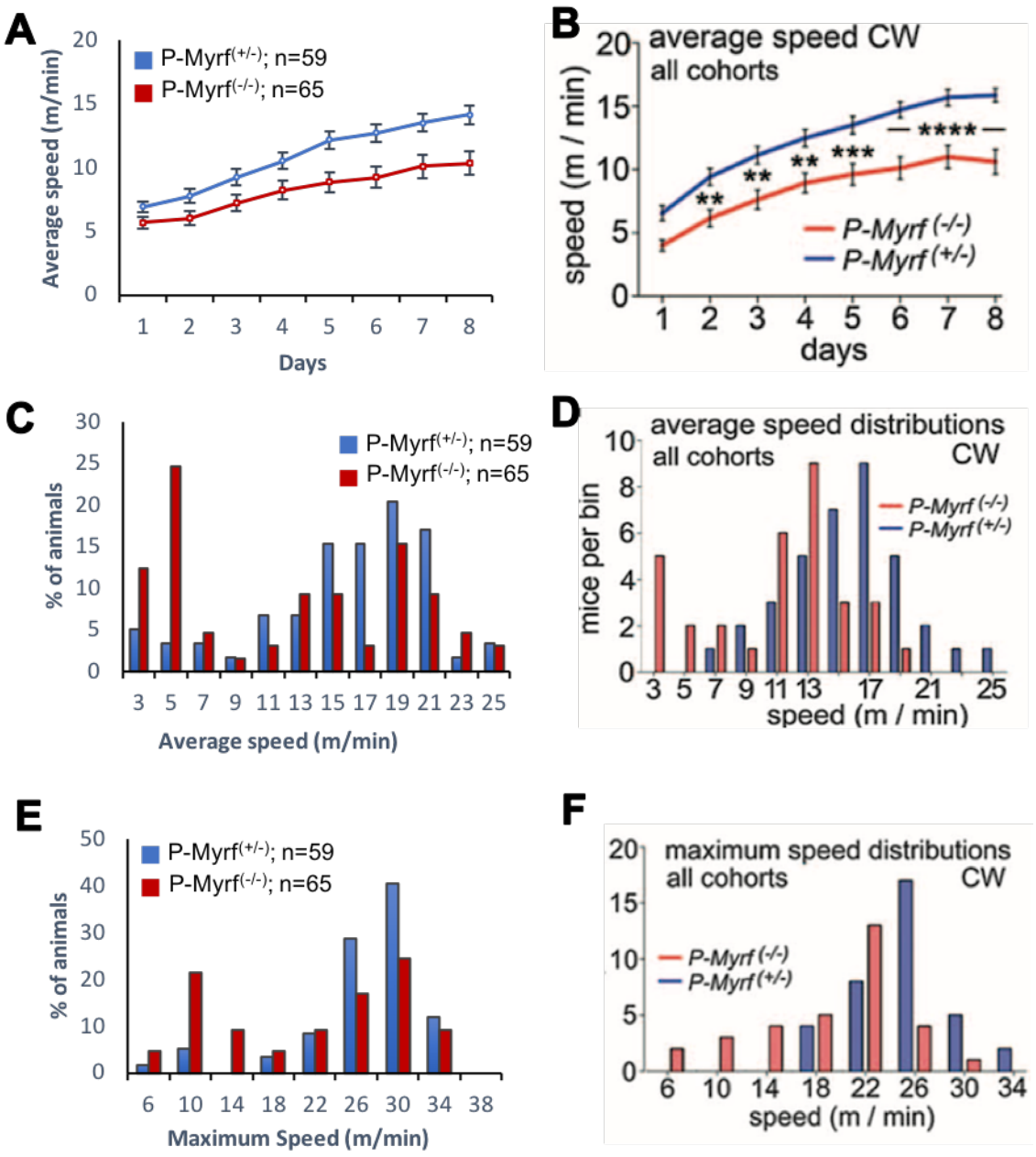


Figure 4.5. ***Comparing running performance results on complex wheel to the results obtained by Mckenzie et al (2014).***

(A) *Average running performance in the current study and* ***(B)*** *results obtained by McKenzie et al (2014) were comparable in their main effect of genotype. The frequency distribution of average running speed in the current study* ***(C)*** *indicates a bimodal distribution in the P-Myrf$^{(-/-)}$ population with a second peak at lower speeds, a trend that was also present in the study by* ***(D)*** *McKenzie et al. (2014). However, McKenzie et al. found that the the peak of the faster P-Myrf$^{(-/-)}$ population (~13 m/min) was lower than in the P-Myrf$^{(+/-)}$ population (~17 m/min). This apparent shift in the normal distribution distinguishing the two populations is not clear in the current study* ***(C)****. The same observations can be be made when comparing the frequency distribution of maximum speeds* ***(E, F)****. Data presented as Mean ± SEM. Data processed in 1 minute long timebins for comparison with McKenzie et al. (2014).*

(~42%) had a cruising speed of <8 m/min, even on their fastest day. Yet, the remaining P-Myrf$^{(-/-)}$ animals showed running performance comparable to their well performing P-Myrf$^{(+/-)}$ littermates, and even a small proportion of controls (~13%) had a cruising speed that was in the lower ranges (<8 m/min). This bimodal distribution in running performance of the P-Myrf$^{(-/-)}$ population can also be observed when plotting the frequency distribution of the highest daily average running speed (Figure 4.5C), maximum running speed (Figure 4.5E), and overall improvement in running speed (Figure 4.4B), indicating that a population of low performing P-Myrf$^{(-/-)}$ mice are driving the group effect of a reduced performance on the CW. McKenzie et al. (2014) reported that the average speeds of P-Myrf$^{(+/-)}$ mice (on the seventh day) had an approximately normal distribution (p = 0.2, K-S test), whereas the average speeds of P-Myrf$^{(-/-)}$ mice were bimodal and skewed toward lower speeds (Independent sample Mann-Whitney U, different distributions, p=0.007) (Figure 4.5D). That means that McKenzie *et al.* (2014) found a similar trend towards a bimodal distribution in running performance (Figure 4.5D), although this low performing group of P-Myrf$^{(-/-)}$ was proportionally smaller in their study and not as pronounced when looking at the frequency distribution of maximum running speed (Figure 4.5F).

4.3.2.4 Quantifying running speed with finer time bins

The robust effect for a difference in running performance between P-Myrf$^{(-/-)}$ mice and P-Myrf$^{(+/-)}$ mice was observed regardless of whether the speed was calculated in 1 minute timebins (Figure 4.3C&D) or 10 second long timebins (Supplementary Figure 3). As about 35-40 % of animal's individual runs were shorter than 1 min, calculating running speed by measuring wheel spins during a 10 sec timebin yielded an overall higher and more accurate estimation of running speed (Supplementary Figure 3A&B). While the data in Figure 4.3 and Figure 4.5 was processed in the same 1-minute timebin as in McKenzie *et al* (2014), 10-sec timebins were used for the calculation of running speed for the remaining analysis to more accurately measure times in which animals were active on the running wheel.

4.3.2.5 Conditional KO of Myrf does not lead to a performance deficit on the Normal Running wheel

To test whether the observed behavioural deficit on the CW was caused by a more general deficit in wheel running *per se*, P-Myrf$^{(-/-)}$ (n=36) and P-Myrf$^{(+/-)}$ (n=35) littermates from the first two generations of P-Myrfs were semi-randomly assigned (meaning, balancing the numbers of sex and littermates in each experimental group) to run either the complex wheel or a normal running wheel (Figure 4.6A). The normal running wheels (NW) used were the same type of wheel without any of the rungs removed. In the subpopulation of animals that ran the complex wheel in parallel to their littermates on the normal wheel, the mean average running speed was lower for the P-Myrf$^{(-/-)}$ animals compared to the P-Myrf$^{(+/-)}$ controls (Figure 4.6B). Statistical analysis using a mixed two-way ANOVA (Within subject factor: Day, Between subject factor: Genotype, Sex) confirmed a significant main effect for Genotype for the average speed on the complex wheel ($F(1,32)=4.732$, $p=0.037$, $\eta_p^2=0.122$, Observed Power=0.561), although the interaction between genotype and day was not significant in this subgroup. No main effect of genotype ($F(1,31)=0.257$, $p=0.616$), or interaction of Day*Genotype, was observed for the animals that ran the normal running wheel, as performance was similar between the two genotype groups (Figure 4.6C).

4.3.2.6 Performance of P-Myrf$^{(-/-)}$ animals on the CW was impaired within the first hours

Previous work by Xiao *et al.* (2016) indicated that P-Myrf$^{(-/-)}$ show an impaired performance on the complex wheel within the first hours of behaviour testing and so we assessed running behaviour over time during the first three nights of running. Average running speed varied across the hour of the night for both genotypes (Figure 4.7A&B). On the first night of testing, average running speed during the first hour of complex wheel running was similar between P-Myrf$^{(-/-)}$ and P-Myrf$^{(+/-)}$ animals (Figure 4.7C), yet running performance within the following hours diverged, with P-Myrf$^{(-/-)}$ animals showing a lower overall average running speed for the remainder of the night. This result was comparable to the data collected by Xiao et al (2016)(Figure 4.7E). The difference in performance

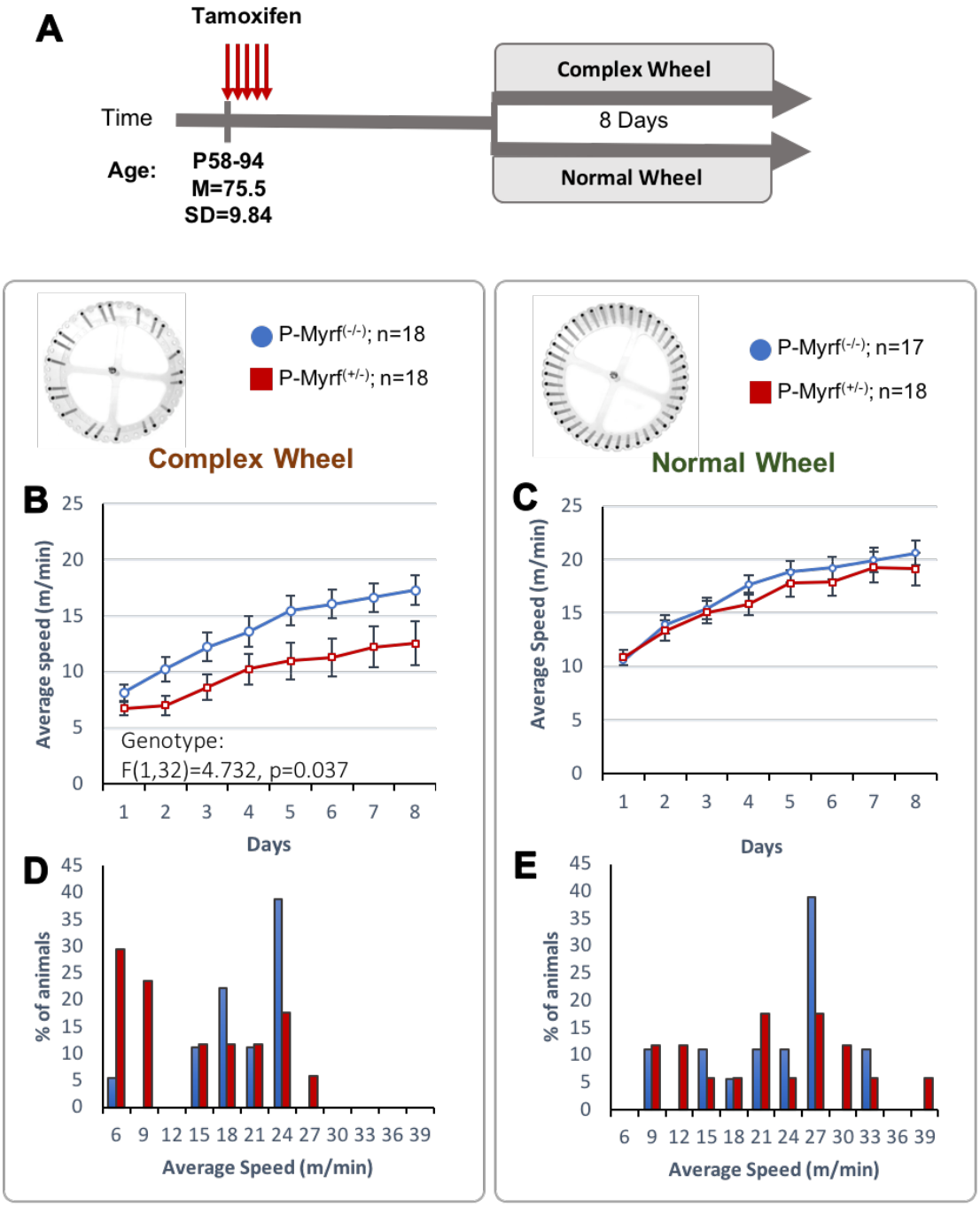


Figure 4.6. ***Performance on the Normal running wheel was not impaired by conditional deletion of Myrf.*** *(**A**) Schematic illustration of the experimental design. Littermates were semi-randomly assigned to either run the complex wheel or a normal running wheel. (**B**) Average running performance was significantly lower for P-Myrf$^{(-/-)}$ animals on the complex wheel, when compared to P-Myrf$^{(+/-)}$ animals, while (**C**) there was no difference between the two genotypes in the littermates that ran the normal wheel. Frequency distribution of the average speeds on the complex wheel (**D**) indicate that a subpopulation of low performing P-Myrf$^{(-/-)}$ were driving the genotype effect. Frequency distribution of average speeds on the normal wheel (**E**) for comparison. Data presented as Mean ± SEM.*

between the genotypes was confirmed to be statistically significant using a mixed two-way ANOVA on average running speed across the first four hours of running on the complex wheel (within-subject factor: Interval (12 intervals of 20 mins), between-subject factors: Genotype, Sex), which indicated a significant Interval*Genotype interaction for running performance ($F(4.83,579.6)= 2.672$, $p=0.036$, η_p^2 =0.021, Observed Power=0.796). The time at which animals were first exposed to the wheel varied between the experiments (total of 14 separate experiments) in our study, ranging from 2,5 hours to 30 min before the lights were switched off. Controlling for this potential covariate in the statistical analysis yielded the same result (Mixed ANOVA, within-subject factor: Interval (12 intervals of 20 mins), between-subject factors: Genotype, Sex, Experiment (14 levels); $F(5.138, 375.04)= 3.074$, $p=0.009$, η_p^2 =0.040, Observed Power=0.980).

To quantify how much animals improved their individual maximum running performance within the first hours, we calculated the difference between the maximum running speed within the first 40 minutes of testing on the first night and their maximum running speed within the subsequent 4 hours of running (Figure 4.7D). P-Myrf$^{(-/-)}$ animals (M=8.43, SD=4.74) showed a lower overall improvement in their maximum speed within the first hours when compared to P-Myrf$^{(+/-)}$ controls (M=10.17, SD=4.41), a difference that was statistically significant (*ANOVA, Fix factors: Genotype, Sex, Experiment; n=124,* $F_(1,92)=7.868$, $p=0.006$, η_p^2 =0.079, Observed Power=0.793). Taken together, this data suggests an early deficit in running performance on the complex wheel in P-Myrf$^{(-/-)}$ animals that was comparable to the deficit observed by Xiao *et al.* (2016) (Figure 4.7B and E).

4.3.2.7 P-Myrf$^{(-/-)}$ animals spent less time running the complex running wheel than P-Myrf$^{(-/+)}$ controls.

As wheel running is a voluntary task and access to running wheels was provided 24 hours a day, animals could vary greatly in the time they spent running and improving their performance on the complex wheel. Hence, we measured the overall time animals were active on the wheel by quantifying the number of 10 second intervals in which the running wheel completed at least 1 full

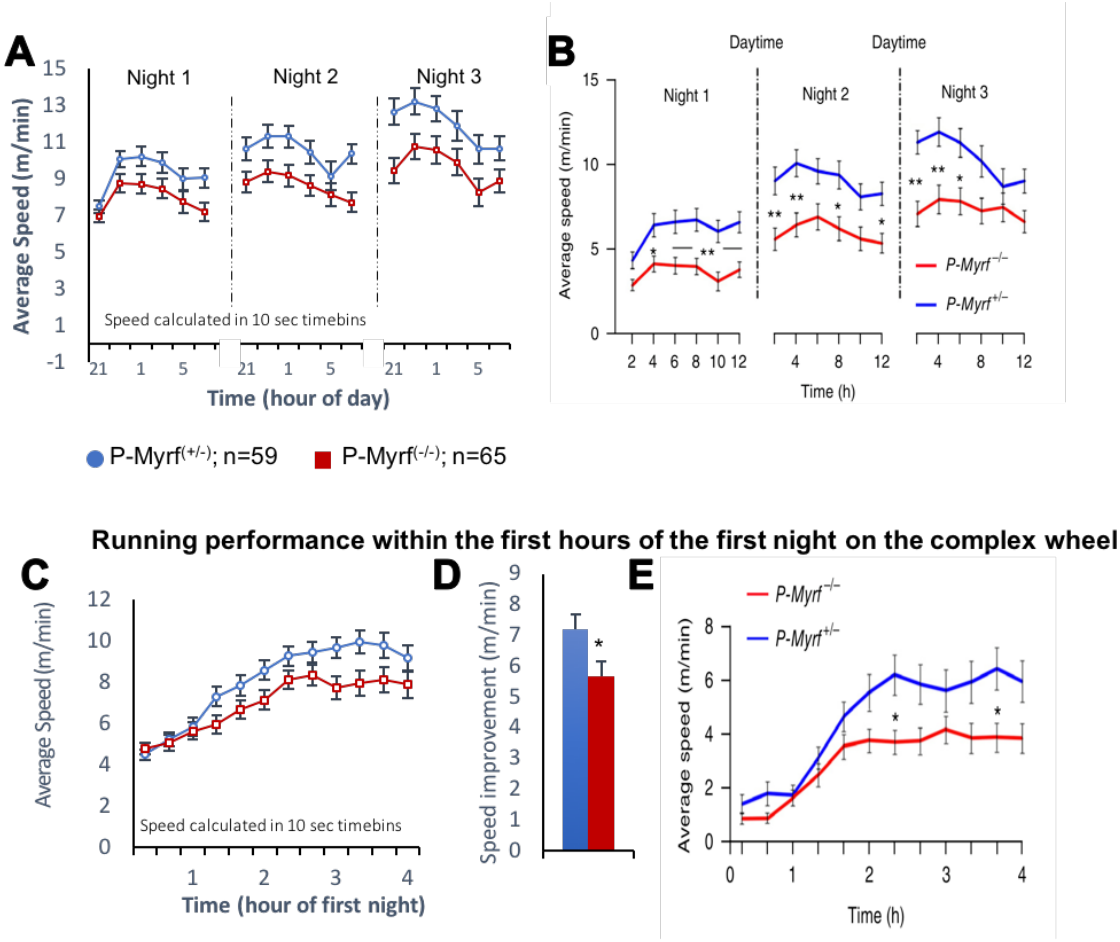


Figure 4.7. ***Performance P-Myrf$^{(-/-)}$ animals on the complex wheel was reduced within the first hours of testing.***

(A) *The group average speed of animals varied across the night, being generally the highest around the first 2-4 hours after the beginning of the dark period. Data presented in 2 hour intervals. Speed was calculated in 10 second timebins.* ***(B)*** *The data collected by Xiao et al. (2016) showed a similar pattern in the data.* ***(C)*** *Average running speed in 20-min intervals during the first 4 hour of the dark period on the first day of testing, starting at the beginning of the first night (21:00). There was a statistically significant Time*Genotype interaction F(4.83,579.6)= 2.672, p=0.036, indicating an early deficit on the complex wheel of P-Myrf$^{(-/-)}$.* ***(D)*** *The overall improvement in maximum running speed made within the first 4 hours of running (Maximum speed within first 40 min - Maximum speed within first 4 hours) was significantly lower in P-Myrf$^{(-/-)}$ animals (*p<0.05).* ***(E)*** *Data from Xiao et al (2016) for comparison, showing average speeds in 20-min intervals during the first 4 hours of the first night. Data presented as Mean ± SEM.*

rotation (referred to as an 'active interval'). Overall, animals were most active within the first hours of the night (Figure 4.8A&B) and spent the most time interacting with the wheel on the first day of running (Figure 4.8A&C). A mixed two-way ANOVA (within subject factors: Day (8 Levels), Hour of Night (12 Levels); between subject factors: Genotype, Sex) revealed an overall main effect for

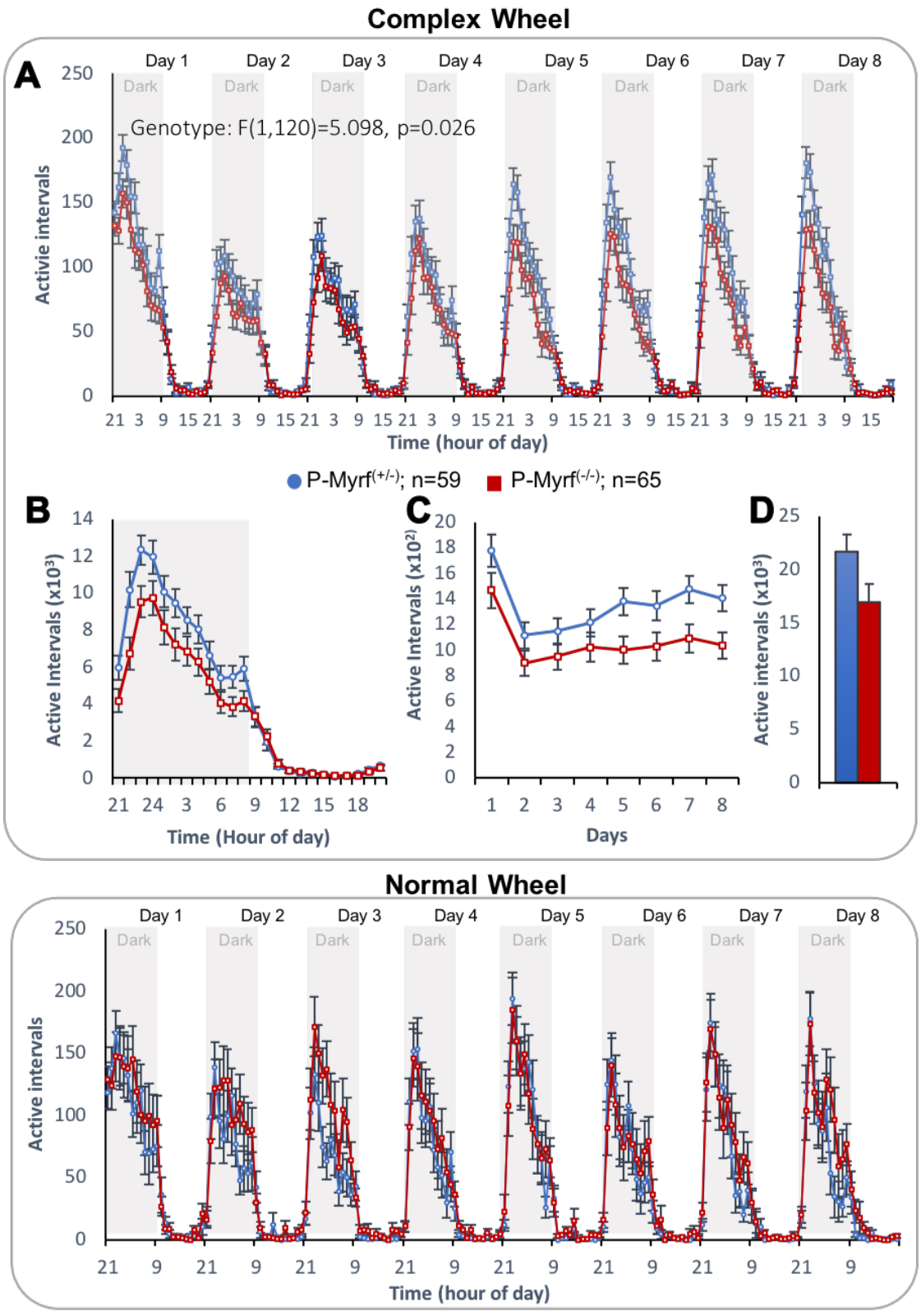


Figure 4.8. ***P-Myrf$^{(-/-)}$ animals spent less time running on the the complex wheel.***

(A) *Active intervals on the complex wheel in 1-hour intervals over the period of 8 days.* ***(B)*** *Sum of the active intervals per hour of the day. Animals were most active on the complex wheel during the beginning of the night.* ***(C)*** *Active intervals per day of running were highest on the first day of exposure to the wheel.* ***(D)*** *Overall, P-Myrf$^{(-/-)}$ spent less time running on the complex…* *(continue next page)*

(Continiuation of legend from Figure 4.8) …wheel than their P-Myrf$^{(+/-)}$ siblings. A mixed two-way ANOVA (within subject factors: Day (8 Levels), Hour of Night (12 Levels); between subject factors: Genotype, Sex) revealed an overall main effect for genotype (F(1,120)=5.098, p=0.026, ηp2=0.041, Observed Power =0.610). ***(E)*** *Active intervals on the normal running wheel in 1-hour intervals over the period of 8 days. No statistically significant differences between genotypes was found using the same analysis as mentioned above. Data presented as Mean ±SEM.*

genotype (F(1,120)=5.098, p=0.026, η_p^2=0.041, Observed Power =0.610), confirming a statistically significant reduction in active intervals in the P-Myrf$^{(-/-)}$ group. Overall running speed on the complex wheel was correlated to the total number of active intervals animals spent on the complex wheel (Spearman's rho; r_s=0.802, n=124, p<0.001, Supplementary Figure 6). Interestingly, this genotype-specific lack of active engagement with the running wheel was not found for the normal running wheel (Figure 4.8E), albeit on a smaller subset of animals, indicating that the observed lack of activity of P-Myrf$^{(-/-)}$ animals did not generalize to wheel running *per se*.

4.3.3 Investigating spontaneous locomotor activity of P-Myrf animals in the home cage using passive infrared (PIR) sensors

The observed reduction in overall running activity on the complex wheel (Figure 4.8) raised the possibility that an underlying deficit in spontaneous locomotor activity may lead to a general deficit in performance on the running wheel. To test this hypothesis, we monitored the spontaneous locomotor activity levels of P-Myrf animals in an environment without wheel access.

4.3.3.1 Assessing differences in spontaneous activity following CW running

After completing behaviour testing on the complex wheel, a subset of animals (P-Myrf$^{(-/-)}$: n=25, 11 females; P-Myrf$^{(+/-)}$: n=15, 7 females) from generation 3 were singly housed in a home cage like environment (referred to as a PIR cage) for 7 days (24h a day) and their spontaneous locomotor activity was monitored using passive infrared (PIR) sensors (Brown *et al.* 2017). A schematic illustration of the experimental design can be found in Fig. 4.9A. The employed sensors measured activity every 100ms, recording if the animal was moving (=1) or not (=0). On average, animals were most active during the first 2-4 hours of the night (Figure 4.9B&C), the same timeframe in which they

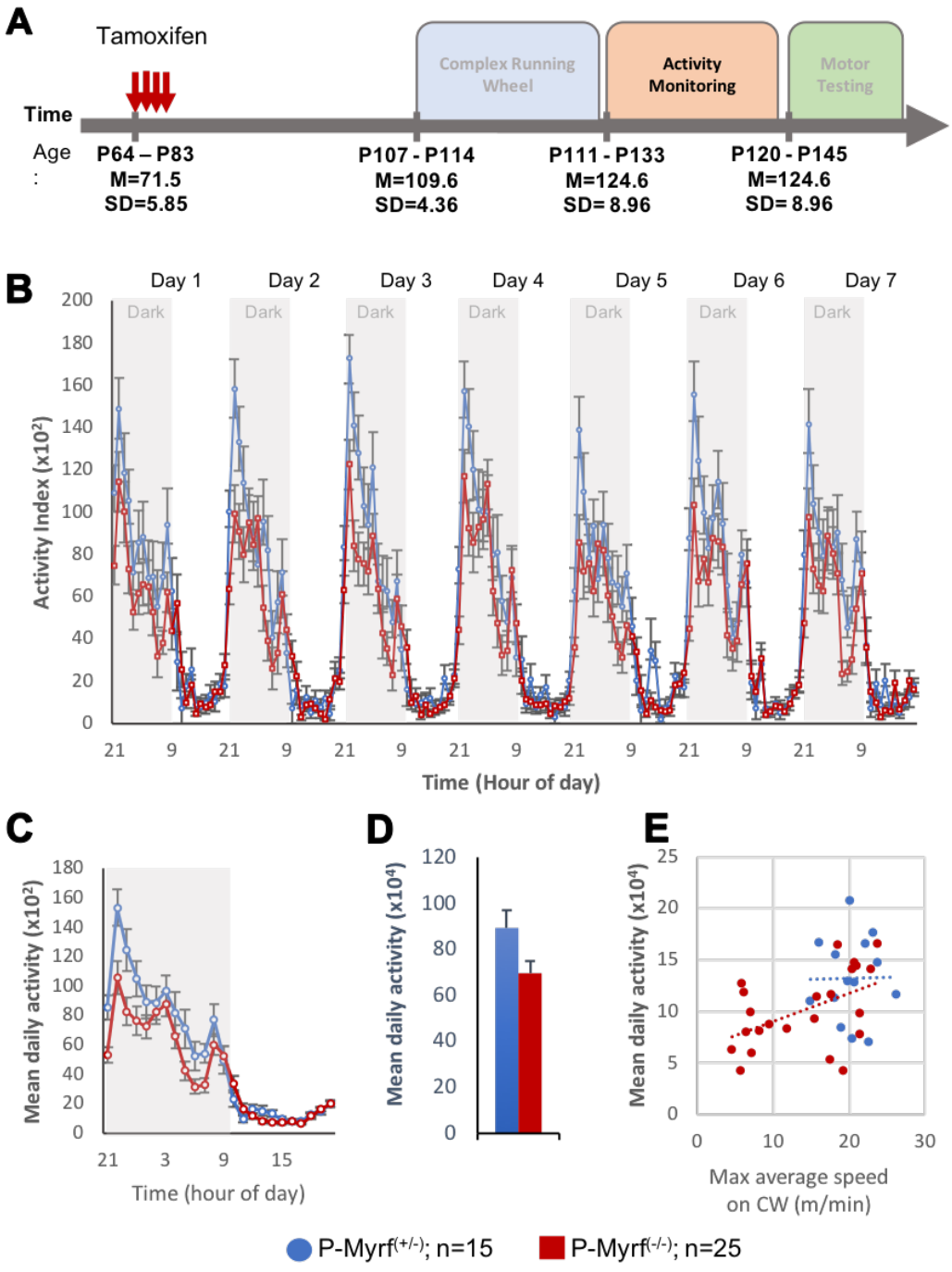


Figure 4.9. ***Spontaneous locomotor activity in home cage was reduced in P-Myrf$^{(-/-)}$ after running the complex wheel. (A)***

Schematic illustration of the experimental design. Animal's activity in the home cage environment was tested after running the complex wheel. ***(B)*** *Activity in the home cage in 1-hour intervals for 7 days. Activity was relatively consistent across days.* ***(C)*** *Mean daily activity in 1-hour intervals compile over a 24h period. Animals were most active during the first hours of the night.* ***(D)*** *Overall, P-Myrf$^{(-/-)}$ animals were less active than their P-Myrf$^{(+/-)}$ siblings. This difference was confirmed to be statistically significant using mixed two-way ANOVA (within subject factors: Day (7 Levels), Hour of Night (12 Levels); between subject factors: Genotype, Sex), which revealed an overall main effect for genotype ($F(1, 36) = 5.795$, $p=0.021$). Data presented as Mean ±SEM.* ***(E)*** *Running speed on the CW and activity levels in the home cage were significantly correlated overall (Spearman's rho; $r_s=0.455$, $n=37$, $p=0.006$).*

were most active on the running wheels (Figure 4.8). P-Myrf$^{(-/-)}$ animals appeared less active in the PIR cage environment when compared to their P-Myrf$^{(+/-)}$ siblings (Figure 4.9C,D). Indeed, testing for this difference statistically using a mixed two-way ANOVA (within subject factors: Day (7 Levels), Hour of Night (12 Levels); between subject factors: Genotype, Sex) revealed an overall main effect for genotype ($F(1, 36) = 5.795$, $p=0.021$, $\eta_p^2=0.139$, Observed Power =0.649), indicating that P-Myrf$^{(-/-)}$ had a lower spontaneous locomotor activity than the P-Myrf$^{(+/-)}$ controls. Activity in the PIR cage after complex wheel running correlated positively with the animal's maximum average running speed on the CW (Spearman's rho; $r_s=0.455$, $n=37$, $p=0.006$; Fig 4.9E), suggesting that animals who engaged in more active bouts on the CW were more spontaneously active in the home cage environment. Separating the analysis by genotype, this correlation was only significant for P-Myrf$^{(-/-)}$ animals ($r_s=0.366$, $n=23$, $p=0.025$; Figure 4.9E) and not for Myrf$^{(+/-)}$ ($r_s=0.011$, $n=14$, $p=0.956$,Figure 4.9E). However, Fisher r-to-z transformation indicated no statistically significant difference between those two correlations ($p=0.322$), providing no evidence that the link between activity in the PIR cage and the activity on the complex wheel was specific to P-Myrf$^{(-/-)}$ animals.

4.3.3.2 Assessing differences in spontaneous activity prior to CW running

As chronic voluntary exercise such as wheel running affects overall fitness and influences and interacts with the circadian rhythm (Yasumoto *et al.* 2015), it is possible that genotype-specific differences in the ability to run the complex wheel may have influenced the amount and pattern of subsequent spontaneous activity in the PIR cage environment. To control for this possibility, we recorded the spontaneous locomotor activity of a subset of experimentally naïve animals in generation 4 (P-Myrf$^{(-/-)}$: n=27, 11 females; P-Myrf$^{(+/-)}$: n=28, 11 females) prior to investigating their performance on the complex running wheel. A schematic illustration of the experimental design can be found in Figure 4.10A. Interestingly, in this experimental set-up, activity levels in the PIR cages were very similar between groups and no main effect for genotype was found (Figure 4.10B-D) in this subset of animals. Additionally, activity in the PIR cage before running the

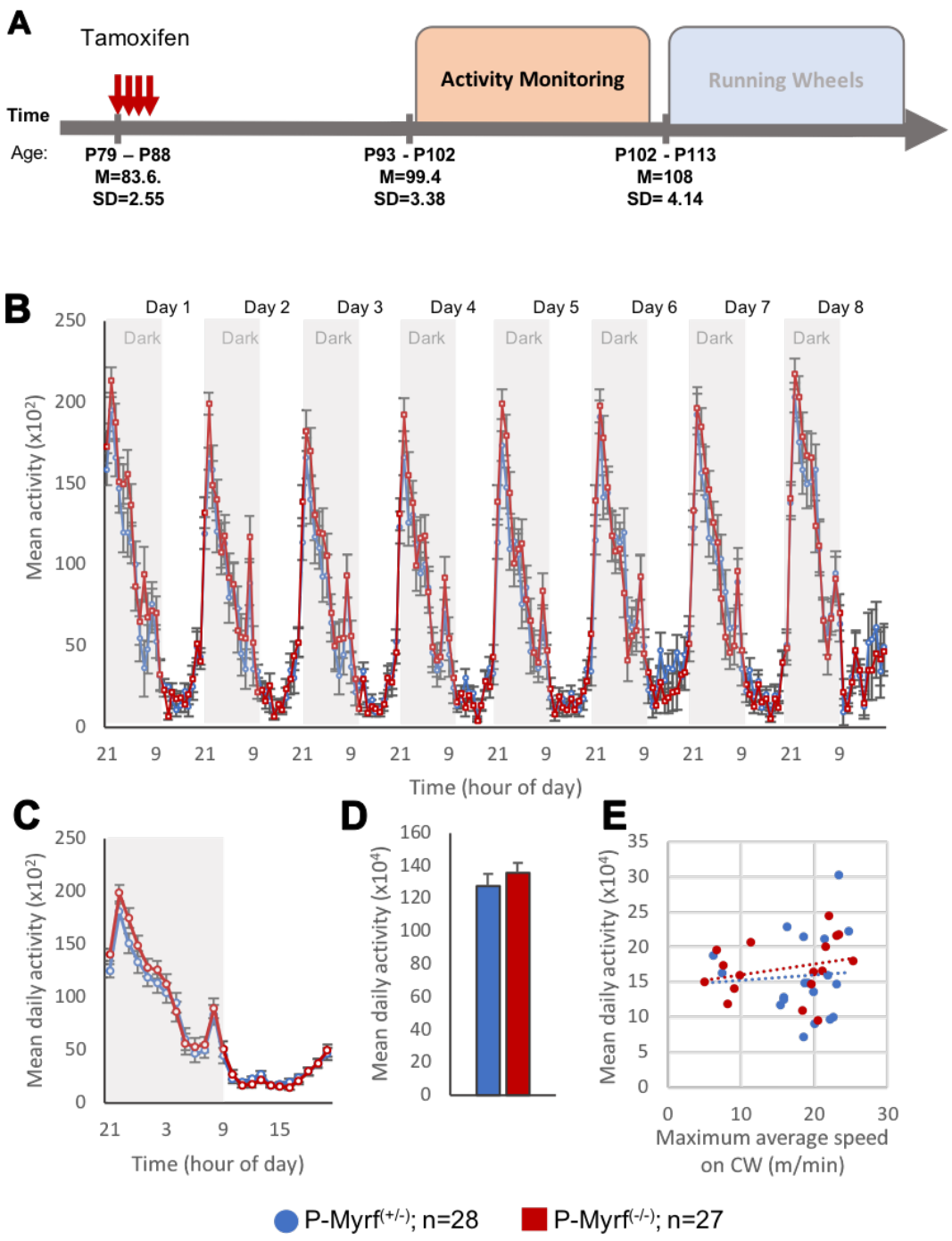


Figure 4.10. ***Spontaneous locomotor activity in home cage was similar between genotypes when tested before running the complex wheel.***

(A) *Schematic illustration of the experimental design. Animal's activity in the home cage environment was tested prior to being introduced to the complex running wheel cages.* ***(B)*** *Activity in the home cage in 1-hour intervals for 7 days. Activity was relatively consistent across days.* ***(C)*** *Mean daily activity in 1-hour intervals compile over a 24h period. Animals were most active during the first hours of the night.* ***(D)*** *Overall, P-Myrf$^{(-/-)}$ animals had similar levels of spontaneous locomotor activity when compared to their P-Myrf$^{(+/-)}$.* ***(E)*** *Relationship between running speed on the CW and activity levels in the home cage. Data presented as Mean ± SEM.*

complex wheel did not correlate with the animal's subsequent running performance on the complex wheel (Spearman's rho; r_s=0.122, n=36, p=0.253; Figure 4.10E), nor with the running performance within the individual genotype groups.

4.3.3.3 Potential confounds

While the results reported in the preceeding sections indicate that genotype specific differences in spontaneous activity were only present *after* testing on the complex running wheel, experimental limitations have to be considered. Different subsets of animals from different breeding generations were tested in the PIR cages for each experiment, instead of testing the same set of animals before and after complex wheel running. Additionally, the ages at which animals of the different subsets of animals received tamoxifen treatment, and the age at which they were tested, were different for both subset of animals (Figure 4.11D). Further, the two experiments differed in whether the primary effect of genotype on CW running was present. In the 'Post CW experiment' (Figure 4.9A), P-Myrf$^{(-/-)}$ animals were significantly less active on the complex wheel than P-Myrf$^{(+/-)}$ animals (Total active intervals, unpaired t-test: t(35)=0.032; Fig 4.11B), replicating the main finding of this chapter – an altered behaviour phenotype of P-Myrf$^{(-/-)}$ on the complex wheel. In contrast, in the 'Pre CW experiment', the amount of active intervals on the complex wheel did not differ between genotypes (Fig 4.11G), indicating a lack of a genotype specific behaviour phenotype on the complex wheel in this subset of animals. In summary, that means that we did not find conclusive evidence for a robust reduction in spontaneous locomotor activity in P-Myrf$^{(-/-)}$ that may contribute to the reduced running performance observed on the CW.

4.3.4 No evidence for a general impairment in locomotor skills or coordination in P-Myrf$^{(-/-)}$ animals.

The complex running wheel task has previously been employed to detect latent motor deficits in mice (Liebetanz and Merkler 2006; Liebetanz *et al.* 2007). Indeed, removing rungs from the running wheel to create an irregular rung pattern is intended to increase the task demand for locomotor skills and

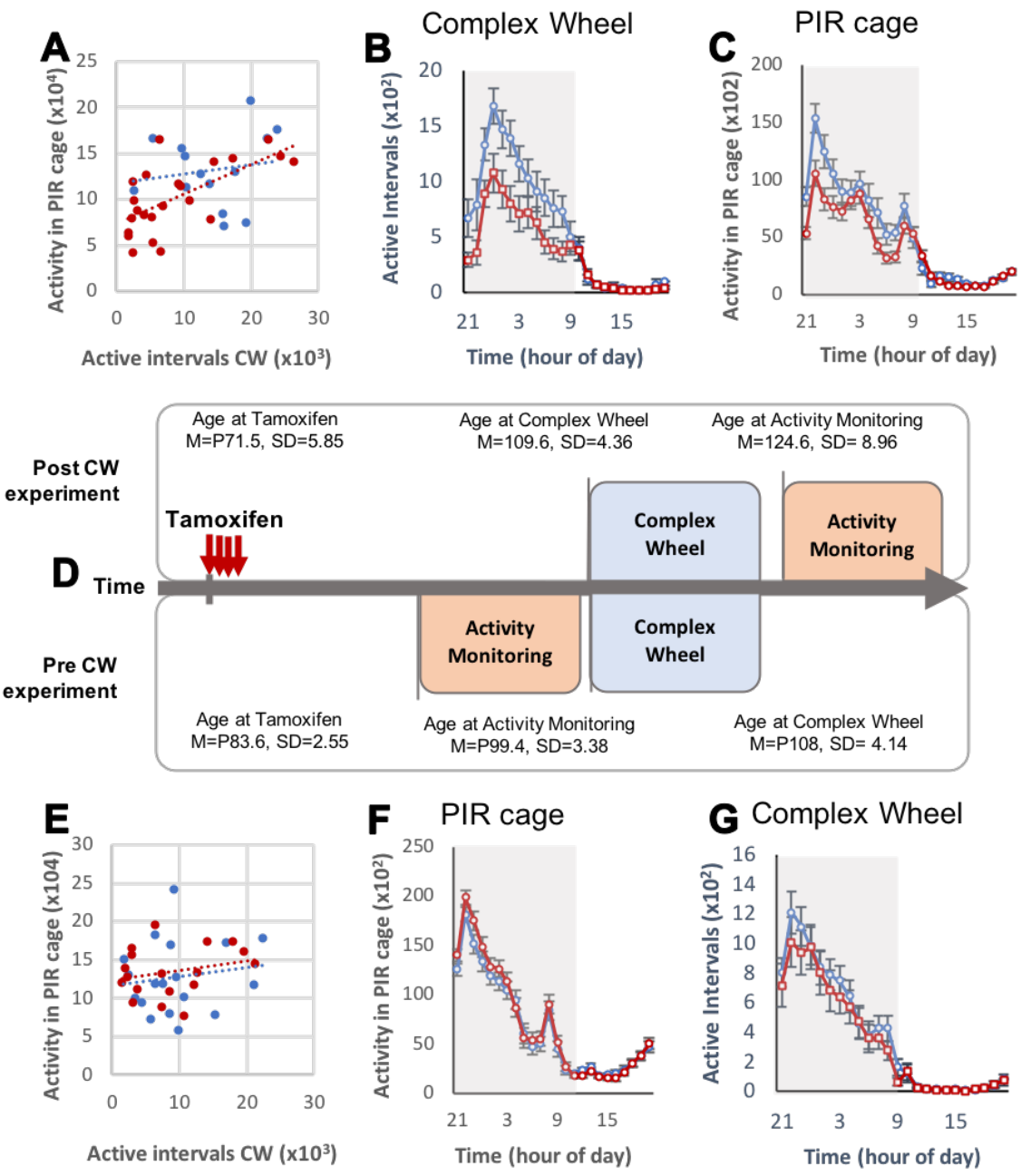


Figure 4.11. ***Comparison of the two experiments investigating spontaneous locomotor activity in P-Myrf animals.***

(A) *Activity on the complex wheel and the activity in the PIR cage environment were significantly correlated (P-Myrf$^{(-/-)}$: n=23, 11 P-Myrf$^{(+/-)}$: n=14) in the experiment outlined in Fig. 4.9. In this experiment, both activity on the complex wheel* ***(B)*** *and activity in the PIR cage* ***(C)*** *were lower for P-Myrf $^{(-/-)}$ when compared to the controls.* ***(D)*** *Schematic illustration of the differences in experimental design between the two experiments assessing spontaneous locomotor activity in the PIR cages. Apart from a reversed order of behavior testing (testing PIR cage activity* ***Pre-*** *or* ***Post*** *complex wheel running) the mean age of tamoxifen treatment and behavior testing varied slightly between groups).* ***(E)*** *Animal's activity on the complex wheel and the activity in the PIR cage environment were not correlated in the* ***Post****-complex wheel running experiment (Figure 4.10). Yet, neither testing environment,* ***(F)*** *PIR cage or* ***(G)*** *complex wheel, revealed a statistically significant difference in spontaneous activity between the two genotype groups in this subset of animals.*

coordination. Hence, it may be possible that an underlying deficit in locomotor coordination and skills prevents the animals from running, and that this in turn prevents them from improving their skills on the complex wheel. In this way, the deficit might be primarily a motor execution deficit rather than a learning deficit. While the absence of genotype differences at the very start of CW testing argues against this (Fig. 4.9C), a floor effect in activity at the beginning of testing may initially mask such a motor execution deficit until performance reaches a certain level in the most active phase (2-4 hours) of the circadian cycle (Figure 4.7).

To test for effects of genotype on simple motor execution, a subset of P-Myrf animals from generation 3 (Figure 4.2B) was examined for their performance on two established behaviour paradigms for the evaluation of motor coordination and balance (Brooks and Dunnett 2009); the Balance beam walking assay and the accelerating rotarod. A schematic illustration of the experimental design can be found in Fig. 4.12A. Animals tested were from the same cohort that had their home cage activity monitored after wheel running and showed a clear behaviour deficit on the complex wheel. Motor skills were tested during the week after activity monitoring was complete.

4.3.4.1 Accelerating rotarod assay revealed no differences between genotypes

The accelerating rotarod (Figure 4.12B) was used to test motor coordination by measuring the animals' ability to remain on a rod of 2 cm in diameter that is rotating (starting speed 4 rpm) while slowly accelerating its rotation at a rate of 20 rpm to a maximum speed of 40 rpm. The latency in falling off the rod was used to quantify performance. Each mouse was tested three times, with a 10 min resting time in between. P-Myrf$^{(-/-)}$ mice performed just as well as their P-Myrf$^{(+/-)}$ siblings, while both groups improved their overall performance from run to run (Figure 4.12D; mixed Two-way ANOVA, within-subject factor: Run (3), between-subject: Genotype, Sex; main effect for Run ($F(2,74)=20.860$, $p<0.001$) but not Genotype).

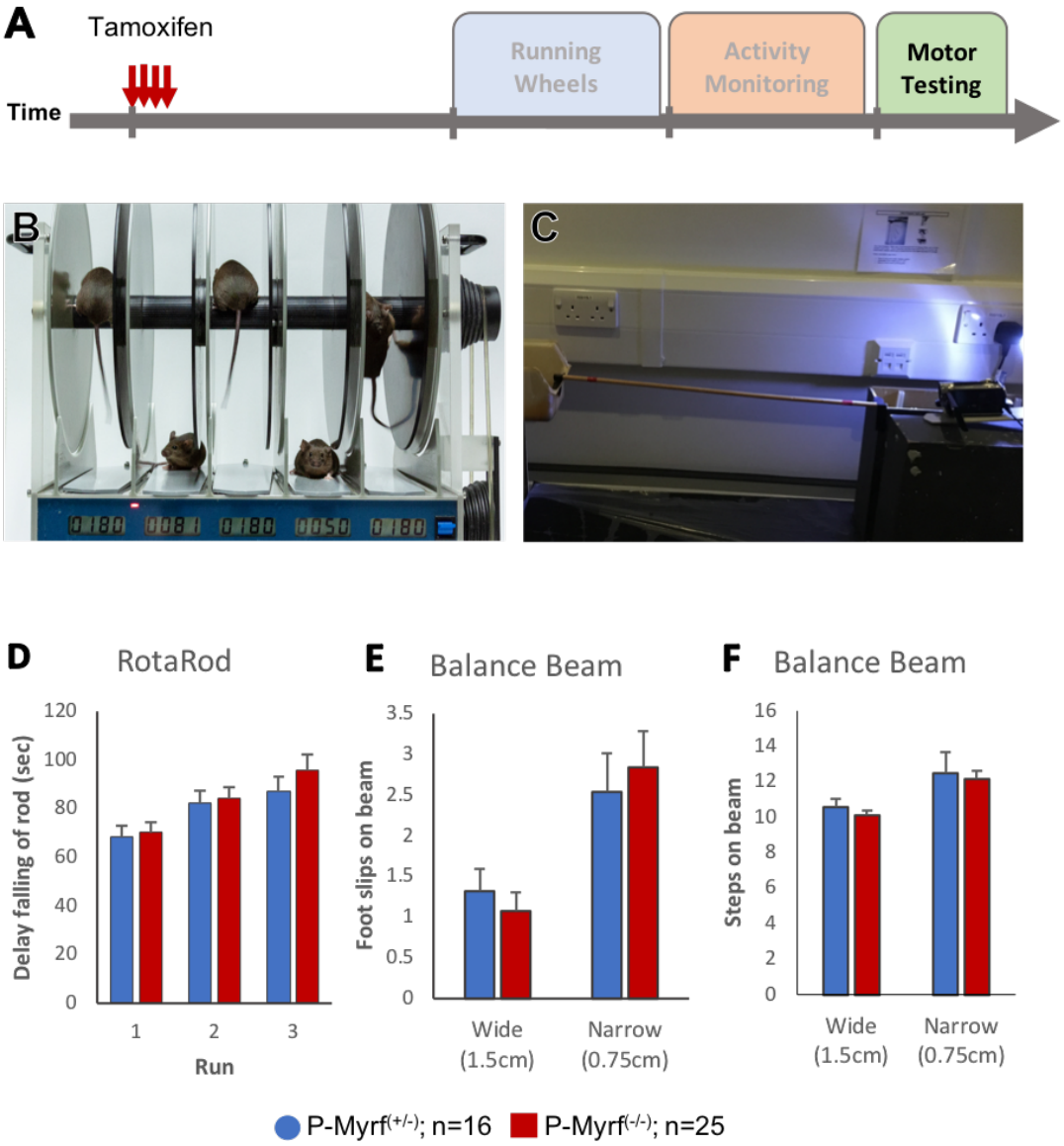


Figure 4.12. ***No evidence for a genotype specific impaired in motor coordination in P-Myrf$^{(-/-)}$ animals.***

(A) Schematic illustration of the experimental design. Animals were tested with two separate for their motor coordination after home cage activity monitoring was completed. Example images of the ***(B)*** *Rotarod and* ***(C)*** *Balance beam apparatus used for behavior testing.* ***(D)*** *Mean delay in falling off the accelerating Rotarod improved with subsequent testing (Main effect for Run $F(2,74)=20.860$, $p<0.001$, Two-Way mixed ANOVA), but was not different between the genotype groups.* ***(E)*** *The overall amount of foot slips while crossing the Balance beam increased with task difficulty (wide vs narrow beam), but was not different between the genotype groups.* ***(F)*** *The average amount of steps taken to cross the Balance beam. Data presented as Mean ± SEM.*

4.3.4.2 Balance beam walking assay revealed no differences between genotypes

The Balance beam walking assay (Figure 4.12C) was used to assess fine motor coordination and balance by testing the animals' ability to cross a 1 m long beam of two different thicknesses (Wide: 1.5 cm; Narrow: 0.75 cm in diameter) to reach their home cage. Animals were first tested on the wider beam. If they successfully crossed the wide beam (100% of animals), animals were assessed for their performance on the narrow beam. Performance was evaluated by measuring the number of times the animals' feet slipped while crossing the beam and how many steps an animal took from one end to the other. Performance between genotypes was similar on both the wide and the narrow beam (Figure 4.12E&F), and no statistically significant differences between the genotypes were detected on either beam type (Statistical test used: unpaired t-test for number of steps, Mann-Whitney U test for number of foot slips). Differences in task difficulty between the two beams were indicated by the fact that animals took more steps on the narrow beam compared to the wide beam (mixed Two-way ANOVA, within-subject factor: Type of Beam, between-subject: Genotype, Sex; main effect for Type of Beam for steps $F(1,36)=21.440$, $p<0.001$).

Taken together, the results from these two behaviour assays provide no evidence for a general impairment in motor skill and coordination in the P-Myrf$^{(-/-)}$ animals that could underlie the observed deficit in running the complex wheel, in agreement with results obtained by McKenzie *et al.* (2014)

4.4. DISCUSSION

The main aim of this chapter was to replicate the behaviour phenotype of transgenic mice with a conditional deletion of *Myrf* in OPCs (P-Myrf animals) that was reported by McKenzie *et al.* (2014) and Xiao *et al.* (2016). In the current study, animals lacking both copies of the *Myrf* gene *(P-Myrf$^{(-/-)}$)* showed a significant reduction in the differentiation of new oligodendrocytes (Figure 4.1) and lower overall running speeds on the complex wheel over time (Figure 4.3), when compared to their siblings which retained one functional copy of the gene *(P-Myrf$^{(+/-)}$).* This deficit in running performance was

not apparent on initial exposure to the complex wheel but emerged during the first four hours of the first night of running (Figure 4.7) and was not observed on a normal running wheel (Figure 4.6), indicating an early and complex wheel specific behaviour deficit. Therefore, the current study replicated the core behaviour phenotype of P-Myrf animals reported by McKenzie *et al* (2014) and Xiao *et al* (2016)(Figure 4.5A&B), which suggests that mice that acquire a significant impairment of their ability to differentiate new oligodendrocytes in early adulthood are on average less able to run the complex wheel.

However, not all aspects of the behaviour phenotype of P-Myrf animals were faithfully replicated. In the current study, *P-Myrf*$^{(-/-)}$ mice also spent significantly less time actively engaging with the complex running wheel (Figure 4.8). However, McKenzie et al (2014) found that the time animals spent turning the wheel >1 m/min did not differ between genotypes, arguing against a difference in motivation or spontaneous locomotor activity. McKenzie et al (2014) also reported no significant differences between males and females, whereas we found that females significantly outperformed males in terms of running speed and activity on the wheel (Supplementary Figure 4). Sex-specific differences in voluntary wheel running are consistently observed across different mouse strains, with females outperforming males in terms of the distance run, running speeds and the amount of time spent on the wheel (Konhilas *et al.* 2004; De Bono *et al.* 2006; Manzanares *et al.* 2019). Our data suggests that these sex-specific difference can also be observed on the complex wheel, despite a potential difference in task demand to the normal wheel. One explanation for this discrepancy between the results of the two studies may be a greater diversity in the mixed genetic background of the animals in the current study. Genetic background of different inbred strains has repeatedly been shown to have a significant influence on performance in behaviour tasks, such motor tasks and voluntary wheel running (Tarantino *et al.* 2000; Lerman *et al.* 2002; Lightfoot *et al.* 2004; Merritt and Rhodes 2015). Indeed, P-Myrf animals were originally created on a background of three mixed inbred strains (C57B6, CBA and 129), yet reported to be predominantly C57B6 with an agouti coat colour derived from the

CBA (McKenzie *et al.* 2014). However, coat colour in the current study varied between black (C57B6) and agouti, indicating a potential larger diversity. Additionally, the genetic background had not been refreshed before or since P-Myrf breeding pairs arrived in our institution, making a genetic drift towards a wider genetic diversity within the colony possible.

A mixed and diverse genetic background within the population may also explain the large variability in performance across the sample of P-Myrfs tested on the complex or normal wheel, which stands in contrast to the relatively narrowly clustered and normally distributed performance distribution across the sample of the cKO-Nrg1 mouse model with a single C57B6 background (Chapter 3, Figure 3.8). McKenzie *et al.* (2014) also reported that individual performance of P-Myrf mice varied widely and, importantly, that average speed performance distribution of P-Myrf$^{(-/-)}$ mice was bimodal and skewed toward lower speeds (Figure 4.5D). Our current study indeed replicated this performance distribution of P-Myrf$^{(-/-)}$ mice, which was bimodal and skewed toward lower speeds regardless of whether looking at running speeds (Figure 4.3F & Figure 4.5C and E) or improvement of running speed (Figure 4.4B).

Yet, some aspects of the performance distribution across the P-Myrf sample differ between the two studies. Firstly, maximum and average speed distribution of better performing P-Myrf$^{(-/-)}$, while still substantially overlapping with the control group, were clearly shifted towards lower speeds in the study by McKenzie *et al.* (2014), indicating a clear performance deficit across the population of animals lacking the ability to differentiate new oligodendrocytes (Figure 4.5D & F). In contrast, in the current study, the performance distribution of the subset of P-Myrf$^{(-/-)}$ with higher performance mostly overlapped with the distribution of the control group of P-Myrf$^{(+/-)}$mice, with very little indication of a shift towards lower performance. Instead, a substantial subset of P-Myrf$^{(-/-)}$ mice show a significant impairment in performance on the complex wheel (Figure 4.3F, Figure 4.4B, Figure 4.5C&E), representing a distinct peak in the sample distributions. Rather than a performance deficit across the population of P-Myrf$^{(-/-)}$ animals, this suggests that only a subset P-Myrf$^{(-/-)}$ animals had a

significantly reduced ability to run and improve their skills on the complex wheel, while the remaining P-Myrf$^{(-/-)}$ animals perform similarly to animals that retain a functional copy of *Myrf.* This would suggest that our data indicates that the conditional deletion of *Myrf* may or may not affect performance on the complex wheel running, rather than causing a reliable and predicable behaviour deficit. That means that while the current study essentially replicates the main behaviour phenotype of McKenzie et al (2014), meaning a deficit on the complex wheel of P-Myrf$^{(-/-)}$ animals along with a skewed and bimodal sample distribution, it less clear what aspects of behaviour are affected by preventing the formation of newly-differentiating oligodendrocytes in the current study.

Mice accustomed to normal wheels experience great difficulty when initially switched to a complex wheel (Liebetanz *et al.* 2007), yet animals can improve their running speeds over time almost to the level seen on the normal wheel. The more demanding task of continuous step-length adaptation and bilateral coordination on the complex wheels seems to require substantial involvement of supraspinal coordination (Liebetanz and Merkler 2006; Liebetanz *et al.* 2007). McKenzie et al (2014) argue that animals learn a specific strategy to run the complex wheel, adapting their gait pattern to cope with irregular rungs in general, rather than learning the specific rung pattern of the wheel. This suggests that adopting a new strategy provides an important threshold in learning to run the complex wheel, after which performance can be successfully improved over time. Hence, the observed deficit of P-Myrf$^{(-/-)}$ may represent an impaired ability to adapt to a new behaviour strategy which is required for a successful running of the complex wheel.

However,, it is not clear which circuits may be involved in learning to run on the complex wheel. If successfully running the complex wheel predominantly requires adapting and adjusting the gait and locomotion, the task requirement would predominantly be considered as a motor adaptation. This would assume that mice learn to adjust their gait by error-based learning, adapting the movement and trajectory of their gait on a trial-by-trial basis until optimised for the new environment (irregular rather than regular running surface). Such motor adaption would predominantly require cerebellar

regions (Diedrichsen and Kornysheva 2015, Wolpert 2011). However, as the major available feedback is either the success (continued running) or failure (false step leading to stopping of the wheel) of staying on the wheel, the learning can be considered as a form of reinforcement learning, which is likely to require integration of information from varies parts of the sensorimotor system to find an optimal strategy in the first place (Diedrichsen and Kornysheva 2015, Wolpert 2011). The integration of sensory information provided by active whisker movement, a complex behaviour in mice with specialised neuronal representation in the sensory cortex (Petersen 2019), is also likely to be involved in the learning process as whiskers may provide important information about the rung location (Pacchiarini et al. 2017). Hence, differences in active whisking or sensory processing, sometimes observed in transgenic mice (Simanaviciute et al. 2020), could also contribute to behaviour differences, a factor that has not been investigated in the current study. Once the gait has been adapted to cope with the irregular rung arrangement, running the complex wheel may require mainly a similar neural circuitry as running a normal wheel to further improve performance on the wheel by motor adaptation and improving other factors like fitness. Hence, learning to run the complex wheel may require a different kind of neural circuitry at different stages of behaviour adaptation. The complex wheel paradigm may also differ from other, more frequently types of motor learning paradigms, such as the skilled reaching task (Chen *et al*. 2014), which trains the fine motors skills in the forlimp of the mice. Such learning of a fine motor skills is more dependent on adaptation in the primary cortical areas and projections through the corticospinal tract (Ueno *et al*. 2018). These potential differences in task demand, types of learning and neural circuitry between motor learning paradigms should be considered when defining a behaviour paradigm and it is currently not clear if disruption of oligodendogensis may impair behaviour performance in other motor learning paradigms.

This may partially explain why P-Myrf$^{(-/-)}$ show behaviour deficits within the first hours on the complex wheel (Figure 4.7), as fewer animals managed to successfully adopt a new strategy to run the wheel

and therefore do not improve their running speed (Figure 4.7). Most importantly, this would partially explain the skewed and bimodal distribution within the P-Myrf$^{(-/-)}$ sample. The subset of P-Myrf$^{(-/-)}$ with very low running speeds may represent animals that never managed to pass the threshold of a crucial behaviour adaptation required to successfully run the complex wheel, which means they never acquire the ability to run at a certain speed (Figure 4.3F) or to improve their running performance over time (Figure 4.4B). While plausible, this hypothesis would have to be tested by recording and comparing running strategies and adaptations of a sufficient number of individual animals with a range of behaviour phenotypes. Such assessments have not yet been conducted either in the experiments presented in this thesis or in previous studies.

Alternatively, the observed deficit on the complex wheel may be caused by an underlying behaviour phenotype other than a motor learning deficit. A general lack of spontaneous locomotor activity and motivation, as well as other factors like discomfort and fatigue (Häger *et al.* 2018; Wolff *et al.* 2018), can lead to reduced engagement with the running wheel, which may subsequently manifest as a reduced performance on the wheel running task (Novak *et al.* 2012). Indeed, we found that P-Myrf$^{(-/-)}$ animals had a lower overall number of active intervals in the complex wheel (Figure 4.8), which may suggest that a more general behaviour deficit affecting the animals' overall activity or motivation may lead to an impaired complex wheel running . The finding that P-Myrf$^{(-/-)}$ animals were less active in a home cage environment after complex wheel running, and that their activity in the home cage correlated with their previous speed on the complex wheel (Figure 4.10) further supported this hypothesis. Yet, running wheels have been demonstrated to alter home cage activity of rodents (Visser *et al.* 2005; Novak *et al.* 2012), which could mean that a lower spontaneous home cage activity may have been influenced by the previous behaviour on the complex running wheel. Importantly, we did not find a reduced home cage activity prior to wheel running (Figure 4.11), nor did we observe a genotype specific difference in activity on the normal running wheel (Figure 4.6). Hence, the current

study does not provide conclusive evidence for a more general deficit in spontaneous locomotor activity in P-Myrf$^{(-/-)}$ animals.

A general motor deficit caused by an inability to form new oligodendrocytes at a time at which continuous myelination in the CNS is still ongoing (Young *et al.* 2013; Hill *et al.* 2018; Hughes *et al.* 2018) may also have contributed to the observed deficit in complex wheel running (Liebetanz and Merkler 2006; Liebetanz *et al.* 2007). The current study employed the accelerating RotaRod and Balance beam paradigm to test motor coordination and balance, two commonly used tests to assess the motor phenotype in mice (Liebetanz *et al.* 2007). Replicating previous findings by McKenzie *et al.* (2014), who found no genotype specific difference on the RotaRod test, our test battery also provided no evidence for a generalised motor deficit on the Balance Beam within the population of P-Myrf$^{(-/-)}$ animals (Figure 4.12). Yet, previous studies have demonstrated that the complex wheel behaviour test can detect and quantify latent motor deficits (Schalomon and Wahlsten 2002; Liebetanz *et al.* 2007; Hibbits *et al.* 2009), which are not revealed by tests like the Rotarod or Balance beam. Complex wheel specific behaviour phenotypes have been demonstrated in association with a range of experimental interventions, such as surgical section and genetic absence of the mouse corpus callosum (Liebetanz *et al.* 2007), cuprizone induced demyelination (Liebetanz and Merkler 2006; Liebetanz *et al.* 2007) and 1-methyl-4-phenyl-1,2,3,6-tetrahydropyridin (MPTP) induced loss of dopaminergic neurons (Liebetanz *et al.* 2007). It is of note that these studies detected a behaviour phenotype similar to the one observed in the current study. Animals that were allowed to recover from cuprizone-induced demyelination and animals with pharmacological loss of dopaminergic neurons both had an impairment in running speeds on the complex wheel that only become apparent after several days of running (Liebetanz and Merkler 2006; Liebetanz *et al.* 2007), with no detectable behaviour phenotype on a normal wheel. Indeed, it is not obvious what distinguishes the behavioural phenotype observed in the current study from the ones observed in these different experimental

mouse models. Hence, it cannot be excluded that a latent motor performance deficit in P-Myrf$^{(-/-)}$ animals may contribute to the observed impairment in motor learning on the complex wheel.

Our study has several limitations. It is of note that the variability in age of tamoxifen treatment, age of behaviour testing on the complex wheel, as well as the period in between timepoints varied across animals in our study (Table 2). While we found no significant correlation between these factors and performance on the complex wheel (Supplementary Figure 5), the differentiation of new oligodendrocytes is a continuous process that declines with age (Hill *et al.* 2018) and adaptive myelination has previously been shown to have critical periods for the effect of social isolation (Makinodan *et al.* 2012). As our experiments were not specifically designed to detect those difference in time, it cannot be excluded that age and time since tamoxifen treatment may have interacted with the observed behaviour phenotype. While McKenzie et al (2014) tested animals that lost their ability to form new-oligodendrocytes at P60 and P90, only 12 (out of 68) animals (5 and 7 per genotype group) were tested within the P90 sample. In our study, age of tamoxifen treatment ranged from P58-93, with a mean age (M=77.1 SD=8.04) greater than that tested by McKenzie et al (2014). It is not clear if this difference in age may have contributed to subtle differences in the observed behaviour phenotype between the two studies. Another limitation of the study is the large variability in behaviour performance among the sample of P-Myrf animals tested, which is caused by apparent sex differences and potentially exacerbated by a mixed genetic background among the population and variations in age across the sample. While the large sample size allows a conclusive effect of genotype to be demonstrated, this variability in performance across the sample makes it difficult to interpret the results, especially if different subsamples of animals provide contradicting data (Fig. 4.11).

Taken together, the current study replicates previous observations by McKenzie *et al.* (2014) and Xiao *et al.* (2016) indicating mice with a significantly reduced ability to differentiate new-oligodendrocytes in early adulthood (Figure 4.1) are less able to run and improve their performance on the complex

running wheel (Figure 4.3, Figure 4.4). However, to understand if and how newly myelinating oligodendrocytes contribute to motor performance and/or learning requires a better understanding of the underlying biological processes that drive the observed behaviour phenotype. Hence, we will investigate the link between the behaviour phenotype, altered oligodendroglia dynamics and white matter integrity of P-Myrf animals in Chapter 5.

Chapter 5 | INVESTIGATING UNDERLYING BIOLOGICAL CHANGES IN WHITE MATTER OF *MYRF*-cKO MODEL

5.1. INTRODUCTION

In the context of accumulating evidence for an active role of oligodendroglia dynamics in brain plasticity the observed behaviour phenotype of the cKO-Myrf model suggested a contribution of newly-differentiated oligodendrocytes to motor performance and learning. However, the link between behaviour performance on the CW and the extend and specificity of related *de novo* myelination has not been thoroughly investigated. If 'motor skill learning requires active central myelination', as suggested by McKenzie et al (2014), changes in oligodendroglia dynamics and the microstructural properties of the brain structures involved should display changes that are associated with behavioural performance.

Along with the behaviour phenotype, McKenzie et al (2014) studied the adaptive response within the oligodendroglia cell population due to running the complex wheel in wild-type mice. Histological analysis in wild-type mice found that OPC proliferation was increased on day 4 on the complex wheel, OPC density was increased on day 6 and the numbers of newly-differentiating oligodendrocytes was increased by day 11 and after 3 weeks in animals that ran the complex wheel, when compared to animals that were housed without a wheel. As the behaviour phenotype of P-Myrf$^{(-/-)}$ was present much earlier than the first observed cellular response (within first 2-3 h; Figure 4.7), Xiao et al (2016) replicated the histological findings mentioned above, but also investigated the cellular response of oligodendroglia with the help of a newly-identified very early marker of oligodendrocyte

differentiation (*Enpp6*). Interestingly, Xiao et al (2016) observed that complex wheel running increased the density of Enpp6-positive cells in the subcortical white matter (within the first 2.5h) and motor cortex (within the first 4h) of wild type mice, indicating an early and rapid response of oligodendroglia to experience. Wild-type animals that had previously trained on the complex wheel and were housed without a wheel for one week after running did not show changes in Enpp6-positive cell densities, nor a change in OPC proliferation, upon re-introduction to the complex wheel. This experience-dependent cellular change suggests that the oligodendroglia response was specific to being introduced to the wheel, not to running the complex wheel *per se*. Learning to run the complex wheel also increased the density of Enpp6-positive cells in P-Myrf$^{(-/-)}$ mice, yet the density of newly-differentiated oligodendrocytes (EdU+|CC1+) cells remained unchanged, suggesting that the successful differentiation of new oligodendrocytes was the main factor underlying the differences in behaviour.

As these experience-dependent cellular events occurred on a similar time scale as the improvement in running performance, which was impaired in P-Myrf$^{(-/-)}$mice that lacked this cellular response, McKenzie *et al.* (2014) and Xiao *et al.* (2016) concluded that newly formed OLs play an important role in motor skill acquisition. Furthermore, the rapid cellular response suggested that oligodendrocyte development may be required for skill acquisition in mice within the first few hours of being introduced to the complex running wheel.

While an accumulating body of evidence suggests a link between skill acquisition and changes in white matter microstructure and/or oligodendroglia dynamics (Blumenfeld-Katzir *et al.* 2011; Hofstetter *et al.* 2013; Sampaio-Baptista *et al.* 2013; Keiner *et al.* 2017), the cKO-Myrf model provided the first evidence that interfering with the adaptive cellular response of oligodendroglia can have behavioural consequences. However, general changes in oligodendroglia dynamics have previously been associated with experience such as environmental enrichment and voluntary exercise on a normal running wheel (Ehninger and Kempermann 2003; Krityakiarana *et al.* 2010; Simon *et al.* 2011;

Keiner *et al.* 2017; Hughes *et al.* 2018). Therefore, the observed adaptive cellular response is not necessarily specific to the type of motor learning required for the complex wheel. Given the large variability in behaviour performance on the complex wheel among P-Myrf animals, it is also not clear if changes in behaviour performance are associated with changes in oligodendroglia dynamics, as the link between performance and cellular dynamics was not studied previously. Indeed, the mechanisms by which an adaptive response in oligodendroglia dynamics subsequently contributes to skill acquisition on the complex wheel is not clear.

While newly-differentiating oligodendrocytes can contribute to a diverse set of functions, including clustering of axonal sodium channels (Blumenfeld-Katzir *et al.* 2011; Hofstetter *et al.* 2013; Sampaio-Baptista *et al.* 2013; Keiner *et al.* 2017) and axonal and metabolic support (Ehninger and Kempermann 2003; Krityakiarana *et al.* 2010; Simon *et al*. 2011; Keiner *et al.* 2017; Hughes *et al.* 2018), myelination of relevant neural circuits and pathways remains a key mechanism by which oligodendroglia dynamics are thought to contribute to behaviour change (Freeman *et al.* 2015). Indeed, previous rodent studies indicate that experience can lead to a region specific increase in the survival, integration and myelination of newly-differentiating oligodendrocytes (Hughes *et al.* 2018) and that neuronal activity increases myelination in an axon-specific manner (Mitew *et al.* 2018). Importantly, learning a fine motor skill (skill-reaching task) has previously been shown to trigger region specific changes in myelination and white matter microstructure in rats (Sampaio-Baptista *et al.* 2013). However, if and how learning to run the complex wheel leads to and requires region specific adaptive myelination in mice, and/or if other, potentially faster, cellular processes play a role, has not been investigated. If the differentiation of new oligodendrocytes significantly contributes to skill acquisition in this behaviour paradigm, experience-dependent cellular and structural changes should be associated with performance improvements, while such changes should be significantly smaller or absent in animals with genetically induced impairment of oligodendrogenisis.

Next to histological methods, magnetic resonance imaging (MRI) provides a valuable tool to study brain-wide changes in tissue microstructure that are translatable to human studies. Diffusion weighted imaging (DWI) is a unique imaging technique that assesses the diffusion of water molecules within the tissue, which is blocked by structures such as cellular membranes in the brain. As cellular membranes of axons and myelin within fibre tracks are often predominantly orientated in one direction, this techniques has proven to be a valuable tool for the assessment of white matter microstructure and for the three-dimensional visualization of the white matter anatomy in the brain (Simmonds *et al.* 2014; Qiu *et al.* 2015). Indeed, human and rodent studies have successfully employed DWI to detect adaptive changes in white matter due to learning (Scholz *et al.* 2009; Blumenfeld-Katzir *et al.* 2011; Sampaio-Baptista *et al.* 2013).

Furthermore, recent developments in MRI acquisition and tissue modelling provide a better characterization and more specific markers for myelin (Heath *et al.* 2018), using techniques such as Magnetization Transfer Imaging Ratio (MTR). MTR allows indirect detection of water bound to macromolecules, such as lipids and proteins, and is thus sensitive to myelin (Deloire-Grassin *et al.* 2000). While MRI methods have limitations and are not sensitive to specific cellular processes, multimodal MRI can provide valuable information about tissue microstructure and region specific changes (Groeschel *et al.* 2016; Petiet *et al.* 2018).

5.1.1 Aim of this Chapter

The aim of this chapter was to investigate the potential link between the underlying biological changes in P-Myrf animals and the associated behaviour phenotype on the complex wheel, as well as the role that newly-differentiating oligodendrocytes play in this process. In order to assess potential biological changes due to running on the complex wheel, we compared P-Myrf animals that had free access to a complex wheel to P-Myrf animals that were exposed to a fixed immovable complex wheel. We employed a combination of histological methods and *ex vivo* MRI to assess changes in cell dynamics and tissue microstructure. Our experiment was designed to:

A) Investigate the effect of complex wheel running on white matter structure and oligodendroglia dynamics and the relationship to performance.
B) Investigate the effect of genetic manipulation on white matter structure and oligodendroglia dynamics
C) Study the interaction between experience-dependent changes and the genetic deletion of *Myrf*.

Our intention was to (I) assess changes in oligodendroglia dynamics in the anterior corpus callosum to compare it to data provided by McKenzie et al (2014), (II) to investigate potential changes in DWI- and MTR-derived metrics of tissue microstructure and to (III) follow up region specific changes in tissue microstructure detected by MRI by histological analysis. However, at the point of writing the MRI analysis was not fully optimised. Hence, the data provided from MRI should be considered preliminary and only an initial exploration of the data.

5.2. MATERIALS AND METHODS

5.2.1 ANIMALS AND BEHAVIOUR TESTING

Breeding and maintenance of P-Myrf animals has previously been described in Chapter 4. A total of 71 P-Myrf animals were used for the experiment illustrated in Figure 5.2. A total of 36 animals were tested on the complex running wheel (P-Myrf$^{(+/-)}$:n=19, 6 females; P-Myrf$^{(-/-)}$:n=17, 5 females) in specific running wheel cages (Figure 3.1). Experimental set up of the complex wheel running cages are described in Chapter 3. Additionally, 35 littermates were exposed to a static fixed complex wheel that was not able to rotate (referred to as fixed wheel, FW) in cages with otherwise identical set up (P-Myrf$^{(+/-)}$:n=17, 5 females; P-Myrf$^{(-/-)}$:n=18, 8 females). As the fixed wheel had the same missing rungs pattern that allow animals to pass between rungs, animals could climb and interact with the wheel as a kind of environmental enrichment yet could not run and turn the wheel. The experiment

consisted of 5 distinct batches of P-Myrf animals bred from the same set of 5 breeding pairs over consecutive litters. Littermates were semi-randomly assigned to cages equipped with either a complex wheel (CW) or a fixed wheel (FW) and were tested in the same environment and time-frame. Semi-random assignment meant that animals were randomly assigned to a wheel type, while attempting to balance the numbers of genotype, sex and littermates equally between experimental groups.

5.2.2 EdU treatment in separate cohort of animals

EdU was administered in animals' drinking water, starting four days before behaviour testing and continuing throughout behaviour testing (Figure 5.4A). The methods for EdU treatment have been described in Chapter 2. A total of 15 animals were tested in this paradigm.

5.2.3 Perfusion and tissue preparation

Animals were sacrificed on day 13 after introduction to the running wheel cages. Animals were transcardially perfused after intraperitoneal injection with sodium pentobarbital, as described in Chapter 3. After perfusion, animal skulls were dissected by removing soft tissue from the outside of the skull (skin, muscle, eyes etc) and the lower jaws. Dissected skulls containing the CNS tissue were stored overnight in 4% PFA at 4°C for 24h. Samples were then washed with phosphate buffer saline (PBS) before being stored in PBS at 4°C. Samples were sent to the Center for Image Sciences, UMCU, Uetrecht, Netherlands for magnetic resonance imaging (MRI). Three samples were slightly damaged during processing at the UMCU (left in a desiccator for two days), yet were included in the preliminary analysis as first inspection of the data did not indicate them to be out of range of the other samples. After MR imaging, tissue samples were sent back to the University of Oxford, cryoprotected with 30% sucrose solution, embedded in OCT and stored at -80°C until processed for histological analysis. A detailed description of the tissue processing for immunohistochemistry has been given in Chapter 3.

5.2.4 Immunohistochemistry

The immunohistochemical analysis of the animal tissue has been previously described in Chapter 3. Data presented in this chapter represents subsets of the data that is presented in Figure 4.1.

5.2.5 MRI ACQUISITION

Ex vivo brains were scanned overnight using a multichannel 7 T MRI scanner (Varian) at the Center for Image Sciences, UMCU, Utrecht, Netherlands. Images were scanned in triplets. Diffusion weighted imaging (DWI) was acquired with an Axial EPI train with 8 shots sequence with the following parameters: 60 diffusion encoding directions; 1 average per image; 5 images with no diffusion weighting; TR/TE 500/38.6 ms, field of view: 24x20x20 mm; resolution of 0.125 mm isotropic; small delta/large delta 5.5/8.91 ms, diffusion gradient (half-sine shape) 73 G/cm, b = 3522 s/mm2; total time 12.3 hrs.

Magnetization transfer was acquired with an Axial EPI train with 8 shots sequence and a train of saturating pulses in front of the image acquisition sequence saturating at 5 kHz, 10 kHz and 100 kHz off resonance with 4 images per offset (TR/TE 500/28ms; field of view: 24x20x20 mm; resolution of 0.125 mm isotropic; total time 2.3 hrs).

5.2.6 MR DATA PROCESSING AND STATISTICAL ANALYSIS

We performed MRI analyses with the FSL (for FMRIB Software Library) package, version 6.0 (www.fmrib.ox.ac.uk/fsl). DWI data were analysed with the FMRIB Diffusion Toolbox. Voxel-wise values of fractional anisotropy (FA) and mean diffusivity (MD) were estimated from the original DWI data using dtifit and then analyzed using Tract-Based Spatial Statistics (TBSS; Smith et al., 2006). Individual brain images were separated out from brain triplets. Brains were digitally extracted from the skull using a brain mask acquired by combining MD, MTR and FA images thresholded to eliminate non-brain areas. Individual mouse FA images were first aligned with linear transformation to an existing mouse brain template to generate the study-specific template. All FA maps were aligned with linear and nonlinear transformations to the study template and averaged to generate the mean FA image, from which the WM skeleton was extracted using the skeletonisation procedure within TBSS.

The skeleton was then thresholded at an FA value of 0.29 (illustrated in Figure 5.1A). This threshold was chosen based on the fact that it generated a skeleton that reliably contained major tracts that can be accurately aligned across individuals. Finally, the FA values of the tract centers (i.e., maximum FA values) were projected onto the skeleton for each mouse brain and fed into statistical analysis.

A similar approach was taken to analyse MTR. Voxel-wise estimates of MTR were acquired by calculating the relative difference between the signal from a sequence with a 5kHz radio pulse signal from a sequence with a 100kHz radio pulse. A threshold of 0.24 was chosen for the MTR. MTR values for voxels along tract centres (I.e. maximum FA values – same voxels as used for FA analysis) were also projected into the skeleton.

We used two statistical approaches to analyse the WM: a region of interest (ROI) based analysis and a voxel-wise analysis approach. First, to explore possible widespread effects, the mean FA and MTR values of the whole WM skeleton (illustrated in Figure 5.1A) were extracted for each animal and fed into SPSS (Version 25, Mac) for statistical analysis. Additionally, the anterior corpus callosum (mask illustrated in Figure 5.1B) was specifically selected as a Region of interest (ROI), as this area was the target of the histological analysis. Mean FA and MTR values of this region were extracted for each animal and fed into SPSS for statistical analysis. ANOVAs were used to compare the data between groups, with fixed factors: Genotype and Wheel Type. As 1 of 5 sets of perfusions were conducted by a different experimenter, experimental batch (5 levels) was included as a fixed factor to control for data variability. Mean MTR and FA data was significantly different ($p<0.05$) between experimental batches when tested with a one-way ANOVA. Correlations between FA and MTR values and histological metrics were assessed in the ROI analysis using Pearsons's r.

Second, we analysed the whole-skeleton using a voxel-wise approach with nonparametric permutation testing with a cluster-forming threshold of $t = 1.95$. 5000 permutations were used to determine corrected p values. Clusters with a corrected significance of $p < 0.05$ were deemed

significant. We tested for differences between the genotype groups (P-Myrf$^{(-/-)}$ vs P-Myrf$^{(+/-)}$) and for differences between animals that ran the complex wheel vs. animals that were exposed to a fixed wheel (CW vs FW). The analysis controlled for wheel type and genotype respectively as they were include as fix factors in the analysis. Analysis also controlled for experimental batch (5 levels) including as a fixed factor, for the reasons mentioned above.

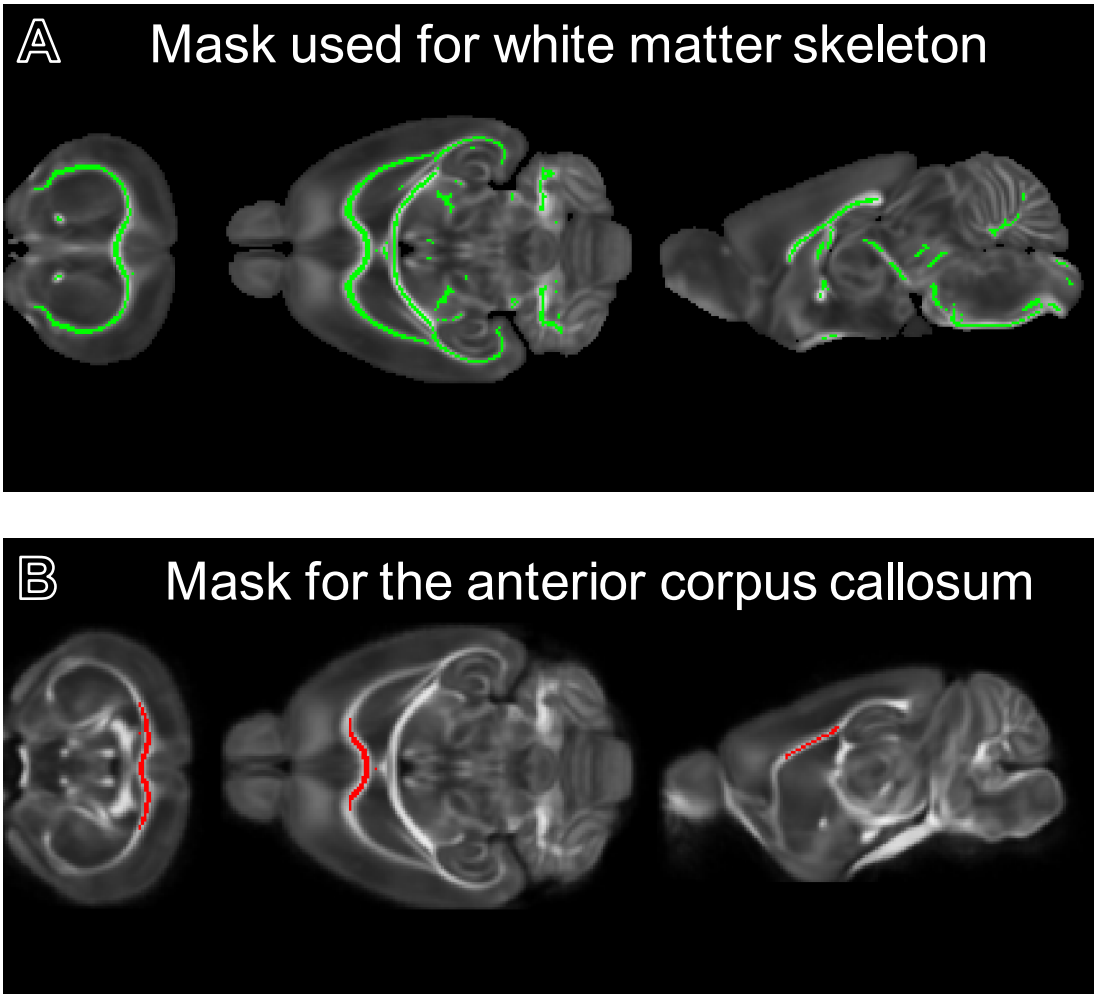


Figure 5.1. ***Example images of the mask used for the current preliminary analysis.***
(A) *Mask (green) used for the analysis of the mouse WM skeleton. (**B**) Mask (red) used to acquire values from the main section of the corpus callosum.*

5.3. RESULTS

The experiment was designed to test effects on white matter microstructure and oligodendroglia dynamics of:

A) the animal's behavioural experience (Wheeltype: FW vs CW)

B) the conditional *Myrf* deletion (Genotype: P-Myrf$^{(-/-)}$ vs P-Myrf$^{(+/-)}$)

C) the interaction between these two factors.

A schematic illustration of the experimental design is depicted in Fig 5.2A.

5.3.1 BEHAVIOURAL PHENOTYPE ON THE COMPLEX WHEEL OF THE SUB-SAMPLE USED FOR BEHAVIOURAL ANALYSIS

We first wished to test whether the behavioural phenotype seen in the overall sample of P-Myrf animals (Chapter 4) could also be detected in the current experimental subsample. Within the subsample of animals tested on the complex wheel, P-Myrf$^{(-/-)}$ showed a lower average (Figure 5.2B) and maximum running speed (Figure 5.2C) when compared to the P-Myrf$^{(-/+)}$ littermates. Yet, the Genotype effect ($F(1, 30)= 0.235$, $p=0.618$, effect size $\eta_p^2 =0.008$, Observed Power=0.078), or Day*Genotype interaction ($F(2.868,86.05)= 6.021$, $p=0.131$, effect size $\eta_p^2 =0.061$, Observed Power=0.475) did not reach statistical significance (Mixed Two-Way ANOVA, Average Speed) and the deficit in running performance was not as pronounced as the effect observed in the complete sample of P-Myrfs tested on the complex wheel (Figure 4.3). Additionally, there was no statistically significant difference between genotypes in the amount of time animals spent interacting with the wheel, as indicated in Chapter 4 (Figure 4.11). However, frequency distributions of running speeds indicated a bimodal distribution within the P-Myrf$^{(-/-)}$ sample (Figure 5.2D), similar to the distributions observed in the full P-Myrf sample and the effect size of the Day*Genotype effect was of a similar magnitude to the one observed in the full sample ($\eta_p^2 =0.061$ and $\eta_p^2 =0.050$, respectively). Overall, while no statistically significant difference between the genotypes was detected in the sub-sample of animals

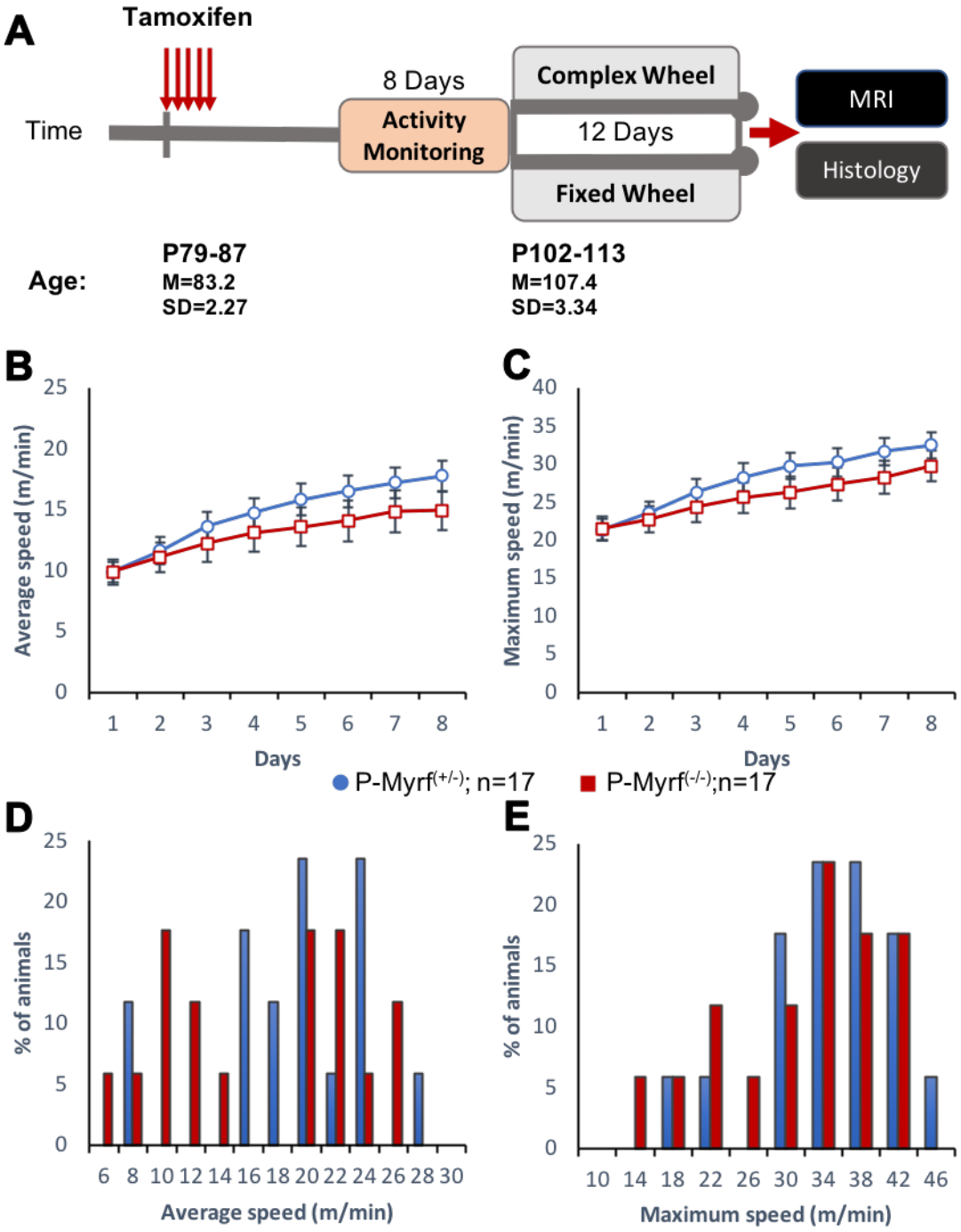


Figure 5.2. ***Experimental design and behavior phenotype of animals used for investigating underlying biology using MRI.***

(A) *Schematic illustration of the experimental design of the experiment. Animals were semi-randomly assigned to a running wheel cage with either a complex wheel (CW) or a fixed wheel (FW) that was prevented from turning. Daily* ***(B)*** *average and* ***(C)*** *maximum running speed in the sub-sample of animals used for the MRI experiment. Data presented as Mean ± SEM. Frequency distributions of* ***(D)*** *average and* ***(E)*** *maximum running speed in the sub-sample of animals used in this experiment.*

assessed for this experiment, trends in the data suggest that the sub-sample in this MRI experiment was at least partly representative of the overall P-Myrf population tested in Chapter 4.

5.3.2 THE EFFECT OF RUNNING AND *MYRF* DELETION ON OLIGODENDROGLIA DYNAMICS IN THE ANTERIOR CORPUS CALLOSUM

5.3.2.1 Density of newly-differentiated OLs not affected by wheel running

In order to understand if the differentiation of new Oligodendrocytes was related to running and/or complex wheel performance, newly differentiated OLs were quantified in the anterior corpus callosum of animals after exposure to either the complex running wheel (CW) or a fixed wheel (FW) for a period of 12 days. Representative images and quantification methods used in this histological analysis are illustrated in Figure 4.1. Overall, the number of newly-differentiated Oligodendrocytes (YFP+|CC1+ cells) was significantly reduced in P-Myrf$^{(-/-)}$ animals (Figure 4.1 & Figure 5.3A&B), when compared to their P-Myrf$^{(+/)}$ littermates, in animals that ran on the complex wheel (unpaired t-test: t(6.25)=4.839, p=0.003) and animals exposed to a fixed wheel (unpaired t-test: t(8)=4.026, p=0.004). However, animals that ran the complex wheel (CW) did not show a significant difference in the assessed cellular densities of newly-differentiated oligodendrocytes when compared to animals that were exposed to a fixed wheel (FW) in the same environment, regardless of genotype (Figure 5.3 A&B). This was statistically tested by analysing the number YFP+|CC1+ cells using a two-way ANOVA (Fixed factors: Experience (FW & CW), Genotype (P-Myrf$^{(-/-)}$, P-Myrf$^{(+/-)}$), revealing a significant effect for Genotype ($F(1,19)=35.018$, $p<0.001$), but no main effect for Experience ($F(1,19)=0.013$, $p=0.910$) nor an Experience*Genotype interaction. This suggests that the experience of running the complex wheel did not affect oligodendrocyte differentiation in the anterior corpus callosum in the sample of P-Myrf animals assessed in this experimental design.

Furthermore, the density of newly differentiated oligodendrocytes in P-Myrf$^{(+/-)}$ animals was not significantly correlated with the maximum daily average running speed (Spearman's rho, $r = -0.643$, $n=7$, $p=0.119$) or the total number of active intervals (Spearman's rho, $r = -0.571$, $n=7$, $p=0.180$) spent

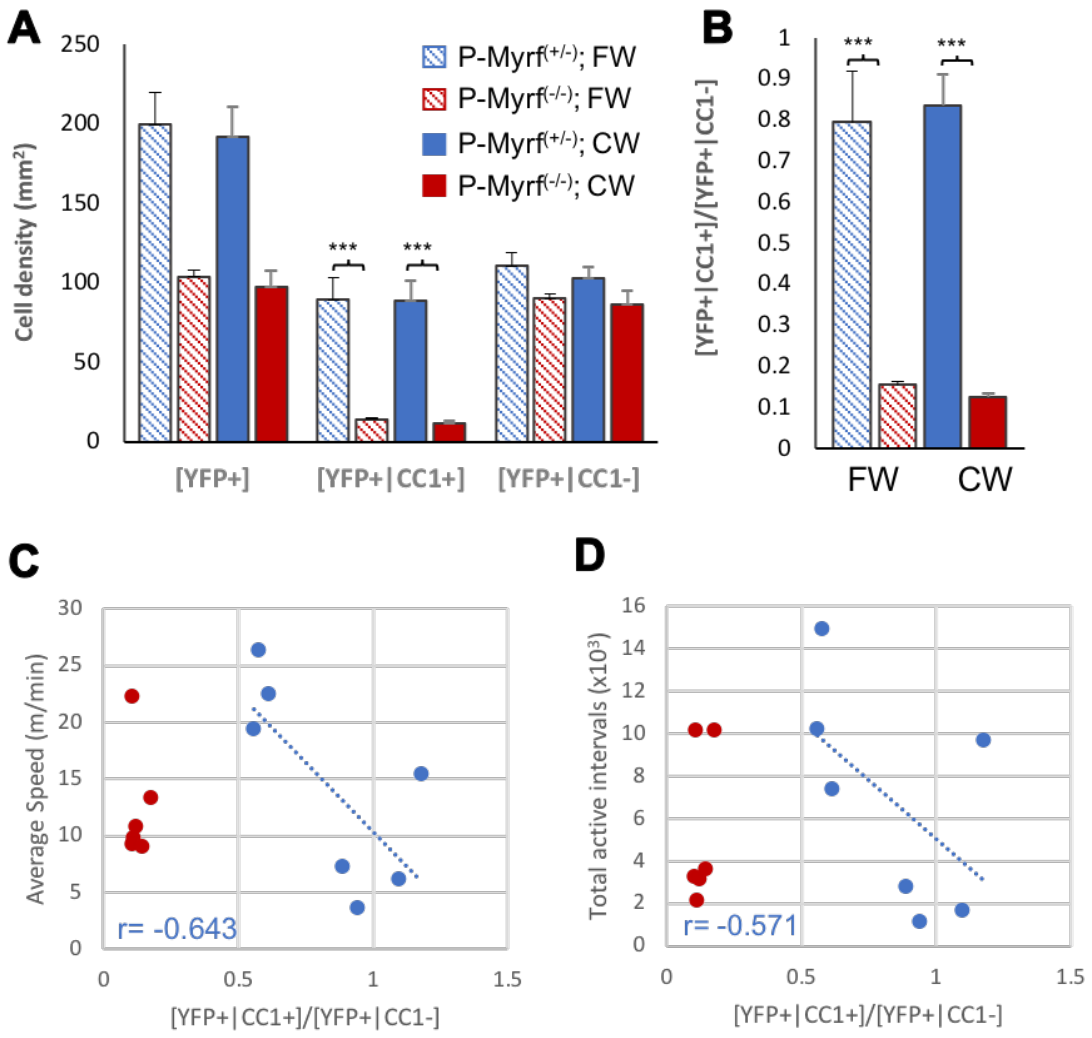


Figure 5.3. ***Complex wheel running did not affect the differentiation of new Oligodendrocytes.***

Histological analysis is illustrated in Figure 4.1. ***(A)*** *The density of newly differentiated OL (YFP+|CC1+),* ***(B)*** *as well as the ratio between differentiated and undifferentiated YFP-positive cells was dependent on genotype. Yet, animals that were exposed to a fixed wheel (FW) that did not move had comparable measures of cellular densities as animals running on the complex wheel (CW). Data presented as Mean ± SEM. Unpaired t-test used for statistical comparison. Asterisks indicated statistical significance: ***:p<0.001. Relationship between cellular densities and* ***(C)*** *average running speed and* ***(D)*** *total number of active intervals run by animals in 8 days. Spearman's rho used for statistical analysis.*

on the complex wheel (Figure 5.3C&D). The ratio between [YFP+|CC1+] cells and [YFP+|CC1-] cells was chosen as a metric to control for potential variations in overall cellular densities. Interestingly, there was an indication towards a negative, rather than a positive, correlation between the parameters of behaviour on the CW and the assessed cellular density in the anterior corpus callosum (Figure 5.3C&D).

5.3.2.2 OPC density and proliferation not affected by deletion of Myrf

While the conditional deletion of *Myrf* should only impair the differentiation of Oligodendrocytes, here we assessed potential nonspecific secondary effects of the *Myrf* deletion on OPCs density and proliferation. Hence, a sub-set of P-Myrf animals from the same cohort that were not included in the MRI analysis were treated with EdU for 4 days prior to running on the complex wheel (in Figure 5.4A).

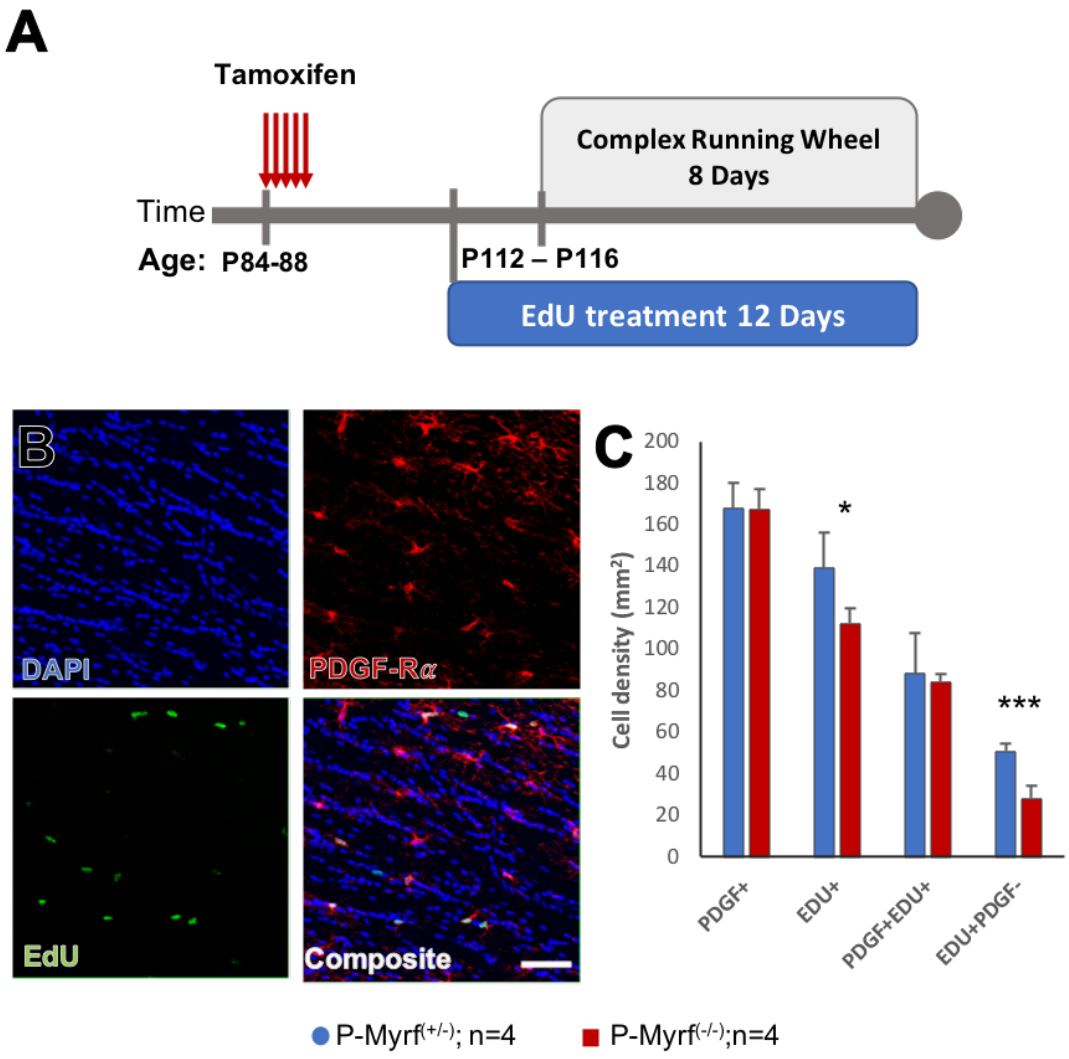


Figure 5.4. ***OPC density and proliferation was not affected by conditional deletion of Myrf. (A)*** *Schematic experimental design. A subset of animas were treated with EdU prior to the exposure to the complex wheel.* ***(B)*** *Representative images of immunohistological analysis. Cell nuclei were stained with DAPI. OPCs were visualized with antibodies against PDGF-Rα. EdU was visualized to assess cell proliferation. The method used for cellular quantification is illustrated on Figure 3.10* ***(C)*** *Quantification of mean cellular densities in the anterior corpus callosum. Data presented as Mean ± SEM. Unpaired t-test used for statistical analysis. Asterisks indicated statistical significance: ***:p<0.001, *:p<0.05.*

Animals were sacrificed after 8 days of wheel running and their tissue processed to assess oligodendroglia dynamics in terms of OPC density and proliferation. The histological method used to assess cell proliferation of OPCs is illustrated in Figure 3.10. Sections of the anterior corpus callosum were stained with antibodies against the OPC marker PDGF-Rα and proliferation marker EdU, while DAPI was used to visualize cell nuclei (Figure 5.4B). The overall density of PDGF-Rα+ cells and PDGF-Rα+|EdU+ positive cells was similar between P-Myrf$^{(-/-)}$ and P-Myrf$^{(+/-)}$ animals (Figure 5.4C), suggesting that OPC proliferation was not affected by the conditional deletion of *Myrf*. As OPCs represent by far the largest population of proliferating cells in the white matter, OPCs that proliferate and subsequently differentiate should represent the majority of EdU+|PDGF-Rα- cells in the observed brain area. Indeed, the overall density of EdU+|PDGF-Rα- cells in P-Myrf$^{(-/-)}$ animals was significantly lower (unpaired t-test, n=4 per group, t(6)=6.297, p=0.001) when compared their P-Myrf$^{(+/-)}$ littermates, in line with the observed overall reduction in newly differentiating Oligodendrocytes (Figure 5.3). This difference in EdU+|PDGF-Rα- likley drove the subtle but significant difference EdU+ between the genotype groups (unpaired t-test, t(3.99)=2.919, p=0.043).

Overall, the histological data suggest conditional homozygous deletion of *Myrf*, but not running on the complex wheel, had a significant effect on the overall differentiation of new oligodendrocytes in the anterior corpus callosum in the assessed experimental design. Furthermore, we found no evidence that performance on the complex wheel was related to the density of newly-differentiating OLs in the anterior corpus callosum. In addition, we found OPC proliferation was not affected by the conditional knock-out of *Myrf*.

5.3.3 Analysis of white matter integrity in *Myrf*-cKO model using MRI (Preliminary data)

WM structure was assessed using *ex vivo* magnetic resonance imaging (MRI) using a multichannel 7 T MRI scanner (Varian). Two different types of MRI-techniques were acquired: Diffusion-weighted imaging (DWI) and Magnetization transfer (MT) imaging. Diffusion-weighted imaging (DWI) is

sensitive to self-diffusion of water molecules in tissue and will therefore be affected by alterations in local tissue microstructure. Magnetization transfer (MT) imaging is an MRI technique that indirectly detects water bound to macromolecules such as lipids and proteins and is thus sensitive to myelin (Kucharczyk *et al.* 1994). Digital brain extraction as well as linear and nonlinear transformations to template were not fully optimised at the stage of writing. Hence, the presented analysis should be considered a preliminary initial exploration of the data.

5.3.3.1 Region of interest analysis in whole WM skeleton: Mean FA and MTR of the whole WM did not reveal an effect of wheel running or genotype

Here we tested the hypothesis that exercise and running results in widespread increases in FA or MTR parameters, and that the prevention of oligodendrocytes differentiation by conditional deletion of *Myrf* results in widespread decreases in the analysed MRI metrics. Individual mean FA values for the whole skeletonised WM were extracted for each animal (Figure 5.5A). An ANOVA (Fixed Factor: Genotype, Wheeltype, Batch (5 level), n=71) was used to test for a statistically significant difference between the groups. The mean FA of the whole WM was not significantly different between the genotype groups (Genotype: $F_(1,51)=.185$, p=0.669), nor did they differ between animals that ran the complex wheel (CW) or animals only exposed to a fixed wheel (FW) (Wheeltype: $F_(1,51)=.1.297$, p=0.260). The same data exploration was performed for the (MTR) weighted images (Figure 5.6), also revealing no wheel ($F(1,51)=.113$, p=0.738) or genotype ($F(1,51)=.973$, p=0.329) effects in the mean WM data using the same statistical approach as above. Neither analysis revealed a Genotype*Wheeltype interaction effect.

5.3.3.2 Voxel-wise analysis of fractional anisotropy (FA) and magnetic transfer ratio (MTR) in the white matter skeleton

Voxel-wise analysis was performed to test for significant regional WM differences between groups across the whole-skeleton. No significant clusters were found when comparing genotypes for either FA or MTR parameters. For visualisation the range and the direction of t-values, t-values from

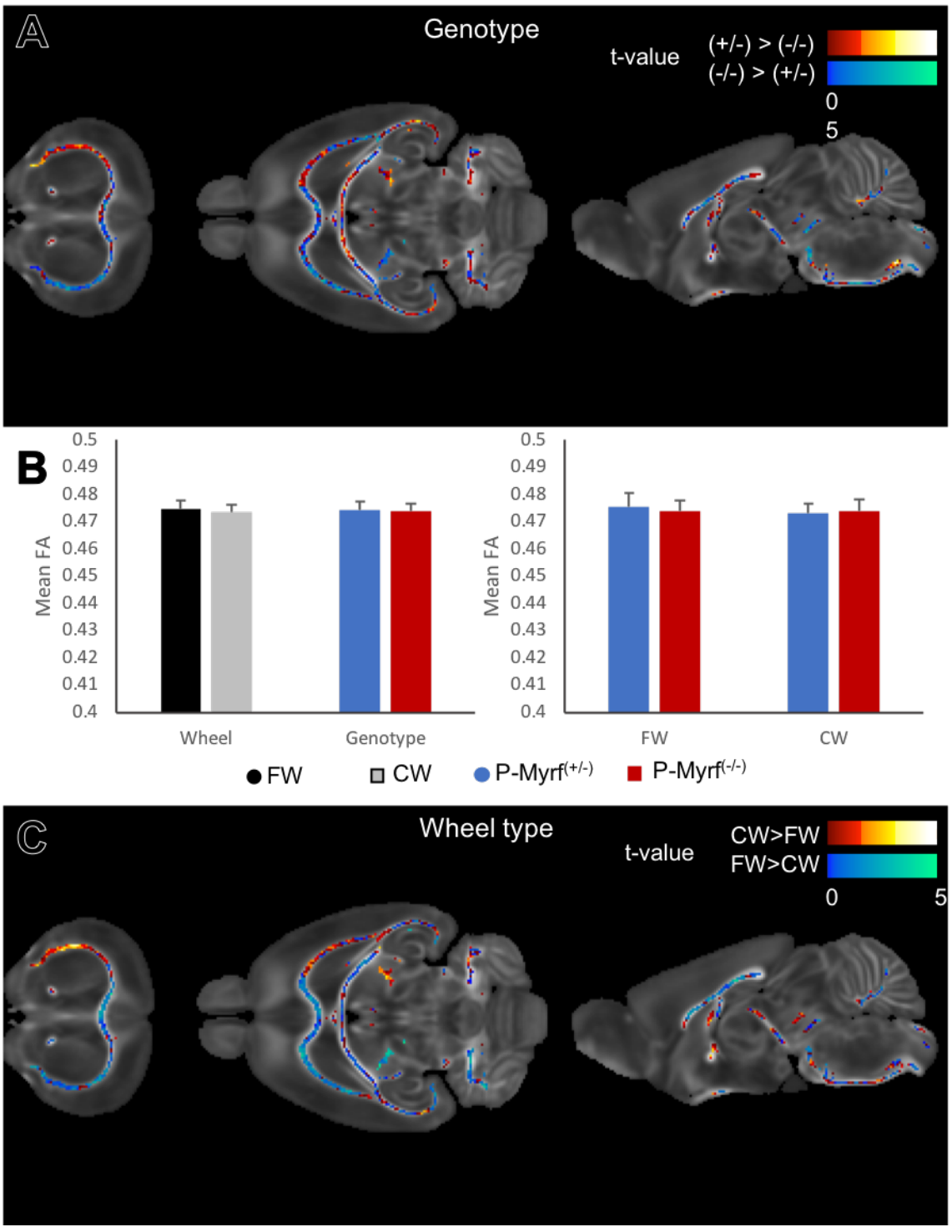


Figure 5.5. ***Tract-Based Spatial Statistics (TBSS) of Fractional anisotropy (FA).***

FA weighted images overlaid with t-value weighted mask of the white matter skeleton acquired by nonparametric permutation testing for a difference between ***(A)*** *Genotype groups and* ***(C)*** *wheel type groups.* ***(B)*** *Mean FA from within the white matter mask plotted to visualize the overall range of values in the wheel type and genotype groups. Data presented as Mean ±SEM. CW=Complex wheel, FW=Fixed Wheel.*

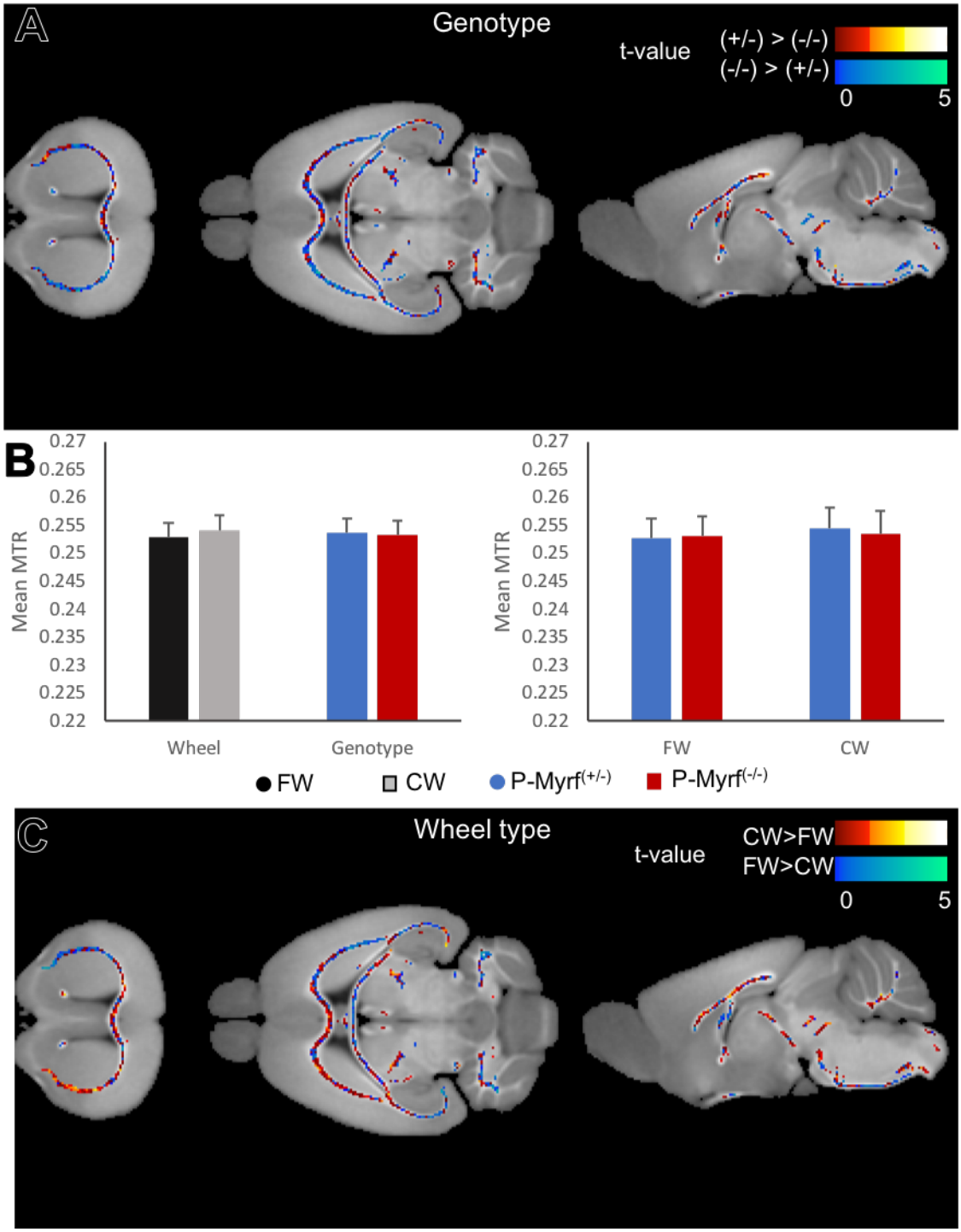


Figure 5.6. ***Tract-Based Spatial Statistics (TBSS) of magnetic transfer ratio (MTR).***

MTR weighted images overlaid with t-value weighted mask of the white matter skeleton acquired by nonparametric permutation testing for a difference between ***(A)*** *genotype groups and* ***(C)*** *wheeltype groups.* ***(B)*** *Mean FA from within the white matter mask plotted to visualize the overall range of values in the wheel type and genotype groups. Data presented as Mean ±SEM. CW=Complex wheel, FW=Fixed Wheel.*

both the FA (Figure 5.5A&C) and MTR (Figure 5.6A&C) metrics were colour-coded and projected onto the FA mouse mean template, indicating location and direction of either Genotype or Wheeltype specific differences.

When comparing animals that ran the complex wheel (CW) to animals that were exposed to a fixed wheel (FW), while controlling for Genotype and Batch as fixed factors, FA values were statistically significantly lower in an area around the left anterior forceps of the corpus callosum ($p<0.05$, corrected, CW: n=36, females 11; NW: n=35, females 13; Figure 5.7A) in animals running the complex wheel. No significant experience-dependent effects for MTR were found.

5.3.3.3 Region of interest analysis in anterior corpus callosum: Mean FA and MTR in the anterior corpus callosum did not significantly correlate with histological measures.

To assess the relationship between the acquired histological measurements and MRI metrics, mean FA and MTR values in the anterior part of the corpus callosum were calculated using a custom designed mask (Figure 5.1B) covering the region where histological analyses were conducted. Mean FA (Fig. 5.8A) and MTR (Figure 5.8B) values from within the masked area of the anterior corpus callosum were extracted. Consistent with the ROI and voxel-wise analyses reported above, mean MRI metrics did not reveal a statistically significant effect of wheel type (FA: $F(1,51)=1.931$, $p=0.173$; MTR: $F(1,51)=.098$, $p=0.755$) or genotype (FA: $F(1,51)=.011$, $p=0.915$; MTR: $F(1,51)=1.322$, $p=0.256$) in the anterior corpus callosum (Figure 5.8A&B) (ANOVA, Fixed Factor: Genotype, Wheeltype, Batch (5 level)). However, there was a subtle but statistically significant Genotype*Wheeltype interaction for the mean MTR metric in the anterior corpus callosum (MTR: $F(1,51)=4.303$, $p=0.043$, Figure 5.8B), and a trend for such an interaction for the mean FA values (FA: $F(1,51)=2.984$, $p=0.090$, Figure 5.8A). This indicates that the effect of wheel running on MR-derived metrics may have depended on animal's genotype, with MTR being higher in P-Myrf$^{(-/-)}$ animals and lower in P-Myrf$^{(-/+)}$ animals that

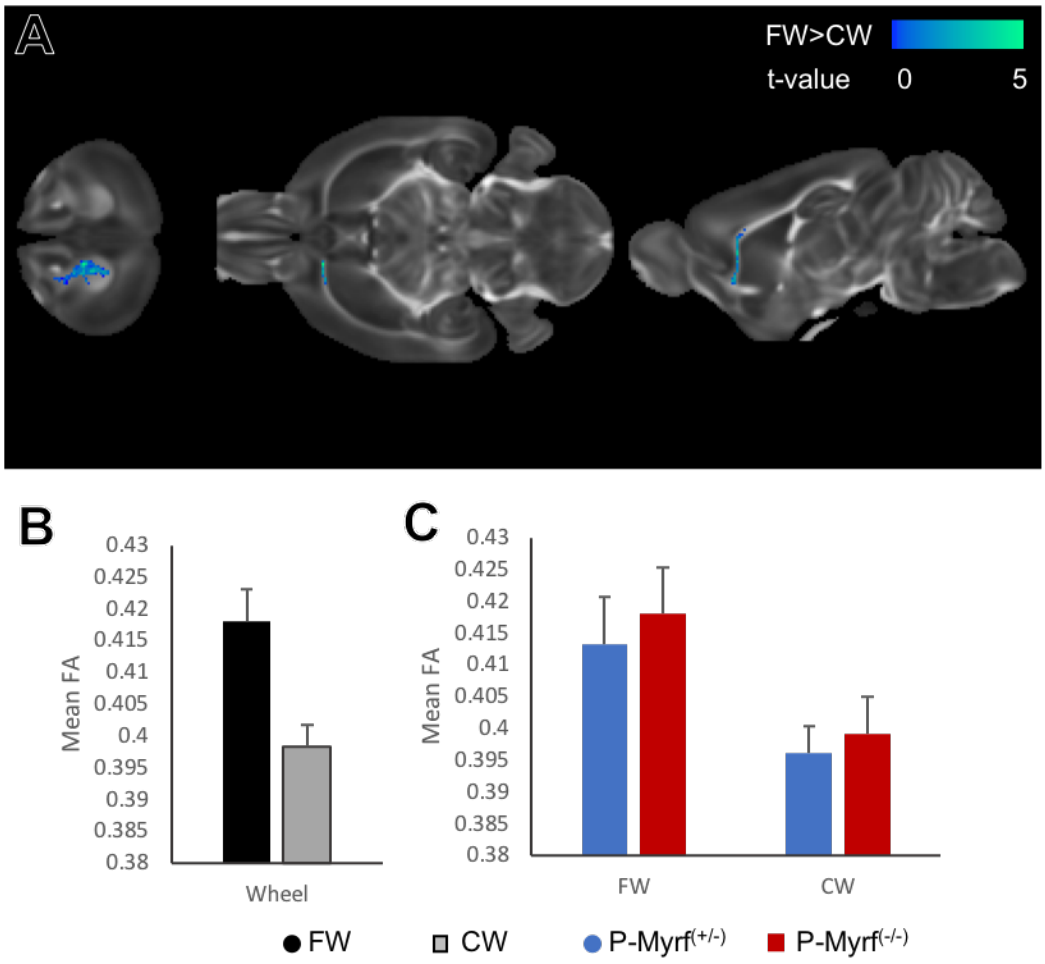


Figure 5.7. ***TBSS between-group analysis revealed a localised reduction in FA in animals running the complex wheel.***

(A) *FA weighted map overlaid with a t-value weighted cluster showing an area in the left anterior forceps of the corpus callosum that had a significantly lower fractional anisotropy (FA) in animals that ran the complex wheel, when compared to animals that were only exposed to a fixed static wheel.* ***(B)*** *Mean FA from within the significant cluster is plotted for each wheel type to visualize the range of values.* ***(C)*** *Mean FA values from within the significant cluster, divided by genotype. Data presented as Mean ±SEM.*

ran the complex wheel, compared to animals only being exposed to a fixed wheel. Assessing the relationship between histological and MRI metrics separately for each genotype, indicated that neither MRI metric was significantly correlated with either the density of newly-differentiated OLs [YFP+|CC1+] (Figure 5.8C&D) or OPCs labelled with yellow fluoresced protein [YFP+|CC1-] (Figure 5.8E&F), therefore providing no indication that oligodendroglia dynamics were directly associated with observed changes in MR-derived metrics.

5.4. DISCUSSION

In this chapter we aimed to investigate the underlying physiological changes associated with the behavioural phenotype of P-Myrf animals. However, the behaviour phenotype in the subsample of P-Myrf animals assessed in this chapter did not indicate a statistically significant difference between genotypes (Figure 5.2), yet revealed trends comparable to the one observed the whole sample of P-Myrfs. Nonetheless, we did confirm that homozygous deletion of *Myrf* in early adulthood significantly impaired the differentiation of new oligodendrocytes in the P-Myrf animals used in this study (Figure 5.3A&B). However, homozygous deletion of *Myrf* did not affect the proliferation and density of OPCs on day 13 of running the wheel, when compared to animals with one remaining copy of the gene (Figure 5.4). Preliminary analysis of our MRI data provided no evidence that this genotype-specific change in oligodendroglia dynamics significantly affected MR-derived parameters of white matter microstructure between the groups. Investigating the effect of animal's experience on oligodendroglia dynamics, we also found no evidence that running on the complex wheel affects the differentiation of new oligodendrocytes in the anterior corpus callosum of mice differently than simply exposing mice to a static complex wheel in a novel environment (Figure 5.3). Additionally, assessment of oligodendroglia dynamics in the anterior corpus callosum did not correlate with behaviour performance of animals that ran the complex wheel (Figure 5.3C&D), nor was this histological data associated with the assessed FA or MTR values in this region of interest (Figure 5.8C-F). However, preliminary voxel-wise analysis of the MR data indicated that the two distinct behaviour experiences affected the fractional anisotropy (FA) differently in an area around the anterior left forceps of the corpus callosum, indicating experience-induced and region-specific changes in white-matter microstructure (Figure 5.7). Interestingly, we found some evidence that the animal's genotype influences the animal's experience-dependent effect on white matter microstructure measured by MTR in the anterior corpus callosum of P-Myrf animals (Figure 5.8B). This provides preliminary evidence that homozygous deletion of *Myrf* can alter experience-dependent adaptive changes in brain structure.

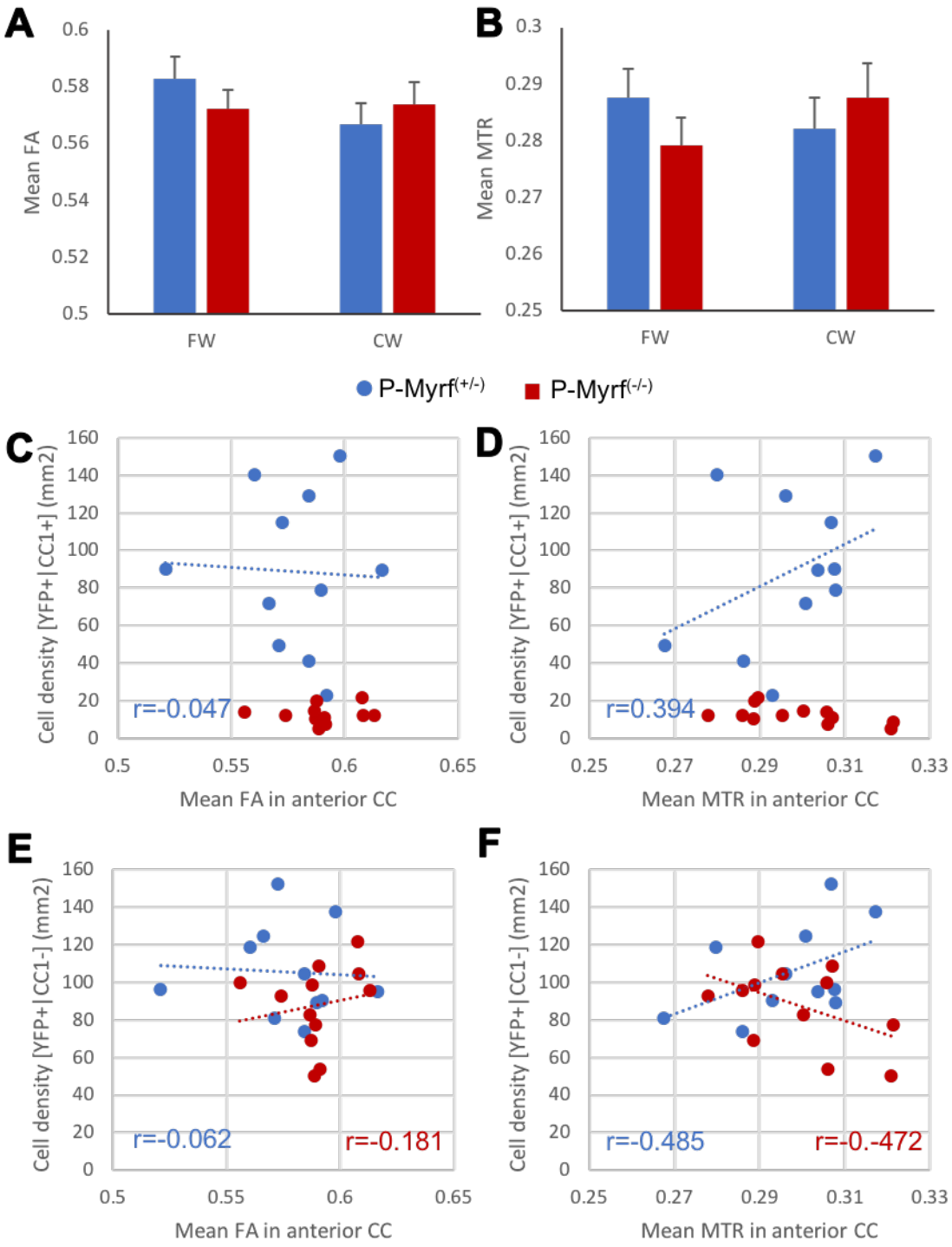


Figure 5.8. ***Relationship between MRI based metrics and cellular densities determined by histology in the anterior corpus callosum.***

*Mean **(A)** FA and **(B)** MTR values from within the masked area of the anterior corpus callosum plotted for each group to visualize the range of values. Data presented as Mean ±SEM. **(C,E)** Plotted relationship between the mean FA values and the **(C)** density of newly differentiated OL or **(E)** YFP-positive OPCs in the anterior corpus callosum. **(D,F)** The relationship between the mean MTR values and the **(D)** density of newly differentiated OL or **(F)** YFP-positive OPCs in the anterior corpus callosum. Pearson's r was used for statistical analysis, with correlation coefficient indicated on the graphs (Red=P-Myrf$^{(-/-)}$;Blue=P-Myrf$^{(-/+)}$. None of the assessed correlation reached statistical significance (p>0.05).*

Experience-dependent changes in oligodendroglia dynamics have been repeatedly demonstrated in a range of studies (Simon *et al.* 2011; McKenzie *et al.* 2014; Tomlinson *et al.* 2016; Xiao *et al.* 2016; Keiner *et al.* 2017; Hughes *et al.* 2018). However, our data does not indicate that running on the complex wheel increased the differentiation of new oligodendrocytes. This is in contrast to previous studies that observed such a physiological response (McKenzie *et al.* 2014; Xiao *et al.* 2016) after 11 days. One reason for the difference in observations may lie in the nature of the control condition used in this study. As we were specifically interested in the effect of running on the complex wheel, the control condition in the current study exposed mice to a static complex wheel in a novel environment, which provided a large object that can be climbed and interacted with as environmental enrichment. However, previous studies used 'housing without a wheel' as a control condition. The lack of any novel and salient object present may make it difficult to attribute observed cellular changes specifically to learning to run the complex wheel, as environmental enrichments (Zhao *et al.* 2011) and running a normal wheel (Krityakiarana *et al.* 2010; Simon *et al.* 2011) can increase the differentiation of oligodendrocytes as well (Tomlinson *et al.* 2016). Indeed, Keiner *et al.* (2017) observed that environmental enrichment and training animals on a fine motor task both increased oligodendroglia dynamics to a similar degree after 10 days, compared to a passive sedentary control condition. Differences between the experience-dependent effects were however observed after 42 days (Keiner *et al.* 2017), a time frame not investigated in the current study.

Moreover, we used a different method to quantify oligodendrocyte differentiation. In the current study PDGF-Rα-positive cells were labelled with YFP at the time of tamoxifen treatment and were later assessed for their expression of the mature oligodendrocyte marker CC1 (Figure 4.1, Figure 5.3). This method labels differentiation for the entire time period after tamoxifen treatment (~5 weeks) and also labels new oligodendrocytes directly differentiating from OPCs, without prior proliferation. In contrast, most other studies use a method to label proliferating cells in order to identify newly-differentiating oligodendrocytes arising from the proliferating cell population (McKenzie *et al.* 2014;

Xiao *et al.* 2016; Keiner *et al.* 2017; Mitew *et al.* 2018), whereas the time at which proliferating cells are being labelled differs between studies. By treating animals with EdU 10 days before behaviour testing, Xiao et al. (2016) demonstrated that OPCs can differentiate into oligodendrocytes without an immediate prior increase in OPC proliferation, an observation supported by the evidence suggesting that only a minority of OPC differentiation events are directly preceeded by proliferation in the cerebral cortex (Hughes *et al.* 2013). Lacking a complete understanding of the exact sequence of these cellular events means that potential differences arising from different methods will have to be considered. Additionally, our study quantified oligodendroglia dynamics in P-Myrf animals, whereas previous studies used wild-type mice (McKenzie *et al.* 2014; Xiao *et al.* 2016). Hence, potential variations in genetic background and the potential effect of heterozygous deletion of *Myrf* on experience-dependent plasticity are possible and have not been investigated. These differences in control conditions, quantification method and genetic background may also explain why we detected an experience-dependent increase in newly-differentiated oligodendrocytes in animals that ran the complex wheel in Chapter 3 (Figure 3.10), but not in the results presented in this chapter.

We found no evidence for a positive linear relationship between performance on the complex wheel and the density of newly-differentiated oligodendrocytes (Figure 5.3). Our study was likely underpowered to detect such a potentially subtle association, as it is likely to be influenced by many other factors and is only an indirect measure of a potential mechanism influencing behaviour performance. However, a trend towards a negative relationship between the density of new oligodendrocytes and running performance indicates a relationship between these two factors that may be more complex. Whereas the absence of newly-differentiating oligodendrocytes can impair performance, better performance may not necessarily require a higher number of differentiating and surviving oligodendroglia. Yet, the histological methods used in this study also label cells that were differentiating prior to running on the complex wheel, making the detection of a potential association between the two factors somewhat inaccurate. Analysing the additional tissue samples available for

the EdU treated animals (Figure 5.4) may provide a more accurate quantification of running and performance related cellular dynamics. However, it may require the quantification of myelination to detect an association with behaviour, as myelination may be the cellular process that lies downstream of oligodendrogenesis. Myelination has previously been correlated to task performance in other rodent studies looking at the effects of motor learning (Sampaio-Baptista *et al.* 2013).

Unfortunately, at the time of writing, our analysis of the data provided by MRI was not fully completed. Hence, the obtained results should be considered with caution. Nonetheless, the preliminary results suggest that the prevention of oligodendrogenesis in early adulthood did not affect the microstructure of the major white matter tracts, as neither our ROI nor voxel-wise analysis revealed any differences between P-Myrf$^{(-/-)}$ animals and their P-Myrf$^{(-/+)}$ littermates. Oligodendrogenesis was significantly impaired in P-Myrf$^{(-/-)}$ animals for about 5 weeks, starting at the age of about P83, during which time the formation of new myelinating oligodendrocytes is ongoing in mice (Young *et al.* 2013; Hill *et al.* 2018; Hughes *et al.* 2018). While it may be possible to pick up such a significant change in oligodendroglia dynamics with MR-derived metrics, the current lack of an observed effect may suggest that the fraction of new myelination that continues in P-Myrf$^{(+/-)}$ controls in this time-frame may be too small to be detectable. Alternatively, concurrent processes affecting the MR-derived signal may mask the effect of myelination, as MTR and DWI derived metrics can be affected by a variety of other processes such as inflammation, changes in astrocytes and axonal morphology (Gareau *et al.* 2000; Walhovd *et al.* 2014).

While our preliminary analysis found no evidence for an experience dependent effect as measured by MTR, we found that running on the complex wheel reduced the FA value in a cluster around the left anterior forceps of the corpus callosum (Figure 5.7). Skill acquisition has previously been associated with increases in FA values in rodents (Blumenfeld-Katzir *et al.* 2011; Sampaio-Baptista *et al.* 2013) and humans (Flöel *et al.* 2009; Scholz *et al.* 2009; Takeuchi *et al.* 2010). However, other studies have also reported a reduction in FA values associated with training. Participants that trained

in a whole-body balancing task showed decreases in FA and a negative correlation between FA changes and performance in prefrontal areas (Taubert et al., 2010). This exemplifies the difficulty in interpreting the changes in metrics like FA without analysing the physiological changes associated with it, as it is not clear which cellular process might have driven the observed changes in FA. It is also not clear why MTR values do not show a significant change in the similar region. A planned histological analysis of this ROI in which significant changes have been identified may help us to understand potentially significant cellular process associated with the observed change. However, correlating histological analysis and MR-derived metrics is not always straightforward either, due to the variety of cellular processes involved. Indeed, previous studies failed to find a correlation between FA and immunobiological measures of myelin expression (Sampaio-Baptista *et al.* 2013). However, the combination of immunolabelling of myelin in a 3D space of the brain, rendered optically transparent by Clear Lipid-exchanged, Anatomically Rigid, Imaging/immunostaining compatible, Tissue hYdrogel (CLARITY), demonstrated that immunofluorescence of myelin basic protein significantly correlated with fractional anisotropy (FA), at least in WM regions with coherent fibre orientations and low fibre dispersion (Chang *et al.* 2017).

Our ROI analysis in the anterior corpus callosum provided some evidence for an interaction between the genetic prevention of oligodendrogenesis and an experience-dependent effect on white matter microstructure (Figure 5.8). Yet, surprisingly, this data suggested that MTR tends to be higher in P-Myrf$^{(-/-)}$ animals and lower in P-Myrf$^{(+/-)}$ animals that experienced running the complex wheel. Hence, it is unlikely that this change represents the formation of myelin by newly differentiating oligodendrocytes and may instead be driven by unrelated cellular processes. Indeed, it is unclear if and how the homozygous deletion of *Myrf* and the subsequent failure of OPCs to successfully differentiated leads to other cellular processes such as inflammation, as such an investigation has not been conducted by previous studies (McKenzie *et al.* 2014; Xiao *et al.* 2016). A histological analysis

looking for markers of potential other cellular process, such as inflammation and cell death, will be required to clarify this outstanding question.

In the cotext of potential inflammatory processes in the P-Myrf model, recent research has indicated that microglia in the adult mouse brain have sex-specific densities, morphology, and immune molecule load, which also depend on age (Kodama and Gan 2019). Transcriptomic phenotypes of microglia are also different between sexes and retain the phenotype of their origin even when microglia have been transplanted into a brain of the opposite sex (Villa *et al.* 2018). The same study also indicated that female microglia can show a more neuroprotective phenotype than male microglia. Hence, if a behavioural or structural phenotype in the P-Myrf animals may be partly driven by, or related to inflammatory processes, a potential sex-dependent differences in microglia phenotype that may relate to a sex-depedent behaviour phenotype should also be further investigated in the P-Myrf mice.

Further analysis of the MRI derived data and subsequent histological analysis is required to understand any potential physiological response to learning to run the complex wheel. While our current analysis only focused on white matter tracts, it is equally likely that changes in grey matter microstructure and cellular dynamics are associated with experience-dependent plasticity. A limitation of our experimental design is that we are looking at cross-sectional changes, rather than investigating longitudinal changes in physiological effects of complex wheel running. While we are comparing siblings and are trying to control for factors other than complex wheel running via an appropriate control condition, the lack of a clear behaviour phenotype in the subsample of animals under investigation, and large variability of performance within the sample, makes it difficult to identify potentially subtle changes between the groups. Our aim was to identify physiological changes that may be driving the observed difference in performance on the complex wheel. Hence, we chose a time point of about 2 weeks after starting training on the complex wheel, as cellular changes were previously consistently identified at this timepoint (McKenzie *et al.* 2014; Xiao *et al.* 2016) and

learning and skill improvement were recent and potentially still ongoing. Yet, it is possible that consistent and quantifiable changes in myelination and cellular changes associated with learning maybe only be detectable at certain timepoints (earlier or later), for reasons not currently understood.

Taking everything into consideration at this stage of analysis, we have currently no conclusive evidence that supports the hypothesis that the formation of new oligodendrocytes or any subsequent changes in myelination or cellular microstructure are driving the behavioural performance on the complex wheel, or that the performance observed on the complex wheel is associated with a specific changes in oligodendroglia dynamics. Yet, this lack of evidence may due to the currently incomplete and insufficient analysis of our available data and biological samples.

Chapter 6 | GENERAL DISCUSSION

6.1. SUMMARY OF THE KEY RESULTS

The aim of this thesis was to contribute to our understanding of myelin dynamics and the axon-glia communication regulating it, as well as develop new *in vitro* co-culture systems to study myelination. We indeed managed to successfully develop a novel myelinating co-culture system between iPSC-derived human sensory neurons and rodent Schwann cells that showed the canonical markers of the axon-glia relationship of the PNS (Figure 2.2), including Nodes of Ranvier formation (Figure 2.3) and the importance of key signalling pathways such as Nrg1-ErbB (Figure 3.2, Figure 3.3). Furthermore, presence of human antigens in the co-culture, as well as its longevity, allowed us to investigate the effect of auto-immune associated antibodies on the formation and maintenance of PNS myelination (Figure 2.7, Figure 2.8, Figure 2.9). Unfortunately, developing an analogous co-culture model using rodent oligodendroglia, rather than Schwann cells, was less successful, as the system did not reliably produce stable myelination that could be studied over time (Figure 3.6), despite initial promising results indicating the presence of myelinated oligodendrocytes.

Another aim of this thesis was to investigate if Nrg1-ErbB signalling can influence adaptive changes in oligodendroglia dynamics. We confirmed that experience such as running the complex wheel indeed leads to an increase in OPC differentiation (Figure 3.10), when compared to a home-cage control. Using a transgenic mouse model that allows the conditional and global knock-out of *Nrg1* we found that deletion of *Nrg1* led to a subtle but significant behaviour deficit in the complex wheel running paradigm (Figure 3.8). Studying the role of Nrg1-ErbB signalling in oligodendroglia dynamics

in vivo, our study did not find sufficient evidence for a change in adaptive oligodendrogenisis in the anterior corpus callosum in the absence of neuregulin signalling (Figure 3.10).

Using the same complex running wheel paradigm, we investigate the role of *de novo* myelination in skill acquisition. Our aim was to replicate and extend previous findings that provided the first evidence indicating a causal relationship between adaptive myelination and behaviour change. Indeed, we were able to replicate findings from these influential studies, indicate that conditional deletion of Myrf, and subsequent inability to form new oligodendrocytes (Figure 4.1), can lead to an impaired performance on the complex wheel (Figure 4.3, Figure 4.4, Figure 4.5). Furthermore, we also confirmed that this impairment in motor skill acquisition can already be detected after a few hours of activity on the wheel (Figure 4.7). However, not all aspects of the behaviour phenotype were faithfully replicated, as sex differences in performance (Supplementary Figure 4) and a reduced time spent on the wheel (Figure 4.8) were not previously reported. Furthermore, we found a large variability in behaviour performance within the transgenic mice population that made interpretation of data from smaller subsamples of animals challenging.

A further aim of this thesis was to test for a link between behaviour performance, histological data about oligodendroglia dynamics, and MRI derived metrics of white matter microstructure within the Myrf-cKO mouse population to understand the underlying biological changes that drive the observed behaviour phenotype on the complex wheel. Surprisingly, we found that complex wheel running does not lead to an increase in adaptive oligodendroglia dynamics when comparing running mice to siblings exposed to a more active control condition that only excludes actually running the complex wheel from the overall experience (Figure 5.3). However, the preliminary analysis of our MRI-derived data indicates experience-dependent changes in white matter microstructure (Figure 5.7) and a potential interaction between the effects of experience and the ability to produce new oligodendrocytes on white matter microstructure (Figure 5.8).

Overall, our work of establishing and studying co-cultures with iPSC-derived co cultures has provided a novel method to study myelination and has provided some valuable insight into the mechanism of autoimmune associated neuropathies (Clark & Kaller et al., 2017). However, our work on the role of Nrg1-ErbB signalling in adaptive oligodendroglia dynamics was limited by the lack of a stable *in vitro* model and the analysis of *in vivo* histological data that is currently underpowered. The work on the role of *de novo* myelination in behaviour acquisition, while replicating the major behaviour deficit found in the original studies, remains partly inconclusive regarding the exact role that *de novo* myelination might play in skill acquisition and further investigation is needed to clarify contradictions and open questions in the data sets. While some limitations in the current data sets are due to incomplete data analysis, other are caused by insufficient experimental design or potential limitations of the experimental models used for the experiments.

6.2. Discussion and Future directions

6.2.1 Theme 1: Establish iPSC- derived myelinating co-cultures to model the axoglial relationship in vitro

The intricate interaction between myelinating glia and axons is essential for the development, maintenance, function and integrity of the nervous system. The study of this cellular relationship relies heavily on animal models, predominantly rodent and zebrafish, and co-cultures between isolated primary rodent neurons and glia. Yet, recent progress iPSC-technology and cell culturing methods allow the exciting opportunity to develop cellular models with human donors and patient derived cells, which can be maintained as a renewable resource. Our study using iPSC-derived sensory neurons with rodent Schwann cells demonstrates the feasibility for the use of iPSC-derived human cells for such models to study aspects of axon-glia relationship and human specific neuropathology (Clark *et al.* 2017; Galino *et al.* 2019; McDermott *et al.* 2019).

Even when studying neuronal physiology *in vitro,* there is a strong argument for using co-cultures containing glia cells. Myelinating glia play a fundamental role in promoting the maturation of the axon

cytoskeleton, regulating axon trafficking parameters, and imposing architectural rearrangements such as the Nodes of Ranvier and their associated molecular domains (Pan and Chan 2017), next to their role in metabolic support and nerve conduction (Nave and Werner 2014). As every axon in the PNS is associated with a Schwann cell, such neuron-glia co-cultures may provide a more physiological relevant model of the conditions found *in vivo*.

A similar argument can be made for the CNS, as the regulation and complexity of CNS myelination may partially depend on interconnected networks with other glia cells (Dutta *et al.* 2018; Fields and Dutta 2019). However, the need for an increased complexity of a culture system will depend on scientific questions under investigation. For example, the fact that aspects like neuronal and oligodendroglia identity can influence dynamics like activity-dependent myelination (Koudelka *et al.* 2016; Bechler *et al.* 2018; Zonouzi *et al.* 2019) emphasises the importance of choosing and controlling these factors carefully when conducting relevant *in vitro* studies. Different types of sensory neurons in the dorsal root ganglia project axons to the spinal cord to convey peripheral information to the central nervous system, which are subsequently myelinated by oligodendrocytes. DRGs are therefore a good model to study oligodendrocyte myelination, which has been frequently used in the past. However, developing a myelinating co-culture system of the CNS using iPSC-derived PNS neurons may not provide a model with the sufficient physiological relevance to study more intricate aspects of the neuron-glia relationship in the CNS, such as adaptive-myelination found in central cortical region and underlying WM tracks. Fortunately, several protocols for the development of iPSC-derived CNS neurons have been developed as a potential alternative (Shi *et al.* 2012; Yan *et al.* 2013), which should be consider for future attempts to develop iPSC-derived myelinating co-cultures to study oligodendroglia dynamics *in vitro.*

The next step of our research is the development of a myelinating co-culture system entirely derived from human iPSC. However, the ability to use iPSC-derived cells relies heavily on the efficacy, specificity and simplicity of the methods used to differentiate them. While advances have been made

in the development of protocols for the differentiation of iPSC-derived Schwann cells (Liu *et al.* 2012b; Ma *et al.* 2014) and oligodendrocytes (Wang *et al.* 2013; Czepiel *et al.* 2015; Douvaras and Fossati 2015), those protocols are currently lengthy, complicated and/or inefficient and the resulting cells fail to develop consistent and reliable myelination *in vitro*. An emerging and alternative model to study cellular development and interaction in an entirely human environment is the generation of three-dimensional organoids (Rookmaaker *et al.* 2015; Kaushik *et al.* 2018). Indeed, a recent study demonstrated a promising new differentiation method of human induced pluripotent stem cells to generate three-dimensional brain organoids that contain oligodendrocytes as well as neurons and astrocytes, which displayed surprisingly complex cellular development, interaction and myelination (Marton *et al.* 2019).

In summary, *in vitro* cultures using iPSC-derived cells are a promising tool for the development of novel co-culture systems that may prove invaluable as a complementary tool for preclinical research. However, the reliability, reproducibility and robustness of such models are important, which will largely depend on the development of efficient differentiation protocols that can easily be established and adopted by research groups and potentially scaled up for high-throughput testing.

6.2.2 THEME 2: INVESTIGATE THE ROLE OF NRG1-ERBB SIGNALLING IN MYELINATION

Neuregulin 1 is member of a family of growth factors that plays essential and diverse roles in the developing and adult nervous system. Nrg1-ErbB contributes to neuronal migration, neuronal differentiation, synaptic formation and function and the development and maintenance of neuromuscular junctions (Mei and Nave 2014). An additional emerging function is the modulation of nervous system injury and repair (Bartus *et al.* 2016; Birchmeier and Bennett 2016; Kataria *et al.* 2019).

Nrg1-ErbB signalling has also been recognised for its central and critical role in PNS myelination, which we were able to demonstrate in our co-culture system. The intra- and extra-cellular signalling cascades of the diverse range of neuregulin isoforms are complex (Mei and Nave 2014) and can be

disrupted by a range of compounds not directly targeting it. The inhibition of BACE1, being pursued as a therapeutic target to treat patients suffering from Alzheimer's disease, is a good example also demonstrated in this thesis. A reliable and durable myelination co-culture model of the PNS, ideally entirely derived from human iPSC, may provide a useful platform to test new compounds for their therapeutic potential or unwanted side effects (Saporta and Shy 2017).

The role of Nrg1-erbB signalling in CNS myelination is little understood, yet does not seem to be as critical and central as in the PNS (Brinkmann *et al.* 2008; Mei and Nave 2014). However, several lines of evidence from different experimental paradigms, including transgenic overexpression and social isolation in mice (Brinkmann *et al.* 2008; Makinodan *et al.* 2012) as well as *in vitro* studies (Lundgaard *et al.* 2013), hint at a more complex involvement in CNS myelination that may be related to activity dependent-myelination and potentially be restricted to critical periods during development. Unfortunately, our co-culture with oligodendroglia lacked the reliability and reproducibility needed to study CNS myelination. However, if such conditions had been optimised, our next steps would be the establishment of tools for the efficient manipulation of neural activity, such as optogenetics (Stockley *et al.* 2017), in cultured neurons to study activity-related effects of Nrg1-ErbB signalling on CNS myelination.

Our studies using the global and conditional deletion of *Nrg1* provide evidence for a subtle and previously unknown behaviour phenotype of animals lacking Neuregulin 1 signalling on the complex wheel. However, the aim of the study was to investigate potential effects of Nrg1-erbB signalling on experience dependent changes in oligodendroglia dynamics. While our current data provides no evidence for such an effect, further investigation of other brain regions and the remaining tissues samples is needed to gain the statistical power needed to exclude a potentially subtle effect on myelination, as well as exclude the possibility of a potentially region-specific effect. Yet, even in the case of a positive result in the paradigm, follow up studies with a more specific knock-out model,

such as an OPC-specific deletion of Erb3/Erb4 would be needed, as a global interference with Nrg1-ErbB could have a wide range of effects not related to the axon-glia communication.

The expression and proteolytic processing of Nrg1 can be influenced by neuronal activity (Ozaki *et al.* 2004; Iwakura *et al.* 2017) and initial *in vitro* studies provide promising results for its potential role in adaptive myelination (Lundgaard *et al.* 2013). Hence, the potential role of Nrg1-erbB signalling in CNS myelination needs further investigation, especially as it may reveal a mechanism by which myelination is switched from an intrinsic into an adaptive mode. Unveiling such a mechanism may help to refine the theoretical concepts trying to explain the complexity and function of oligodendroglia dynamics in the CNS during development and adulthood. Unfortunately, the results presented in this thesis contribute little conclusive evidence that may help to advance our understanding of Nrg1-ErbB signalling in CNS myelination at this point in time. However, the presence of a subtle behavioural phenotype of Nrg1-cKO mice on the complex wheel hints at an underlying factor that may be worth pursuing with a more detailed histological analysis and more specific transgenic model.

6.2.3 Theme 3: Replicating and extending evidence for role of de novo myelination in motor learning

While the link between behaviour, myelin integrity and developmental myelination had been recognised in the past, the plastic regulation of myelination, even during adulthood, has gained increased recognition as an additional mechanism by which experience can shape brain structure. However, the role of adaptive myelination in the CNS is relatively unclear and its potential to facilitate and shape behavioural change remains elusive. Work by McKenzie *et al.* (2014) and Xiao *et al.* (2016) have provided the first evidence for a causal link between experience-dependent myelin remodelling and behaviour change in the form of motor skill acquisition.

The results presented in this thesis replicated previous observations by McKenzie *et al.* (2014) and Xiao *et al.* (2016) indicating that mice with a significantly reduced ability to differentiate new-

oligodendrocytes in early adulthood can be less able to run and/or improve their performance on the complex running wheel. However, several aspects of the behavioural phenotype, such as a bimodal distribution of performance and an overall reduced activity level on the wheel, make it difficult to define exactly which aspect of behaviour is impaired. This is further complicated by the fact that the complex wheel has not previously been used or cross validated as a motor learning task. Hence, further investigation of the behavioural phenotype using more established motor learning task, such as the skilled reaching task, is needed to clarify if conditional deletion of *Myrf* affects motor skill acquisition in general. Additionally, it would be ideal to replicate the behavioural phenotype in a different rodent model that allows the conditional prevention of oligodendrogenisis using a set of different gene targets, as this would make it unlikely that the observed behavioural deficit is caused by secondary factors other than a lack of *de novo* myelination, a secondary and unknown factor that may be specific to the Myrf-cKO model investigated in this study.

Furthermore, it is essential to understand the underlying biological changes that are associated with learning to run the complex wheel. If *de novo* myelination actively contributes to skill acquisition, relevant changes in myelination and tissue microstructure should be associated with behavioural performance or improvement. While it is methodologically challenging to detect such specific and potentially subtle changes, the detection of general experience-dependent changes in oligodendroglia dynamics, which may also be caused by a range of other novel experiences, provides little evidence for their contribution to skill acquisition. Further analysis of our histological and MRI-derived data is required before we can determine if the methods and experimental design presented in this thesis are sufficient to reveal such performance and learning specific biological changes, and to demonstrate that such changes are associated with *de novo* myelination. While our preliminary data indicates potential experience and learning-specific changes, the lack of a clear behavioural deficit in the relevant subsample of mice may make it challenging to link biological changes to the behavioural phenotype of interest.

Providing conclusive evidence for the contribution of myelin plasticity and oligodendroglia dynamics to learning and behavioural changes remains a key challenge in the field. On the one hand, the presented work replicating the behavioural deficit of the Myrf-cKO model provides support for the hypothesis that *de novo* myelination contributions to skill acquisition. On the other hand, it is not fully clear which aspect of behaviour is affected in this model and if physiological changes associated with performance and learning can be linked to adaptive oligodendrogenesis and *de novo* myelination. Hence, further work is needed to clarify the contribution of myelin plasticity to skill acquisition and adaptive behaviour change in general. Future studies should make use of technological advances, such as electron microscopic volumetric reconstruction of brain tissue (Briggman and Bock 2012; Kasthuri *et al.* 2015) and models to translate between MRI signals and microscopy (Chen *et al.* 2013; Stüber *et al.* 2014; Morawski *et al.* 2018), which present promising tools to relate evidence across the different experimental approaches and to address the many unanswered questions regarding the role myelin plasticity might play in the nervous system.

BIBLIOGRAPHY

Almeida RG. The Rules of Attraction in Central Nervous System Myelination. *Front Cell Neurosci* 2018;**12**, DOI: 10.3389/fncel.2018.00367.

Alonso-Ortiz E, Levesque IR, Pike GB. MRI-based myelin water imaging: A technical review. *Magn Reson Med* 2015;**73**:70–81.

Arancibia-Cárcamo IL, Ford MC, Cossell L *et al.* Node of Ranvier length as a potential regulator of myelinated axon conduction speed. *eLife* 2017, DOI: 10.7554/eLife.23329.

Arnau J, Bendayan R, Blanca MJ *et al.* The effect of skewness and kurtosis on the robustness of linear mixed models. *Behav Res Methods* 2013;**45**:873–9.

Barkovich AJ, Kjos BO, Jackson DE *et al.* Normal maturation of the neonatal and infant brain: MR imaging at 1.5 T. *Radiology* 1988;**166**:173–80.

Bartus K, Galino J, James ND *et al.* Neuregulin-1 controls an endogenous repair mechanism after spinal cord injury. *Brain* 2016;**139**:1394–416.

Bartzokis G, Lu PH, Tingus K *et al.* Lifespan trajectory of myelin integrity and maximum motor speed. *Neurobiol Aging* 2010;**31**:1554–62.

Bech E, Orntoft TF, Andersen LP *et al.* IgM anti-GM1 antibodies in the Guillain-Barré syndrome: a serological predictor of the clinical course. *J Neuroimmunol* 1997;**72**:59–66.

Bechler ME, Byrne L, ffrench-Constant C. CNS Myelin Sheath Lengths Are an Intrinsic Property of Oligodendrocytes. *Curr Biol* 2015a;**25**:2411–6.

Bechler ME, Swire M, ffrench-Constant C. Intrinsic and adaptive myelination—A sequential mechanism for smart wiring in the brain. *Devel Neurobio* 2018;**78**:68–79.

Bells S, Lefebvre J, Longoni G *et al.* White matter plasticity and maturation in human cognition. *Glia* 2019, DOI: 10.1002/glia.23661.

Bennett IJ, Madden DJ. Disconnected aging: Cerebral white matter integrity and age-related differences in cognition. *Neuroscience* 2014;**276**:187–205.

Bergles DE, Richardson WD. Oligodendrocyte Development and Plasticity. *Cold Spring Harb Perspect Biol* 2016;**8**:a020453.

Birchmeier C, Bennett DLH. Chapter Four - Neuregulin/ErbB Signaling in Developmental Myelin Formation and Nerve Repair. In: Wassarman PM (ed.). *Current Topics in Developmental Biology*. Vol 116. Academic Press, 2016, 45–64.

Blanca MJ, Alarcón R, Arnau J *et al.* Non-normal data: Is ANOVA still a valid option? *Psicothema* 2017;**29**:552–7.

Blanca MJ, Alarcón R, Arnau J *et al.* Effect of variance ratio on ANOVA robustness: Might 1.5 be the limit? *Behav Res Methods* 2018;**50**:937–62.

Blumenfeld-Katzir T, Pasternak O, Dagan M *et al.* Diffusion MRI of Structural Brain Plasticity Induced by a Learning and Memory Task. *PLOS ONE* 2011;**6**:e20678.

Boffey J, Odaka M, Nicoll D *et al.* Characterisation of the immunoglobulin variable region gene usage encoding the murine anti-ganglioside antibody repertoire. *Journal of Neuroimmunology* 2005;**165**:92–103.

Bos W van den, Rodriguez CA, Schweitzer JB *et al.* Adolescent impatience decreases with increased frontostriatal connectivity. *PNAS* 2015;**112**:E3765–74.

Briggman KL, Bock DD. Volume electron microscopy for neuronal circuit reconstruction. *Current Opinion in Neurobiology* 2012;**22**:154–61.

Brinkmann BG, Agarwal A, Sereda MW *et al.* Neuregulin-1/ErbB Signaling Serves Distinct Functions in Myelination of the Peripheral and Central Nervous System. *Neuron* 2008a;**59**:581–95.

Brooks SP, Dunnett SB. Tests to assess motor phenotype in mice: a user's guide. *Nature Reviews Neuroscience* 2009;**10**:519–29.

Brown LA, Hasan S, Foster RG *et al.* COMPASS: Continuous Open Mouse Phenotyping of Activity and Sleep Status. *Wellcome Open Research* 2017;**1**:2.

Caeyenberghs K, Metzler-Baddeley C, Foley S *et al.* Dynamics of the Human Structural Connectome Underlying Working Memory Training. *J Neurosci* 2016;**36**:4056–66.

Calaora V, Rogister B, Bismuth K *et al.* Neuregulin Signaling Regulates Neural Precursor Growth and the Generation of Oligodendrocytes In Vitro. *J Neurosci* 2001;**21**:4740–51.

Canoll PD, Kraemer R, Teng KK *et al.* GGF/Neuregulin Induces a Phenotypic Reversion of Oligodendrocytes. *Molecular and Cellular Neuroscience* 1999;**13**:79–94.

Canoll PD, Musacchio JM, Hardy R *et al.* GGF/Neuregulin Is a Neuronal Signal That Promotes the Proliferation and Survival and Inhibits the Differentiation of Oligodendrocyte Progenitors. *Neuron* 1996;**17**:229–43.

Castelfranco AM, Hartline DK. Evolution of rapid nerve conduction. *Brain Research* 2016;**1641**:11–33.

Chambers SM, Qi Y, Mica Y *et al.* Combined small-molecule inhibition accelerates developmental timing and converts human pluripotent stem cells into nociceptors. *Nat Biotechnol* 2012;**30**:715–20.

Chang EH, Argyelan M, Aggarwal M *et al.* The role of myelination in measures of white matter integrity: Combination of diffusion tensor imaging and two-photon microscopy of CLARITY intact brains. *NeuroImage* 2017;**147**:253–61.

Chang K-J, Redmond SA, Chan JR. Remodeling myelination: implications for mechanisms of neural plasticity. *Nat Neurosci* 2016;**19**:190–7.

Chen S, Rio C, Ji R-R *et al.* Disruption of ErbB receptor signaling in adult non-myelinating Schwann cells causes progressive sensory loss. *Nat Neurosci* 2003;**6**:1186–93.

Chen WC, Foxley S, Miller KL. Detecting microstructural properties of white matter based on compartmentalization of magnetic susceptibility. *NeuroImage* 2013;**70**:1–9.

Cheret C, Willem M, Fricker FR *et al.* Bace1 and Neuregulin-1 cooperate to control formation and maintenance of muscle spindles. *The EMBO Journal* 2013;**32**:2015–28.

Chomiak T, Hu B. What Is the Optimal Value of the g-Ratio for Myelinated Fibers in the Rat CNS? A Theoretical Approach. *PLOS ONE* 2009;**4**:e7754.

Chorghay Z, Káradóttir RT, Ruthazer ES. White Matter Plasticity Keeps the Brain in Tune: Axons Conduct While Glia Wrap. *Front Cell Neurosci* 2018;**12**, DOI: 10.3389/fncel.2018.00428.

Chvátal A, Verkhratsky A. An Early History of Neuroglial Research: Personalities. *Neuroglia* 2018;**1**:245–57.

Clark AJ, Kaller MS, Galino J *et al.* Co-cultures with stem cell-derived human sensory neurons reveal regulators of peripheral myelination. *Brain* 2017;**140**:898–913.

Corti S, Faravelli I, Cardano M *et al.* Human pluripotent stem cells as tools for neurodegenerative and neurodevelopmental disease modeling and drug discovery. *Expert Opin Drug Discov* 2015;**10**:615–29.

Cox SR, Ritchie SJ, Tucker-Drob EM *et al.* Ageing and brain white matter structure in 3,513 UK Biobank participants. *Nature Communications* 2016;**7**:13629.

Czepiel M, Boddeke E, Copray S. Human oligodendrocytes in remyelination research. *Glia* 2015;**63**:513–30.

Czopka T. Insights into mechanisms of central nervous system myelination using zebrafish. *Glia* 2016;**64**:333–49.

Czopka T, ffrench-Constant C, Lyons DA. Individual Oligodendrocytes Have Only a Few Hours in which to Generate New Myelin Sheaths In Vivo. *Developmental Cell* 2013;**25**:599–609.

Dan Y, Poo M-M. Spike timing-dependent plasticity: from synapse to perception. *Physiol Rev* 2006;**86**:1033–48.

Darki F, Klingberg T. The Role of Fronto-Parietal and Fronto-Striatal Networks in the Development of Working Memory: A Longitudinal Study. *Cereb Cortex* 2015;**25**:1587–95.

Dawson MRL, Polito A, Levine JM *et al.* NG2-expressing glial progenitor cells: an abundant and widespread population of cycling cells in the adult rat CNS. *Mol Cell Neurosci* 2003;**24**:476–88.

De Bono JP, Adlam D, Paterson DJ *et al.* Novel quantitative phenotypes of exercise training in mouse models. *American Journal of Physiology-Regulatory, Integrative and Comparative Physiology* 2006;**290**:R926–34.

Deloire-Grassin MSA, Brochet B, Quesson B *et al.* In vivo evaluation of remyelination in rat brain by magnetization transfer imaging. *Journal of the Neurological Sciences* 2000;**178**:10–6.

Demerens C, Stankoff B, Logak M *et al.* Induction of myelination in the central nervous system by electrical activity. *PNAS* 1996;**93**:9887–92.

Deoni SCL, Mercure E, Blasi A *et al.* Mapping Infant Brain Myelination with Magnetic Resonance Imaging. *J Neurosci* 2011;**31**:784–91.

Devaux JJ, Odaka M, Yuki N. Nodal proteins are target antigens in Guillain-Barré syndrome. *J Peripher Nerv Syst* 2012;**17**:62–71.

Diedrichsen J, Kornysheva K. Motor skill learning between selection and execution. *Trends Cogn Sci* 2015;**19**:227–33.

Dimou L, Gallo V. NG2-glia and their functions in the central nervous system. *Glia* 2015;**63**:1429–51.

Dimou L, Simons M. Diversity of oligodendrocytes and their progenitors. *Current Opinion in Neurobiology* 2017;**47**:73–9.

Douaud G, Groves AR, Tamnes CK *et al.* A common brain network links development, aging, and vulnerability to disease. *PNAS* 2014;**111**:17648–53.

Douvaras P, Fossati V. Generation and isolation of oligodendrocyte progenitor cells from human pluripotent stem cells. *Nat Protocols* 2015;**10**:1143–54.

Dugas JC, Emery B. Purification of Oligodendrocyte Precursor Cells from Rat Cortices by Immunopanning. *Cold Spring Harb Protoc* 2013a;**2013**:pdb.prot070862.

Dugas JC, Emery B. Purification and Culture of Oligodendrocyte Lineage Cells. *Cold Spring Harb Protoc* 2013b;**2013**:pdb.top074898.

Dutta DJ, Woo DH, Lee PR *et al.* Regulation of myelin structure and conduction velocity by perinodal astrocytes. *Proc Natl Acad Sci USA* 2018;**115**:11832–7.

Ehninger D, Kempermann G. Regional Effects of Wheel Running and Environmental Enrichment on Cell Genesis and Microglia Proliferation in the Adult Murine Neocortex. *Cereb Cortex* 2003;**13**:845–51.

Emery B, Agalliu D, Cahoy JD *et al.* Myelin Gene Regulatory Factor Is a Critical Transcriptional Regulator Required for CNS Myelination. *Cell* 2009;**138**:172–85.

Etxeberria A, Hokanson KC, Dao DQ *et al.* Dynamic Modulation of Myelination in Response to Visual Stimuli Alters Optic Nerve Conduction Velocity. *J Neurosci* 2016;**36**:6937–48.

de Faria O, Gonsalvez DG, Nicholson M *et al.* Activity-dependent central nervous system myelination throughout life. *J Neurochem* 2019;**148**:447–61.

de Faria O, Pama EAC, Evans K *et al.* Neuroglial interactions underpinning myelin plasticity. *Devel Neurobio* 2018;**78**:93–107.

Fehmi J, Scherer SS, Willison HJ *et al.* Nodes, paranodes and neuropathies. *J Neurol Neurosurg Psychiatry* 2018;**89**:61–71.

Fields RD. White matter in learning, cognition and psychiatric disorders. *Trends in Neurosciences* 2008;**31**:361–70.

Fields RD. A new mechanism of nervous system plasticity: activity-dependent myelination. *Nat Rev Neurosci* 2015;**16**:756–67.

Fields RD, Dutta DJ. Treadmilling Model for Plasticity of the Myelin Sheath. *Trends Neurosci* 2019;**42**:443–7.

Fleck D, van Bebber F, Colombo A *et al.* Dual cleavage of neuregulin 1 type III by BACE1 and ADAM17 liberates its EGF-like domain and allows paracrine signaling. *J Neurosci* 2013;**33**:7856–69.

Flöel A, de Vries MH, Scholz J *et al.* White matter integrity in the vicinity of Broca's area predicts grammar learning success. *NeuroImage* 2009;**47**:1974–81.

Flores AI, Mallon BS, Matsui T *et al.* Akt-mediated survival of oligodendrocytes induced by neuregulins. *J Neurosci* 2000;**20**:7622–30.

Ford MC, Alexandrova O, Cossell L *et al.* Tuning of Ranvier node and internode properties in myelinated axons to adjust action potential timing. *Nat Commun* 2015;**6**, DOI: 10.1038/ncomms9073.

Freeman SA, Desmazières A, Simonnet J *et al.* Acceleration of conduction velocity linked to clustering of nodal components precedes myelination. *PNAS* 2015;**112**:E321–8.

Fricker FR, Antunes-Martins A, Galino J *et al.* Axonal neuregulin 1 is a rate limiting but not essential factor for nerve remyelination. *Brain* 2013;**136**:2279–97.

Friede RL. The Significance of Internode Length for Saltatory Conduction: Looking Back at the Age of 90. *J Neuropathol Exp Neurol* 2017;**76**:258–9.

Friede RL, Meier T, Diem M. How is the exact length of an internode determined. *J Neurol Sci* 1981;**50**:217–28.

Fünfschilling U, Supplie LM, Mahad D *et al.* Glycolytic oligodendrocytes maintain myelin and long-term axonal integrity. *Nature* 2012;**485**:517–21.

Galino J, Cervellini I, Zhu N *et al.* RalGTPases contribute to Schwann cell repair after nerve injury via regulation of process formation. *J Cell Biol* 2019;**218**:2370–87.

Gareau PJ, Rutt BK, Karlik SJ *et al.* Magnetization transfer and multicomponent T2 relaxation measurements with histopathologic correlation in an experimental model of MS. *Journal of Magnetic Resonance Imaging* 2000;**11**:586–95.

Garratt AN, Voiculescu O, Topilko P *et al.* A dual role of erbB2 in myelination and in expansion of the schwann cell precursor pool. *J Cell Biol* 2000;**148**:1035–46.

Gerber D, Ghidinelli M, Tinelli E *et al.* Schwann cells, but not Oligodendrocytes, Depend Strictly on Dynamin 2 Function. *eLife* 2019, DOI: 10.7554/eLife.42404.

Gibson EM, Purger D, Mount CW *et al.* Neuronal Activity Promotes Oligodendrogenesis and Adaptive Myelination in the Mammalian Brain. *Science* 2014;**344**:1252304.

Goebbels S, Oltrogge JH, Kemper R *et al.* Elevated phosphatidylinositol 3,4,5-trisphosphate in glia triggers cell-autonomous membrane wrapping and myelination. *J Neurosci* 2010;**30**:8953–64.

Grätsch S, Büschges A, Dubuc R. Descending control of locomotor circuits. *Current Opinion in Physiology* 2019;**8**:94–8.

Greenshields KN, Halstead SK, Zitman FMP *et al.* The neuropathic potential of anti-GM1 autoantibodies is regulated by the local glycolipid environment in mice. *J Clin Invest* 2009;**119**:595–610.

Groeschel S, Hagberg GE, Schultz T *et al.* Assessing White Matter Microstructure in Brain Regions with Different Myelin Architecture Using MRI. *PLoS One* 2016;**11**, DOI: 10.1371/journal.pone.0167274.

Häger C, Keubler LM, Talbot SR *et al.* Running in the wheel: Defining individual severity levels in mice. *PLOS Biology* 2018;**16**:e2006159.

Handel AE, Chintawar S, Lalic T *et al.* Assessing similarity to primary tissue and cortical layer identity in induced pluripotent stem cell-derived cortical neurons through single-cell transcriptomics. *Hum Mol Genet* 2016;**25**:989–1000.

Haney CA, Sahenk Z, Li C *et al.* Heterophilic binding of L1 on unmyelinated sensory axons mediates Schwann cell adhesion and is required for axonal survival. *J Cell Biol* 1999;**146**:1173–84.

Harboe M, Torvund-Jensen J, Kjaer-Sorensen K *et al.* Ephrin-A1-EphA4 signaling negatively regulates myelination in the central nervous system. *Glia* 2018;**66**:934–50.

Harris JJ, Attwell D. The energetics of central nervous system white matter. *J Neurosci* 2012;**32**:356–71.

Hartfield EM, Yamasaki-Mann M, Ribeiro Fernandes HJ *et al.* Physiological characterisation of human iPS-derived dopaminergic neurons. *PLoS ONE* 2014;**9**:e87388.

Hayashi S, McMahon AP. Efficient recombination in diverse tissues by a tamoxifen-inducible form of Cre: a tool for temporally regulated gene activation/inactivation in the mouse. *Dev Biol* 2002;**244**:305–18.

Heath F, Hurley SA, Johansen-Berg H *et al.* Advances in noninvasive myelin imaging. *Devel Neurobio* 2018;**78**:136–51.

Herbert AL, Monk KR. Advances in myelinating glial cell development. *Current Opinion in Neurobiology* 2017;**42**:53–60.

Hibbits N, Pannu R, John Wu T *et al.* Cuprizone demyelination of the corpus callosum in mice correlates with altered social interaction and impaired bilateral sensorimotor coordination. *ASN Neuro* 2009;**1**, DOI: 10.1042/AN20090032.

Hildebrand C, Remahl S, Persson H *et al.* Myelinated nerve fibres in the CNS. *Prog Neurobiol* 1993;**40**:319–84.

Hill RA, Li AM, Grutzendler J. Lifelong cortical myelin plasticity and age-related degeneration in the live mammalian brain. *Nature Neuroscience* 2018:1.

Hines JH, Ravanelli AM, Schwindt R *et al.* Neuronal activity biases axon selection for myelination in vivo. *Nat Neurosci* 2015;**18**:683–9.

Hitoshi S, Kusunoki S, Murayama S *et al.* Rabbit experimental sensory ataxic neuropathy: anti-GD1b antibody-mediated trkC downregulation of dorsal root ganglia neurons. *Neurosci Lett* 1999;**260**:157–60.

Hockemeyer D, Jaenisch R. Induced Pluripotent Stem Cells Meet Genome Editing. *Cell Stem Cell* 2016;**18**:573–86.

Hofstetter S, Tavor I, Moryosef ST *et al.* Short-Term Learning Induces White Matter Plasticity in the Fornix. *J Neurosci* 2013;**33**:12844–50.

de Hoz L, Simons M. The emerging functions of oligodendrocytes in regulating neuronal network behaviour. *BioEssays* 2015;**37**:60–9.

Hu X, Hicks CW, He W *et al.* Bace1 modulates myelination in the central and peripheral nervous system. *Nat Neurosci* 2006;**9**:1520–5.

Hughes EG, Kang SH, Fukaya M *et al.* Oligodendrocyte progenitors balance growth with self-repulsion to achieve homeostasis in the adult brain. *Nature Neuroscience* 2013a;**16**:nn.3390.

Hughes EG, Orthmann-Murphy JL, Langseth AJ *et al.* Myelin remodeling through experience-dependent oligodendrogenesis in the adult somatosensory cortex. *Nature Neuroscience* 2018:1.

Huxley AF, Stampfli R. Evidence for saltatory conduction in peripheral myelinated nerve fibres. *J Physiol (Lond)* 1949;**108**:315–39.

Iwakura Y, Wang R, Inamura N *et al.* Glutamate-dependent ectodomain shedding of neuregulin-1 type II precursors in rat forebrain neurons. *PLOS ONE* 2017;**12**:e0174780.

Jeffries MA, Urbanek K, Torres L *et al.* ERK1/2 Activation in Preexisting Oligodendrocytes of Adult Mice Drives New Myelin Synthesis and Enhanced CNS Function. *J Neurosci* 2016;**36**:9186–200.

Jessen KR, Mirsky R. The repair Schwann cell and its function in regenerating nerves. *J Physiol (Lond)* 2016;**594**:3521–31.

Jessen KR, Mirsky R. Schwann Cell Precursors; Multipotent Glial Cells in Embryonic Nerves. *Front Mol Neurosci* 2019;**12**:69.

Jessen KR, Mirsky R, Lloyd AC. Schwann Cells: Development and Role in Nerve Repair. *Cold Spring Harb Perspect Biol* 2015;**7**:a020487.

Jha MK, Morrison BM. Glia-neuron energy metabolism in health and diseases: New insights into the role of nervous system metabolic transporters. *Exp Neurol* 2018;**309**:23–31.

Kamil K, Yazid MD, Idrus RBH *et al.* Peripheral Demyelinating Diseases: From Biology to Translational Medicine. *Front Neurol* 2019;**10**:87.

Karl T, Duffy L, Scimone A *et al.* Altered motor activity, exploration and anxiety in heterozygous neuregulin 1 mutant mice: implications for understanding schizophrenia. *Genes, Brain and Behavior* 2007;**6**:677–87.

Kasthuri N, Hayworth KJ, Berger DR *et al.* Saturated Reconstruction of a Volume of Neocortex. *Cell* 2015;**162**:648–61.

Kataria H, Alizadeh A, Karimi-Abdolrezaee S. Neuregulin-1/ErbB network: An emerging modulator of nervous system injury and repair. *Progress in Neurobiology* 2019:101643.

Kaushik G, Ponnusamy MP, Batra SK. Concise Review: Current Status of Three-Dimensional Organoids as Preclinical Models. *Stem Cells* 2018;**36**:1329–40.

Keiner S, Niv F, Neumann S *et al.* Effect of skilled reaching training and enriched environment on generation of oligodendrocytes in the adult sensorimotor cortex and corpus callosum. *BMC Neuroscience* 2017;**18**:31.

Kessaris N, Fogarty M, Iannarelli P *et al.* Competing waves of oligodendrocytes in the forebrain and postnatal elimination of an embryonic lineage. *Nat Neurosci* 2006;**9**:173–9.

Keswani SC, Buldanlioglu U, Fischer A *et al.* A novel endogenous erythropoietin mediated pathway prevents axonal degeneration. *Ann Neurol* 2004;**56**:815–26.

Kinney HC, Brody BA, Kloman AS *et al.* Sequence of Central Nervous System Myelination in Human InfancyII. Patterns of Myelination in Autopsied Infants. *J Neuropathol Exp Neurol* 1988;**47**:217–34.

Kıray H, Lindsay SL, Hosseinzadeh S *et al.* The multifaceted role of astrocytes in regulating myelination. *Exp Neurol* 2016;**283**:541–9.

Knowles L. The Evolution of Myelin: Theories and Application to Human Disease. *Journal of Evolutionary Medicine* 2017;**5**:1–23.

Koenning M, Jackson S, Hay CM *et al.* Myelin Gene Regulatory Factor Is Required for Maintenance of Myelin and Mature Oligodendrocyte Identity in the Adult CNS. *J Neurosci* 2012;**32**:12528–42.

Konhilas JP, Maass AH, Luckey SW *et al.* Sex modifies exercise and cardiac adaptation in mice. *Am J Physiol Heart Circ Physiol* 2004;**287**:H2768-2776.

Koudelka S, Voas MG, Almeida RG *et al.* Individual Neuronal Subtypes Exhibit Diversity in CNS Myelination Mediated by Synaptic Vesicle Release. *Current Biology* 2016;**26**:1447–55.

Kodama L, Gan L. Do Microglial Sex Differences Contribute to Sex Differences in Neurodegenerative Diseases? *Trends in Molecular Medicine* 2019;**25**:741–9.

Kreutz MR, Sala C. *Synaptic Plasticity: Dynamics, Development and Disease*. Springer Science & Business Media, 2012.

Krityakiarana W, Espinosa-Jeffrey A, Ghiani CA *et al.* VOLUNTARY EXERCISE INCREASES OLIGODENDROGENESIS IN SPINAL CORD. *Int J Neurosci* 2010;**120**:280–90.

Kucharczyk W, Macdonald PM, Stanisz GJ *et al.* Relaxivity and magnetization transfer of white matter lipids at MR imaging: importance of cerebrosides and pH. *Radiology* 1994;**192**:521–9.

Kusunoki S, Shimizu J, Chiba A *et al.* Experimental sensory neuropathy induced by sensitization with ganglioside GD1b. *Ann Neurol* 1996;**39**:424–31.

Lakhani B, Borich MR, Jackson JN *et al.* Motor Skill Acquisition Promotes Human Brain Myelin Plasticity. *Neural Plasticity* 2016;**2016**:e7526135.

Lee S, Leach MK, Redmond SA *et al.* A culture system to study oligodendrocyte myelination-processes using engineered nanofibers. *Nat Methods* 2012;**9**:917–22.

Lerman I, Harrison BC, Freeman K *et al.* Genetic variability in forced and voluntary endurance exercise performance in seven inbred mouse strains. *J Appl Physiol* 2002;**92**:2245–55.

Liebetanz D, Baier PC, Paulus W *et al.* A highly sensitive automated complex running wheel test to detect latent motor deficits in the mouse MPTP model of Parkinson's disease. *Exp Neurol* 2007;**205**:207–13.

Liebetanz D, Merkler D. Effects of commissural de- and remyelination on motor skill behaviour in the cuprizone mouse model of multiple sclerosis. *Exp Neurol* 2006;**202**:217–24.

Lightfoot JT, Turner MJ, Daves M *et al.* Genetic influence on daily wheel running activity level. *Physiol Genomics* 2004;**19**:270–6.

Liston C, Malter Cohen M, Teslovich T *et al.* Atypical prefrontal connectivity in attention-deficit/hyperactivity disorder: pathway to disease or pathological end point? *Biol Psychiatry* 2011;**69**:1168–77.

Liu J, Dietz K, DeLoyht JM *et al.* Impaired adult myelination in the prefrontal cortex of socially isolated mice. *Nat Neurosci* 2012a;**15**:1621–3.

Liu Q, Spusta SC, Mi R *et al.* Human Neural Crest Stem Cells Derived from Human ESCs and Induced Pluripotent Stem Cells: Induction, Maintenance, and Differentiation into Functional Schwann Cells. *Stem Cells Trans Med* 2012b;**1**:266–78.

Lundgaard I, Luzhynskaya A, Stockley JH *et al.* Neuregulin and BDNF Induce a Switch to NMDA Receptor-Dependent Myelination by Oligodendrocytes. *PLOS Biol* 2013;**11**:e1001743.

Ma M-S, Boddeke E, Copray S. Pluripotent Stem Cells for Schwann Cell Engineering. *Stem Cell Rev and Rep* 2014;**11**:205–18.

Mabbott DJ, Noseworthy M, Bouffet E *et al.* White matter growth as a mechanism of cognitive development in children. *NeuroImage* 2006;**33**:936–46.

Makino H, Hwang EJ, Hedrick NG *et al.* Circuit Mechanisms of Sensorimotor Learning. *Neuron* 2016;**92**:705–21.

Makinodan M, Rosen KM, Ito S *et al.* A Critical Period for Social Experience–Dependent Oligodendrocyte Maturation and Myelination. *Science* 2012;**337**:1357–60.

Manzanares G, Brito-da-Silva G, Gandra PG *et al.* Voluntary wheel running: patterns and physiological effects in mice. *Brazilian Journal of Medical and Biological Research* 2019;**52**, DOI: 10.1590/1414-431x20187830.

Marner L, Nyengaard JR, Tang Y *et al.* Marked loss of myelinated nerve fibers in the human brain with age. *J Comp Neurol* 2003;**462**:144–52.

Marques S, Zeisel A, Codeluppi S *et al.* Oligodendrocyte heterogeneity in the mouse juvenile and adult central nervous system. *Science* 2016;**352**:1326–9.

Marton RM, Miura Y, Sloan SA *et al.* Differentiation and maturation of oligodendrocytes in human three-dimensional neural cultures. *Nat Neurosci* 2019, DOI: 10.1038/s41593-018-0316-9.

Martyn CN, Hughes RA. Epidemiology of peripheral neuropathy. *J Neurol Neurosurg Psychiatry* 1997;**62**:310–8.

Meijer JH, Robbers Y. Wheel running in the wild. *Proceedings of the Royal Society B: Biological Sciences* 2014;**281**:20140210.

McDermott LA, Weir GA, Themistocleous AC *et al.* Defining the Functional Role of NaV1.7 in Human Nociception. *Neuron* 2019;**101**:905-919.e8.

McGonigal R, Rowan EG, Greenshields KN *et al.* Anti-GD1a antibodies activate complement and calpain to injure distal motor nodes of Ranvier in mice. *Brain* 2010;**133**:1944–60.

McKenzie IA, Ohayon D, Li H *et al.* Motor skill learning requires active central myelination. *Science* 2014;**346**:318–22.

Mei L, Nave K-A. Neuregulin-ERBB Signaling in the Nervous System and Neuropsychiatric Diseases. *Neuron* 2014;**83**:27–49.

Mensch S, Baraban M, Almeida R *et al.* Synaptic vesicle release regulates myelin sheath number of individual oligodendrocytes in vivo. *Nat Neurosci* 2015;**18**:628–30.

Merritt J, Rhodes JS. Mouse genetic differences in voluntary wheel running, adult hippocampal neurogenesis and learning on the multi-strain-adapted plus water maze. *Behav Brain Res* 2015;**280**:62–71.

Mertens J, Marchetto MC, Bardy C *et al.* Evaluating cell reprogramming, differentiation and conversion technologies in neuroscience. *Nat Rev Neurosci* 2016;**17**:424–37.

Meyer D, Birchmeier C. Multiple essential functions of neuregulin in development. *Nature* 1995;**378**:386–90.

Michailov GV, Sereda MW, Brinkmann BG *et al.* Axonal neuregulin-1 regulates myelin sheath thickness. *Science* 2004;**304**:700–3.

Michalski J-P, Kothary R. Oligodendrocytes in a nutshell. *Front Cell Neurosci* 2015:340.

Min R, Knaap MS van der. Genetic defects disrupting glial ion and water homeostasis in the brain. *Brain Pathology* 2018;**28**:372–87.

Mitew S, Gobius I, Fenlon LR *et al.* Pharmacogenetic stimulation of neuronal activity increases myelination in an axon-specific manner. *Nature Communications* 2018;**9**:306.

Miyazaki T, Kusunoki S, Kaida K *et al.* Guillain–Barré syndrome associated with IgG monospecific to ganglioside GD1b. *Neurology* 2001;**56**:1227–9.

Monk KR, Feltri ML, Taveggia C. New insights on schwann cell development. *Glia* 2015:n/a-n/a.

Montag D, Giese KP, Bartsch U *et al.* Mice deficient for the glycoprotein show subtle abnormalities in myelin. *Neuron* 1994;**13**:229–46.

Morawski M, Kirilina E, Scherf N *et al.* Developing 3D microscopy with CLARITY on human brain tissue: Towards a tool for informing and validating MRI-based histology. *NeuroImage* 2018;**182**:417–28.

Morrissey TK, Bunge RP, Kleitman N. Human schwann cells in vitro. I. Failure to differentiate and support neuronal health under co-culture conditions that promote full function of rodent cells. *J Neurobiol* 1995;**28**:171–89.

Mount CW, Monje M. Wrapped to Adapt: Experience-Dependent Myelination. *Neuron* 2017;**95**:743–56.

Nagy Z, Westerberg H, Klingberg T. Maturation of White Matter is Associated with the Development of Cognitive Functions during Childhood. *Journal of Cognitive Neuroscience* 2004;**16**:1227–33.

Nave K-A. Myelination and support of axonal integrity by glia. *Nature* 2010a;**468**:244–52.

Nave K-A. Myelination and the trophic support of long axons. *Nature Reviews Neuroscience* 2010b;**11**:275–83.

Nave K-A, Werner HB. Myelination of the Nervous System: Mechanisms and Functions. *Annual Review of Cell and Developmental Biology* 2014;**30**:503–33.

Nishimura K, Sano M, Ohtaka M *et al.* Development of defective and persistent Sendai virus vector: a unique gene delivery/expression system ideal for cell reprogramming. *J Biol Chem* 2011;**286**:4760–71.

Nishimura T, Kaneko S, Kawana-Tachikawa A *et al.* Generation of Rejuvenated Antigen-Specific T Cells by Reprogramming to Pluripotency and Redifferentiation. *Cell Stem Cell* 2013;**12**:114–26.

Novak CM, Burghardt PR, Levine JA. The use of a running wheel to measure activity in rodents: Relationship to energy balance, general activity, and reward. *Neurosci Biobehav Rev* 2012;**36**:1001–14.

O'Hanlon GM, Plomp JJ, Chakrabarti M *et al.* Anti-GQ1b ganglioside antibodies mediate complement-dependent destruction of the motor nerve terminal. *Brain* 2001;**124**:893–906.

Owens GC, Boyd CJ, Bunge RP *et al.* Expression of recombinant myelin-associated glycoprotein in primary Schwann cells promotes the initial investment of axons by myelinating Schwann cells. *The Journal of Cell Biology* 1990;**111**:1171–82.

Owens GC, Bunge RP. Schwann cells infected with a recombinant retrovirus expressing myelin-associated glycoprotein antisense RNA do not form myelin. *Neuron* 1991;**7**:565–75.

Ozaki M, Itoh K, Miyakawa Y *et al.* Protein processing and releases of neuregulin-1 are regulated in an activity-dependent manner. *J Neurochem* 2004;**91**:176–88.

Pajevic S, Basser PJ, Fields RD. Role of myelin plasticity in oscillations and synchrony of neuronal activity. *Neuroscience* 2014;**276**:135–47.

Pan S, Chan JR. Regulation and dysregulation of axon infrastructure by myelinating glia. *J Cell Biol* 2017;**216**:3903–16.

Pang Y, Zheng B, Kimberly SL *et al.* Neuron-oligodendrocyte myelination co-culture derived from embryonic rat spinal cord and cerebral cortex. *Brain and Behavior* 2012;**2**:53–67.

Parkinson DB, Bhaskaran A, Arthur-Farraj P *et al.* c-Jun is a negative regulator of myelination. *J Cell Biol* 2008;**181**:625–37.

Paus T, Collins DL, Evans AC *et al.* Maturation of white matter in the human brain: a review of magnetic resonance studies. *Brain Res Bull* 2001;**54**:255–66.

Peters A. The effects of normal aging on myelin and nerve fibers: A review. *J Neurocytol* 2002;**31**:581–93.

Peters BD, Ikuta T, DeRosse P *et al.* Age-Related Differences in White Matter Tract Microstructure Are Associated with Cognitive Performance from Childhood to Adulthood. *Biological Psychiatry* 2014;**75**:248–56.

Petiet A, Adanyeguh I, Aigrot M-S *et al.* Ultrahigh field imaging of myelin disease models: Toward specific markers of myelin integrity? *J Comp Neurol* 2018, DOI: 10.1002/cne.24598.

Purger D, Gibson EM, Monje M. Myelin plasticity in the central nervous system. *Neuropharmacology* 2016;**110, Part B**:563–73.

Qiu A, Mori S, Miller MI. Diffusion Tensor Imaging for Understanding Brain Development in Early Life. *Annu Rev Psychol* 2015;**66**:853–76.

Querol L, Nogales-Gadea G, Rojas-Garcia R *et al.* Antibodies to contactin-1 in chronic inflammatory demyelinating polyneuropathy. *Ann Neurol* 2013;**73**:370–80.

Rasband MN, Peles E. The Nodes of Ranvier: Molecular Assembly and Maintenance. *Cold Spring Harb Perspect Biol* 2016;**8**:a020495.

Richardson WD, Kessaris N, Pringle N. Oligodendrocyte wars. *Nature Reviews Neuroscience* 2006;**7**:11.

Richardson WD, Pringle N, Mosley MJ *et al.* A role for platelet-derived growth factor in normal gliogenesis in the central nervous system. *Cell* 1988;**53**:309–19.

Riethmacher D, Sonnenberg-Riethmacher E, Brinkmann V *et al.* Severe neuropathies in mice with targeted mutations in the ErbB3 receptor. *Nature* 1997;**389**:725–30.

Rinaldi S, Brennan KM, Kalna G *et al.* Antibodies to Heteromeric Glycolipid Complexes in Guillain-Barré Syndrome. *PLoS One* 2013;**8**, DOI: 10.1371/journal.pone.0082337.

Ritchie Joseph Murdoch. On the relation between fibre diameter and conduction velocity in myelinated nerve fibres. *Proceedings of the Royal Society of London Series B Biological Sciences* 1982;**217**:29–35.

Rivers LE, Young KM, Rizzi M *et al.* PDGFRA/NG2 glia generate myelinating oligodendrocytes and piriform projection neurons in adult mice. *Nat Neurosci* 2008;**11**:1392–401.

Rookmaaker MB, Schutgens F, Verhaar MC *et al.* Development and application of human adult stem or progenitor cell organoids. *Nat Rev Nephrol* 2015;**11**:546–54.

Roy K, Murtie JC, El-Khodor BF *et al.* Loss of erbB signaling in oligodendrocytes alters myelin and dopaminergic function, a potential mechanism for neuropsychiatric disorders. *PNAS* 2007;**104**:8131–6.

Rozés Salvador V, Heredia F, Berardo A *et al.* Anti-glycan antibodies halt axon regeneration in a model of Guillain Barrè Syndrome axonal neuropathy by inducing microtubule disorganization via RhoA–ROCK-dependent inactivation of CRMP-2. *Experimental Neurology* 2016;**278**:42–53.

Rushton WAH. A theory of the effects of fibre size in medullated nerve. *J Physiol* 1951;**115**:101–22.

Saab AS, Nave K-A. Myelin dynamics: protecting and shaping neuronal functions. *Current Opinion in Neurobiology* 2017;**47**:104–12.

Saporta MA, Shy ME. A human cellular model to study peripheral myelination and demyelinating neuropathies. *Brain* 2017;**140**:856–9.

Salzer JL. Schwann Cell Myelination. *Cold Spring Harb Perspect Biol* 2015:a020529.

Salzer JL, Williams AK, Glaser L *et al.* Studies of Schwann cell proliferation. II. Characterization of the stimulation and specificity of the response to a neurite membrane fraction. *J Cell Biol* 1980;**84**:753–66.

Salzer JL, Zalc B. Myelination. *Current Biology* 2016;**26**:R971–5.

Sampaio-Baptista C, Johansen-Berg H. White Matter Plasticity in the Adult Brain. *Neuron* 2017;**96**:1239–51.

Sampaio-Baptista C, Khrapitchev AA, Foxley S *et al.* Motor Skill Learning Induces Changes in White Matter Microstructure and Myelination. *J Neurosci* 2013;**33**:19499–503.

Sandoe J, Eggan K. Opportunities and challenges of pluripotent stem cell neurodegenerative disease models. *Nature Neuroscience* 2013;**16**:780–9.

Schalomon PM, Wahlsten D. Wheel running behavior is impaired by both surgical section and genetic absence of the mouse corpus callosum. *Brain Research Bulletin* 2002a;**57**:27–33.

Schneider S, Götz K, Birchmeier C *et al.* Neuregulin-1 mutant mice indicate motor and sensory deficits, indeed few references for schizophrenia endophenotype model. *Behavioural Brain Research* 2017;**322**:177–85.

Schneider S, Gruart A, Grade S *et al.* Decrease in newly generated oligodendrocytes leads to motor dysfunctions and changed myelin structures that can be rescued by transplanted cells. *Glia* 2016;**64**:2201–18.

Scholz J, Klein MC, Behrens TEJ *et al.* Training induces changes in white matter architecture. *Nat Neurosci* 2009;**12**:1370–1.

Seidl AH. Regulation of Conduction Time along Axons. *Neuroscience* 2014;**0**:126–34.

Sevc J, Matiašová A, Kútna V *et al.* Evidence that the central canal lining of the spinal cord contributes to oligodendrogenesis during postnatal development and adulthood in intact rats. *J Comp Neurol* 2014;**522**:3194–207.

Sheikh KA, Sun J, Liu Y *et al.* Mice lacking complex gangliosides develop Wallerian degeneration and myelination defects. *Proc Natl Acad Sci U S A* 1999;**96**:7532–7.

Shi Y, Kirwan P, Livesey FJ. Directed differentiation of human pluripotent stem cells to cerebral cortex neurons and neural networks. *Nature Protocols* 2012;**7**:1836–46.

Sim FJ, Windrem MS, Goldman SA. Fate determination of adult human glial progenitor cells. *Neuron Glia Biology* 2009;**5**:45–55.

Simmonds DJ, Hallquist MN, Asato M *et al.* Developmental stages and sex differences of white matter and behavioral development through adolescence: A longitudinal diffusion tensor imaging (DTI) study. *NeuroImage* 2014;**92**:356–68.

Simon C, Götz M, Dimou L. Progenitors in the adult cerebral cortex: Cell cycle properties and regulation by physiological stimuli and injury. *Glia* 2011;**59**:869–81.

Simon CM, Jablonka S, Ruiz R *et al.* Ciliary neurotrophic factor-induced sprouting preserves motor function in a mouse model of mild spinal muscular atrophy. *Hum Mol Genet* 2010;**19**:973–86.

Simons M, Nave K-A. Oligodendrocytes: Myelination and Axonal Support. *Cold Spring Harb Perspect Biol* 2016;**8**:a020479.

Simanaviciute U, Ahmed J, Brown RE *et al.* Recommendations for measuring whisker movements and locomotion in mice with sensory, motor and cognitive deficits. *Journal of Neuroscience Methods* 2020;**331**:108532.

Sinclair JL, Fischl MJ, Alexandrova O *et al.* Sound-Evoked Activity Influences Myelination of Brainstem Axons in the Trapezoid Body. *J Neurosci* 2017;**37**:8239–55.

Snaidero N, Möbius W, Czopka T *et al.* Myelin Membrane Wrapping of CNS Axons by PI(3,4,5)P3-Dependent Polarized Growth at the Inner Tongue. *Cell* 2014;**156**:277–90.

Snaidero N, Simons M. Myelination at a glance. *J Cell Sci* 2014;**127**:2999–3004.

Sock E, Wegner M. Transcriptional control of myelination and remyelination. *Glia* 2019, DOI: 10.1002/glia.23636.

Soldner F, Jaenisch R. iPSC Disease Modeling. *Science* 2012;**338**:1155–6.

Spitzer SO, Sitnikov S, Kamen Y *et al.* Oligodendrocyte Progenitor Cells Become Regionally Diverse and Heterogeneous with Age. *Neuron* 2019;**101**:459-471.e5.

Srinivas S, Watanabe T, Lin C-S *et al.* Cre reporter strains produced by targeted insertion of EYFP and ECFP into the ROSA26 locus. *BMC Dev Biol* 2001;**1**:4.

Stassart RM, Möbius W, Nave K-A *et al.* The Axon-Myelin Unit in Development and Degenerative Disease. *Front Neurosci* 2018;**12**:467.

Sterneckert JL, Reinhardt P, Schöler HR. Investigating human disease using stem cell models. *Nat Rev Genet* 2014;**15**:625–39.

Stevens B, Tanner S, Fields RD. Control of Myelination by Specific Patterns of Neural Impulses. *J Neurosci* 1998;**18**:9303–11.

Stierli S, Imperatore V, Lloyd AC. Schwann cell plasticity-roles in tissue homeostasis, regeneration, and disease. *Glia* 2019, DOI: 10.1002/glia.23643.

Stierli S, Napoli I, White IJ *et al.* The regulation of the homeostasis and regeneration of peripheral nerve is distinct from the CNS and independent of a stem cell population. *Development* 2018;**145**, DOI: 10.1242/dev.170316.

Stockley JH, Evans K, Matthey M *et al.* Surpassing light-induced cell damage in vitro with novel cell culture media. *Scientific Reports* 2017;**7**:849.

Stüber C, Morawski M, Schäfer A *et al.* Myelin and iron concentration in the human brain: A quantitative study of MRI contrast. *NeuroImage* 2014;**93**:95–106.

Takahashi K, Yamanaka S. Induction of Pluripotent Stem Cells from Mouse Embryonic and Adult Fibroblast Cultures by Defined Factors. *Cell* 2006;**126**:663–76.

Takeuchi H, Sekiguchi A, Taki Y *et al.* Training of Working Memory Impacts Structural Connectivity. *J Neurosci* 2010;**30**:3297–303.

Tarantino LM, Gould TJ, Druhan JP *et al.* Behavior and mutagenesis screens: the importance of baseline analysis of inbred strains. *Mamm Genome* 2000;**11**:555–64.

Tasaki I. Conduction of Impulses in the Myelinated Nerve Fiber. *Cold Spring Harb Symp Quant Biol* 1952;**17**:37–41.

Taubert M, Draganski B, Anwander A *et al.* Dynamic Properties of Human Brain Structure: Learning-Related Changes in Cortical Areas and Associated Fiber Connections. *J Neurosci* 2010;**30**:11670–7.

Taveggia C. Schwann cells-axon interaction in myelination. *Curr Opin Neurobiol* 2016;**39**:24–9.

Taveggia C, Feltri ML, Wrabetz L. Signals to promote myelin formation and repair. *Nat Rev Neurol* 2010;**6**:276–87.

Taveggia C, Thaker P, Petrylak A *et al.* Type III neuregulin-1 promotes oligodendrocyte myelination. *Glia* 2008;**56**:284–93.

Taveggia C, Zanazzi G, Petrylak A *et al.* Neuregulin-1 type III determines the ensheathment fate of axons. *Neuron* 2005;**47**:681–94.

Tomassy GS, Berger DR, Chen H-H *et al.* Distinct Profiles of Myelin Distribution Along Single Axons of Pyramidal Neurons in the Neocortex. *Science* 2014;**344**:319–24.

Tomassy GS, Dershowitz LB, Arlotta P. Diversity Matters: A Revised Guide to Myelination. *Trends in Cell Biology* 2016;**26**:135–47.

Tomlinson L, Leiton CV, Colognato H. Behavioral experiences as drivers of oligodendrocyte lineage dynamics and myelin plasticity. *Neuropharmacology* 2016;**110**:548–62.

Tripathi RB, Jackiewicz M, McKenzie IA *et al.* Remarkable Stability of Myelinating Oligodendrocytes in Mice. *Cell Reports* 2017;**21**:316–23.

Turrigiano G. Too many cooks? Intrinsic and synaptic homeostatic mechanisms in cortical circuit refinement. *Annu Rev Neurosci* 2011;**34**:89–103.

Vartanian T, Goodearl A, Viehöver A *et al.* Axonal Neuregulin Signals Cells of the Oligodendrocyte Lineage through Activation of HER4 and Schwann Cells through HER2 and HER3. *J Cell Biol* 1997;**137**:211–20.

Vassar R. Bace 1. *J Mol Neurosci* 2004;**23**:105–13.

Vassar R. BACE1 inhibitor drugs in clinical trials for Alzheimer's disease. *Alzheimers Res Ther* 2014;**6**, DOI: 10.1186/s13195-014-0089-7.

Verkhratsky A, Butt AM. The History of the Decline and Fall of the Glial Numbers Legend. *Neuroglia* 2018;**1**:188–92.

Villa A, Gelosa P, Castiglioni L *et al.* Sex-Specific Features of Microglia from Adult Mice. *Cell Rep* 2018;**23**:3501–11.

Visser L de, Bos R van den, Spruijt BM. Automated home cage observations as a tool to measure the effects of wheel running on cage floor locomotion. *Behavioural Brain Research* 2005;**160**:382–8.

Wake H, Lee PR, Fields RD. Control of Local Protein Synthesis and Initial Events in Myelination by Action Potentials. *Science* 2011;**333**:1647–51.

Walhovd KB, Johansen-Berg H, Káradóttir RT. Unraveling the secrets of white matter – Bridging the gap between cellular, animal and human imaging studies. *Neuroscience* 2014;**276**:2–13.

Wang JY, Miller SJ, Falls DL. The N-terminal region of neuregulin isoforms determines the accumulation of cell surface and released neuregulin ectodomain. *J Biol Chem* 2001;**276**:2841–51.

Wang S, Bates J, Li X *et al.* Human iPSC-derived oligodendrocyte progenitor cells can myelinate and rescue a mouse model of congenital hypomyelination. *Cell Stem Cell* 2013;**12**:252–64.

Wang Z, Colognato H, ffrench-Constant C. Contrasting effects of mitogenic growth factors on myelination in neuron–oligodendrocyte co-cultures. *Glia* 2007;**55**:537–45.

Watkins TA, Emery B, Mulinyawe S *et al.* Distinct stages of myelination regulated by gamma-secretase and astrocytes in a rapidly myelinating CNS coculture system. *Neuron* 2008;**60**:555–69.

Waxman SG. Electron-microscopic observations on preterminal fibers in the oculomotor nucleus of the cat. With special reference to the relation between axon diameter and myelin thickness in mammalian gray matter. *J Neurol Sci* 1975;**26**:395–400.

Wicklein EM, Pfeiffer G, Yuki N *et al.* Prominent sensory ataxia in Guillain-Barré syndrome associated with IgG anti-GD1b antibody. *J Neurol Sci* 1997;**151**:227–9.

Willem M, Garratt AN, Novak B *et al.* Control of peripheral nerve myelination by the beta-secretase BACE1. *Science* 2006;**314**:664–6.

Williamson JM, Lyons DA. Myelin Dynamics Throughout Life: An Ever-Changing Landscape? *Front Cell Neurosci* 2018;**12**, DOI: 10.3389/fncel.2018.00424.

Willison HJ, O'Hanlon GM, Paterson G *et al.* A somatically mutated human antiganglioside IgM antibody that induces experimental neuropathy in mice is encoded by the variable region heavy chain gene, V1-18. *J Clin Invest* 1996;**97**:1155–64.

Willison HJ, O'Leary CP, Veitch J *et al.* The clinical and laboratory features of chronic sensory ataxic neuropathy with anti-disialosyl IgM antibodies. *Brain* 2001;**124**:1968–77.

Willison HJ, Yuki N. Peripheral neuropathies and anti-glycolipid antibodies. *Brain* 2002;**125**:2591–625.

Wolff BS, Raheem SA, Saligan LN. Comparing passive measures of fatigue-like behavior in mice. *Scientific Reports* 2018;**8**:14238.

Wolpert DM, Diedrichsen J, Flanagan JR. Principles of sensorimotor learning. *Nat Rev Neurosci* 2011;**12**:739–51.

Wood PM, Bunge RP. Evidence that sensory axons are mitogenic for Schwann cells. *Nature* 1975;**256**:662–4.

Wu Yi-Ying, Chiu Feng-Lan, Yeh Chan-Shien *et al.* Opportunities and challenges for the use of induced pluripotent stem cells in modelling neurodegenerative disease. *Open Biology* **9**:180177.

Xiao L, Ohayon D, McKenzie IA *et al.* Rapid production of new oligodendrocytes is required in the earliest stages of motor-skill learning. *Nat Neurosci* 2016a;**19**:1210–7.

Xu K, Terakawa S. Three Mechanisms or Strategies for Increasing Conduction Velocity of Nerve Fibers. In: Xu K, Terakawa S (eds.). *Myelinated Fibers and Saltatory Conduction in the Shrimp: The Fastest Impulse Conduction in the Animal Kingdom*. Tokyo: Springer Japan, 2013, 83–90.

Yan Y, Shin S, Jha BS *et al.* Efficient and rapid derivation of primitive neural stem cells and generation of brain subtype neurons from human pluripotent stem cells. *Stem Cells Transl Med* 2013;**2**:862–70.

Yang LJ, Zeller CB, Shaper NL *et al.* Gangliosides are neuronal ligands for myelin-associated glycoprotein. *Proc Natl Acad Sci USA* 1996;**93**:814–8.

Yasumoto Y, Nakao R, Oishi K. Free Access to a Running-Wheel Advances the Phase of Behavioral and Physiological Circadian Rhythms and Peripheral Molecular Clocks in Mice. *PLOS ONE* 2015;**10**:e0116476.

Yeung MSY, Zdunek S, Bergmann O *et al.* Dynamics of Oligodendrocyte Generation and Myelination in the Human Brain. *Cell* 2014;**159**:766–74.

Young GT, Gutteridge A, Fox HD *et al.* Characterizing Human Stem Cell–derived Sensory Neurons at the Single-cell Level Reveals Their Ion Channel Expression and Utility in Pain Research. *Mol Ther* 2014;**22**:1530–43.

Young KM, Psachoulia K, Tripathi RB *et al.* Oligodendrocyte Dynamics in the Healthy Adult CNS: Evidence for Myelin Remodeling. *Neuron* 2013;**77**:873–85.

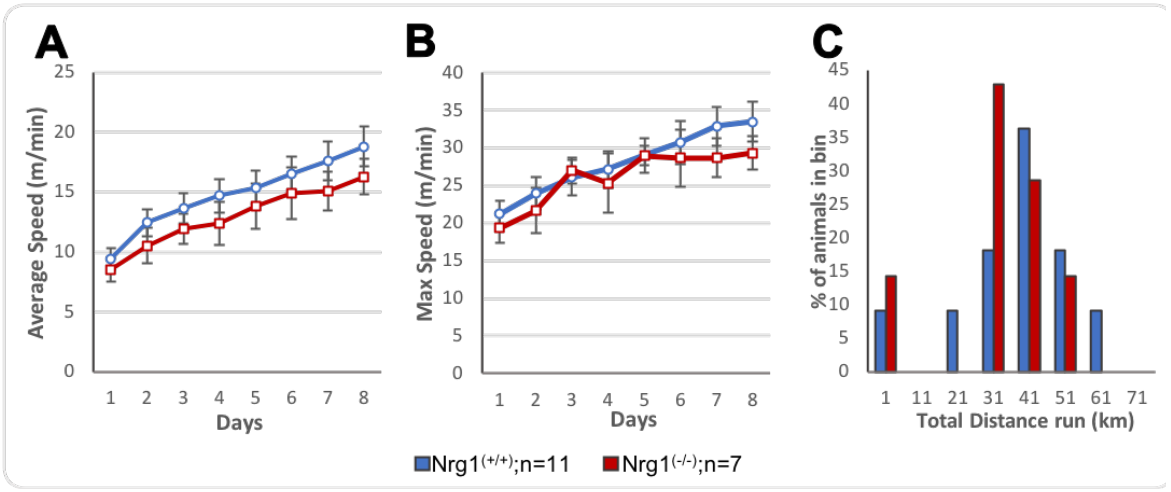
Yu DX, Marchetto MC, Gage FH. Therapeutic Translation of iPSCs for Treating Neurological Disease. *Cell Stem Cell* 2013;**12**:678–88.

Zalc B, Goujet D, Colman D. The origin of the myelination program in vertebrates. *Curr Biol* 2008;**18**:R511-512.

Zhao Y-Y, Shi X-Y, Qiu X *et al.* Enriched environment increases the total number of CNPase positive cells in the corpus callosum of middle-aged rats. *Acta Neurobiol Exp (Wars)* 2011;**71**:322–30.

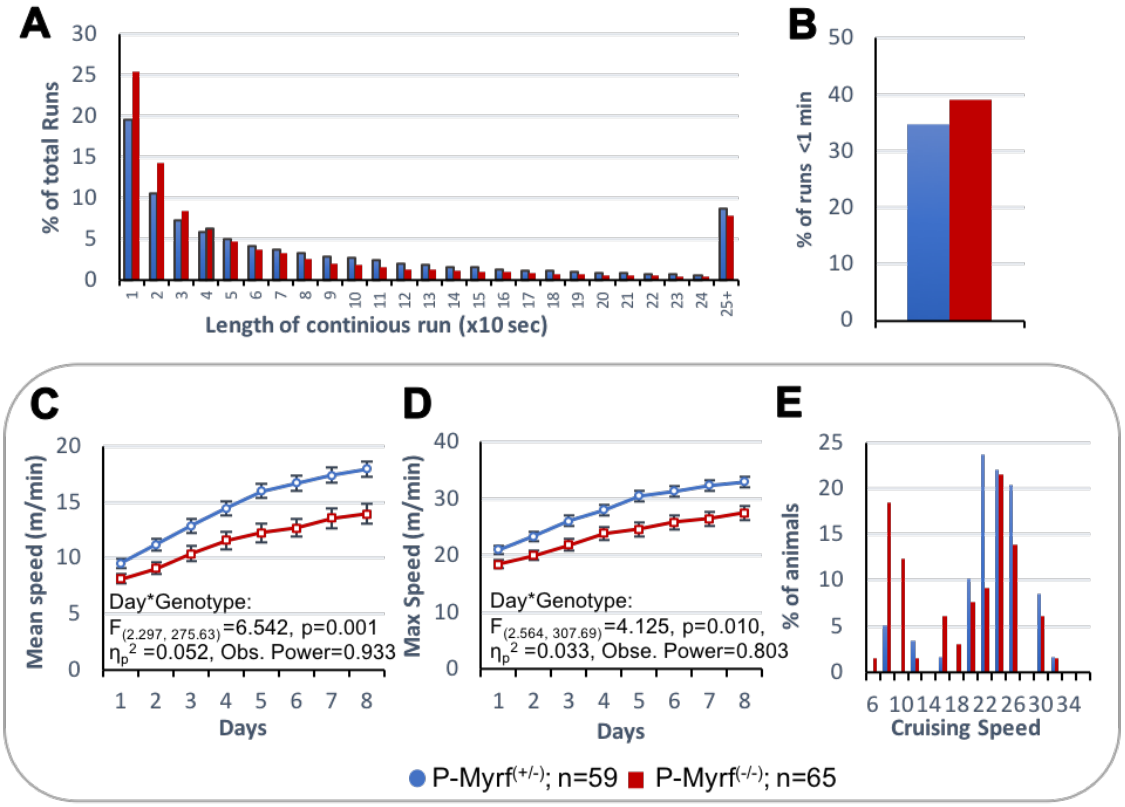
Zonouzi M, Berger D, Jokhi V *et al.* Individual Oligodendrocytes Show Bias for Inhibitory Axons in the Neocortex. *Cell Reports* 2019;**27**:2799-2808.e3.

SUPPLEMENTARY FIGURES



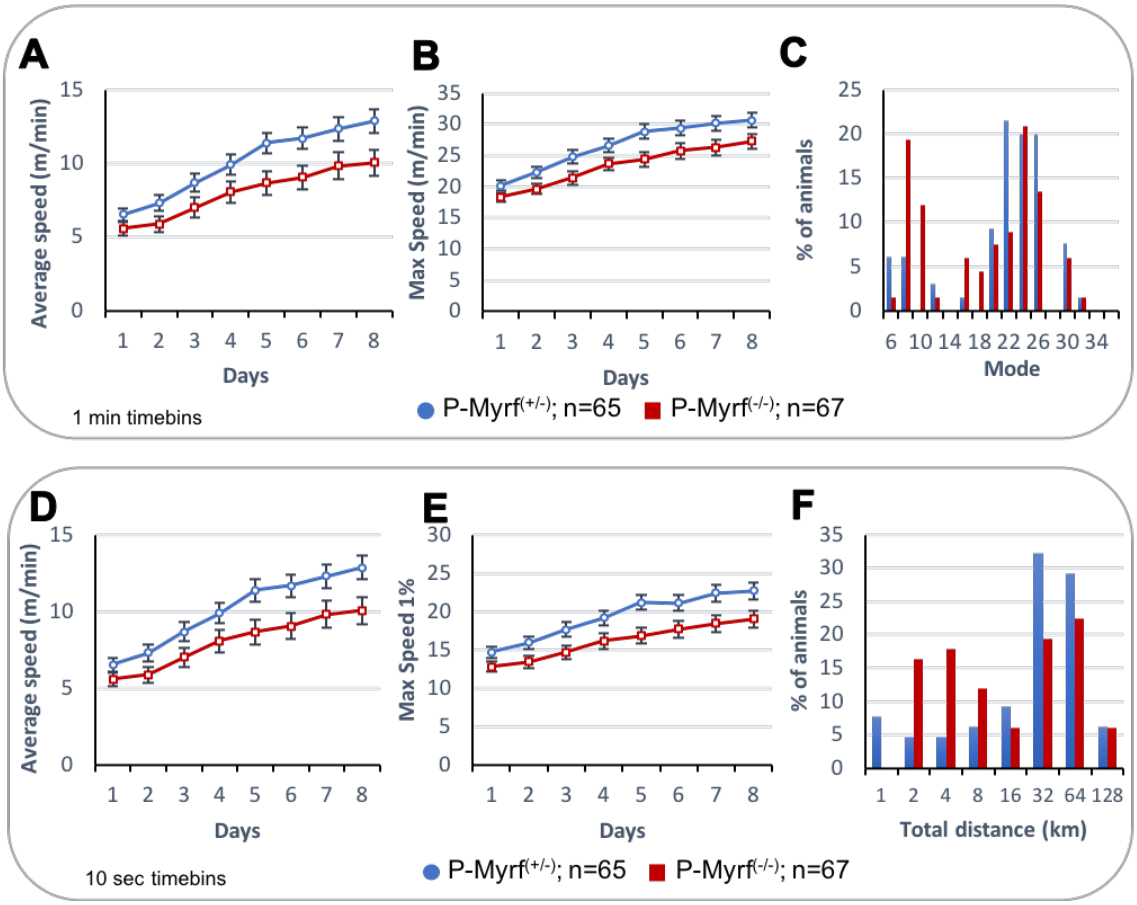
Supplementary Figure 1. ***CW running performance of Nrg1-cKO model prior to data exclusion***

(A) *Average and* ***(B)*** *maximum running speed without any exclusion of animals from analysis, in which case no statistically significant difference between the genotype groups was detected.* ***(C)*** *Frequency distribution of total distance run of all animals, separated by genotype. One animal from each group met the predetermined exclusion criteria due to a consistent lack of running behavior.*



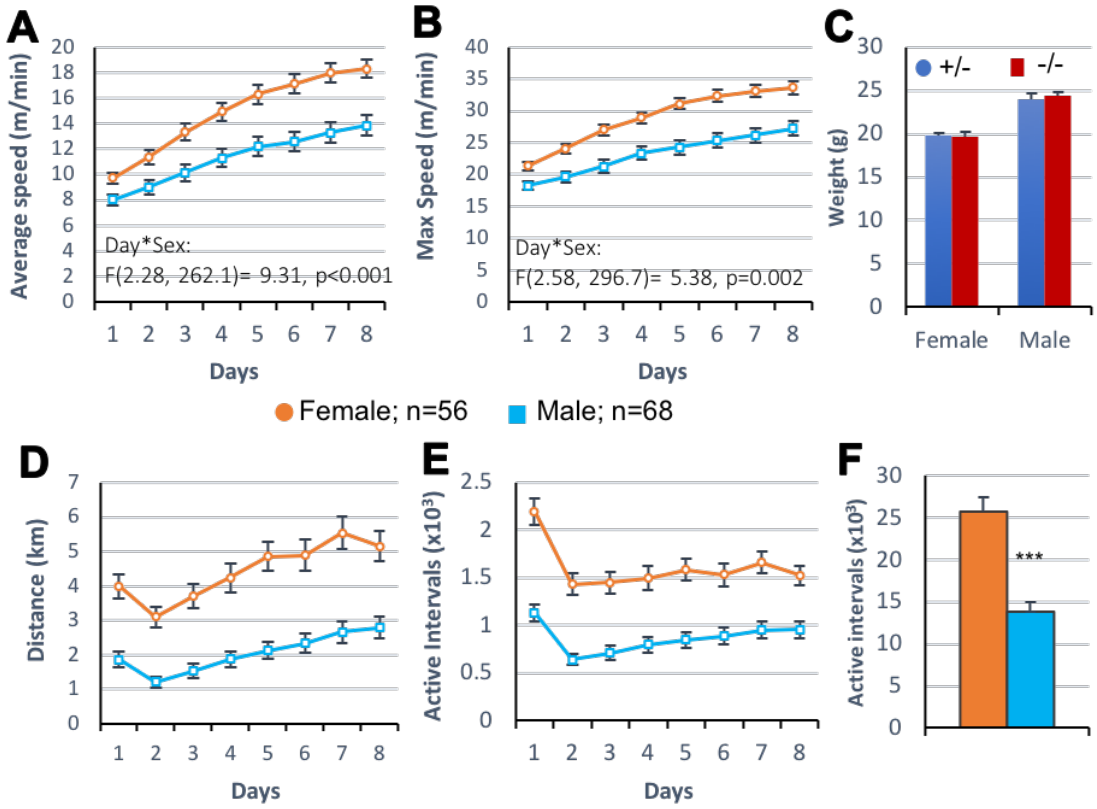
Supplementary Figure 2. ***Processing overall running performance in 10 sec long intervals leads to the same conclusion that preventing differentiation of new OL leads to impaired performance on the complex wheel.***

Speed calculated in 10 sec long timebins, rather than 1 min long bins (Figure 4.3&5) as was done by McKenzie et al (2014). ***(A)*** *The length of individual runs as the % of total runs.* ***(D)*** *In total, between 35-40 % of individual runs were shorter than 1 min, which means that calculating running speed in bins of 1 min often underestimates the actual running speed per animal.* ***(C)*** *Average and* ***(D)*** *Maximum running speeds over 8 days per genotype group. A statistically significant Day*Genotype interaction was also observed if running speed was estimated using 10 sec bins. Data presented as Mean ± SEM.* ***(E)*** *Frequency distribution of the cruising speeds indicated when a bimodal distribution in the population of P-Myrf$^{(-/-)}$ that was driving the observed behavior deficit observed in* ***(C)*** *and* ***(D).*** *Statistical analysis was performed using a mixed two-way ANOVA.*



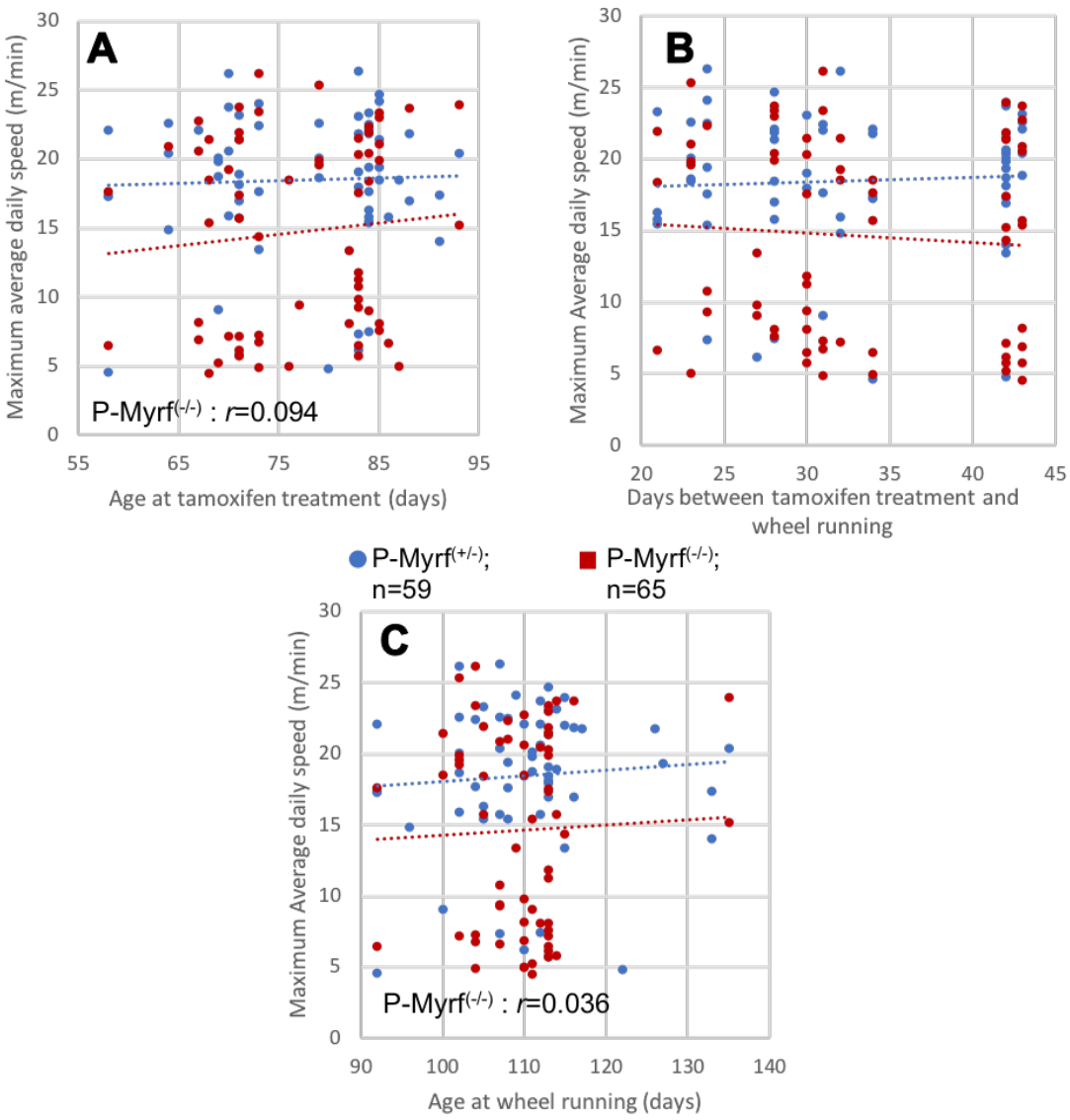
Supplementary Figure 3. ***Running performance on the complex wheel without exclusion of any animals.***

A. B. C. *= 1 min time bins* ***D. E. F. =*** *10 sec timebins. Data presented as Mean ±SEM. While the exclusion of animals that did not run sufficiently and/or consistently (see methods for details) did not change the overall shape and trend of the data, it reduced variability within the data. Analyzing daily running speeds (10 sec timebins) using a mixed two-way ANOVA still indicated a significant Day*Genotype interaction for average speed (F(2.3, 292.1)=4.567. p=0.008) and a Genotype main effect for maximum speed (F(1,128)=6.846, p=0.01), even if non-runners were not excluded from data set.*



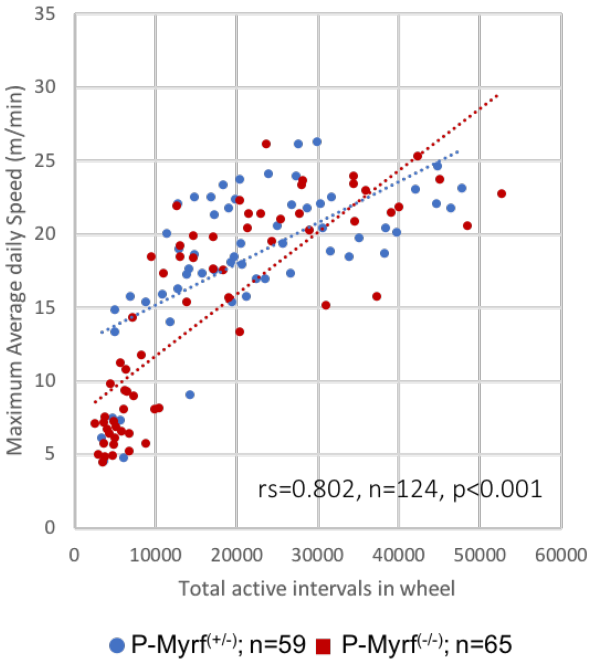
Supplementary Figure 4. ***Sex difference in running speed and activity level.***

Females outperformed males on the complex running wheel in terms of ***(A)*** *average and* ***(B)*** *maximum speed.* ***(C)*** *Body weights were lower in females, but not different between genotypes. Females not only consistently ran larger distances* ***(D)****, but also spent more time active on the wheel* ***(E,F)****. Data presented as Mean ± SEM. Data processed in 10 sec intervals. Statistical test used was a mixed two-way ANOVA (Within subject factor: Daily running speed over 8 days; Between subject factors: Sex, Generation). Independent t-test was used to compare two groups. Asterix note statistical significance: ***=<0.001.*



Supplementary Figure 5. ***Running performance on the complex wheel did not correlate with age parameters in the current study.***

Formation of new oligodendrocytes was disrupted in P-Myrf$^{(-/-)}$ animals during a time in which myelination is still ongoing. However, performance on the complex running wheel, measured in the maximum average daily running speed achieved by animals during 8 days of testing, did not correlate to either ***(A)*** *the postnatal day at which tamoxifen was administered,* ***(B)*** *the number of days between tamoxifen treatment and behavior testing on the complex wheel, or the* ***(C)*** *age at which behavior testing was started. Correlation was statistically tested using Spearman's rho (all p>0.05).*



Supplementary Figure 6. ***The amount of active intervals on the complex wheel correlated with overall running speed.***

Spearman's rho was used for statistical analysis.

TABLE OF FIGURES

MAIN FIGURES:

Figure 1.1. Myelin and the node of Ranvier. 3

Figure 1.2. Development of Myelinating and Non-myelinating Schwann Cells in the PNS. 4

Figure 1.3. Development of Oligodendroglia in the CNS. 5

Figure 1.4. Myelination can be dynamically remodelled by neural activity and experience even during adulthood, yet its role in learning remains elusive. 18

Figure 1.5. Different cellular processes may lead to dynamic changes in myelination during adulthood. 20

Figure 2.1. The number of MBP positive internodes and MBP area (as a proportion of NF200 immunoreactive axons) is highly correlated (Pearson's R; r = 0.962, n =18, P <0.001). 38

Figure 2.2. Rat Schwann cells align and myelinate human iPSC-derived sensory neurons. 42

Figure 2.3. Nodes of Ranvier and the basal lamina successfully form in co-cultures. 44

Figure 2.4. Myelination increases over time in culture. 46

Figure 2.5. Myelinating co-cultures can be maintained in culture for many months. 47

Figure 2.6. The levels of myelination are similar across three different iPSC lines. 48

Figure 2.7. Mouse IgG anti-disialosyl antibodies cause acute, complement dependent axonal degeneration while prolonged application without a source of complement impairs myelination. .49

Figure 2.8. A CANOMAD associated human IgM anti-disialosyl antibody (HA1) also causes acute, complement dependent axonal degeneration while prolonged application without a source of complement impairs myelination. 50

Figure 2.9. Prolonged (4 week) incubation with control antibodies (normal mouse IgG, nIgG) does not significantly alter either (A) axonal or (B) myelin coverage. 52

Figure 2.10. A CANOMAD associated human IgM anti-disialosyl antibody induces complement independent demyelination without evidence of axonal injury. 53

Figure 3.1. Equipment used for behavior testing with a complex wheel. 64

Figure 3.2. Overexpression of TIIINRG1 significantly increases myelination in the co-cultures. 68

Figure 3.3. Pharmacological blockade of NRG1/ErbB signalling impairs myelination in the human/rat co-cultures. 70

Figure 3.4. Co-cultures of rat OPCs and iPSC-derived sensory neurons. 72

Figure 3.5. Co-cultures in the pilot experiment contained both intact and fragmented Oligodendrocytes. 74

Figure 3.6. Oligodendrocyte do not remain stable across experiments. 75

Figure 3.7. . Experiment to investigate NRG1-ErbB signaling in co-culture system with Oligodendrocytes. 77

Figure 3.8. Conditional KO of Nrg1 caused a deficit in performance on complex wheel running. 80

Figure 3.9. Conditional KO of Nrg1 did not effect total running distance or spontaneous activity patterns in mice. 81

Figure 3.10. Effect of running and cKO of Nrg1 on oligodendroglia dynamics. 83

Figure 4.1. Deleting MYRF expression in OPCs significantly reduced the formation of new oligodendrocytes. 101

Figure 4.2. Schematic illutrations of experimental designs used to test the phenotype of P-Myrfs. 103

Figure 4.3. Preventing differentiation of new OL leads to impaired performance on the complex wheel. 106

Figure 4.4. P-Myrf$^{(-/-)}$ animals had a significantly lower improvement of their overall running speed. 107

Figure 4.5. Comparing running performance results on complex wheel to the results obtained by Mckenzie et al (2014). 108

Figure 4.6. Performance on the Normal running wheel was not impaired by conditional deletion of Myrf. 111

Figure 4.7. Performance P-Myrf$^{(-/-)}$ animals on the complex wheel was reduced within the first hours of testing. 113

Figure 4.8. P-Myrf$^{(-/-)}$ animals spent less time running on the the complex wheel. 114

Figure 4.9. Spontaneous locomotor activity in home cage was reduced in P-Myrf$^{(-/-)}$ after running the complex wheel. (A) 116

Figure 4.10. Spontaneous locomotor activity in home cage was similar between genotypes when tested before running the complex wheel. 118

Figure 4.11. Comparison of the two experiments investigating spontaneous locomotor activity in P-Myrf animals. 120

Figure 4.12. No evidence for a genotype specific impaired in motor coordination in P-Myrf$^{(-/-)}$ animals. 122

Figure 5.1. Example images of the mask used for the current preliminary analysis. 140

Figure 5.2. Experimental design and behavior phenotype of animals used for investigating underlying biology using MRI. 142

Figure 5.3. Complex wheel running did not affect the differentiation of new Oligodendrocytes. 144

Figure 5.4. OPC density and proliferation was not affected by conditional deletion of Myrf. (A) 145

Figure 5.5. Tract-Based Spatial Statistics (TBSS) of Fractional anisotropy (FA). 148

Figure 5.6. Tract-Based Spatial Statistics (TBSS) of magnetic transfer ratio (MTR). 149

Figure 5.7. TBSS between-group analysis revealed a localised reduction in FA in animals running the complex wheel. 151

Figure 5.8. Relationship between MRI based metrics and cellular densities determined by histology in the anterior corpus callosum. 153

SUPPLEMENTARY FIGURES:

Supplementary Figure 1. CW running performance of Nrg1-cKO model prior to data exclusion 189

Supplementary Figure 2. Processing overall running performance in 10 sec long intervals leads to the same conclusion that preventing differentiation of new OL leads to impaired performance on the complex wheel.....190

Supplementary Figure 3. Running performance on the complex wheel without exclusion of any animals.....191

Supplementary Figure 4. Sex difference in running speed and activity level. 192

Supplementary Figure 5. Running performance on the complex wheel did not correlate with age parameters in the current study.....193

Supplementary Figure 6. The amount of active intervals on the complex wheel correlated with overall running speed.....194

TABLES

Table 1. Primary Antibodies used for immunohistochemistry and their dilutions.....37

Table 2. Variability of animal's age at important experimental timepoints within different generations of Myrf-cKO animals.....105